

WARSAW UNIVERSITY OF TECHNOLOGY

MECHANICAL ENGINEERING

MACHINE DESIGN AND MAINTENANCE

# Ph.D. Thesis

Mateusz Żurawski, M.Sc.

**Experimental study, numerical analysis and predictive control  
of the Adaptive Tuned Particle Impact Damper**

Supervisor:

Professor Robert Zalewski, PhD, DSc

Additional supervisor:

Cezary Graczykowski, PhD

Warsaw 2023



## **Abstract**

The doctoral dissertation presents the concept of the Adaptive Tuned Particle Impact Damper (ATPID) and its application for adaptive mechanical vibration damping. The proposed concept involves modification of the classical Impact Damper (ID), which consists of a container and an additional element (usually grains) capable of free movement. The ATPID damper is enhanced with additional electromechanical elements, mainly an electric motor that changes the position of the upper container wall, allowing for real-time changes in the volume of the damper. The proposed damper prototype is equipped with a measurement system, creating a device with tunable vibration damping by adaptation to the actual excitation.

The thesis attempts to present a complete description of subsequent stages of development of the ATPID. The dissertation starts with a literature review of similar technical solutions. The main types of impact dampers and their practical applications in the engineering environment are described. In the following chapter, an experimental research methodology is proposed. For this purpose, an ATPID prototype is constructed, and a test stand is built along with a measurement system. The research plan is described in details, including free and harmonic vibration analyses of a cantilever beam with the ATPID damper attached at its free end. Over 100 experimental measurements are conducted for various system parameters, such as excitation frequency or amplitude, grain mass, and the damper height. Both displacement and acceleration of the beam at the damper attachment point are measured using a laser sensor, accelerometer, measuring cards and dedicated measurement software.

The further part of the dissertation concerns the development of a numerical model of the ATPID damper and the test stand. Theoretical analyses are based on the grain collisions with the damper walls using the theory of soft contact. Additionally, a tuned container height allowing control of the damper wall position is taken into account. The numerical model is validated based on previously conducted experimental measurements. A series of sensitivity analyses were performed to describe the detailed operation principle of the proposed device. Furthermore, an energy balance analysis is carried out to define the influence of the collisions on the change in the dynamics of the tested system. A parametric optimization is performed, which allows for the formulation of the criteria for the optimal particle movement from the perspective of vibration damping. In the following part, a general concept of the Adaptive Impact Damper control strategy is formulated. A predictive control algorithm is presented, facilitating the search for optimal damper heights for adopted system parameters and current operating conditions.

The dissertation presents a comprehensive study of the Adaptive Tuned Particle Impact Damper concept, including experimental research, numerical modelling, and control strategy development. The proposed concept has a significant potential for practical applications in various mechanical systems, used in aerospace and automotive engineering.

**Keywords:** Adaptive Tuned Particle Impact Damper, Damping of vibrations, Adaptive passive damping, Controllable damper, Control function, Sensitivity analysis, System optimization, Real-time control strategy.

## Streszczenie

W rozprawie doktorskiej przedstawiono koncepcję Adaptacyjnego Tłumika Uderzeniowego (ang. Adaptive Tuned Particle Impact Damper - ATPID) i jego zastosowanie do tłumienia drgań mechanicznych. Zaproponowana koncepcja polega na modyfikacji klasycznego Tłumika Uderzeniowego (ang. Impact Damper - ID), który składa się z obudowy oraz dodatkowego elementu (najczęściej granulatu) zdolnego do swobodnego ruchu wewnątrz obudowy. Amortyzator ATPID został wzbogacony o dodatkowe elementy elektromechaniczne, głównie silnik elektryczny zmieniający położenie sufitu obudowy, co pozwala na zmianę objętości tłumika w czasie rzeczywistym. Proponowany prototyp tłumika wyposażony jest w układ pomiarowy, tworzącym urządzenie o możliwościach adaptacyjnych poprzez dostosowywanie się do aktualnie występującego wymuszenia.

W pracy podjęto próbę przedstawienia pełnego opisu kolejnych etapów rozwoju tłumika ATPID. W pierwszym rozdziale rozprawy dokonano przeglądu literatury dotyczącej podobnych rozwiązań technicznych. Opisano główne typy amortyzatorów oraz ich praktyczne zastosowanie w środowisku inżynierskim. W kolejnym rozdziale zaproponowano metodologię badań eksperymentalnych. W tym celu skonstruowano prototyp urządzenia oraz zbudowano stanowisko badawcze uwzględniające układ pomiarowy. Szczegółowo opisano plan badań obejmujący analizę drgań swobodnych i harmonicznym belki wspornikowej z tłumikiem ATPID zamocowanym na jej swobodnym końcu. Przeprowadzono ponad 100 pomiarów eksperymentalnych dla różnych parametrów układu, takich jak amplituda i częstotliwość wymuszenia, masa granulatu i wysokość tłumika. Zarówno przemieszczenie, jak i przyspieszenie belki w punkcie mocowania amortyzatora mierzono za pomocą czujnika laserowego, akcelerometru, kart pomiarowych oraz dedykowanego oprogramowania pomiarowego.

Dalsza część rozprawy dotyczy opracowania modelu numerycznego tłumika ATPID oraz zaproponowanego stanowiska badawczego. Analizy teoretyczne opierają się na odwzorowaniu zderzenia granulatu ze ściankami obudowy z wykorzystaniem teorii miękkiego kontaktu. Dodatkowo uwzględniono zmienną wysokość obudowy, umożliwiającą kontrolę położenia sufitu urządzenia. Model numeryczny został zweryfikowany na podstawie wcześniej przeprowadzonych badań eksperymentalnych. Wykonano szereg analiz wrażliwości w celu szczegółowego opisanie zasady działania proponowanego tłumika. Ponadto przeprowadzono analizę energetyczną w celu określenia wpływu poszczególnych zderzeń na zmianę dynamiki badanego układu. Przeprowadzono optymalizację parametryczną, która pozwoliła

na sformułowanie kryteriów optymalnego ruchu granulatu z punktu widzenia tłumienia drgań. W dalszej części sformułowano ogólną koncepcję strategii sterowania Adaptacyjnym Tłumikiem Uderzeniowym. Przedstawiono algorytm sterowania predykcyjnego, ułatwiający poszukiwanie optymalnych wysokości obudowy dla przyjętych parametrów układu i aktualnych warunków pracy.

Rozprawa przedstawia kompleksowe badanie koncepcji Adaptacyjnego Tłumika Uderzenia, w tym badania eksperymentalne, modelowanie numeryczne i rozwój predykcyjnego algorytmu sterowania. Proponowana koncepcja ma znaczny potencjał praktycznych zastosowań w różnych układach mechanicznych, wykorzystywanych w inżynierii lotniczej i motoryzacji.

**Słowa kluczowe:** Adaptacyjny Tłumik Uderzeniowy, tłumienie drgań, adaptacyjno-pasywne tłumienie, sterowalny tłumik, funkcja sterująca, analiza wrażliwości, optymalizacja parametryczna, strategia sterowania w czasie rzeczywistym, .

# Contents

- List of Abbreviations** **9**
  
- List of Symbols** **11**
  
- 1 Introduction** **15**
  - 1.1 Motivation . . . . . 15
  - 1.2 State of the art . . . . . 17
    - 1.2.1 Classical PID damper . . . . . 17
    - 1.2.2 Types of PID dampers . . . . . 18
    - 1.2.3 Applications of the PID dampers . . . . . 28
  - 1.3 Objectives and plan of the thesis . . . . . 35
  
- 2 Adaptive Tuned Particle Impact Damper - the prototype and experimental studies** **37**
  - 2.1 The concept and design of the ATPID damper . . . . . 38
  - 2.2 Description of the test stand . . . . . 40
  - 2.3 Experimental results . . . . . 43
    - 2.3.1 Free vibrations . . . . . 45
    - 2.3.2 Harmonic vibrations . . . . . 54
  
- 3 Adaptive Tuned Particle Impact Damper - numerical analysis** **69**
  - 3.1 Contact modelling - state of the art . . . . . 69
  - 3.2 Numerical model of the ATPID damper . . . . . 79
  - 3.3 Validation of the numerical model . . . . . 87
  - 3.4 Detailed analysis of the ATPID damper operating principle . . . . . 90
  - 3.5 Sensitivity analysis . . . . . 98

3.5.1	Influence of the container height . . . . .	98
3.5.2	Influence of the grain mass . . . . .	101
3.5.3	Influence of the excitation amplitude . . . . .	102
3.6	Energy analysis . . . . .	105
3.6.1	Overlaps, overlaps rates and contact forces . . . . .	105
3.6.2	Balance of system energy . . . . .	106
3.7	Parameters optimization . . . . .	113
<b>4</b>	<b>ATPID damper control algorithm</b>	<b>119</b>
4.1	State of the art . . . . .	119
4.2	General concept of the control strategy . . . . .	122
4.3	Numerical simulations of real-time control algorithm . . . . .	126
4.4	Predictive control algorithm (PCA) . . . . .	132
<b>5</b>	<b>Summary</b>	<b>163</b>

# List of Abbreviations

PID - Particles Impact Damper

AID - Adaptive Impact Damper

PD - Particles Damper

ID - Impact Damper

MUID - Multi-Unit Impact Damper

MUPD - Multi-Unit Particles Damper

BID - Buffered Impact Damper

FPID - Fine Particle Impact Damper

PPD - Polymeric Particle Damper

TMD - Tuned Mass Damper

TLCD - Tuned Liquid Column Damper

DPID - Double Pendulum Impact Damper

TPID - Tuned Particles Impact Damper

DEM - Discrete Element Method

FEM - Finite Element Method

PCB - Printed Circuit Board

ATPID - Adaptive Tuned Particle Impact Damper

LH - Lee and Herrmann

KK - Kuwabara and Kono

CK45 - Cash-Karp fourth-fifth order Runge-Kutta method

LSODE - Livermore Solver for Ordinary Differential Equations

DOF - Degree Of Freedom

RMSE - Root Mean Square Errors

MME - Mass Modification Effect

PIFE - Pseudo-Inertial Force Effect

SDC - Specific Damping Coefficient  
PCA - Predictive Control Algorithm  
SM - Simplified Model  
PM - Predictive Model  
CM - Complex Model

# List of Symbols

$F^n$  - normal contact force

$F_{el}^n$  - normal elastic contact force

$F_{diss}^n$  - normal dissipative contact force

$F_c$  - indenter force

$F_{ATPID}$  - total force generated by the ATPID damper

$F_{c_1}$  - grain - floor contact forces

$F_{c_2}$  - grain - ceiling contact force

$F_{iner}$  - inertial force

$k^n$  - non-linear reduced stiffness

$k_{lin}^n$  - equivalent stiffness spring

$\gamma_{lin}^n$  - equivalent linear damping

$\gamma_{LH}^n$  - phenomenological dissipative factor (from Lee and Hermann model)

$\gamma_{KK}^n$  - dissipative factor (from Kuwabara and Kono model)

$\gamma_T^n$  - phenomenological dissipative factor (from Tsuji model)

$a$  - radius of the contact circle

$R$  - indenter radius

$r$  - grain radius

$E_w$  - specimen Young's modulus

$E_p$  - indenter Young's modulus

$E_{eff}$  - effective Young's modulus of the specimen and indenter

$\nu_w$  - specimen Poisson's ratio

$\nu_p$  - indenter Poisson's ratio

$\alpha$  - damping factor

$\beta$  - system damping ratio

$\xi$  - overlap

$\dot{\xi}$  - overlap rate  
 $\xi_{c_1}$  - lower overlap  
 $\xi_{c_2}$  - upper overlap  
 $\dot{\xi}_{c_1}$  - lower overlap rate  
 $\dot{\xi}_{c_2}$  - upper overlap rate  
 $m_s$  - reduced beam mass  
 $m_g$  - grain mass  
 $M$  - total mass of the system  
 $m$  - system mass  
 $\Delta m$  - change in system mass  
 $k$  - system stiffness  
 $k_s$  - reduced beam stiffness  
 $k_c$  - reduced effective stiffness  
 $k_{eff}$  - effective stiffness  
 $c_s$  - reduced beam damping  
 $c_c$  - reduced effective damping  
 $c_{eff}$  - effective damping  
 $h$  - controllable container height  
 $\dot{h}$  - container ceiling velocity  
 $h_{min}$  - minimal container height  
 $h_{max}$  - maximum container height  
 $\Delta h$  - ceiling's controllable range of movement  
 $t$  - time  
 $\psi$  - dimensionless control function  
 $t_1$  - activation start time  
 $t_2$  - saturation start time  
 $\Delta t_{12}$  - activation period  
 $x_s$  - beam (and container floor) displacement  
 $\dot{x}_s$  - beam (and container floor) velocity  
 $\ddot{x}_s$  - beam (and container floor) acceleration  
 $x_g$  - grain displacement  
 $\dot{x}_g$  - grain velocity

$\ddot{x}_g$  - grain acceleration  
 $x_{g_i}$  - initial position of the grain in the container  
 $X_{Sim}$  - amplitude of the numerical beam vibration  
 $X_{Exp}$  - amplitude of the experimental beam vibration  
 $u_s$  - excitation displacement  
 $\dot{u}_s$  - excitation velocity  
 $A$  - amplitude of excitation  
 $f$  - resonance frequency  
 $f_0$  - natural frequency of the system  
 $Q_s$  - beam gravity force  
 $Q_g$  - grain gravity force  
 $g$  - gravity  
 $E_{tot}^s$  - total energy of the beam  
 $\Delta E_k^s$  - change of beam kinetic energy  
 $\Delta E_{el}^s$  - change of beam elastic energy  
 $\Delta E_p^s$  - change of potential energy of the beam  
 $\Delta E_{tot}^s$  - change of total energy of the beam  
 $\Delta E_k^g$  - change of grain kinetic energy  
 $\Delta E_p^g$  - change of grain potential energy  
 $\Delta E_p^c$  - change of potential energy of the contact spring  
 $E(t_i)$  - initial energy per one cycle of vibrations  
 $D$  - energy dissipation in the contact element  
 $W_d^s$  - viscous dissipation  
 $W_{F_c}^s$  - work of contact forces  
 $\Delta W_{F_{ext}}^s$  - work done by excitation force on beam displacement  
 $\Delta W_{F_c}^s$  - work done by both contact forces on beam displacement  
 $\Delta W_{F_c}^g$  - work done by both contact forces on grain displacement  
 $\overline{W}_{F_c}^s$  - work done by the system due to interaction with the grain  
 $W(t_i)$  - ratio of the energy lost per one cycle of vibrations  
 $\Psi(t_i)$  - Specific Damping Coefficient  
 $d$  - damper efficiency for different excitation amplitudes  
 $x_s^d$  - amplitudes of damped steady-state vibrations

$x_s^{ud}$  - amplitudes of undamped steady-state vibrations  
 $\gamma$  - parameter related to the non-sticking effect  
 $x_{pred}^s$  - predicted response of the vibrating system  
 $x_{pred}^h$  - predicted displacement of the ceiling of the damper  
 $h_{pred}$  - predicted height of the damper  
 $D_{red}$  - reduced amplitude  
 $A_0$  - the first component of the reduced amplitude  $D_{red}$   
 $B_0$  - the second component of the reduced amplitude  $D_{red}$   
 $\phi$  - phase shift  
 $T$  - one period of beam oscillation  
 $t_c$  - single contact time  
 $t_{c_1}$  - time of the particle's impact with the lower part of the container  
 $x_{pred}^{t_{c_1}}$  - predicted beam displacement at the time  $t_{c_1}$   
 $t_{c_2}$  - time of the particle's impact with the upper part of the container  
 $x_{pred}^{t_{c_2}}$  - predicted beam displacement at the time  $t_{c_2}$   
 $x_{k_i}$  - initial condition of the grain displacement  
 $V_{k_0}$  - initial velocity of the grain  
 $X_g$  - predicted grain displacement at the time  $t_{c_2}$   
 $X_{beam}$  - beam position from the Complex Model  
 $X_{grain}$  - grain position from the Complex Model  
 $V_{beam}$  - beam velocity from the Complex Model  
 $V_{grain}$  - grain velocity from the Complex Model  
 $n$  - number of iterations of the searching process  
 $\Delta h_{opt}$  - parameter of the PCA algorithm effectiveness

# Chapter 1

## Introduction

### 1.1 Motivation

The purpose of this research is to develop a highly efficient device that can adaptively damp mechanical vibrations, providing a practical alternative to the classical absorbers widely used in mechanical engineering. Mechanical systems are often subjected to dynamic excitations, and effective damping of the corresponding vibrations is crucial for a system safety and reliability. Improper damping strategies can cause significant damage of the protected objects. By improving vibration attenuation techniques, failures can be prevented, durability can be enhanced, and employee comfort can be maximized in the design of various objects, such as machines, buildings, bridges, cranes, and cars. Currently, passive vibration damping systems are the most commonly used, but without information about actual excitations acting on the equipment, they often lead to sub-optimal vibration damping in rapidly changing environments with varying internal and external forces.

Since 1960, the Particle Impact Damper (PID) was introduced a novel device for vibration attenuation. According to the first concept, it was a passive system with a simple design and operating principle. The PID damper consists of a container and grain enclosed inside the absorber. During the vibrations, grain can move and collides with the walls, and as a result, reduces system vibrations by modifying the structure's natural frequency and generating additional forces acting on the structure. Despite scientific efforts to improve its construction, the PID damper has not been widely used in engineering due to limitations that prevent optimal adaptation to dynamic operating

conditions [1]. Hence, there is a need for innovative technology to effectively adapt the damper to real excitation.

Adaptive devices are complex systems that merge the theoretical modelling of various physical phenomena with technical solutions in the form of well-designed structures. These models cover areas such as fluid mechanics, electricity, magnetism, and machine mechanics. Developed mathematical models enable simulation of the system behaviour in real conditions and form the basis for optimizing the structure and achieving the most efficient damping of vibrations caused by given excitation. Despite scientific advancements in this area, there is a noticeable lack of adaptive devices that integrate with classic PID dampers. The modelling and control of Adaptive Impact Dampers (AID) are not widely recognized in the scientific literature, according to the author's understanding.

The dissertation introduces the concept of the "Adaptive Tuned Particle Impact Damper" (ATPID), a tuneable device with a container that can change its volume in real-time and a control algorithm that predicts optimal parameters for maximum vibration damping caused by dynamic excitation. The prototype design, modelling methods, predictive control algorithm development, and applications of the ATPID damper are extensively examined. Thus, the research appears significant both from a practical and theoretical point of view.

## 1.2 State of the art

### 1.2.1 Classical PID damper

Devices that reduce mechanical vibrations have been of interest to researchers and engineers for many years. There are various types of vibration dampers designs used in everyday engineering applications, including passive shock absorbers that use elastomers with viscous properties. Recently, Particle Impact Dampers have gained importance in the domain of vibration damping. The classical PID (Fig 1.1) operates through the particles inelastic collisions enclosed in a special container or cavity. Energy dissipation is also due to the frictional contact between the particles and the damper walls. When subjected to a vibrating system, the PID device absorbs some of the structure's kinetic energy, reducing its vibration amplitudes. The effectiveness of this damping approach is mainly due to the combination of impact and friction phenomena [2].

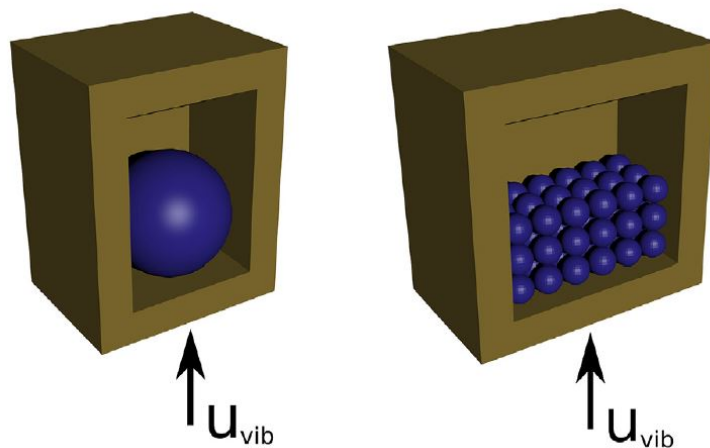


Figure 1.1: Simplified construction of the PID dampers [3]

Most frequently utilized damping devices exhibit energy dissipation typically related to friction or visco-elastic material deformation, which leads to increased operating temperature, material wear and reduced damping properties. In the light of these limitations, granular dampers, where the influence of temperature and material degradation is less significant, are particularly appealing. PIDs offer additional advantages, such as the ability to operate at a wide range of frequencies, the use of recyclable materials, lower cost, and a lower overall system mass compared to traditional dampers. These features make PIDs well-suited for dynamic systems operating in harsh envi-

ronments [4]. However, the adjustment of damping properties in this class of shock absorbers is limited and mainly involves selecting the proper type, shape, and size of grains for the specific application [5, 6].

### 1.2.2 Types of PID dampers

The traditional particle dampers have undergone several modifications, which provided their unique characteristics and made them suitable for selected technical applications [3, 7, 8]. These modifications can be divided into three main categories, as shown in Fig. 1.2. The categories are based on the various components of modifications made to the standard Particle Dampers (PD), including configuration, material type, and combination type.

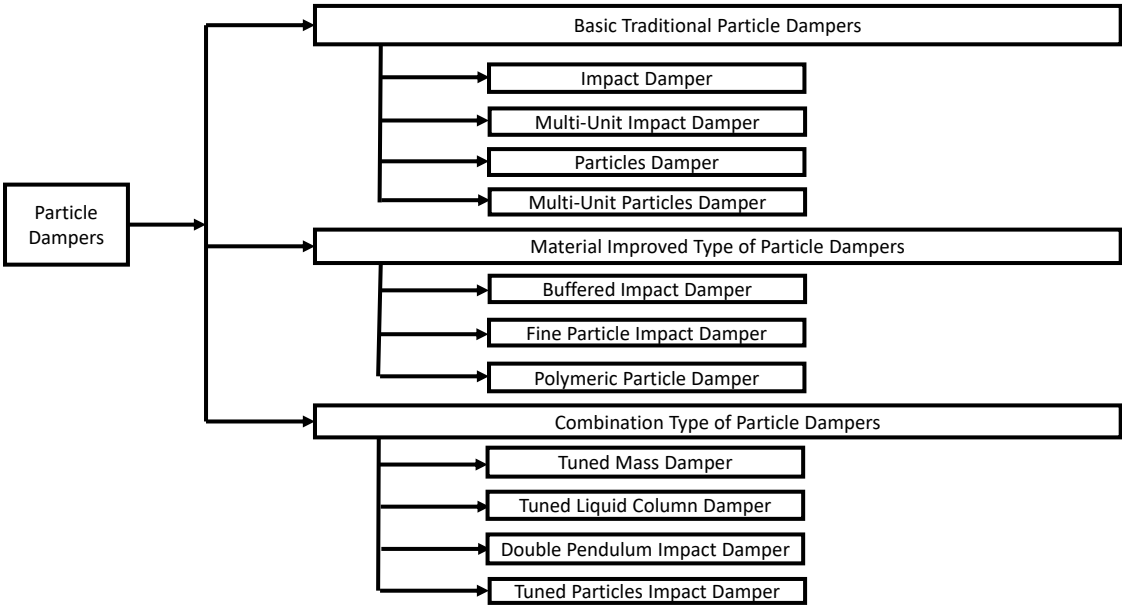


Figure 1.2: Main categories of the Particle Dampers

#### *Basic traditional Particle Dampers*

Single Particle Impact Damper (SPID) is a specific type of Impact Damper (ID). The classic Impact Damper uses a freely moving mass inside the absorber, whose shape and material can be arbitrary [9, 10]. The SPID is characterised by high noise levels and high impact forces due to the presence of only one particle being involved in the collision process (as shown in Fig. 1.3). As a result, the effectiveness of the SPID depends

on changes in excitation parameters such as excitation amplitude and frequency [11, 12]. Despite their extension from the initial idea of using a moving mass (taking a different shape than a sphere) to reduce mechanical system vibration, Single Particle Impact Dampers have significant limitation in the form of fixed container size. This disadvantage hinders their potential for implementation and improvement in various industries.

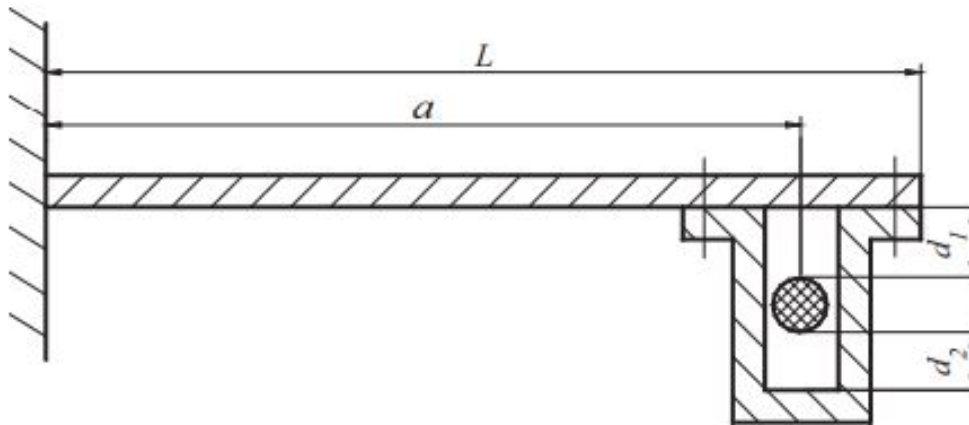


Figure 1.3: The scheme of the Single Particle Impact Damper [13]

The size of the cavity is a crucial factor in determining the efficiency of particle damping in an impact damper. This parameter affects the overall vibration reduction of the system. Although, when the optimal size of the container is too large, it may not be feasible to incorporate such a cavity into the main structure due to practical constraints in construction. Furthermore, the collision between the particle and the container can generate a significant amount of noise. To address these issues, some researchers have proposed using Multi-Unit Impact Dampers that consist of multiple small cavities with appropriate dimensions (Fig. 1.4). MUID is an advanced form of Single Particle Impact Damper [14]. The study investigated the effect of the number and size of cavities on the damper's effectiveness.

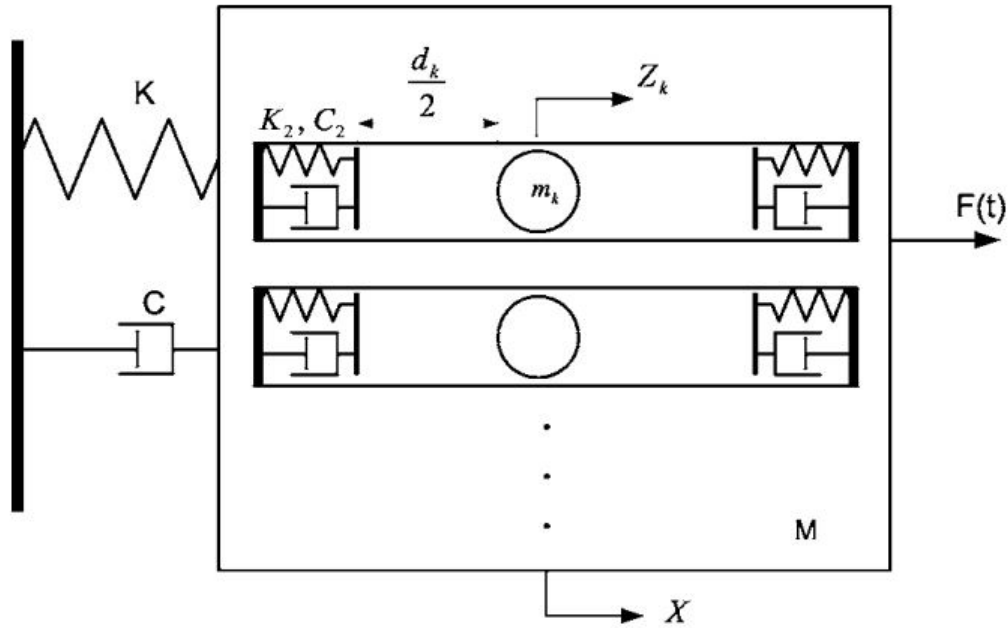


Figure 1.4: The scheme of the MUID damper [14]

The MUID has been the subject of various theoretical, numerical, and experimental researches. In 1969, Masri conducted a theoretical analysis of the MUID under harmonic excitation and obtained an analytical method for the stationary motion, which agrees with both numerical simulations and experimental investigation [15]. Cempel [16] proposed the application of an equivalent continuous force as a method for estimating the effects of impact interactions and analyzed the oscillations of the MUID accordingly. Meanwhile, in [17] the authors examined the impact of Coulomb friction on the MUID's performance through theoretical investigation and computational modeling.

Vibration reduction in a structure can be achieved through the use of Particle Dampers [18, 19, 20]. This passive damping technology involves filling a single cavity (as shown in Fig. 1.5a) or multiple cavities (Fig. 1.5b for Multi-Unit Particle Dampers - MUPD) with small particles. The grains can be formed of ceramics or metals that are thermally stable, which causes that the damping mechanism is independent on viscoelastic properties and insensitive to temperature changes. This is a key advantage of particle dampers. However, modelling the complex interactions between the particles and walls as well as the development of simplified models that account for various non-linear physical phenomena [21] is a challenging problem.

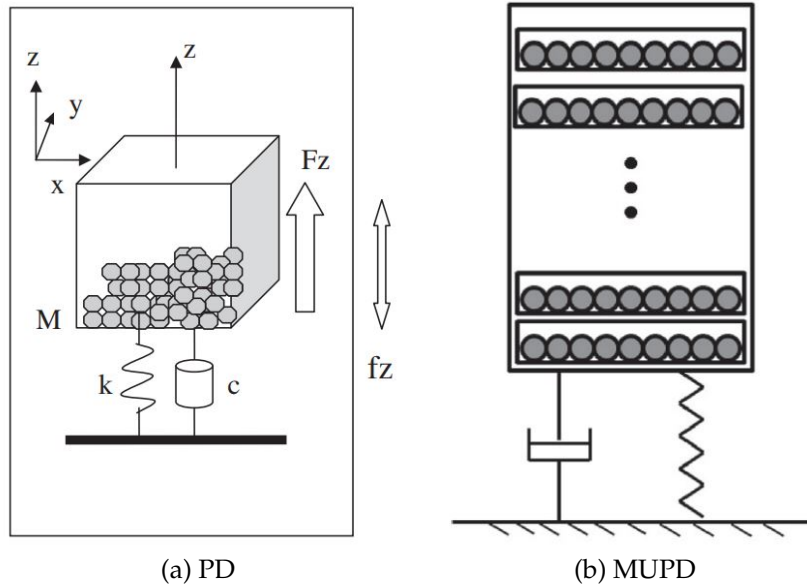


Figure 1.5: The scheme of the Particles Damper [22] and Multi-Unit Particles Damper [23]

*Material Improved Type of Particle Dampers*

The Buffered Impact Damper (BID) is a variant of the traditional Impact Damper that incorporates soft, elastic buffers connecting the stops (Fig. 1.6). This design modification helps to reduce the drawbacks associated with ID absorbers, such as extreme noise levels, large accelerations, and significant impact force. The buffer significantly reduces the peak value of the impact force and increases the contact time during impact, leading to improved damping performance [24, 25, 26].

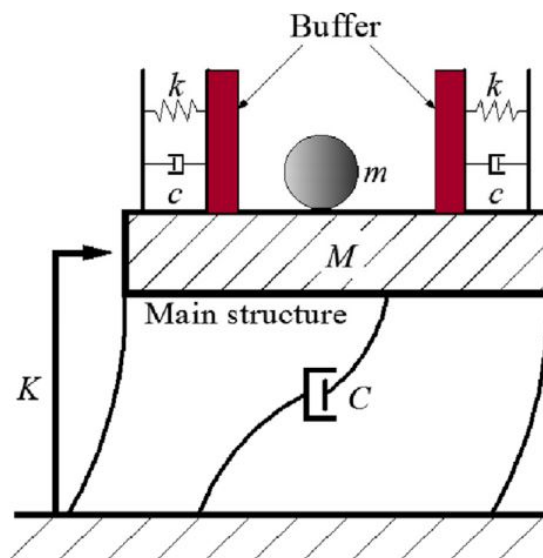


Figure 1.6: Scheme of the Buffered Impact Damper [3]

The purpose of the study in [25] was to conduct systematic experimental research to investigate the mechanism of buffered impact dampers. Seven different materials were selected for testing on a shake table, and parameters such as gap distance, material, mass ratio, and excitation characteristics were examined. The mechanism of the attenuation was presented, and several design guidelines for buffered impact dampers were described. The study proposed collision hardness as a critical factor that can reveal momentum exchange, also the issue of the restitution coefficient was thoroughly discussed. The main finding of the study reveals that increasing the mass ratio causes a greater reduction of vibration. The mass ratio plays a crucial role and affects the optimal gap distance. Therefore, when designing buffered impact dampers, the mass ratio should be considered before the gap distance. If there are no practical limitations on the damper mass, a higher mass ratio is recommended. However, if a higher mass ratio is not feasible, a lower mass ratio with an optimal gap distance can also be a viable alternative. To achieve a better impact reduction, it is important to use a moderate gap distance. However, the optimal value for the gap distance depends on the characteristics of the excitation. Experimental analysis has shown that a larger response from the structure requires a larger gap distance. The restitution coefficient's impact on the vibration effect is complex and cannot be used as the sole indicator of a buffer impact attenuator performance. When designing the buffer, it is also important to consider the hardness of the buffering particle, as a softened particle may have a smaller effect when the response is small. It is recommended to use a hard particle and a soft inner container wall for practical applications.

The Fine Particle Impact Damper (FPID) provides a plastic deformation of small particles resulting in continuous energy loss in a vibration system. A small number of microparticles serve as the damping element in the FPID (Fig. 1.7). Due to the surface attraction being greater than the gravitational force, fine particles often completely cover the impact components, including the oscillators and cavity. FPID introduces a new mechanism that relies on the ability of particles compressed between two large bodies during a normal impact to absorb a significant amount of kinetic energy. Systems with FPID technology can effectively operate in a vibratory environment as described [27].

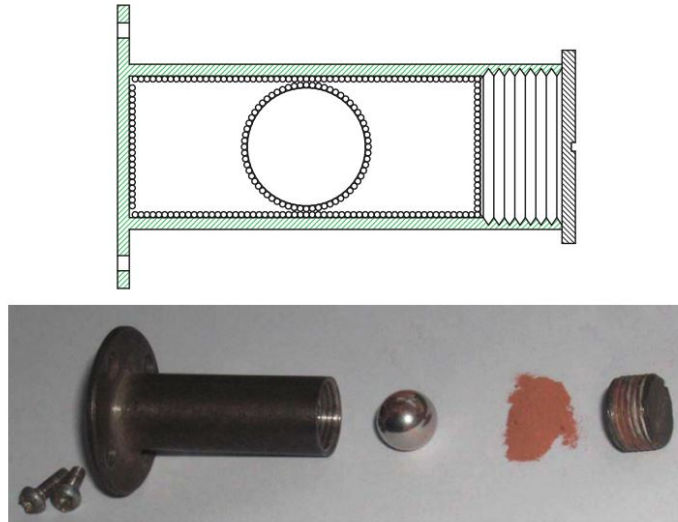


Figure 1.7: The concept of the Fine Particle Impact Damper [27]

The repeatability of operation in a Fine Particle Impact Damper (FPID) may not be maintained due to permanent plastic deformation of the fine particles. However, there are methods that ensure the repeatability despite plastic deformation. One approach is to intentionally design the FPID to include a specific amount of plastic deformation. This can be achieved by selecting appropriate materials and applying a careful technical design. By considering a predetermined level of deformation, the FPID can operate within an acceptable range without being affected by deformation. Another approach is to monitor the amount of plastic deformation that occurs during operation and adjust the FPID accordingly, if necessary, to maintain an optimal performance. This can be achieved through regular inspections and tests and making any necessary adjustments or replacements. Additionally, the fine particles used in FPID can be periodically replaced to ensure that they have not undergone excessive plastic deformation [28].

The conventional impact damper usually features a container partially filled with metal grains. However, materials with varying physical properties can impact the damper's functionality. Viscoelastic polymers, known for their frequency and temperature dependent properties, are commonly used in engineering structures as amplitude-independent damping elements. In contrast to traditional linear dampers, which lose their effectiveness at higher amplitudes, PPDs can provide constant damping over a wide range of vibration amplitudes. In view of this, [29] proposed a Particle Damper filled with polymeric particles (Fig. 1.8) to introduce new, promising properties that enhance the vibration damping efficiency of the structure.

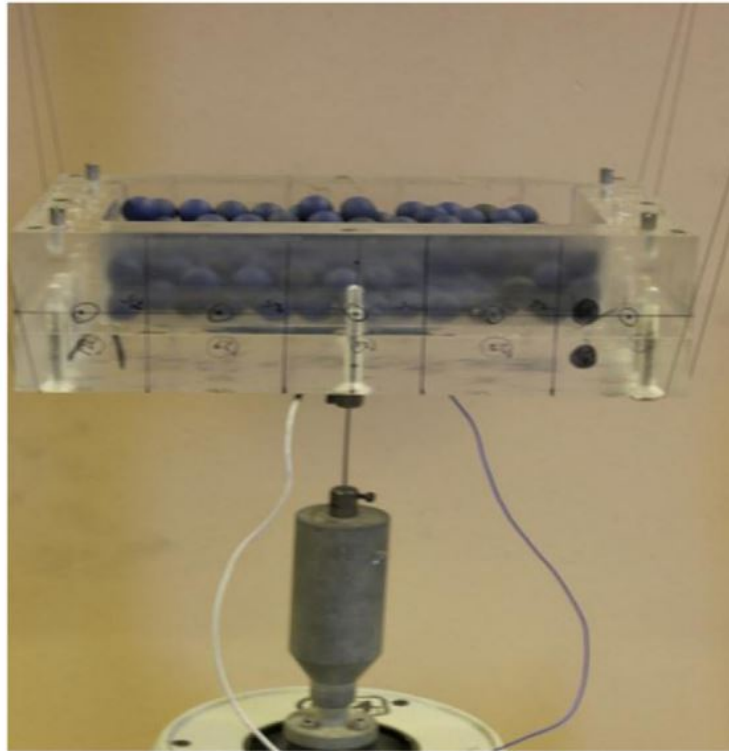


Figure 1.8: The construction of the Polymeric Particle Damper (PPD) [29]

#### *Combination Type of Particle Dampers*

From the damping of vibration point of view, the effectiveness of Particle Impact Dampers can be seen in the reduction of vibration amplitudes, especially in the frequency range where the excitation is close to resonant. In some situations, the impact of PID can be considered as similar to that of a Tuned Mass Damper (TMD). The authors of [30, 31, 32] compared the effect of both devices on vibration damping and suggested modelling both absorbers as single or multi-degree-of-freedom systems with similar operating principles. The damping performance of TMD and PD was evaluated through tests conducted under various dynamic conditions such as seismic excitations and wind loads. The study also investigated the impact of factors like maximum ground accelerations and wind attack angles on the effectiveness of these devices. Results demonstrated that TMD and PD are effective passive control devices, capable of reducing the response of a primary structure in various dynamic scenarios.

When comparing the vibration damping capabilities of mass dampers (PD) and mechanical vibration dampers (TMD), PD damping was generally found to be superior to TMD damping due to different energy dissipation mechanisms. However, the damping effectiveness of TMD was more sensitive to wind attack angles and seismic input

characteristics than PD, and TMD only worked effectively within a narrow resonance frequency band. PD, on the other hand, displayed more stable vibration reduction effects that were less sensitive to changes in parameters under different types of seismic excitations or wind attack angles. This makes PD a preferred option in practical engineering designs, as they exhibit a small amplitude of vibration and lower sensitivity to different parameters.

Tests conducted in an aerodynamic tunnel with aeroelasticity also demonstrated that PD performance was typically better than TMD in various mass ratio cases. The application of PD dampers may contribute to favourable and stable dynamic behaviour of primary structures in the field of civil engineering. The systematic experimental studies and damping mechanisms investigated for these two devices under different dynamic loads are a step forwards promoting passive PD-based control technologies. However, further theoretical and numerical comparative analyses of TMD and PD are still being investigated.

Since 1980, the idea of using a Tuned Liquid Damper (TLD) to reduce vibrations in civil and marine engineering structures has been developed and described. The application of a rectangular container filled with two non-mixing liquids to damp the response through interface motion was initially proposed by Bauer [33]. Welt and Modi [34] implemented Tuned Liquid Dampers (TLDs) in building structures with the objective of diminishing the overall response during severe weather conditions like strong winds and seismic activities such as earthquakes. Hayama [35] investigated the behaviour of the liquid in the container and the effectiveness of TLD. Scientists suggested the U-shaped Tuned Liquid Column Damper (TLCD) filled with liquid (usually water) and has a controlled valve, as an extension of TLD. Through the mobility of the liquid inside the container, which balances off external forces, TLCD can decrease structural vibrations. The damping effect of TLCD is produced by a hydraulic pressure drop of the liquid due to the opening installed inside the container. The use of TLCD in engineering structures was first proposed and studied by Sakai and Takeda [36].

Research on the impact of PD and TLD on vibration reduction is being conducted separately, but there is a lack of comparisons between them. Previous studies have focused mainly on the damping effect of PD or on the comparison between PD and TMD. The authors of [37] propose the use of a specific TLCD, which consists of both liquid

and grains (Fig. 1.9). Such an approach allows for the extension of the functionality of the device, which cannot be observed when they are used separately. Numerous numerical and experimental research have been carried out, demonstrating the high effectiveness of vibration damping in structures such as high-rise buildings.

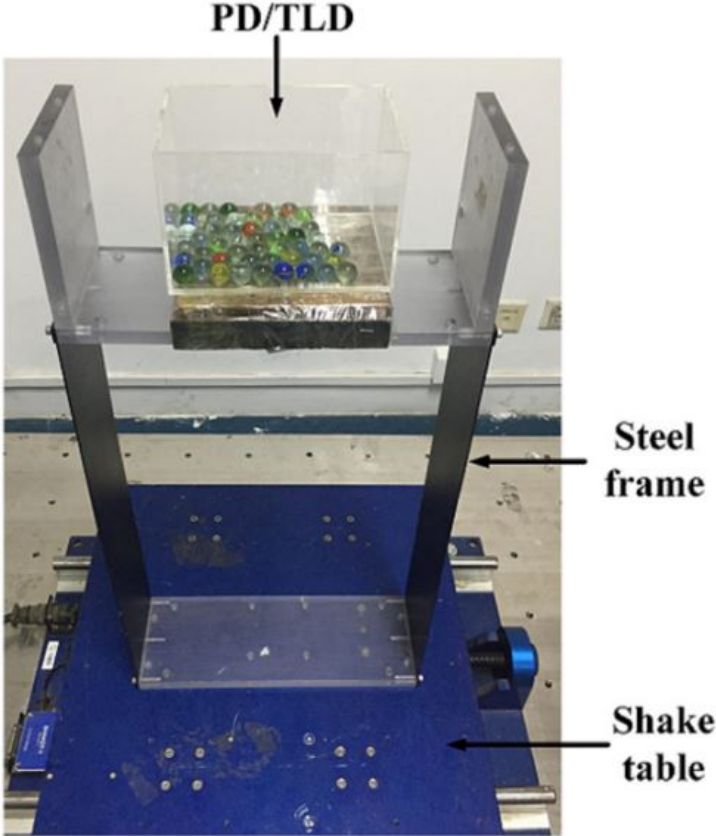


Figure 1.9: The prototype of Tuned Liquid Column Damper [37]

The paper [38] explores an interesting subject of Particles Impact Damper functioning as a double pendulum striking element, referred to as a Double Pendulum Impact Damper (DPID) (Fig. 1.10). DPID consists of two pendulums connected in series. The first pendulum is attached to the structure while the second pendulum is attached to the first one. This type of damper is designed to have different natural frequencies, allowing for effective vibration damping over a wide range of frequencies. During vibration, the Double Pendulum Impact Damper responds to the movement of the structure by oscillating. It absorbs the kinetic energy of the structure, which is then dissipated in the form of heat. This reduces the amplitude of vibrations, preventing damage to the structure from excessive movement. The authors found that DPID is highly effective in reducing vibrations of slender elements and conducted experiments

considering various excitation rules and DPID parameters.

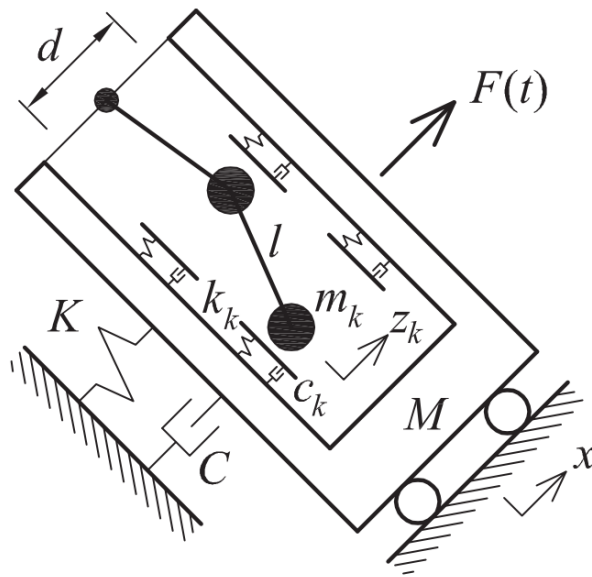


Figure 1.10: Scheme of the Double Pendulum Impact Damper [38]

Previous studies on the use of PIDs in dynamic systems suggested that altering their damping properties could only be accomplished through passive methods such as modifying the container size, grain mass, particle material, or shape. However, the author of the dissertation aimed to enhance traditional PIDs by introducing the Tuned Particles Impact Damper (TPID) [39]. The proposed adaptive-passive system allows the user to actively change the damping properties, as depicted in Fig. 1.11. This constitutes an improvement over classical passive damping strategies, as adaptive-passive methods have been shown to be more effective in controlling vibrations.

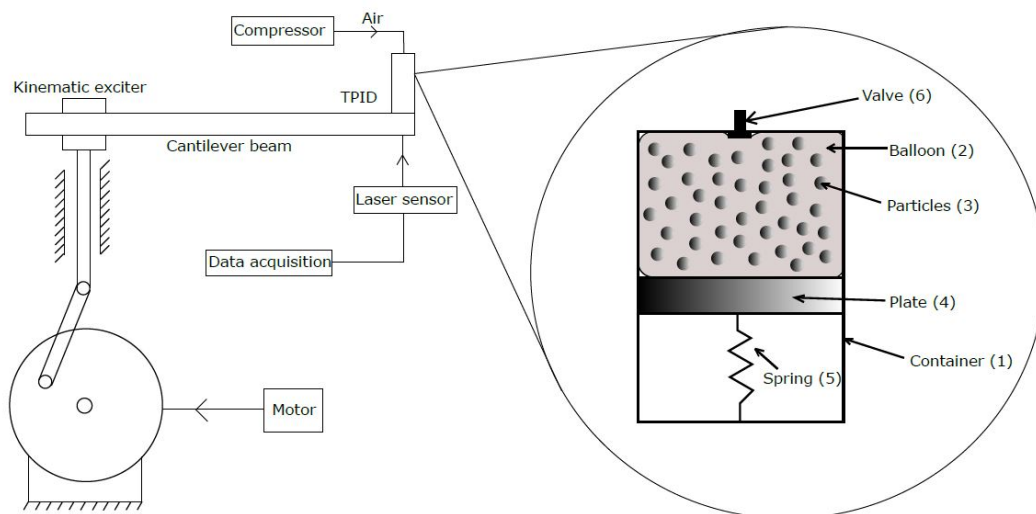


Figure 1.11: Scheme of the Tuned Particles Impact Damper [40]

The TPID as a novel device that can be attached to various mechanical systems to adjust their dynamic characteristics and minimize their mechanical vibrations. The considered TPID prototype has a container with a varying volume range (0.2 to 0.79 [dm<sup>3</sup>]), controlled by an inner balloon. The balloon initially holds loose granular material and acts as a concentrated mass. Discs and springs limit the container's minimum volume, and the balloon has a valve for connecting an external pump. Increasing the pressure inside the balloon results in the expansion of the container's volume, which is a novel method for adaptive-passive control of the system. The TPID is also favoured for its simple design and eco-friendliness.

The proposed device presented in Fig. 1.11 should be treated as starting point for research on real-time controllable PID dampers and offers a preliminary evaluation of their efficiency. However, it is important to emphasize that the described construction is patented [41] but the experimental and numerical studies reported in [40] do not constitute the main part of the dissertation.

### **1.2.3 Applications of the PID dampers**

Particle Impact Dampers have a wide range of applications in mechanical engineering, including some practical and noteworthy examples of their application presented below. The transmission system's vibrations can have an adverse effect on the machine's performance and durability. Addressing this problem is crucial for ensuring a seamless and efficient operation. To minimize the machine transmission system's vibrations, techniques such as balancing, dampening, and decoupling can be utilized. By controlling the transmission vibrations, the stability, durability, and efficiency of the machinery can be improved. One example of using granular dampers for reducing vibrations in centrifugal gear transmissions [42, 43]. This is accomplished by inserting tightly packed loose granular material into specifically designed holes in the gears, as shown in Figure 1.12. The reliability of particle impact dampers has been proven through comparisons between actual system responses and numerical simulations based on the Discrete Element Method.

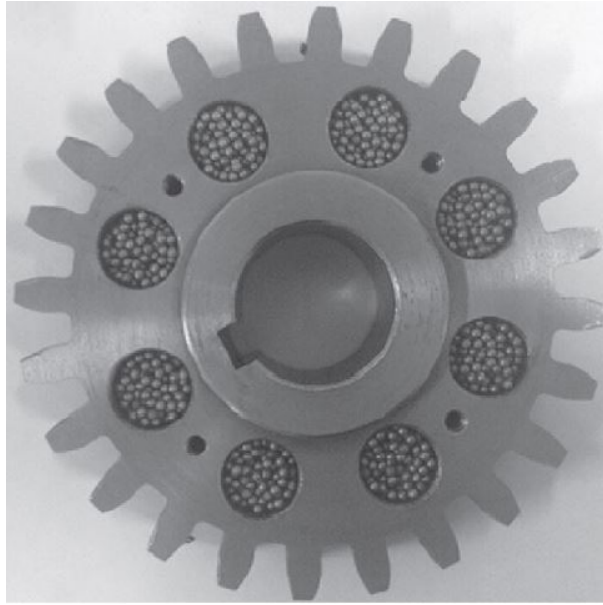


Figure 1.12: The prototype of the gear with PID damper [42]

The study described in [42] involved the implementation of a Particle Damper in order to reduce vibrations in a gearbox. The researchers carried out both theoretical analysis and experimental testing to investigate how the filling ratio of particles affected the reduction of vibrations under different operating conditions. The results showed that the damping effect was greatly influenced by the filling ratio of particles, with a more pronounced effect observed as particle velocity increased. However, once the rotational speed surpassed a certain critical value, the damping effect of particles decreased sharply due to the centrifugal force becoming too large. Therefore, in the case of the tested gearbox system, the smallest structural response and the best particle damping effect were observed when the particle filling ratio was 88 %. To effectively apply particle damping in gearboxes, it is crucial to consider rotational speed, which has a significant impact on the effectiveness of the damper.

An interesting approach is presented in [44], where oscillations in sawing machines negatively affecting the precision and quality of cuts are reduced by the implementation of the MUID dampers (Fig. 1.13). Causes of saw oscillations include improper blade tension, worn or damaged guide bearings, and an unbalanced or dull blade. Excessive saw oscillations can lead to increased wear and tear on the saw and its components, resulting in decreased lifespan and higher maintenance costs. Regular monitoring and maintenance of the saw are crucial in preventing oscillations and ensuring accurate and consistent cuts.

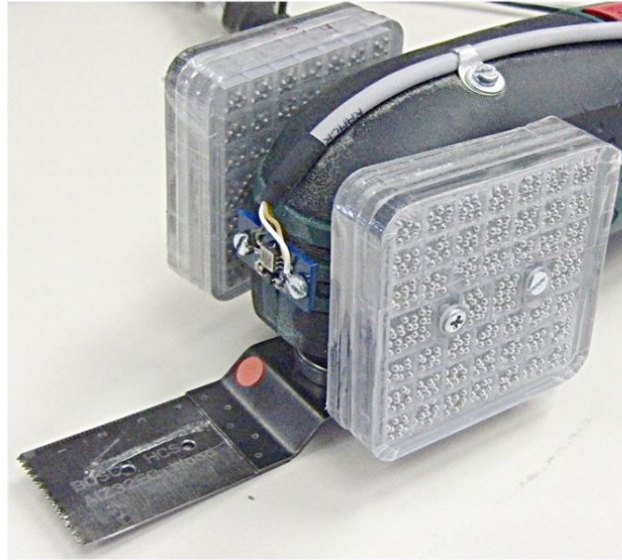


Figure 1.13: Implementation of the MUID into the mechanical saw [44]

The handle of an oscillating saw was subjected to vibration damping experiments using a passive damping method. Granular dampers were attached to the handle to dissipate some of the kinetic energy through inelastic collisions. The size of the granular dampers was chosen to achieve optimal dissipation rates. According to the study, when the geometry of the dampers is modified for the particular vibration amplitude, granular dampers exceed solid mass dampers. This indicates that granular dampers can be used to provide more effective damping while maintaining the weight of the saw, or reduce the weight of the saw while keeping the handle's residual vibration constant. The purpose of the study was to demonstrate the practical application of granular dampers, rather than to find the most effective attenuation method, which would depend on the specific application.

A dump truck is a vehicle created for carrying materials like gravel, sand, and dirt (Fig. 1.14). The cab and seat of a dump truck may be impacted by unpleasant vibrations as a result of rough roads and heavy loads. These vibrations can cause not only discomfort to the driver and passengers but also contribute to increased damage to the truck's components. In order to minimize the negative vibrations and enhance ride comfort, dump trucks may be equipped with shock absorbers, spring isolators, cab mounts, and air suspension systems. These parts help to absorb the road vibrations and decrease their transfer to the cab and seat, resulting in a smoother and more comfortable ride [45].



Figure 1.14: The photograph of the dump truck with PID absorber [45]

A numerical model for reducing vibrations of the cab seat of a dump truck using particle damping is presented in the paper [45]. The Discrete Element Method is utilized to simulate various damper schemes, particle diameters, and particle filling rates to obtain optimal parameters. Tests are used to confirm the modelling results, and the field test yields satisfactory outcomes, where the RMS acceleration of the seat plinth decreases by 26.8 %, 46.8 %, and 38.4 % in both horizontal directions and vertical direction, respectively, at a speed of 40 [km/h]. Human vibration comfort in the cab of a dump truck is also analyzed. After adding damping particles, the comfort duration increases by 85 % at 6.3 [Hz], 20 % at 8 [Hz], and 29.6 % at 20 [Hz] when the velocity reaches 40 [km/h]. As a result, it has been shown that particle damping can effectively decrease the vibration associated with sensitive frequencies in human organs while extending operating comfort.

High-rise buildings and wind turbines are susceptible to vibrations caused by factors such as earthquakes, wind, mechanical equipment, and pedestrian traffic (Fig. 1.15). These vibrations can pose a threat to the building's structure and make it uncomfortable for the people inside. To minimize these impacts, engineers utilize various techniques such as dampers, isolators, and tuned mass dampers. Dampers are designed to absorb energy and reduce vibrations, while isolators disconnect the build-

ing's structure from the sources of vibrations [46]. A tuned mass damper is constructed using a large mass placed inside the building that operates in opposition to the building's vibrations in order to counteract them. By utilizing these techniques, engineers can reduce the effects of vibrations on high-rise buildings, ensuring the safety and comfort of people inside. The use of Particles Impact Dampers (PIDs) is a possibility for large structures, like high-rise buildings, which often face seismic vibrations and heavy dynamic loads. Research on vibration reduction in these types of structures using PID dampers can be found in the references [46, 31, 47].

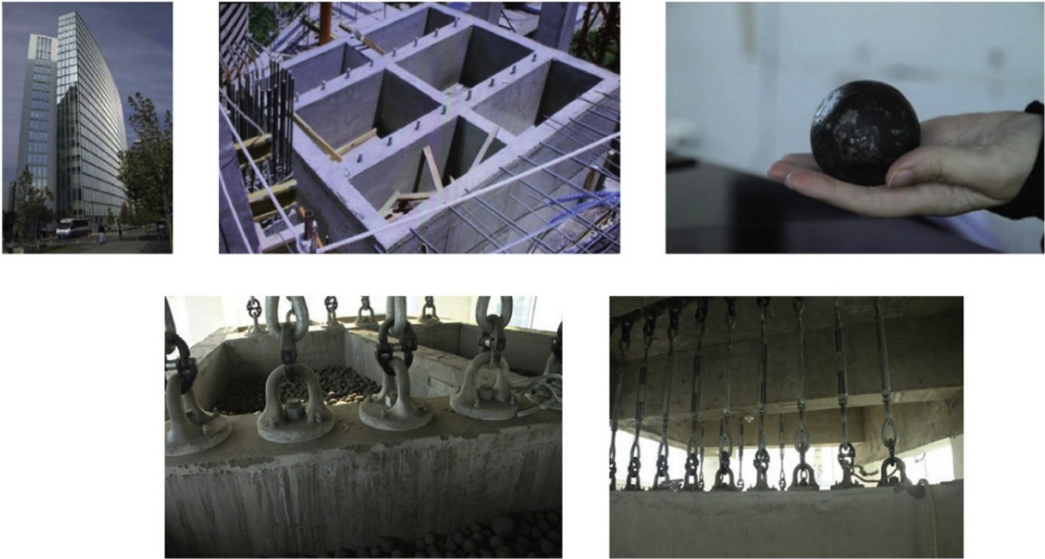


Figure 1.15: Examples of the high-rise building with PID dampers [46]

The study in [46] focuses on the evaluation of the effectiveness of particle dampers with buffering material in controlling the vibrations of structures with multiple degrees of freedom under dynamic loads. It has been observed that the mass ratio of particles is important for effective momentum transfer from the primary system to particles with better vibration damping. The particle damper system with buffering material performs well in reducing structural responses under both random excitations and seismic shocks, with higher efficiency in the case of random excitations. The reduction of responses includes acceleration, displacement, and Root Means Square (RMS) displacement, where the effectiveness of reducing RMS responses is the highest. An experiment on a shake table showed that the particle damper with buffering material is more effective in controlling vibrations than conventional dampers. However, the exact reasons for the increased effectiveness of control require further investigation. The

research takes into account all significant forces of interaction between particles and container walls, including friction, gravitational forces, and inclined impacts, using discrete particle modelling methods. Drawing upon both experimental and analytical findings, it can be inferred that appropriately engineered particle dampers, in combination with buffering materials, can proficiently mitigate the response of primary systems featuring multiple degrees of freedom that possess limited damping. Furthermore, this damping method achieves notable effectiveness while introducing only a negligible increase in mass load, proving its efficacy across diverse load conditions.

Vibrations are a significant factor in the aerospace industry and require careful attention during the design and operation of aircraft. These vibrations can have a negative impact on the aircraft's performance, comfort, and safety of passengers. They are caused by a variety of factors, such as engine operation, aerodynamic forces, and the partially damaged structure of the aircraft. Aerospace engineers involve a range of techniques to prevent and control vibrations, including structural changes, passive damping systems, and active control systems. Passive damping systems, like viscoelastic materials or tuned mass dampers, help to reduce vibrations, while active control systems, such as control surfaces or actuators, actively counteract vibrations in real-time.

It is essential to understand and manage vibrations in aerospace engineering, especially in the electric Printed Circuit Board (PCB) presented in Fig. 1.16 to ensure the safe and efficient operation of aircraft. Precise prediction and analysis of vibrations during the design phase are crucial to minimizing the risk of vibration-related problems during flight.

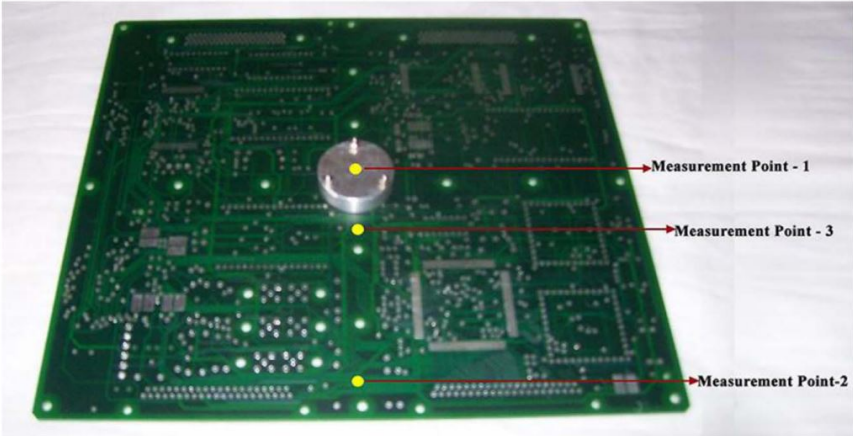


Figure 1.16: Application of the PID damper for Printed Circuit Board [48]

Aerospace engineering is an area where PID dampers are particularly popular. According to [48], PIDs can be used to reduce vibrations in highly sensitive electrical circuits on the Printed Circuit Board (PCB). Damping of the vibrations in Printed Circuit Boards is crucial because excessive vibrations can result in damage or malfunction of both the PCB and the components such as transistors, capacitors and integrated circuits. These vibrations can generate stress causing cracks, breakages, or loose connections which then lead to decreased reliability and an increased risk of failure in the electronic system. Furthermore, vibrations can generate electrical noise in signals, negatively impacting the performance of the electronic system. By reducing vibrations through damping, the reliability and performance of the electronic system can be enhanced and the chance of failure reduced. As a result, considering damping is an important aspect in the design of PCBs for ensuring reliable and efficient electronic systems.

The PID dampers can play an additional role in energy harvesting (Fig. 1.17) [49]. Energy harvesters are equipment that gathers and transforms available energy sources into usable electrical energy [50]. These devices are utilized in numerous fields, including supplying energy to low-power electronics like sensors and wearable technology, as well as serving as a substitute energy source for isolated systems. Energy harvesters are gaining more recognition due to their ability to reduce reliance on conventional energy sources and decrease carbon emissions [51, 52].

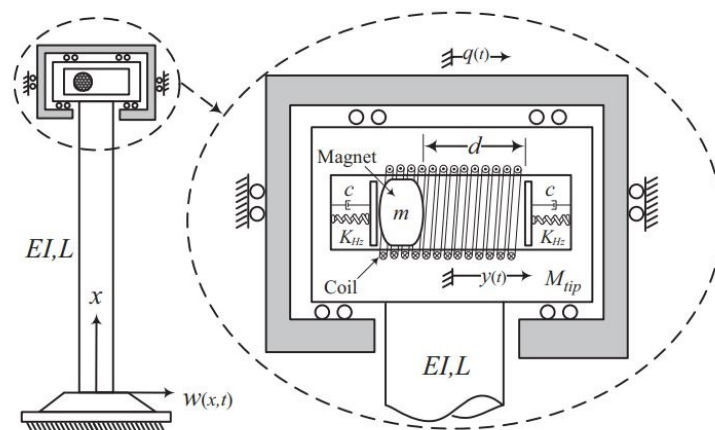


Figure 1.17: Scheme of the PID energy harvester [49]

In the aforementioned energy harvester [49], a moving magnet replaces the traditional grains. First of all, both the classical PID and the colliding magnet with the con-

tainer walls operate in the same manner, retaining the equivalent damping properties. Secondly, the device can be improved with an extra feature called energy harvesting due to the magnet's motion inside the coils. Finding the parameters at which the best operating conditions exist for both vibration damping and energy harvesting makes the analysis of the problem challenging. Research revealed that magnetic shock absorbers can convert more than 33 % of kinetic energy into electrical energy. To improve the energy behaviour and vibration of the magnetic shock absorber system, the impact of changing load resistance and coupling coefficient was studied. The study found that changing only the load resistance can increase damping efficiency by over 27.6 %. Additionally, increasing the gap size at a constant load resistance can increase the average collected power and damping efficiency. When the coupling coefficients are sufficiently large, increasing the gap size at constant coupling coefficient values slowly increases the average power. An interesting aspect, not discussed in the manuscript [49], is the possibility of using an electromagnetic field to influence the movement of the magnet in the container. Such an approach would allow for introducing an additional case to modify the form of collisions between elements, which is important for the most effective vibration damping.

### **1.3 Objectives and plan of the thesis**

The objectives of the Ph.D. thesis can be divided into three groups related to:

1. Designing an effective prototype of the Adaptive Tuned Particle Impact Damper (ATPID) and conducting experimental research to determine its dynamic characteristics and validate the numerical model.
2. Proposing a numerical model of the ATPID damper that accurately reflects physical phenomena and serves as a basis for the development of a predictive control algorithm.
3. Development of a predictive control algorithm that can determine the optimal damper height under various dynamic excitations.

The first objective of the thesis involves proposing an innovative design for the Adaptive Tuned Particle Impact Damper (ATPID). This design modifies the classic PID damper by adding an electric motor and a suitable mechanical system to the upper

wall of the damper. This enables dynamic adjustments of the damper volume and enables control of the particle movement. The electric motor will be connected to a power supply and real-time controller. The damper will be attached to the free end of a cantilever beam, which serves as the main component of the test stand. The beam will be subjected to various kinetic excitations such as harmonic motions with different amplitudes and frequencies. Measurements of displacements and accelerations of the beam free end will be made to assess the performance of the ATPID damper. Additionally, tests will be performed to determine the damping characteristics of the absorber during free vibrations caused by initial beam deflections. These tests will be used to validate the numerical model, which will be described in the later chapter of the thesis.

The second objective focuses on developing a numerical model for the ATPID damper and test stand. A simplified model will be proposed to describe the non-linear viscoelastic collisions of the grain with the damper walls. This model will reflect the response of the system to each type of excitation used in the experimental studies. The possibility of proposing various functions describing the real-time change of the damper height. The parameters will be identified and the model will be validated using experimental results. A sensitivity analysis of the system will be performed to provide the damper's operating principle and determine the criteria for optimal particle movement and maximal damping effectiveness. The process of parametric optimization of the system will be also carried out. An energy analysis will be conducted to describe the influence of grain-wall collisions on the movement and dynamic disturbances of the entire structure.

The third objective is to propose and develop a predictive control algorithm for the ATPID damper. Taking into account the various excitations affecting real mechanical systems, it is important to examine the possibilities of controlling the innovative damper in order to provide optimal adaptation to existing operating conditions. An algorithm based on criteria determined from the sensitivity analysis of the numerical model will be proposed. Further, a series of numerical tests will be carried out to determine if the predicted damper height for a given excitation is close to optimal. The effectiveness of the method will be analysed for different combinations of parameters that could vary in real conditions.

## Chapter 2

# Adaptive Tuned Particle Impact Damper - the prototype and experimental studies

Popular granular vibration attenuators are devices that introduce additional damping to a system. The literature review concerning PID dampers primarily focuses on passive damping strategies. The vibrations of structures are damped by loose materials and can be adjusted mainly by the grain volume ratio, granular material mass, or its material properties. While it has been demonstrated that PIDs are comparable to other damping techniques, granular dampers have not been used as part of adaptive damping systems until now. The dynamic characteristics of such structures are influenced by several factors, with the key ones including the dimensions, configuration, and capacity of the container, the proportion of granular material filling, and the attributes of the individual grains, encompassing density, shape, and surface.

Previous investigations into the implementation of Particle Impact Dampers (PIDs) in dynamic systems have operated under the assumption that modifying damping properties can solely be accomplished by making passive modifications to the parameters mentioned above. Considering the advantages of adaptive passive damping methods over traditional passive strategies, the author aims to improve classical PIDs by introducing the Adaptive Tuned Particle Impact Damper that enables the user to tune the damping properties.

## 2.1 The concept and design of the ATPID damper

The classical Particle Impact Damper design consists of a container filled with granular material. External excitations applied to the attached mechanical system result in particle movements and impacts with the container walls, thus reducing the amplitudes of vibrations. The damper volume is a main factor that affects its damping effectiveness. In order to enhance the efficiency of damping, the author aims to develop an Adaptive Tuned Particle Impact Damper (ATPID) that can dynamically adjust its container height (as depicted in Fig. 2.1) during vibration mitigation process.

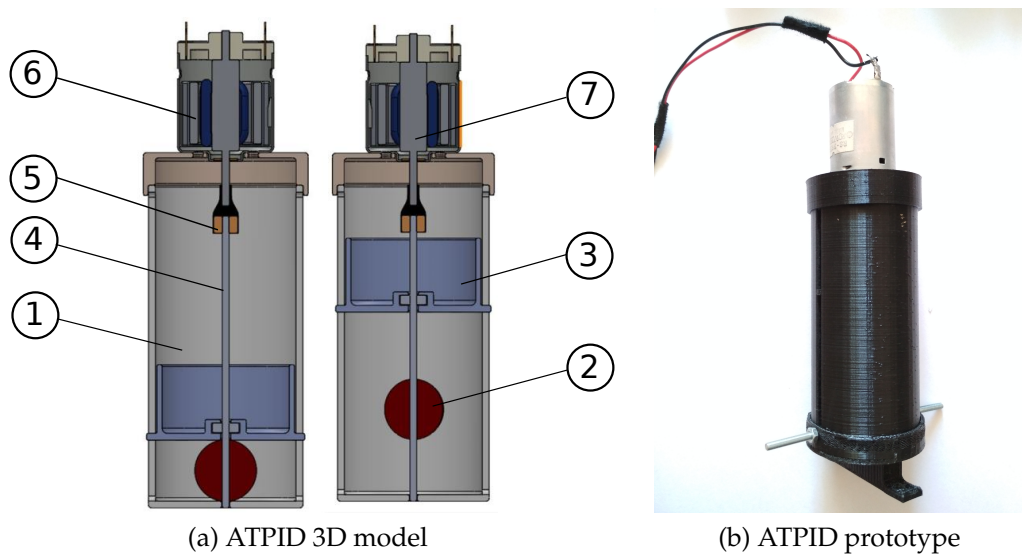


Figure 2.1: ATPID model and prototype

A single-grain system is often used to describe PID operations, and the proposed concept also uses this approach. Figs. 2.1a and 2.1b show the 3D model and prototype of the ATPID damper, respectively. The considered ATPID absorber consists of the cylindrical container (1) containing a single grain (2) made of the Polylactide (PLA), a moveable plate (3) joined by screw connections (4) and clutch (5) with an electric engine (6). The rotation of the engine shaft (7) is transformed into the linear movement of the ceiling in a vertical direction. A simple electromechanical control system can change the direction and speed of the upper damper wall's movement. This method enables the real-time volume modification of the particle's chamber as well as dynamic tuning of the distance between the damper lower (floor) and higher (ceiling) walls. The damper container was made with the use of 3D printer from PLA material. The Ender 3 printer, shown in Fig. 2.2, was applied for this purpose.

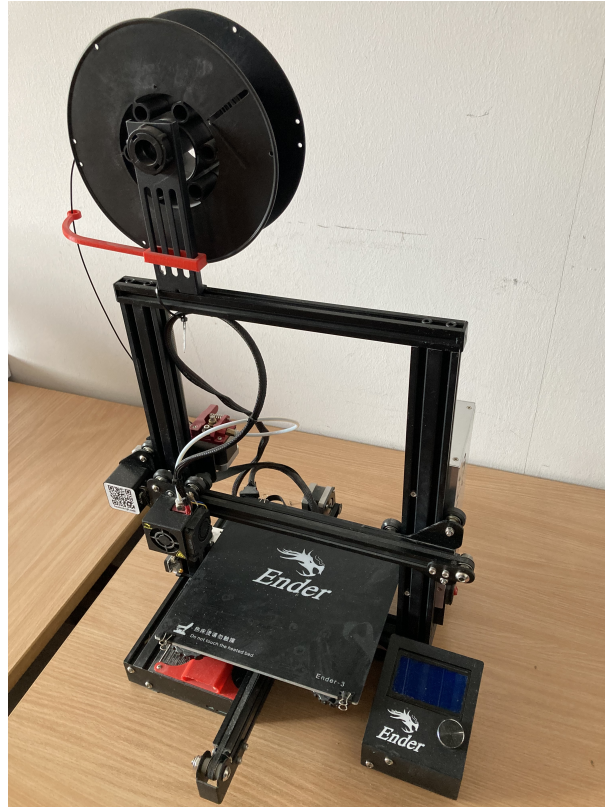


Figure 2.2: The 3D printer used in the process of the ATPID prototyping

3D printing methods refer to a range of technologies that allow to create 3D objects based on digital designs. In this case, the Fused Deposition Modelling (FDM) method was utilized, which involves constructing objects by depositing soluble synthetic material in the form of thin threads layer by layer. The threads are then melted and fused together to produce a robust structure. 3D printing enables the production of objects with complex shapes and geometries that are difficult to achieve using traditional manufacturing techniques. This technology is widely applied in diverse fields such as medicine, aerospace, and architecture.

For this specific damper construction, 3D printing was used to manufacture an ax-symmetric container to which the electric motor responsible for controlling the ceiling position was attached. It is worth noting that the entire procedure of constructing the device prototype required skills in modelling systems using CAD software and generating G-code based on a 3D model in Cura software. G-code is a script that is implemented into the 3D printer, which describes the position of the extruder (heating and extruding element of PLA material) at each time interval. As a result, it is possible to observe the final process of printing.

## 2.2 Description of the test stand

The carefully designed laboratory test stand enables investigation of the ATPID damper efficiency in reducing vibrations of the cantilever beam (Fig. 2.3 and Fig. 2.4). The test stand is composed of an electric motor with an eccentric disc (1), a mechanism that transforms rotational motion into linear motion (2), a beam (3), an ATPID damper (4), a data transmission system (5), a control system (6), two inverters (7), a power supply (8), and a data analysis system (9). The displacement of the beam's free end was the quantity that was measured during the experiment. To carry out the experiment, a laser sensor (Omron ZX1-LD300A81), accelerometer (PCB 351B03), measuring cards (Labjack T7-pro and National Instruments NI 9230) and dedicated LABVIEW software were used.

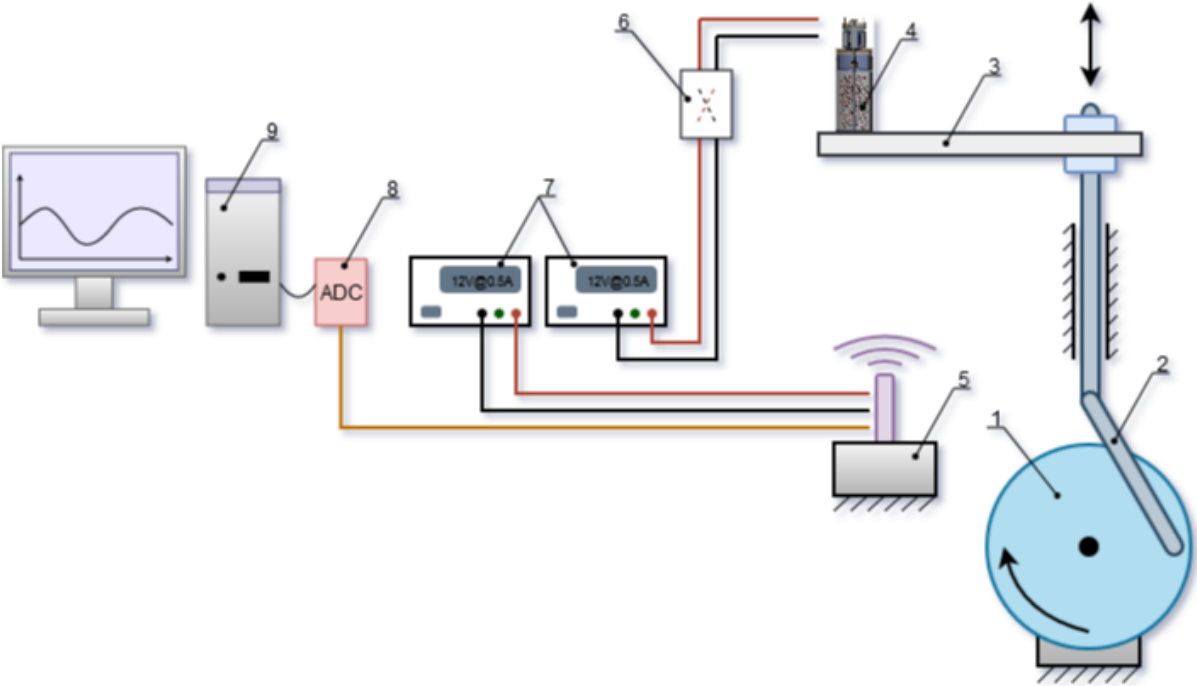


Figure 2.3: Scheme of the experimental test stand

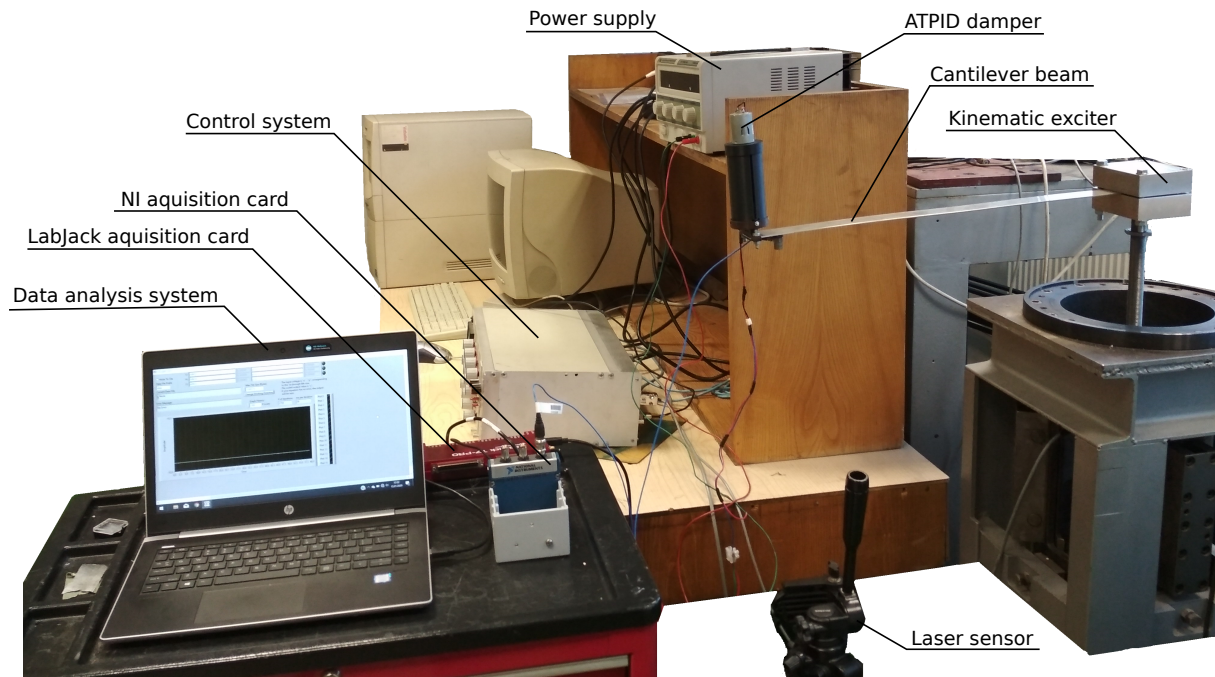


Figure 2.4: Experimental test stand

In the free vibrations test, the cantilever beam was positioned horizontally. For the harmonic vibrations testing, displayed in Fig. 2.4, the horizontal beam was allowed to move in a transverse direction up and down along the vertical axis. An electrically powered motor, equipped with a gear and linear inverter, enabled the operator to manually adjust the excitation frequencies from 0 to 60 [Hz]. Due to the mechanical design of the eccentric discs, the amplitude of excitation varied between  $\pm 5$  [mm] and  $\pm 10$  [mm]. The main focus of the experimental research was the analysis of resonance vibrations, where the damper demonstrated its greatest effectiveness. Both laser sensors and accelerometers were utilized to measure the amplitude and acceleration of the beam tip under various conditions, including changes in excitation amplitude and frequency, grain mass, and damper heights. Detailed modifications to the parameters are described in the next section, which pertains to the research methodology.

A cantilever beam is a basic structure which dynamics will be analyzed to verify the effectiveness of vibration damping achieved by the attached ATPID damper. Therefore, it is necessary to clearly define the geometric parameters of the used beam. All relevant parameters are presented in Fig. 2.5 and in Tab. 2.1.

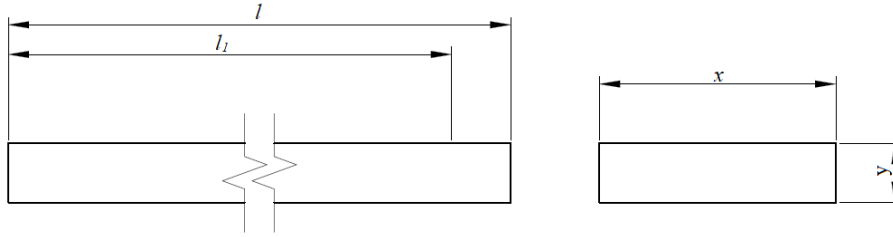
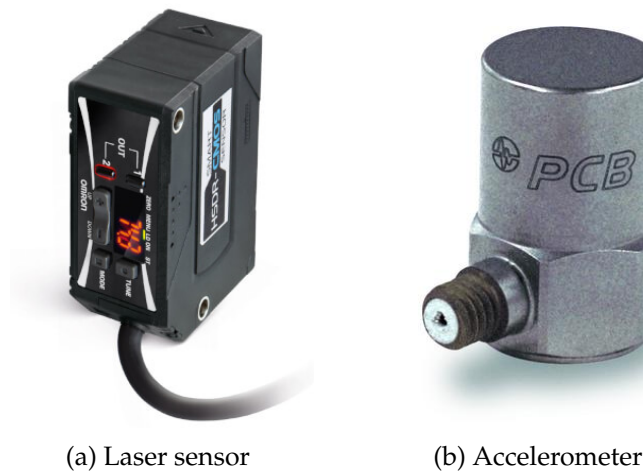


Figure 2.5: Scheme of the experimental cantilever beam

Table 2.1: Basic parameters of the cantilever beam

Symbol	Description	Value	Unit
$m_s$	Beam mass	0.360	[kg]
$y$	Section height	0.008	[m]
$x$	Section width	0.040	[m]
$l$	Beam length	0.450	[m]
$l_1$	Beam attachment point	0.400	[m]

The cantilever beam has a total mass of 0.35 [kg] and its total length is 0.45 [m]. The distance between the place of attachment of the exciter clamp to the point of attachment of the ATPID damper is 0.4 [m]. The beam has a rectangular cross-section 0.04 [m] x 0.008 [m]. Transverse displacement at both the beam's free end (where ATPID damper is attached) and excitation point were measured using an Omron ZX1-LD300A81 laser sensor (Fig. 2.6a) and a PCB 351B03 accelerometer (Fig 2.6b). The laser sensor provided a measurement resolution of at least 20 [ $\mu$ m] at 1 [kHz] sampling frequency, which exceeds the assumed test requirements. The accelerometer was sensitive up to 10 [mV/g], with a measurement range of  $\pm 150$  [g] and a frequency range of 1 to 6000 [Hz].



(a) Laser sensor

(b) Accelerometer

Figure 2.6: Photo of the sensors

The data was collected using National Instruments 9230 and Labjack T7-pro data acquisition cards. The NI-9230 is a device with a 3-Channel Vibration Input Module and an analog input voltage range from -30 [V] to 30 [V]. The three input channels of the NI-9230 can simultaneously measure signals at 12.8 [kS/s] per channel. On the other hand, the Labjack T7-pro has 14 analog input channels, with an input voltage range of  $\pm 10$  [V],  $\pm 1$  [V],  $\pm 0.1$  [V], and  $\pm 0.01$  [V], and a transducer resolution of 16-bit at 100k [samples/s]. The Labjack T7-pro can communicate using various protocols such as USB, Ethernet, and WiFi.

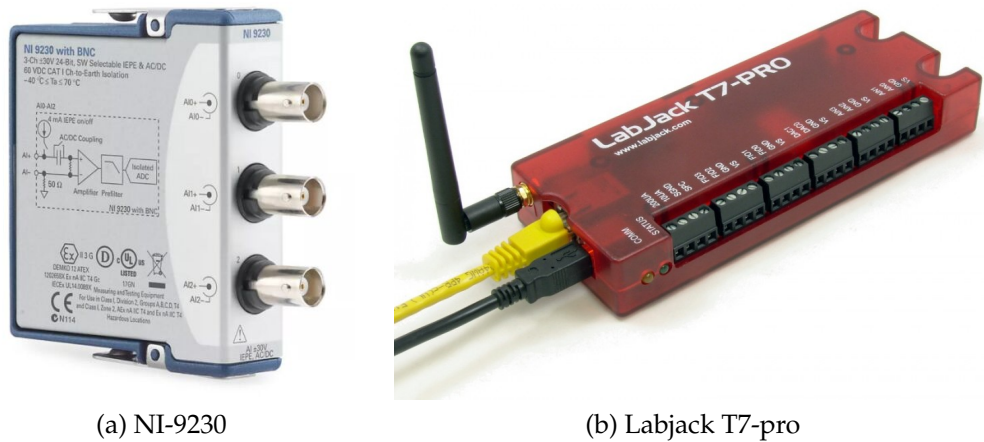


Figure 2.7: Measuring cards used during experimental tests

Two single-channel laboratory power supplies were employed to operate the AT-PID damper engine. The output of each power supply permitted the setting of voltage within the 0 to 30 [V] DC range and also offered the flexibility of establishing a current limit ranging from 0 to 5 [A].

## 2.3 Experimental results

Before beginning the experimental studies, it is essential to establish a correct research methodology. Considering the laboratory equipment and the experimental setup limitations, a research plan was proposed and graphically presented in Fig. 2.8. The scheme outlines the experimental research plan and subsequent numerical analyses that correspond directly to the conducted study. The experimental measurements will be performed for various types of parameters of the excitations. Furthermore, differ-

ent masses of grains will be used inside the ATPID damper and the container will have varying heights.

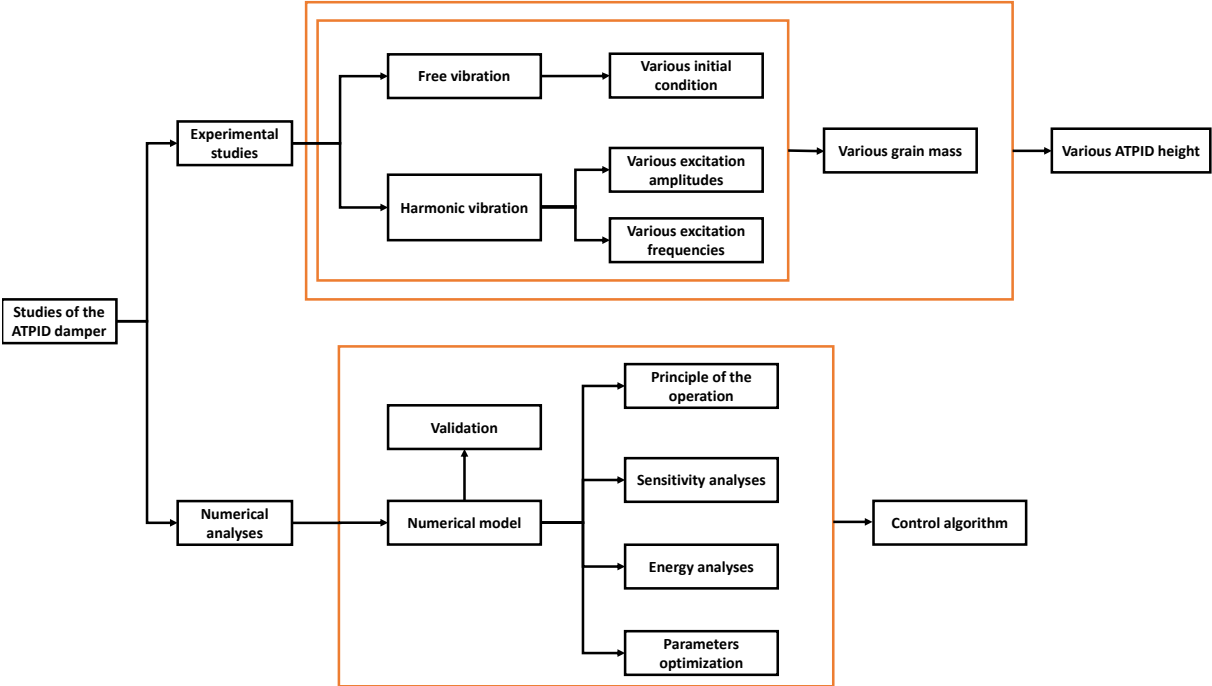


Figure 2.8: Scheme of the experimental and numerical research plan

The experimental study will focus on two types of vibrations: free vibrations of the beam due to initial deflection, and harmonic vibrations resulting from kinematic excitation. For free vibrations, various cases corresponding to different initial beam deflections ranging from 0.1 [m] to 0.3 [m] will be analyzed. In the case of harmonic vibrations, the amplitude of kinematic excitation ( $\pm 5$  [mm] and  $\pm 10$  [mm]) and frequency will be varied to analyze vibrations 'in' and 'out' of resonance. Particles of 5 different masses will be used for all types of vibrations, with the lightest grain having a mass equal to 2.5% of the total system mass (combined mass of the grain and beam), and the heaviest particle having a mass of 30% of the total system mass. Additionally, the height of the damper will be changed to 5 different values for each combination of excitation parameters and grains mass.

In order to conduct holistic analysis of the system response, the experimental research was carried out for 40 different cases of free vibrations and approximately 100 different parameters variations for harmonic vibrations. The most important parts of these studies have been presented to draw the most significant conclusions, ensuring the transparency and readability of the doctoral thesis.

### 2.3.1 Free vibrations

The first type of conducted research was the analysis of free vibrations of a beam for a constant value of initial deflection equal to 0.2 [m]. Grain with a mass equal to 2.5 % of the total system mass ( $M_s$ ) was used, and 5 different values of damper height were assumed, which were set from the beginning of the experiments. The minimum damper height was  $h_1 = 0.017$  [m], which corresponded to the situation where the damper was deactivated, i.e., the grain was blocked and could not move inside the container. The remaining studies referred to cases in which the damper heights were equal:  $h_2 = 0.05$  [m],  $h_3 = 0.1$  [m],  $h_4 = 0.15$  [m], and  $h_5 = 0.2$  [m]. The height  $h_5$  is the maximum damper height due to design limitations. The measurements of the displacement of the beam free end for each of the 5 different damper height variations are presented in Fig. 2.9.

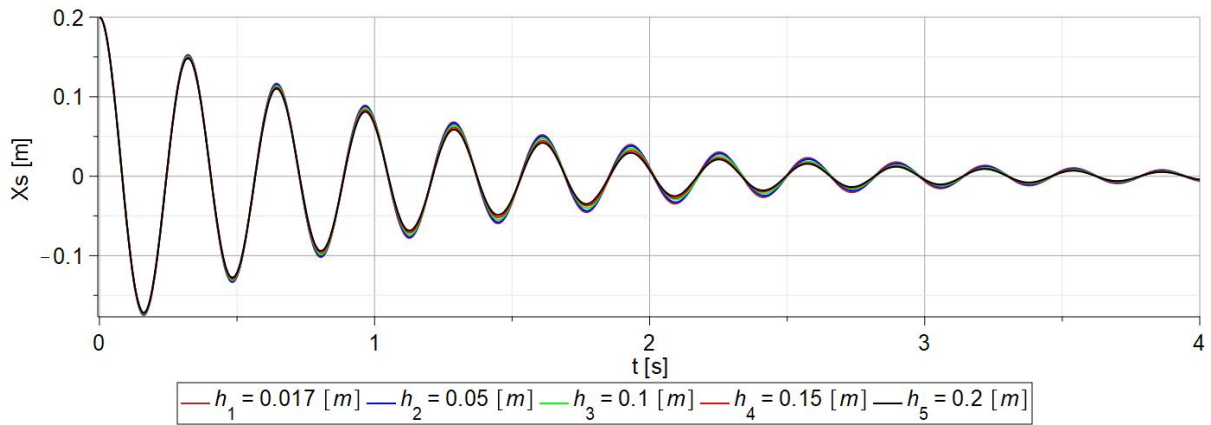


Figure 2.9: Response of the beam for grain mass  $m_g = 0.025M_s$  and for 5 various damper heights  $h_1 \rightarrow h_5$

Upon analyzing the response of the beam (Fig. 2.9), it can be observed that it is similar for each case. Despite the absence of significant differences, a relatively small variance in vibration amplitudes can be noticed. This is due to the motion and collisions of the grain with the walls of the damper. However, due to their small mass, these collisions do not introduce significant disturbances that would allow for significant damping of the system. In order to quantify the small differences in the results, for each case the damping decrement ( $\delta$ ) was determined according to the formula:

$$\delta = \frac{As_n}{As_{n+1}} \quad (2.1)$$

where  $As_n$  is the amplitude of the  $n$ 'th period of vibration system,  $As_{n+1}$  is the amplitude of the next period of system oscillation.

Generally, for a system characterized only by the internal damping of the beam, i.e. for the case  $h_1$ , the damping decrement is a constant value and for the assumed parameters, it takes an approximate value of 1.31. In the remaining cases, the grain moves inside the container, but its motion differs in each subsequent vibration period due to the decreasing vibration amplitudes. These differences are directly related to the various collisions of the particle with the containers walls, which affect the change in vibration amplitude in subsequent periods  $T_i$ . Therefore, for cases  $h_2 \rightarrow h_5$ , the damping decrement changes in each subsequent vibration period. The obtained results are presented in Fig. 2.10

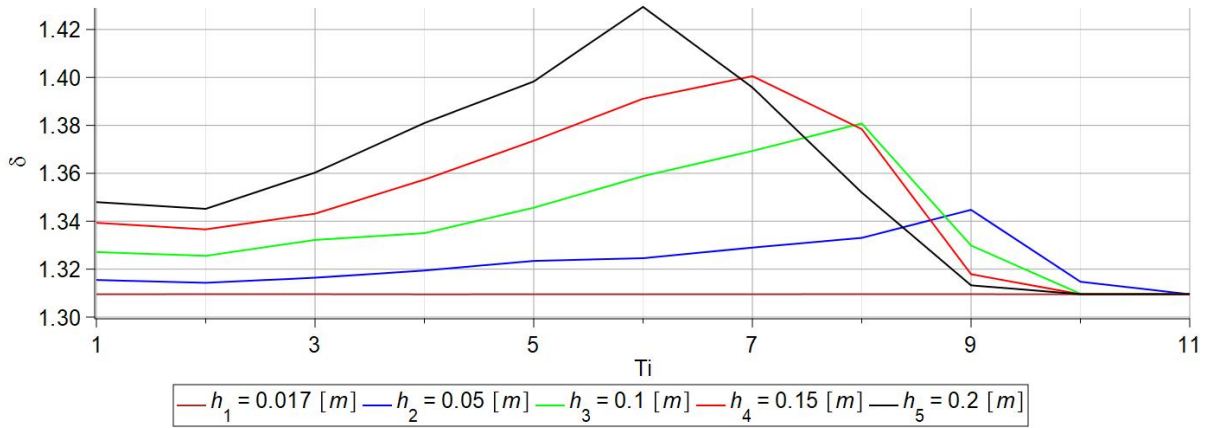


Figure 2.10: Damping decrement of the beam free vibrations for grain mass  $m_g = 0.025M_s$  and for 5 various damper heights  $h_1 \rightarrow h_5$

For the case  $h_1$ , it remains constant at a level of approximately 1.31. In the remaining cases, the damping decrement for each iteration of vibration periods changes, reaching a maximum value of approximately 1.345 for  $h_2$  (for the ninth vibration period), 1.38 for  $h_3$  ( $T_i = 8$ ), 1.4 for  $h_4$  (for  $T_i = 7$ ), and over 1.42 for the case  $h_5$ , where  $T_i = 6$ . These values differ maximally by about 9 % compared to the damping decrement corresponding to the internal damping of the beam. Therefore, the effectiveness of vibration reduction is small for the presented cases. It should be noted that the maximum values are achieved at different vibration periods. It has been observed that the larger damper height corresponds to the greater damping decrement value occurring in the earlier stage of vibration. This means that the impacts of the grain on the top or bottom of the damper introduce the most effective disturbance from the point of

view of vibration damping. A detailed description of the conditions of optimal particle movement will be presented in the further numerical part of the doctoral thesis.

The next step involved conducting similar experimental studies of the free vibrations of the beam for variants in which the mass of the grain amounted to 5 %, 10 %, 20 %, and 30 % of the total system mass. The responses of the system are presented in Figs. 2.11, 2.13, 2.15, and 2.17, respectively. Additionally, the damping decrement was determined for each discussed case of grain mass and damper height, and the results are shown in Figs. 2.12, 2.14, 2.16, and 2.18, respectively.

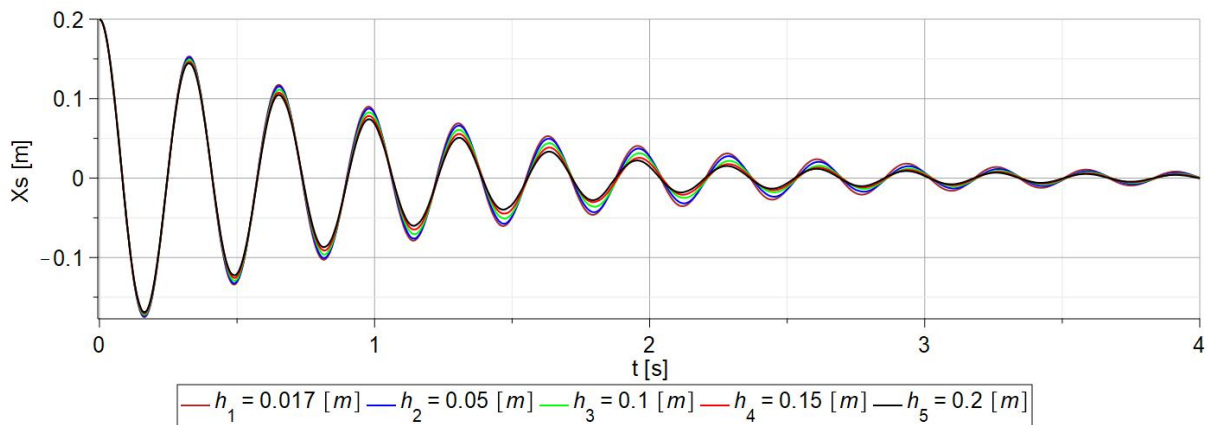


Figure 2.11: Response of the beam for grain mass  $m_g = 0.05M_s$  and for 5 various damper heights  $h_1 \rightarrow h_5$

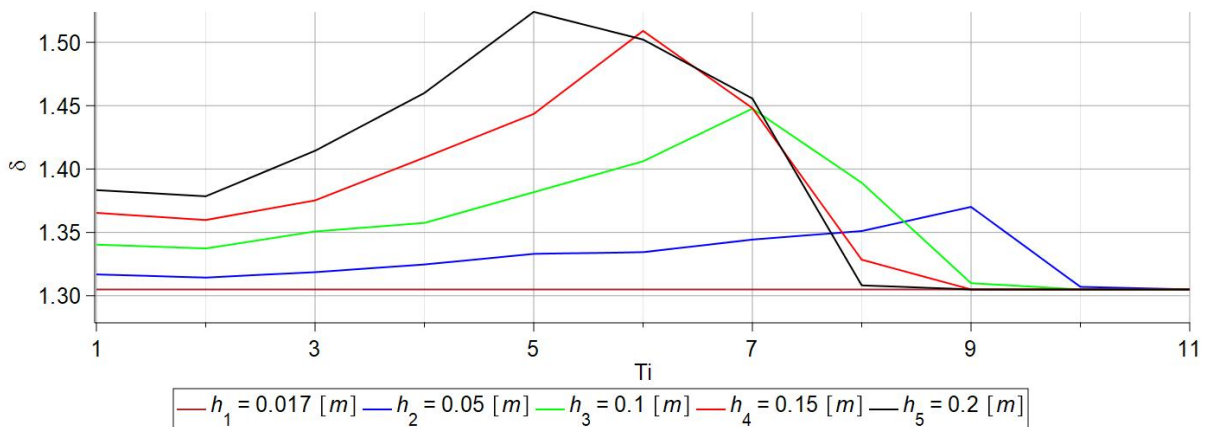


Figure 2.12: Damping decrement of the beam free vibrations for grain mass  $m_g = 0.05M_s$  and for 5 various damper heights  $h_1 \rightarrow h_5$

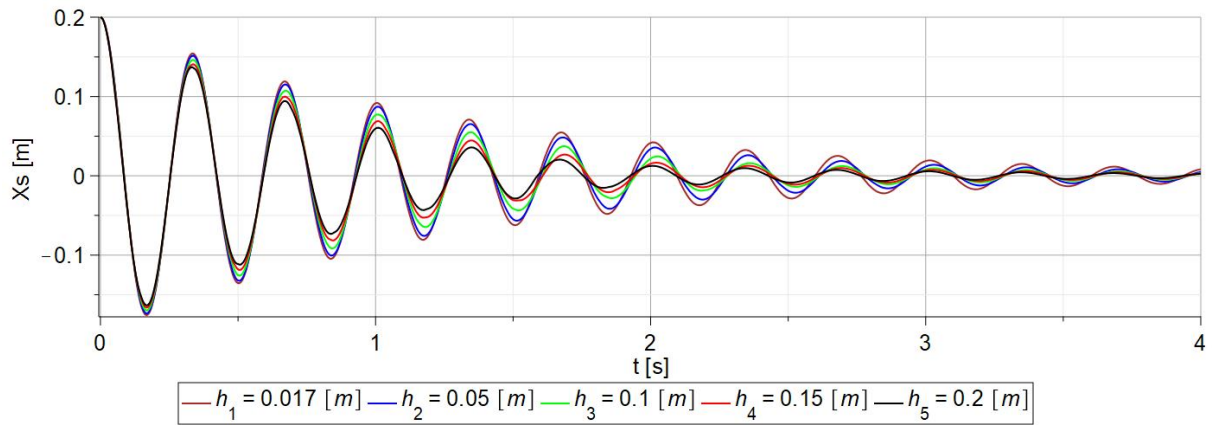


Figure 2.13: Response of the beam for grain mass  $m_g = 0.1 M_s$  and for 5 various damper heights  $h_1 \rightarrow h_5$

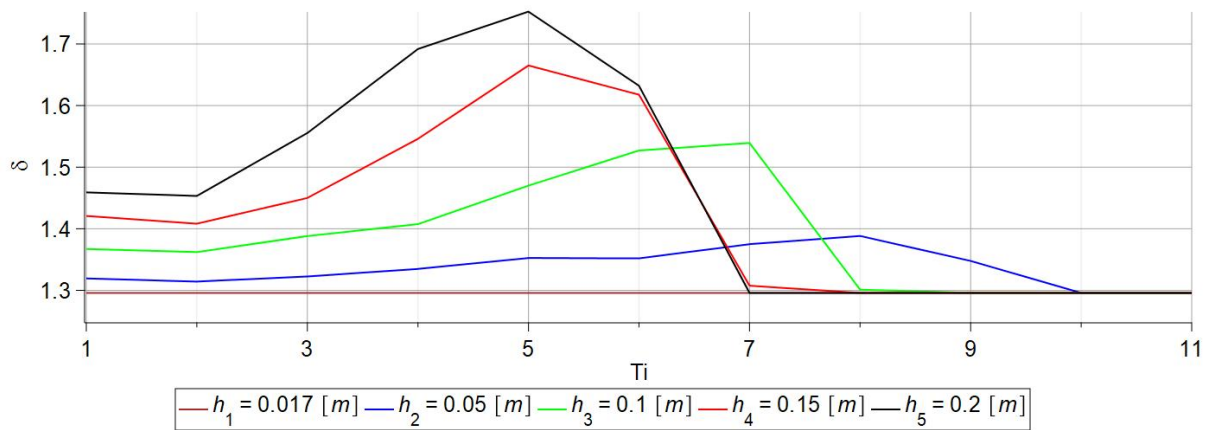


Figure 2.14: Damping decrement of the beam free vibrations for grain mass  $m_g = 0.1 M_s$  and for 5 various damper heights  $h_1 \rightarrow h_5$

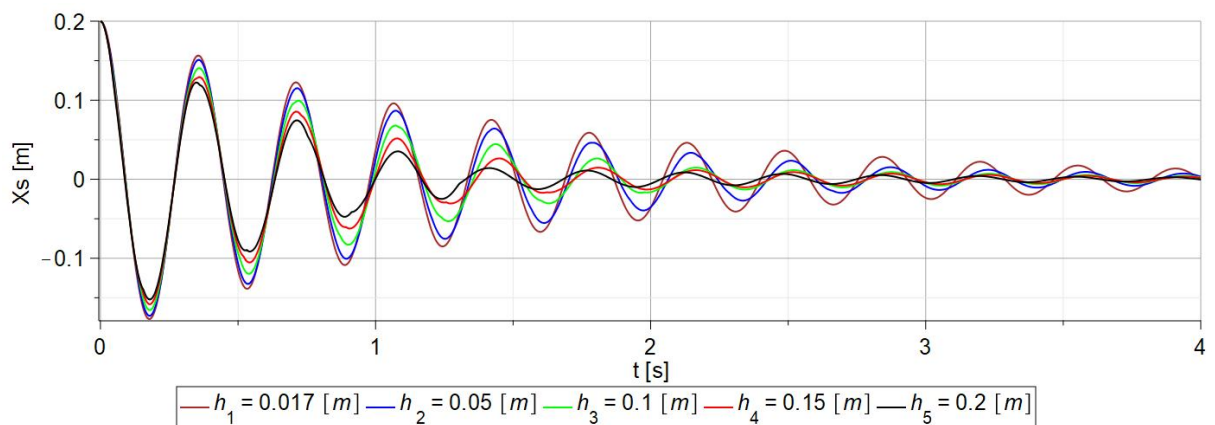


Figure 2.15: Response of the beam for grain mass  $m_g = 0.2 M_s$  and for 5 various damper heights  $h_1 \rightarrow h_5$

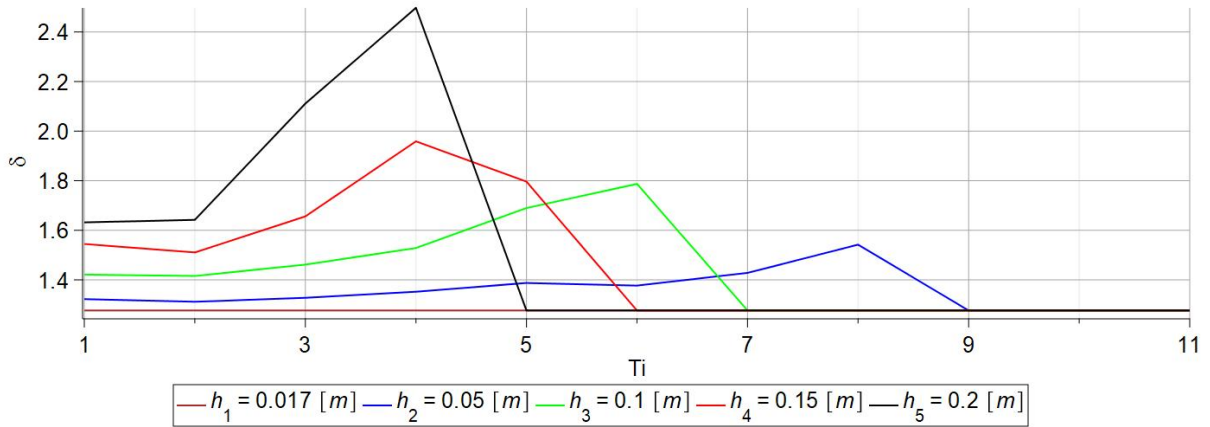


Figure 2.16: Damping decrement of the beam free vibrations for grain mass  $m_g = 0.2M_s$  and for 5 various damper heights  $h_1 \rightarrow h_5$

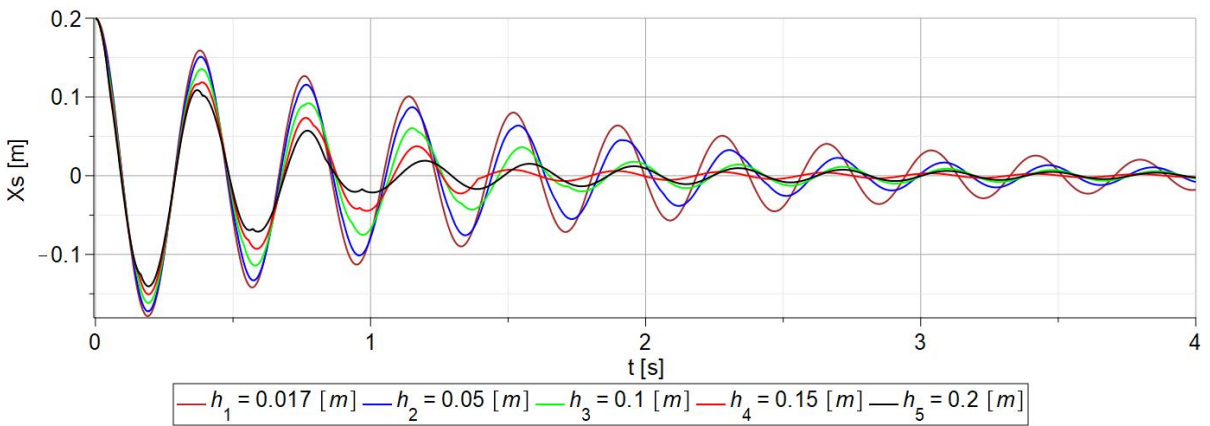


Figure 2.17: Response of the beam for grain mass  $m_g = 0.3M_s$  and for 5 various damper heights  $h_1 \rightarrow h_5$

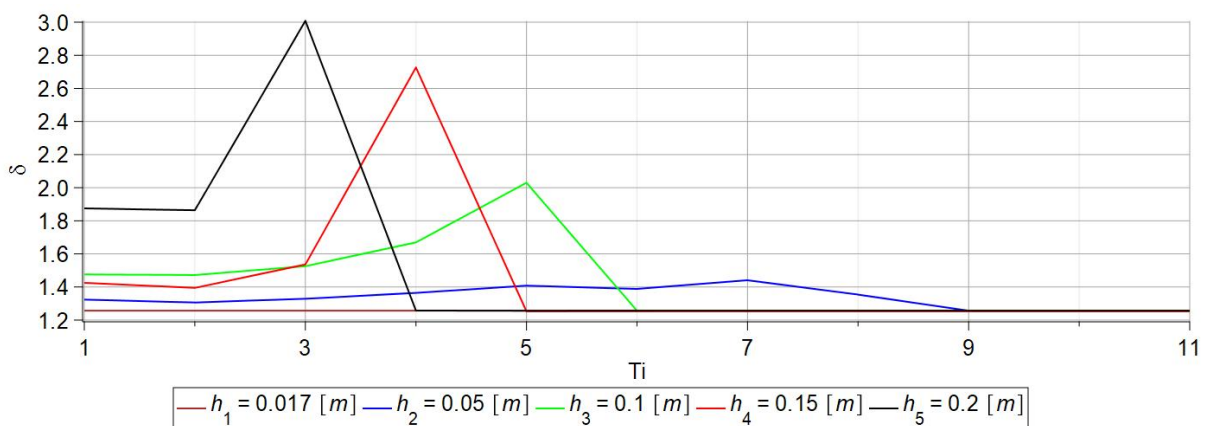


Figure 2.18: Damping decrement of the beam free vibrations for grain mass  $m_g = 0.3M_s$  and for 5 various damper heights  $h_1 \rightarrow h_5$

Analysis of the results allows to observe that using grain of a mass of 5 % of the total system mass to damp free vibrations of the beam is similarly effective as using

a particle of a mass of 2.5 % of  $M_s$ . Fig. 2.11 shows that there are only small differences in the dynamic response of the beam. The maximum damping decrement for  $h_5$  is 16 % higher than the constant decrement value for the  $h_1$  case and it equals approximately 1.52. The maximum decrement values for the remaining cases ( $h_2 \rightarrow h_4$ ) are smaller and are achieved in later vibration periods. However, when the grain mass was sequentially increased to 10 %, 20 %, and 30 %, significant differences in the beam vibration displacement plots were observed, as shown in Figs. 2.13, 2.15, and 2.17. In particular, higher vibration damping is visible in the damping decrement graphs (Figs. 2.14, 2.16 and 2.18). The maximum damping decrement for  $m_g = 0.1M_s$  is about 30 % higher than the minimum value of the decrement for this case (for the height  $h_1$ ) and for  $m_g = 0.2M_s$  and  $m_g = 0.3M_s$ , the maximum damping decrement values exceed 2.4 and 3, respectively, which are almost more than 2 times greater than the value of the minimum decrement (for the height  $h_1$ ). The most effective vibration damping occurs during the initial phase of vibrations, corresponding to the third and fourth vibration periods ( $T_i = 3$  and  $T_i = 4$ ).

To compare the effectiveness of beam vibration damping due to changes in the grain mass, the maximum damping decrement values were compared. From the above results, it is clear that the maximum damping decrement values were consistently achieved for the  $h_5$  case, irrespectively of the grain mass. Therefore, the decrement values for the  $h_5$  case for different grain masses ( $m_{g1} = 0.025M_s \rightarrow m_{g5} = 0.3M_s$ ) were compared and presented in Fig. 2.19.

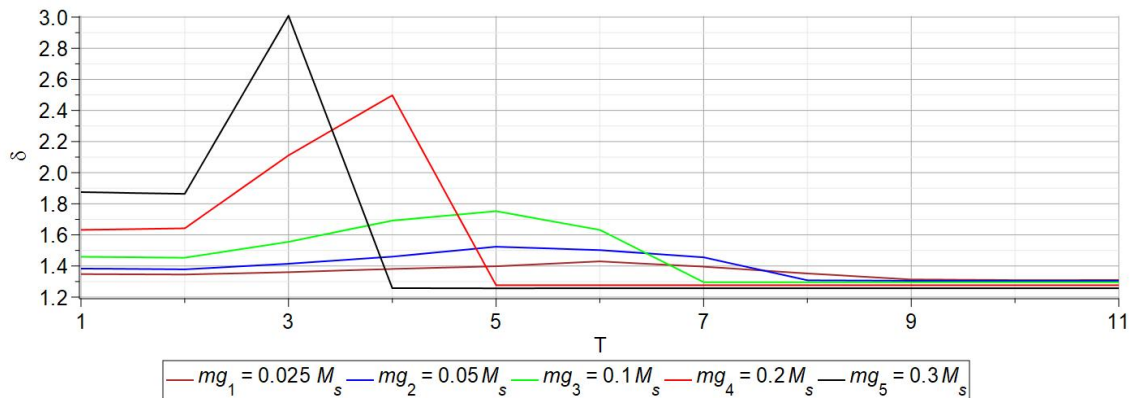


Figure 2.19: Damping decrement of the beam free vibrations for container height  $h_5 = 0.2$  [m] and for 5 various grain mass  $m_{g1} \rightarrow m_{g5}$

The results presented in Fig. 2.19 show that increasing the mass of the grain leads to higher maximum damping decrements in the early stages of vibrations. This indicates that free vibrations are reduced more quickly which is important from a damping point of view. However, it should be noted that using heavier grain can significantly alter the dynamic properties of the structure, making the particle the dominant element of the system. Furthermore, during the design of the damper, the mass of the grain must be chosen appropriately based on the frequency and amplitude. If the system is expected to work at low levels of vibration, it may be difficult to set a very heavy grain in motion, and it may be impossible to achieve additional damping factors. In such cases, the lighter particles can move more effectively within the enclosure, making the ATPID damper more efficient.

In addition, the effect of the initial deflection of the beam (change of the initial potential energy) on the beam response was analyzed for three different grain masses (10 %, 20 %, and 30 % of the total system mass) and for a damper height equal to  $h_5 = 0.2$  [m]. The cases of particle masses representing 2.5 % and 5 % of the system mass were omitted because the results obtained so far indicated relatively low damping effectiveness. The results are presented in Figs. 2.20-2.22.

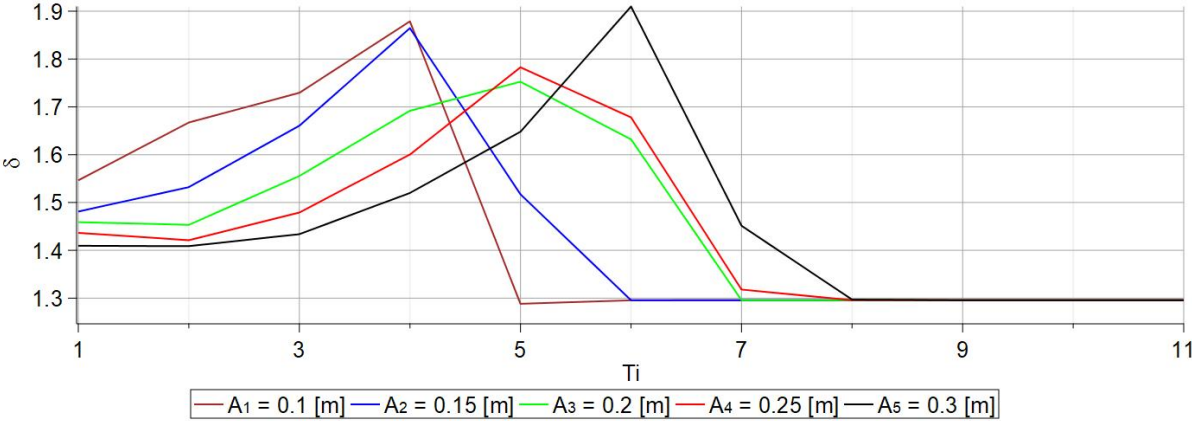


Figure 2.20: Damping decrement of the beam free vibrations for container height  $h_5 = 0.2$  [m], constant grain mass  $m_g = 0.1M_s$  and for 5 various initial beam deflections  $A_1 \rightarrow A_5$

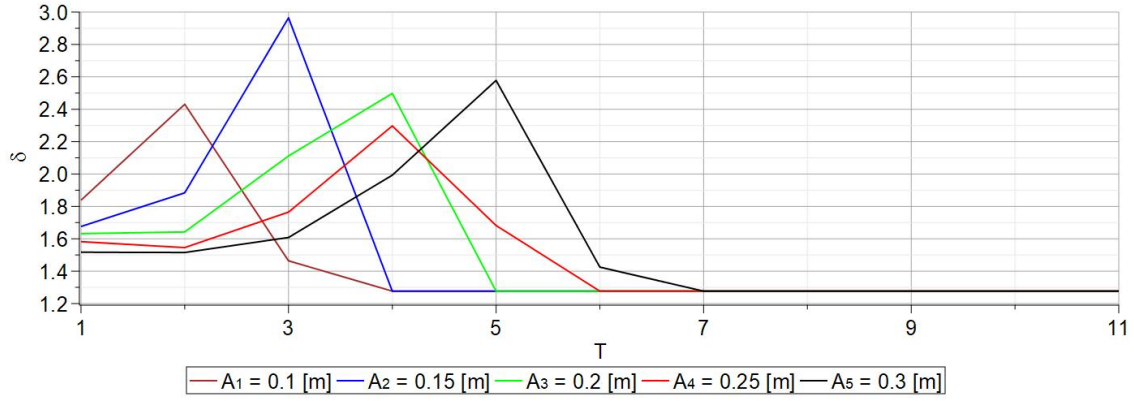


Figure 2.21: Damping decrement of the beam free vibrations for container height  $h_5 = 0.2$  [m], constant grain mass  $m_g = 0.2M_s$  and for 5 various initial beam deflections  $A_1 \rightarrow A_5$

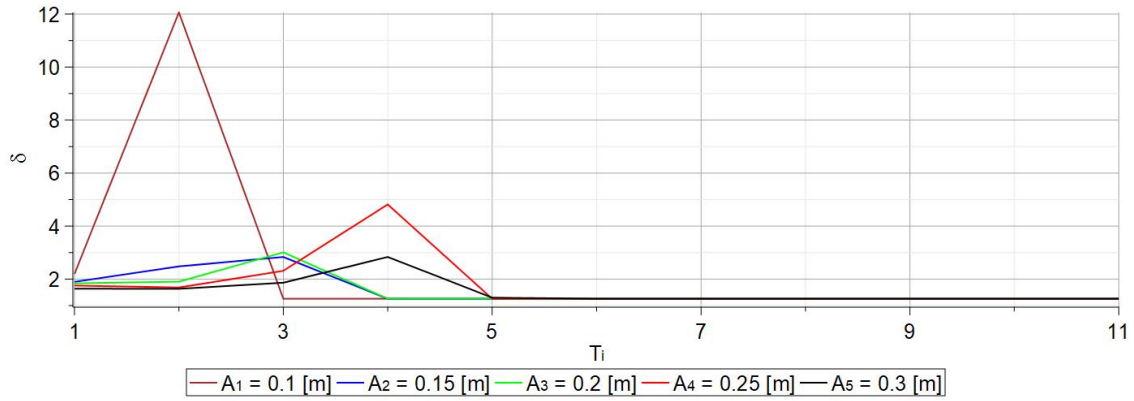


Figure 2.22: Damping decrement of the beam free vibrations for container height  $h_5 = 0.2$  [m], constant grain mass  $m_g = 0.3M_s$  and for 5 various initial beam deflections  $A_1 \rightarrow A_5$

Analysis of the first two figures allows to observe that for all five proposed beam deflection cases, the maximum decrement of damping for the mass  $m_g = 0.1M_s$  and  $m_g = 0.2M_s$  equals approximately 1.8 and 2.5, respectively. The bigger the initial deflection of the beam, the more effective vibration damping occurs in later vibration periods. In Fig. 2.21, it can be observed that the maximum damping decrement for the initial deflection of  $A_2 = 0.15$  [m] is close to 3, which is significantly greater than the maximum values for the other considered cases. A similar, but more visible case, is shown in Fig. 2.22, where the maximum value of the damping decrement for the initial deflection of 0.1 [m] equals 12, which is approximately from 2.5 to 4 times greater than the other maximum damping decrement values. These cases indicate that in order to achieve optimal vibration damping, the movement of the grain inside the encl-

sure must be appropriate, which corresponds to effective impacts of the grain with the container walls and introducing additional damping disturbances into the system. In order to check how the system responds to the specific case described above, the response of the beam for the granular mass  $m_g = 0.3M_s$  is presented in Fig. 2.23, where the damper height was  $h_5 = 0.2$  [m], and the amplitude of the initial deflection is  $A_1 = 0.1$  [m].

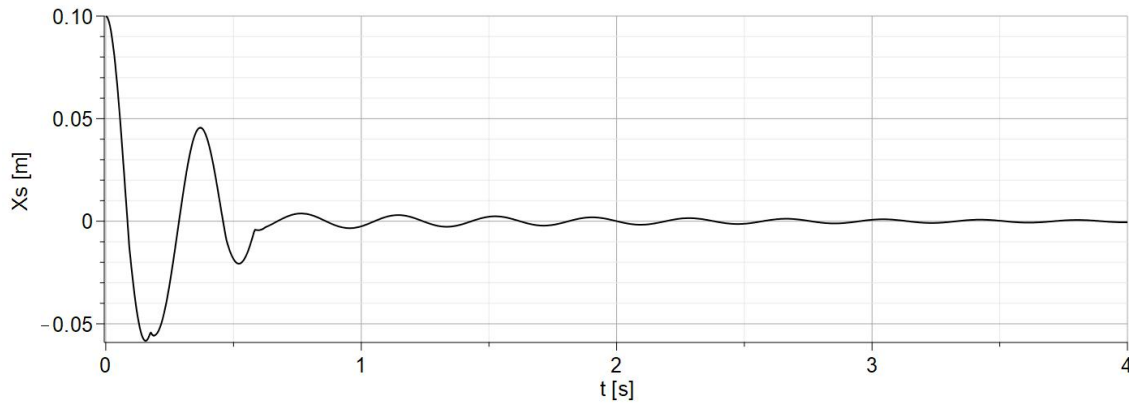


Figure 2.23: Response of the beam for grain mass  $m_g = 0.3M_s$ , damper height  $h_5 = 0.2$  [m] and amplitude of the initial deflection  $A_1 = 0.1$  [m]

The above graph shows a significant influence of the proper impact of the particle against the container wall, which results in relevant damping occurring in the second vibration period ( $T_2$ ). The impact location is visible as a sudden change in the beam response (presented by black colour) around 0.5 seconds after the start of the analysis. The collision occurred when the beam deflection was equal to 0 which corresponds to the maximum beam velocity. This may suggest that the most effective reduction of beam vibrations is obtained when the collisions occur when the system reaches the maximal kinetic energy.

The conducted experimental research based solely on free vibrations initially revealed the fundamental characteristics of the ATPID damper. It was observed that a key aspect is to ensure the appropriate level of vibrations (initial deflection of the beam), to use a suitable grain mass for a given case, and to apply appropriate damper height. The combined application of all these factors allows to optimize damping properties of the system. Despite conducting about 40 studies based on different cases, the basic behaviour of the ATPID damper can be described. Generally, it can be postulated that an increase of granular mass can potentially result in improved damping

efficiency. However, the complexity arises due to the sensitivity of the investigated system to various parameters. For example, changes of the container height, while maintaining the same granular mass, can result in different ratio of vibration damping. This issue is further complicated by components such as the amplitude of vibrations and the inappropriate choice of the granular mass and damper's height. Notably, in the context of free vibrations, even single impacts can significantly reduce vibrations. However, it is not certain whether this effect is also observed in the harmonic vibrations. Considering the current stage of the research, formulating a concrete set of guidelines for the design and parameter selection of the ATPID damper is a complex procedure. For this purpose, the necessary element for further research is to determine the behaviour of the absorber for harmonic vibrations induced by kinematic excitation and to attempt to observe how the response of the system changes when the damper height changes in real time.

### 2.3.2 Harmonic vibrations

The next type of conducted experimental research concerned harmonic vibrations of a cantilever beam subjected to kinematic excitations. Initially, preliminary measurements of the beam vibrations were conducted for various excitation frequencies in order to observe whether there was a significant difference in vibration damping efficiency caused by the use of an ATPID damper. The research was carried out for an excitation amplitudes of 0.005 [m] and 0.01 [m], excitation frequencies ranging from  $0.7f_{res}$  to  $1.3f_{res}$  (where  $f_{res}$  denotes the first natural frequency of the system). Additionally, three different grain masses ( $0.1M_s$ ,  $0.2M_s$ , and  $0.3M_s$ ) were used, and the damper height varied from the minimum height of  $h_1 = 0.017$  [m] to the maximum values of  $h_2 = 0.05$  [m],  $h_3 = 0.1$  [m],  $h_4 = 0.15$  [m], and  $h_5 = 0.2$  [m], respectively. The damper ceiling position change occurred approximately at the sixth second of each analysis and was tuned at a constant speed (resulting from the power supply of the electric motor). Out of the 50 different analysed cases, five plots that represent the beam vibration response for five different excitation frequencies ( $0.9f_{res}$ ,  $0.95f_{res}$ ,  $f_{res}$ ,  $1.05f_{res}$ ,  $1.1f_{res}$ ) were selected. In each case, the excitation amplitude was 0.01 [m], the mass of the grain was equal to  $0.2M_s$ , and the maximum damper height was  $h_5 = 0.2$ m. The obtained results are presented in Figs. 2.24 - 2.28.

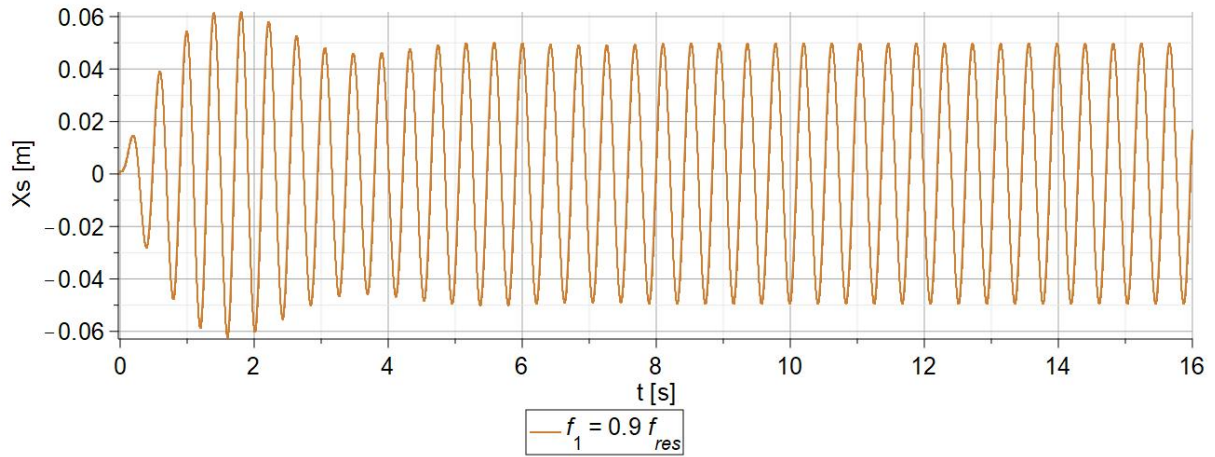


Figure 2.24: The amplitude of the beam harmonic vibration for  $f_1 = 0.9 f_{res}$ ,  $A = 0.01$  [m],  $h_5 = 0.2$  [m] and  $m_g = 0.2 M_s$

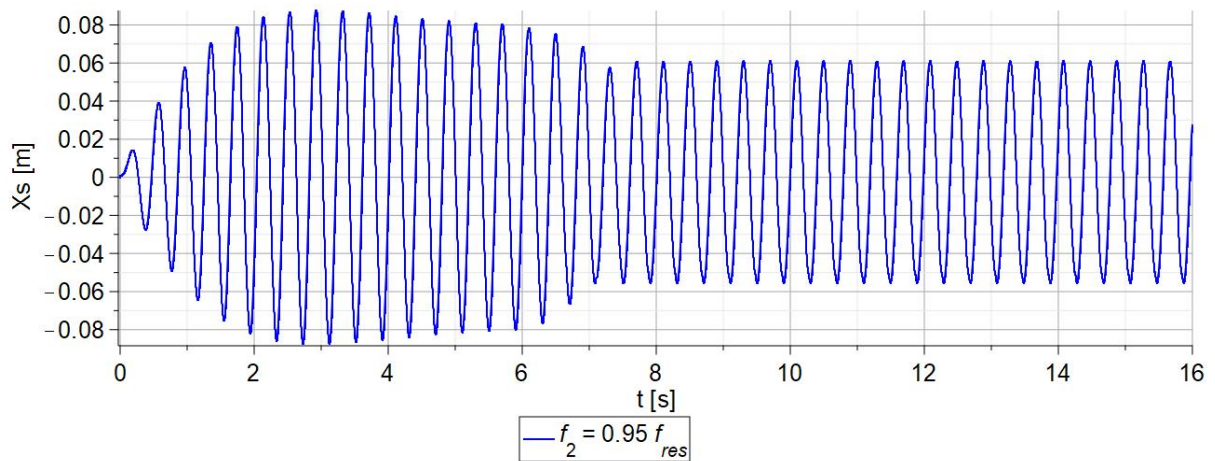


Figure 2.25: The amplitude of the beam harmonic vibration for  $f_1 = 0.95 f_{res}$ ,  $A = 0.01$  [m],  $h_5 = 0.2$  [m] and  $m_g = 0.2 M_s$

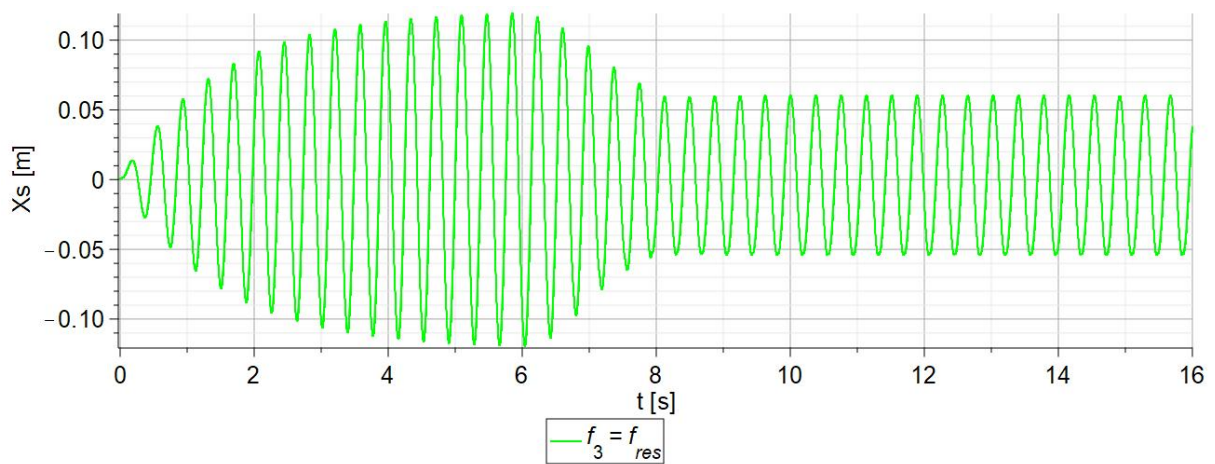


Figure 2.26: The amplitude of the beam harmonic vibration for  $f_1 = f_{res}$ ,  $A = 0.01$  [m],  $h_5 = 0.2$  [m] and  $m_g = 0.2 M_s$

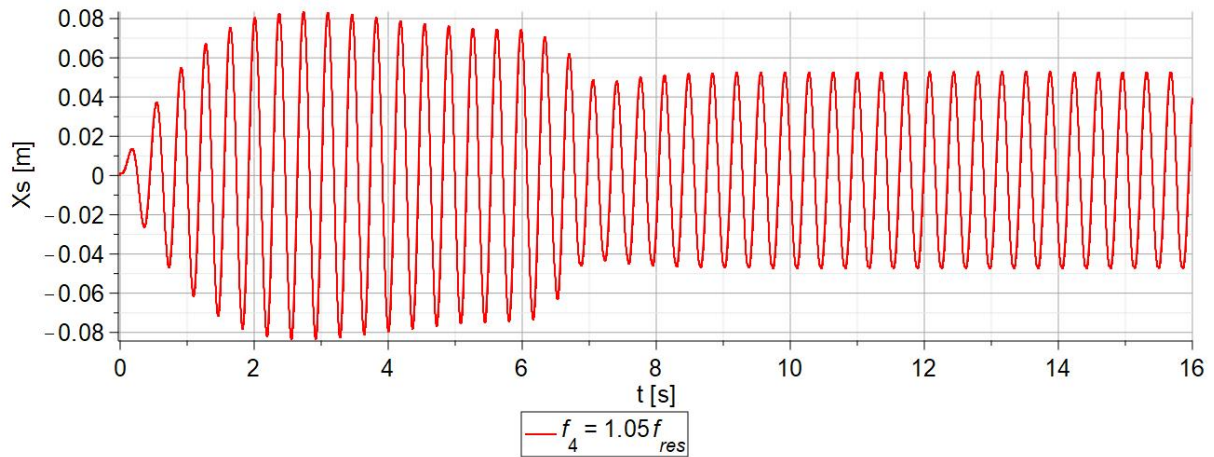


Figure 2.27: The amplitude of the beam harmonic vibration for  $f_1 = 1.05f_{res}$ ,  $A = 0.01$  [m],  $h_5 = 0.2$  [m] and  $m_g = 0.2M_s$

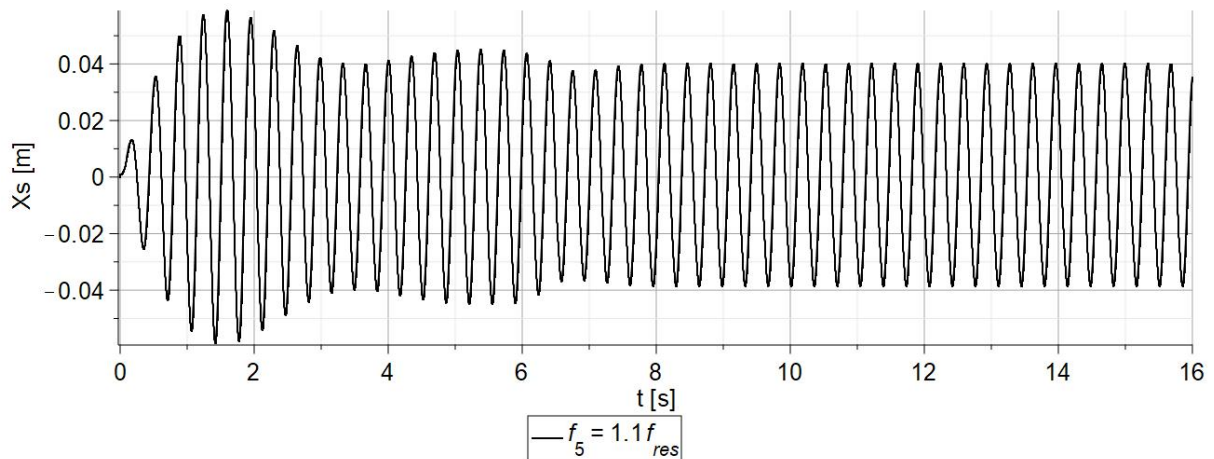


Figure 2.28: The amplitude of the beam harmonic vibration for  $f_1 = 1.1f_{res}$ ,  $A = 0.01$  [m],  $h_5 = 0.2$  [m] and  $m_g = 0.2M_s$

Fig. 2.26 shows the response of the beam that was in resonance during the initial phase of vibration (up to 6 [s]) due to the minimum height  $h_1$  of the damper. Subsequently, the damper was opened to a height of  $h_5$  which caused the start of vibration damping process. Fully damped and stabilized vibrations can be observed starting from approximately 8 seconds of the experiment. Comparing the amplitude of beam vibrations in the damped and undamped (resonant) ranges, it can be stated that for the case where the mass of the grain is 20 % of the total mass of the system, the vibrations were reduced by approximately by 50 %.

Other conducted experiments, including the results presented in Figs. 2.24, 2.25, 2.27, and 2.28, concerned the response of the beam for excitation that does not cause

resonance and for the same tuning strategy of the damper. For the cases close to resonance (Figs. 2.25 and 2.27), relatively small additional damping of the system vibrations can be observed around the sixth second of the experiment. For the case of  $f_2 = 0.95f_{res}$ , the amplitude of vibrations decreased by about 30 %, and for the case of  $f_4 = 0.105f_{res}$ , the vibrations were damped by about 40 %. For other cases, the greater was the difference between the excitation frequency and the natural frequency of vibrations, the smaller was the amplitude of the system response for a deactivated damper. The lack of resonance directly affects the dynamics of the beam and the particle. The obtained system accelerations are so small that it is difficult to obtain detachment of the grain from the container bottom.

It should be noticed that the ATPID damper operates similarly to the Tuned Mass Damper. Even when the grain moves inside the container vibrating beyond the resonance range, the change in the dynamic structure of the system will not cause a significant reduction in its vibrations. In such a case, contact forces occurring during collisions could possibly cause the process of vibration damping. However, again, for non-resonant vibrations for the selected parameters of the conducted experiments, the effect of the occurring forces on vibration damping was not observed, which is presented in Figs. 2.24 and 2.28.

Analyzing all the obtained results, it can be stated that the proposed ATPID damper is an effective construction in reducing vibrations of the system in resonance. In the preliminary stage of experimental research the applied construction allowed for achieving a vibration damping efficiency of 50%, which means that the amplitude of the beam vibrations decreased by half after opening the damper. Similar studies for non-resonant beam vibrations showed that the effectiveness of the damper decreases along the shifting from the resonance. It may seem that for ordinary harmonic vibrations, the prototype damper construction is ineffective. However, it should be noticed that these are preliminary studies for a construction whose size and parameters resulted from the available materials and laboratory limitations. The main goal of this stage of research is to generally determine the usefulness of the ATPID damper and the potential directions of its development.

The next group of experimental studies focused on the influence of the ATPID damper on reducing vibrations of the beam only in resonance. The research was

carried out for 50 different cases, where the parameters of the system assumed similar values as in the studies concerning free vibrations, i.e., the excitation amplitude was equal to 0.005 [m] and 0.01 [m], five different grains whose mass changes in the range was  $0.025M_s \leq m_g \leq 0.3M_s$ , and five different heights of the damper were  $h_1 = 0.017$  [m]  $\rightarrow h_5 = 0.2$  [m]. The results of individual measurements are presented in Figs. 2.29, 2.31, 2.33, 2.35, and 2.37. Summary results allowing to compare the system response for different damper heights and the use of different masses of grains are presented in Figs. 2.30, 2.32, 2.34, 2.36, and 2.38 - 2.43.

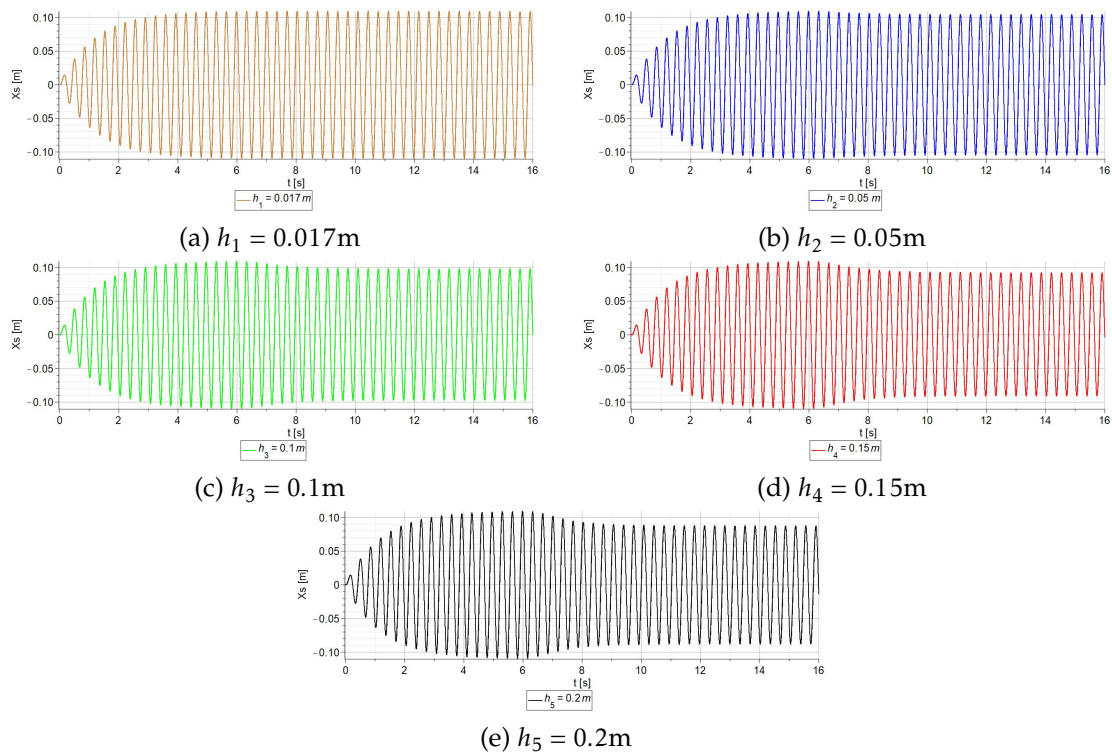


Figure 2.29: Response of the beam for  $A = 0.01$  [m],  $m_g = 0.025M_s$ , and five different ATPID heights  $h_1 \rightarrow h_5$

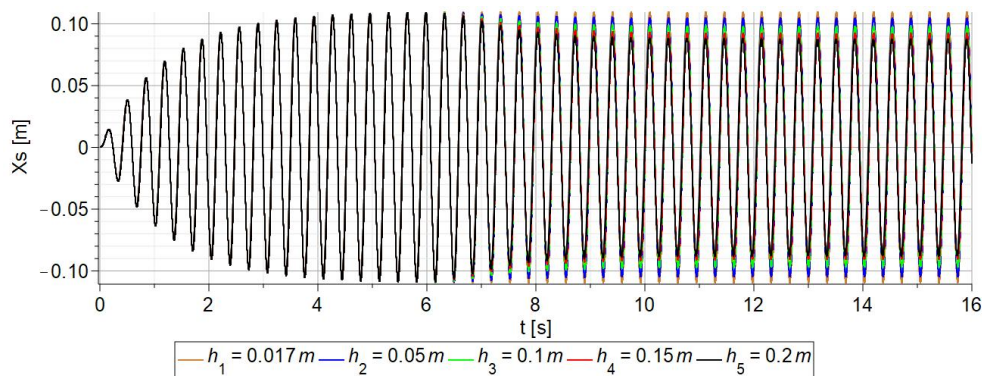


Figure 2.30: Comparison of the beam response for  $A = 0.01$  [m],  $m_g = 0.025M_s$ , and five different ATPID heights  $h_1 \rightarrow h_5$

The initial obtained results of the beam response  $X_s$  show that by using a grain with a small mass equal to 2.5% of the total system mass, it is possible to achieve only a slight damping of vibrations. In particular, for the most effective  $h_5$  case, the amplitude of the oscillations is decreased by 20 % in comparison to the range of resonance vibrations (during first 6-second analysis). For smaller heights, correspondingly lower vibration damping efficiency was achieved.

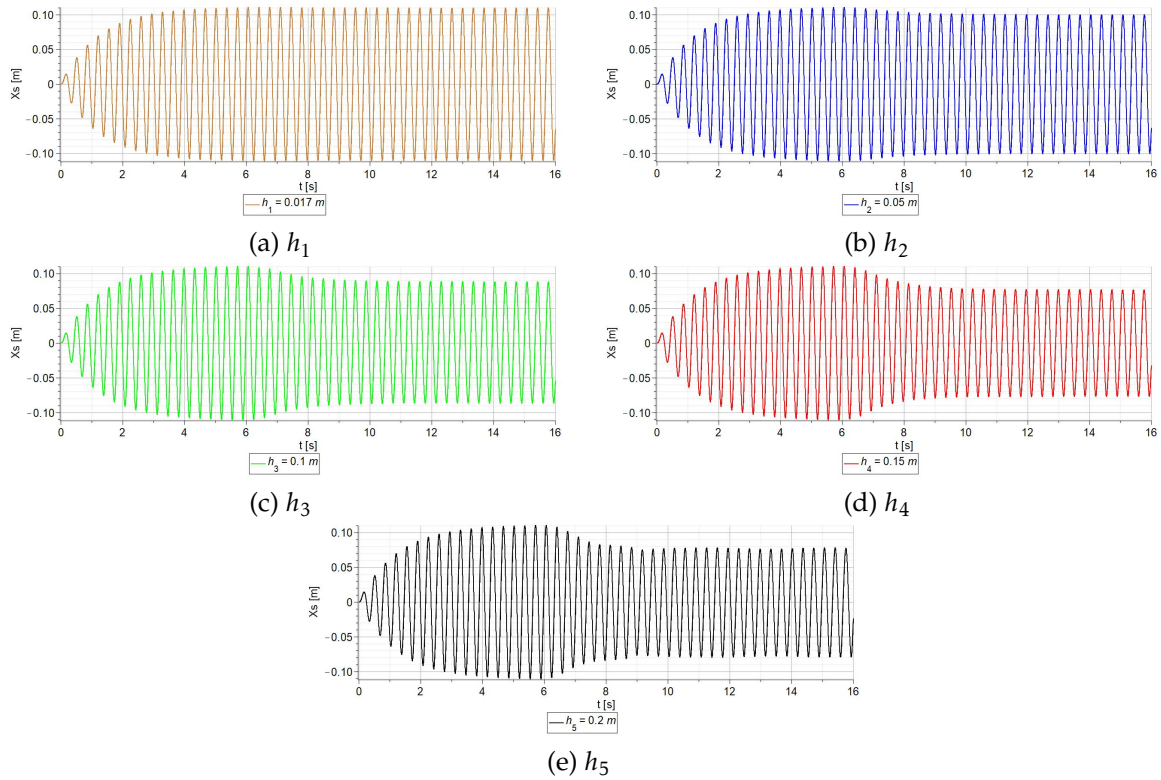


Figure 2.31: Response of the beam for  $A = 0.01$  [m],  $m_g = 0.05M_s$ , and five different ATPID heights  $h_1 \rightarrow h_5$

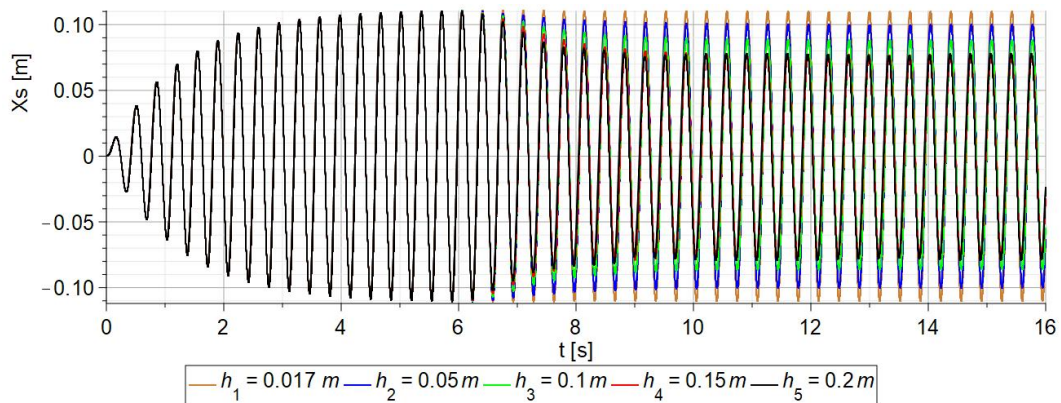


Figure 2.32: Comparison of the beam response for  $A = 0.01$  [m],  $m_g = 0.05M_s$ , and five different ATPID heights  $h_1 \rightarrow h_5$

In the case when the mass of the particle is  $m_g = 0.05M_s$ , similar conclusions can be drawn as in the previous case ( $m_g = 0.025M_s$ ). The highest effectiveness was achieved again for the height  $h_5$ , and vibrations were reduced by about 32 %. This result should be treated as another example revealing that using a heavier grain can lead to improved damping properties.

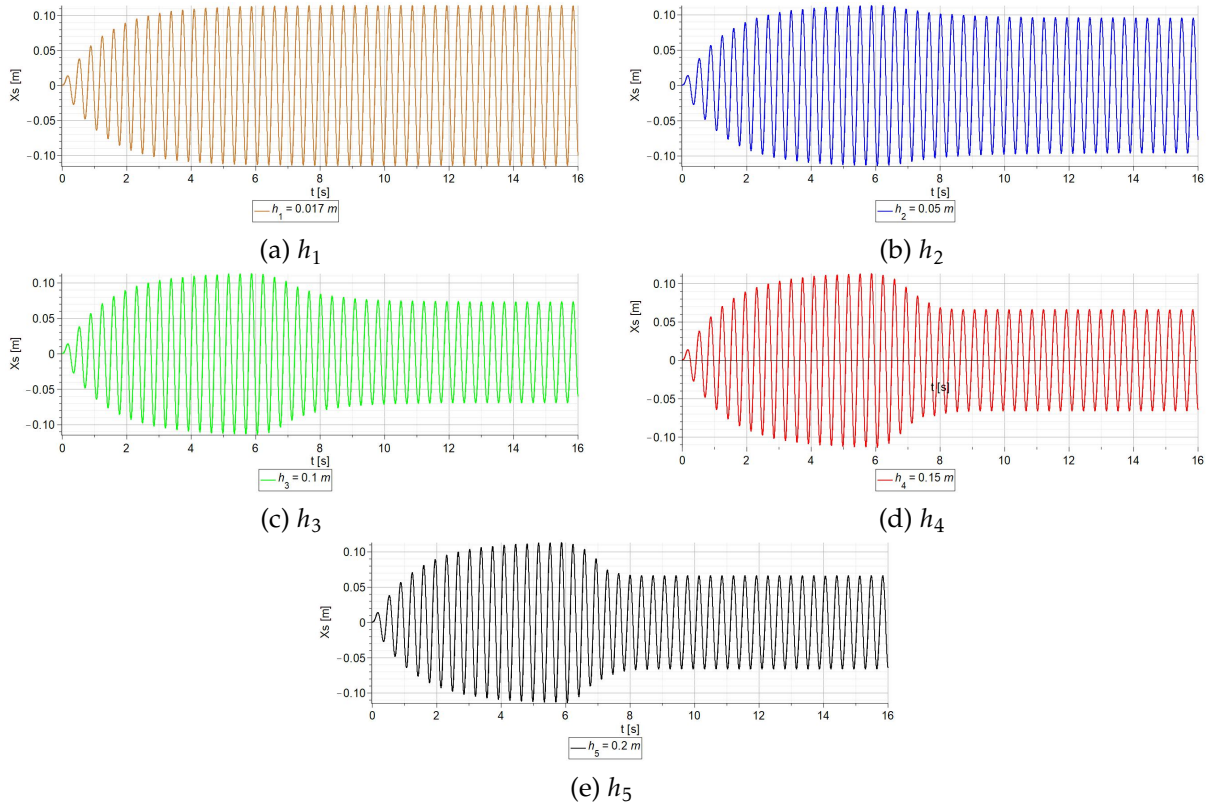


Figure 2.33: Response of the beam for  $A = 0.01 \text{ [m]}$ ,  $m_g = 0.1M_s$ , and five different ATPID heights  $h_1 \rightarrow h_5$

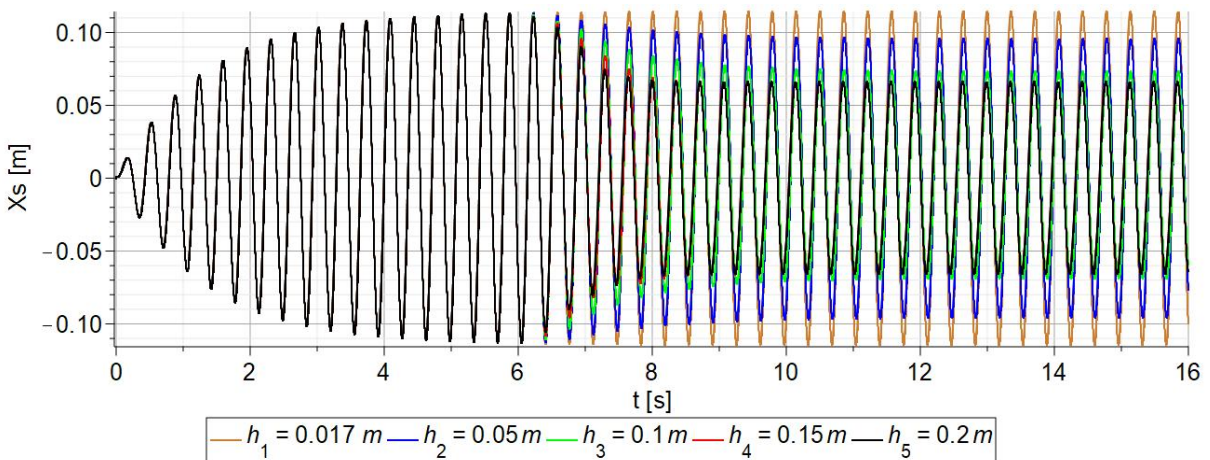


Figure 2.34: Comparison of the beam response for  $A = 0.01 \text{ [m]}$ ,  $m_g = 0.1M_s$ , and five different ATPID heights  $h_1 \rightarrow h_5$

In the case where a grain with a mass of 10 % of the total system mass was used, the resonant vibrations were damped maximally approximately 45 %. This value was obtained for two different cases when the height of the damper was equal to  $h_4 = 0.15$  [m] and  $h_5 = 0.2$  [m]. The only difference was that the time required to obtain a completely damped (stabilized) system was shorter for the higher damper height. A slightly smaller vibration reduction was achieved for the case of  $h_3$ .

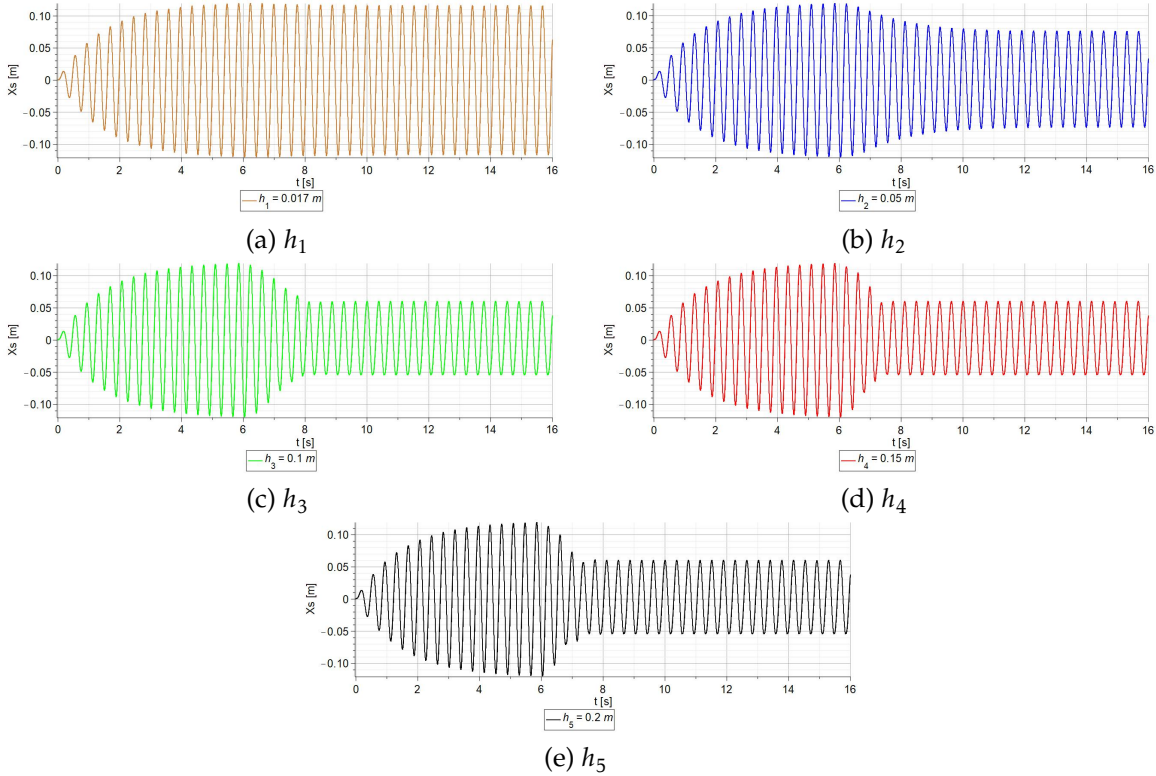


Figure 2.35: Response of the beam for  $A = 0.01$  [m],  $m_g = 0.2M_s$ , and five different ATPID heights  $h_1 \rightarrow h_5$

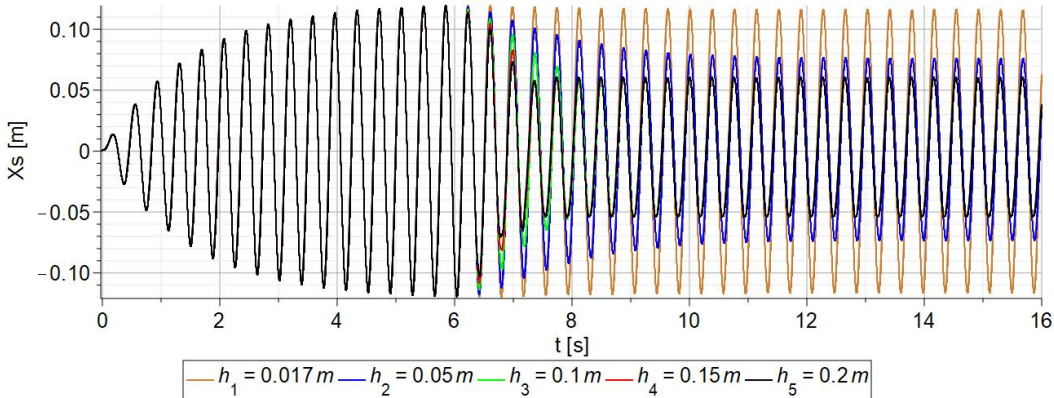


Figure 2.36: Comparison of the beam response for  $A = 0.01$  [m],  $m_g = 0.2M_s$ , and five different ATPID heights  $h_1 \rightarrow h_5$

The use of grain with a mass of  $m_g = 0.2M_s$  allows to reduce the amplitude of resonant vibrations by approximately 50 % by using one of the three available damper heights  $h_3 \rightarrow h_5$ . Moreover, there is a noticeable difference in the time required to stabilize the vibrations in these three cases. The shortest time is observed for the highest container ( $h_5$ ).

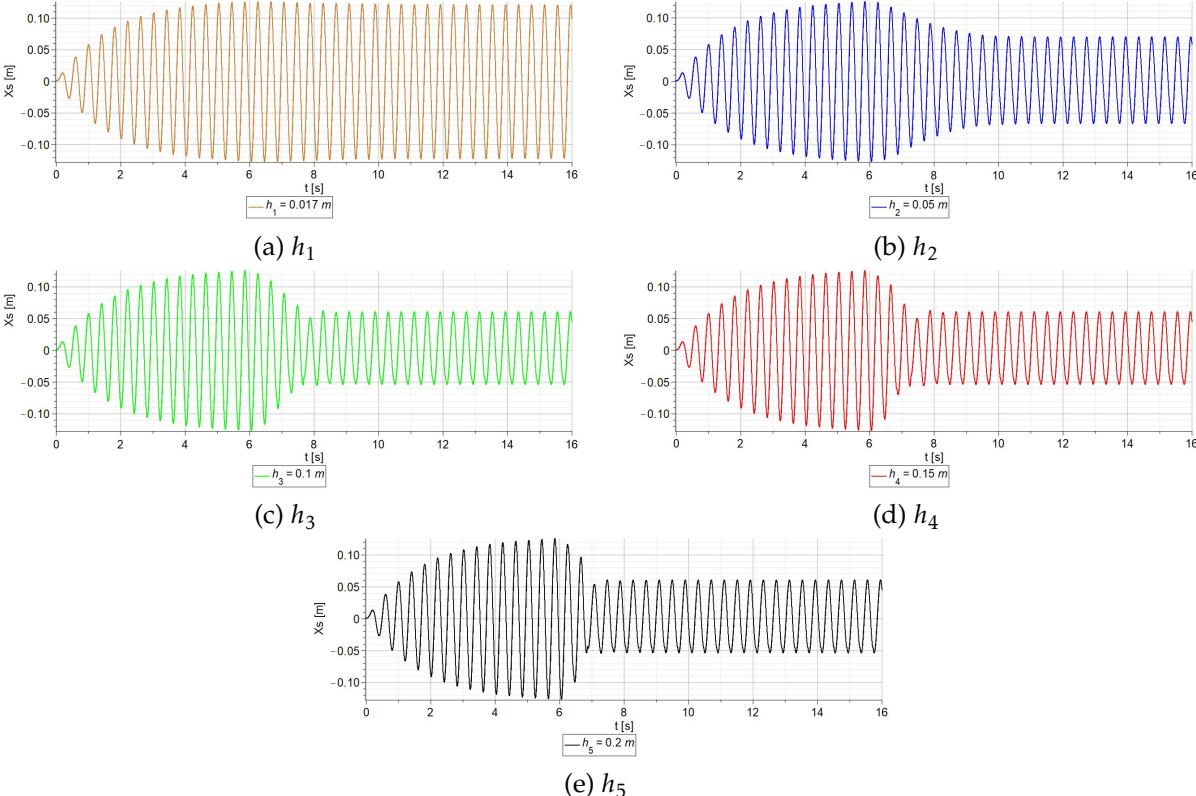


Figure 2.37: Response of the beam for  $A = 0.01$  [m],  $m_g = 0.3M_s$ , and five different ATPID heights  $h_1 \rightarrow h_5$

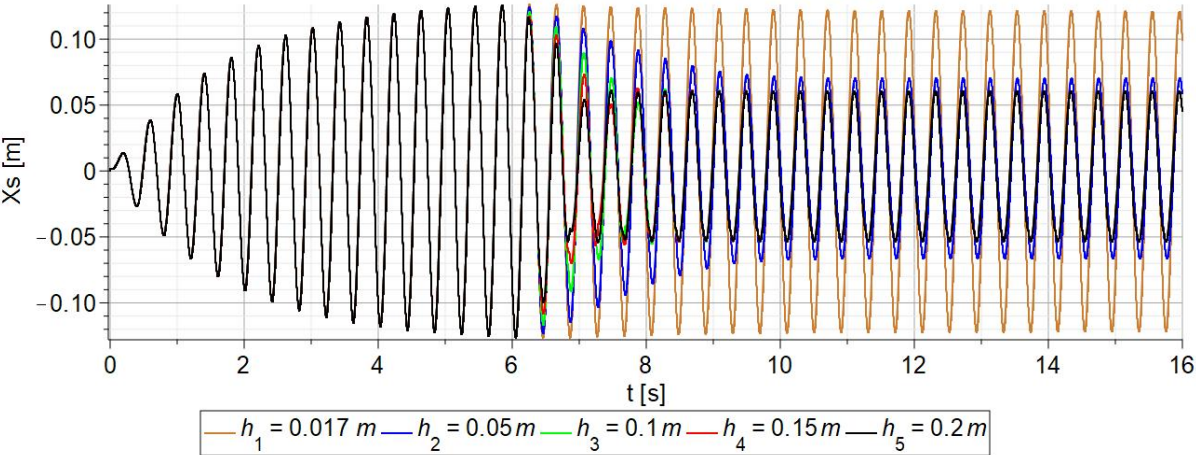


Figure 2.38: Comparison of the beam response for  $A = 0.01$  [m],  $m_g = 0.3M_s$ , and five different ATPID heights  $h_1 \rightarrow h_5$

The results presented in Fig. 2.38 are further examples confirming the fact that one of the main factors positively affecting the level of vibration damping is the mass of the grain placed inside the container. In the above case, it is possible to reduce the amplitude of the vibrations by 53 %. Similarly, in the case of the particle mass equal to  $0.2M_s$ , there is a difference in the time of obtaining stabilized damped vibrations, and the maximum damping can be achieved for 3 selected heights ( $h_3$ ,  $h_4$  and  $h_5$ ). Only slightly worse damping was obtained using height  $h_2$ . This means that the grain, under the assumed excitation parameters, moves inside the container in such a way that its influence on vibration reduction for all 4 cases of the height of the damper is similar.

In the next stage, the experimental tests were carried out for the same particle masses and damper heights, changing the excitation amplitude in the range between 0.01 [m] and 0.005 [m]. The aggregated results of beam displacements for the applied variants are presented in Figs. 2.39 - 2.43.

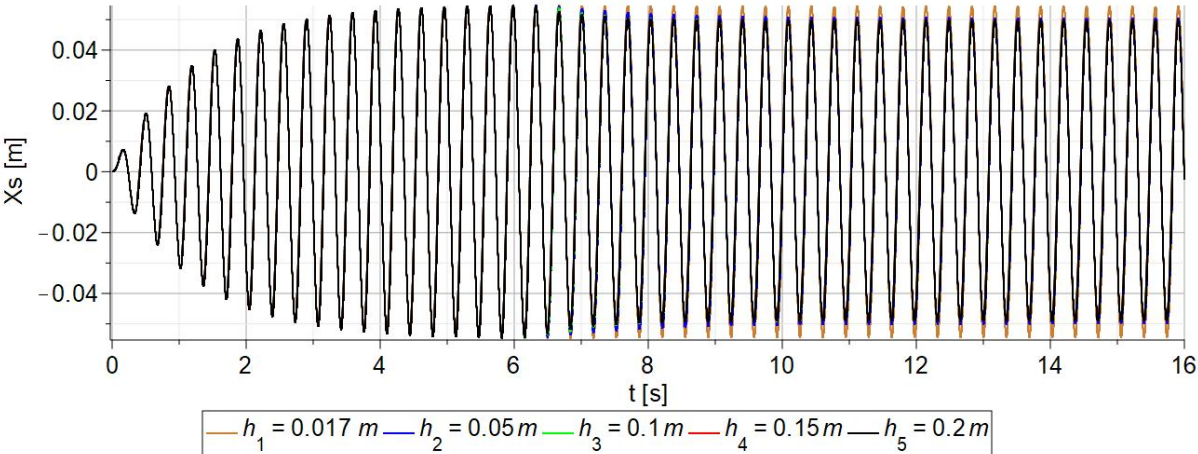


Figure 2.39: Response of the beam for  $A = 0.005$  [m],  $m_g = 0.025M_s$ , and five different ATPID heights  $h_1 \rightarrow h_5$

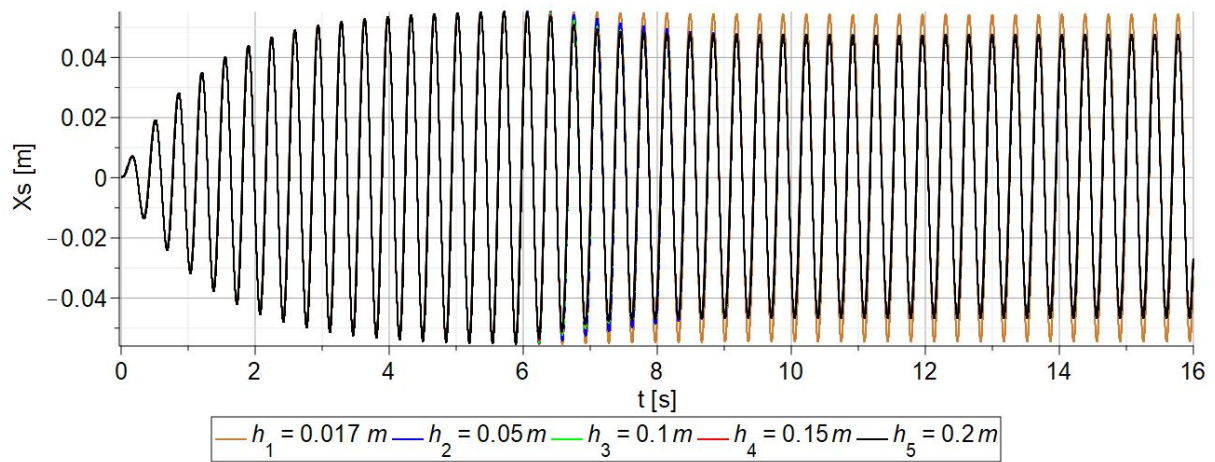


Figure 2.40: Response of the beam for  $A = 0.005$  [m],  $m_g = 0.05M_s$ , and five different ATPID heights  $h_1 \rightarrow h_5$

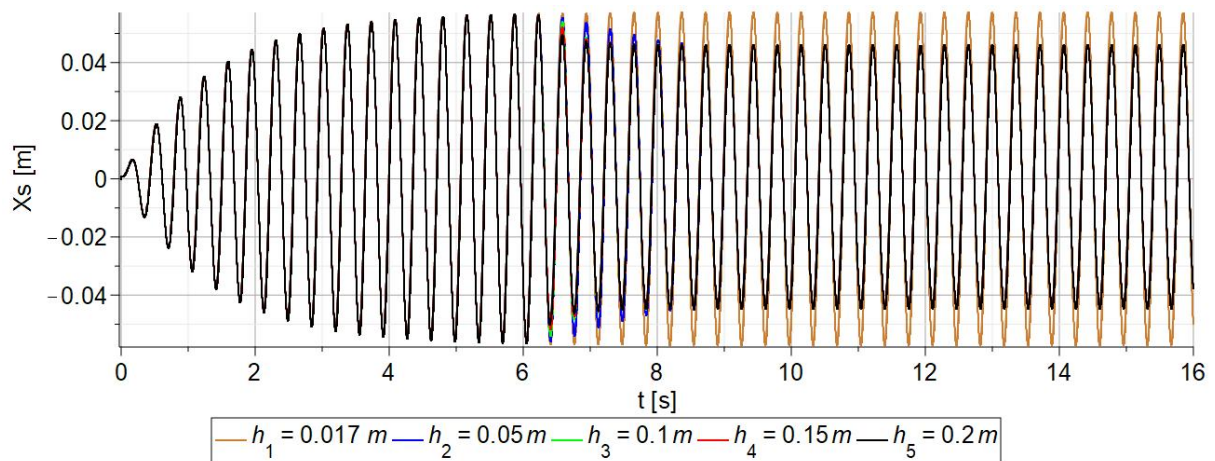


Figure 2.41: Response of the beam for  $A = 0.005$  [m],  $m_g = 0.1M_s$ , and five different ATPID heights  $h_1 \rightarrow h_5$

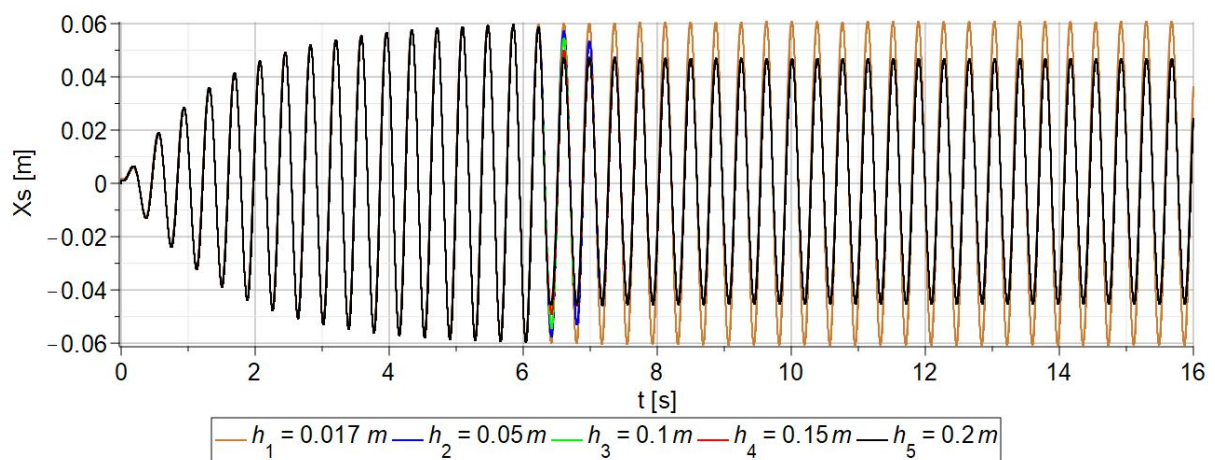


Figure 2.42: Response of the beam for  $A = 0.005$  [m],  $m_g = 0.2M_s$ , and five different ATPID heights  $h_1 \rightarrow h_5$

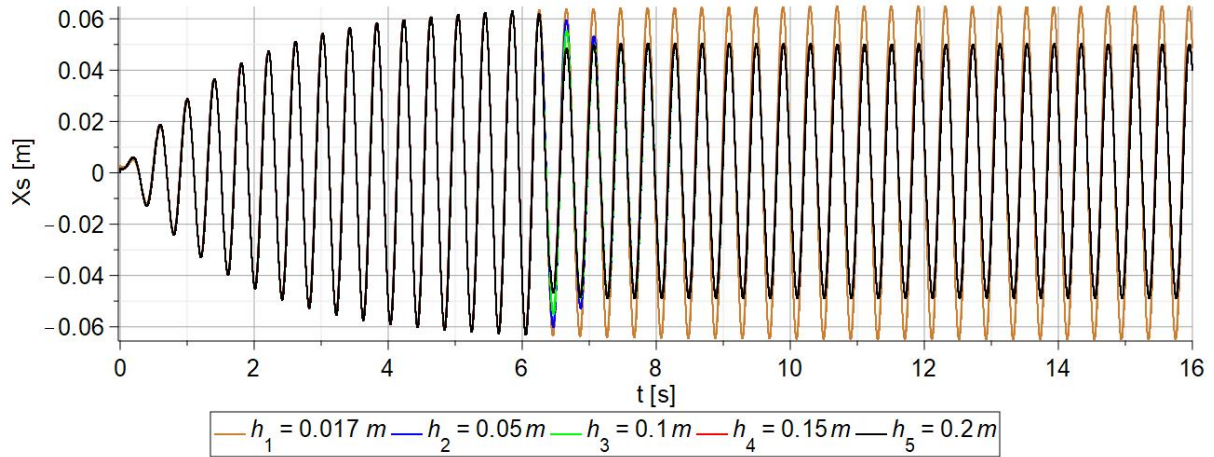


Figure 2.43: Response of the beam for  $A = 0.005$  [m],  $m_g = 0.3M_s$ , and five different ATPID heights  $h_1 \rightarrow h_5$

The results presented in the above figures allow for the analysis of the effects of excitation amplitude and the dynamics of the primary structure (cantilever beam) on the effectiveness of resonant vibration damping using the ATPID damper. The conclusions that can be drawn are analogous to those presented for the case where the excitation amplitude was 0.01 [m]. Regardless of the damper height (excluding  $h_1$ , which indicates the deactivated damper), a noticeable reduction in the vibration amplitude of the beam can be observed. The possibility of using heavier grain results in an improvement in the effectiveness of vibration damping. For the case when the grain mass was the largest ( $0.3M_s$ ), a maximum vibration damping of about 20 % was observed. For a lower grain mass, this value decreased. Additionally, it should be noted that the maximum vibration reduction value for the case with an excitation amplitude of 0.01 [m] was above 50 %.

The last graphical form of the obtained results is a comparison of the maximum amplitude of damped beam vibrations for each case of particle mass and damper height plot presented in Fig. 2.46. Therefore, in Figs. 2.44 and 2.45, the response curves for these variants are presented. The last second of the experimental measurements was considered as the damped and stabilized range of the system response. For the clarity, only the curves corresponding to two selected heights indicating deactivated damper  $h_1$  (Fig. 2.44) and most effectively tuned vibrations  $h_5$  (Fig. 2.45) were presented.

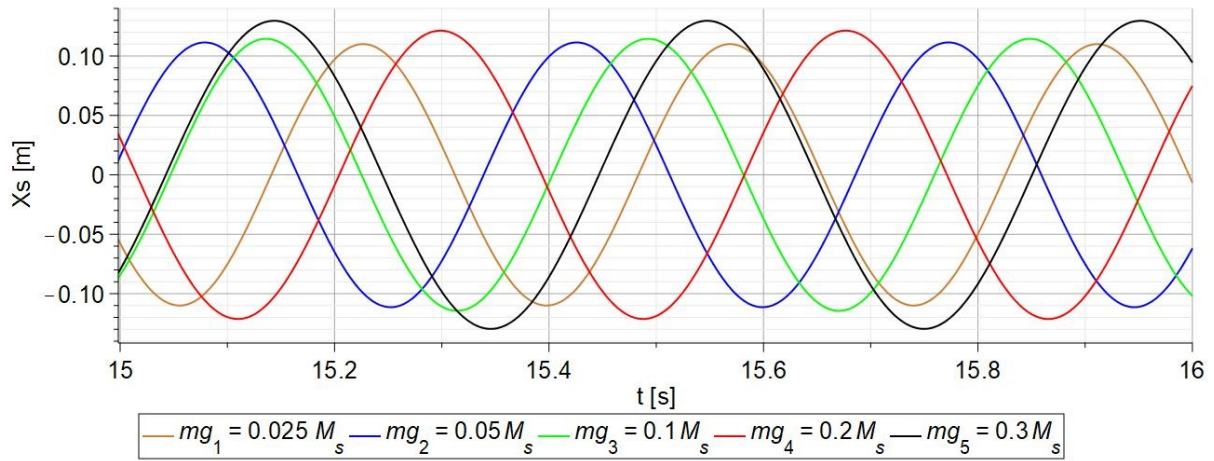


Figure 2.44: Response of the beam for  $A = 0.01\text{m}$ ,  $h_1$  and five different grain mass  $m_{g_1} \rightarrow m_{g_5}$

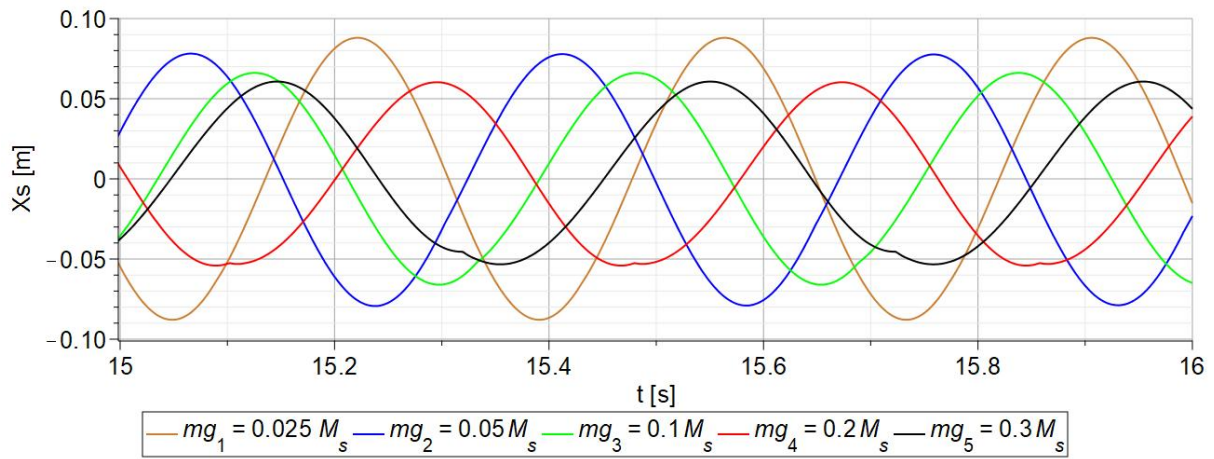


Figure 2.45: Response of the beam for  $A = 0.01\text{m}$ ,  $h_5$  and five different grain mass  $m_{g_1} \rightarrow m_{g_5}$

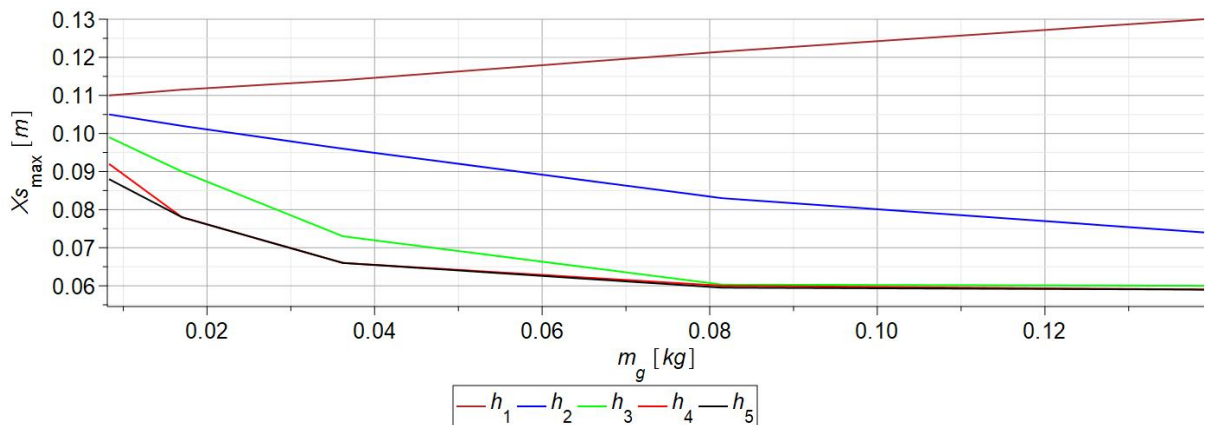


Figure 2.46: Maximum amplitude of the damped beam vibration for  $A = 0.01$  [m], five different grain mass  $m_{g_1} \rightarrow m_{g_5}$  and for five different damper heights  $h_1 \rightarrow h_5$

From Fig. 2.46 it can be directly inferred that changing the mass of the grain affects the beam response. The conducted research has shown that the greater the mass, the higher the efficiency of vibration damping. Additionally, by changing the damper height, it is possible to influence the particle movement, which translates into the effectiveness of oscillation reduction. For the  $h_1$  height (when the grain is blocked in the damper), an increase in vibration amplitude is observed with the use of heavier grains due to the phenomenon of resonance. Each of the proposed damper tuning strategies results in a reduction of the maximum amplitude of damped vibrations. For the used cantilever beam and excitation amplitude, the system response amplitude was approximately 0.06 [m], indicating a reduction of resonant vibrations by more than half of their value. A similar maximum damping ratio was identified for the combination of several different damper heights  $h_4$  and  $h_5$  and for most of the used grain masses (with the exception of a value equal to 2.5 % of the total system mass) as well as for the height  $h_3$  and grain mass equal to 20 % and 30 % of the total system mass. It is expected that a stiffer beam and a higher height could lead to better absorber performance. At the preliminary research stage, validation of this hypothesis was not possible due to laboratory limitations and a lack of sufficient knowledge about the appropriate height of the damper for every case. Further research based on the heuristical method would be possible, but at this stage, it was decided to develop mathematical model of the test stand, conduct numerical sensitivity analyses, and thus determine optimal parameters from the perspective of vibration damping.



# Chapter 3

## Adaptive Tuned Particle Impact Damper - numerical analysis

### 3.1 Contact modelling - state of the art

It is crucial to propose a numerical model for both the absorber and the test stand. There is an abundance of fascinating scientific articles concerning PID dampers available due to the extensive scientific research on this topic. These papers present various methods for modelling of such absorbers. Although the operating principle of Impact Dampers remains the same, all numerical models presented in the literature propose different approaches to modelling collisions between grains, and between grains and walls of the damper. This section offers a comprehensive literature review on contact modelling, which facilitates the selection of the most appropriate method to model the ATPID damper. The study of collisions is a crucial area of research in fields like physics and engineering where there is a need to comprehend how interacting objects behave. Generally, collisions can be classified into two types: elastic and inelastic [53]. Elastic collisions are characterized by the conservation of both the momentum and the kinetic energy. This implies that the total momentum of the objects prior to the collision equals the total momentum after the collision, while the total kinetic energy is conserved. On the other hand, inelastic collisions are characterized by the lost of kinetic energy, which is converted into other forms such as heat. The momentum is still conserved, but the final velocities of the objects are generally different from their initial velocities [54].

To model collisions, it is necessary to understand the physical principles involved in the interaction between objects and the influence of properties of the objects themselves, such as their mass, velocity, and material characteristics. Mathematical models can be developed to describe the motion of objects before and after the collision, taking into account factors such as the angles of collision, the coefficient of restitution, and the nature of the forces involved. Additionally, computer simulations and experimental studies can be employed to better comprehend the behaviour of objects in real collisions and design materials and structures that can better withstand impacts and collisions [55, 56].

### **Hard contact theory**

The hard contact theory of collisions is a physical concept which explains how two objects interact when they collide and bounce off each other. This theory is based on several assumptions concerning the nature of the collision. Firstly, it assumes that the objects do not deform or break apart when they collide. Secondly, it assumes that the collision duration is very short. Thirdly, it is possible to model perfectly elastic as well as inelastic collisions. Lastly, it assumes that the forces acting on the objects during the collision are conservative, meaning that energy is not lost due to non-conservative forces like friction or air resistance. Using these assumptions, the hard contact theory predicts that the forces acting on the objects during the collision can be calculated using simple formulas based on the masses and velocities of the objects before and after the collision [57, 10].

As the first case, let us consider central perfectly elastic collisions. When two rigid objects collide, the forces between them are assumed to be conservative, so no energy is lost from the system. In this case, it is also possible to apply the law of conservation of momentum, which states that the total momentum of objects before and after the collision must be equal [58]. A collision is considered central if the bodies involved move initially in the same straight line, resulting in the total momentum having a direction parallel to this line. For a clearer description of the hard contact theory, let us consider the collision of two bodies, which are labelled with subscripts 1 and 2. Their velocities before the collision are represented by  $-$ , while their velocities after the collision are represented by  $+$ . Additionally, the masses of the bodies are denoted by the variable  $m$ . The total momentum after the collision is equal to the momentum before

the collision:

$$m_1\dot{y}_1^+ + m_2\dot{y}_2^+ = m_1\dot{y}_1^- + m_2\dot{y}_2^- \quad (3.1)$$

The total kinetic energy after the collision is equal to the kinetic energy of the bodies before the collision:

$$\frac{m_1\dot{y}_1^{+2}}{2} + \frac{m_2\dot{y}_2^{+2}}{2} = \frac{m_1\dot{y}_1^{-2}}{2} + \frac{m_2\dot{y}_2^{-2}}{2} \quad (3.2)$$

From Eqs. 3.1 and 3.2 it is possible to determine the velocities of the systems after the collision:

$$\dot{y}_1^+ = \frac{(m_1 - m_2)\dot{y}_1^- + 2m_2\dot{y}_2^-}{m_1 + m_2} \quad (3.3)$$

$$\dot{y}_2^+ = \frac{(m_2 - m_1)\dot{y}_2^- + 2m_1\dot{y}_1^-}{m_1 + m_2} \quad (3.4)$$

In the case of the perfectly elastic collision the coefficient of restitution (COR) for an impact can be defined as the negative value of the ratio between the relative velocity of the elements after impact to the relative velocity before impact:

$$e = -\frac{\dot{y}_1^+ - \dot{y}_2^+}{\dot{y}_1^- - \dot{y}_2^-} \quad (3.5)$$

In the case of the perfectly elastic collision, COR is equal to 1 where there is no loss of kinetic energy, and the objects have the same relative velocity as they had before the collision. Eqs. 3.1 - 3.5 utilizing the restitution coefficient can be used to describe an inelastic collision. The velocities of the systems after the elastic collision are as follows:

$$\dot{y}_1^+ = (1 + e)\frac{m_1\dot{y}_1^- + m_2\dot{y}_2^-}{m_1 + m_2} - e\dot{y}_1^- \quad (3.6)$$

$$\dot{y}_2^+ = (1 + e)\frac{m_1\dot{y}_1^- + m_2\dot{y}_2^-}{m_1 + m_2} - e\dot{y}_2^- \quad (3.7)$$

In an inelastic collision, it is assumed that the COR takes values within the range of  $0 < e < 1$ . The coefficients of restitution are influenced by various factors, such as the material properties (e.g. elastic modulus and rheology), the angle of impact,

the shapes of the colliding objects, the coefficient of friction between them, and their adhesive properties. When two bodies collide at a non-central angle, their paths do not align on a single straight line. If I observe the collision from a reference frame where one body is stationary before the collision or their velocities are parallel, the law of conservation of momentum implies that the momentum vectors after the collision must lie in the same plane as the momenta before the collision. Hence, by selecting the right coordinate system, I can examine this event on a two-dimensional plane. The use of hard contact theory to explain collisions can be found in various literature examples [59, 60, 61, 62, 63, 64, 65].

However, this theory is not applicable to all types of collisions. For instance, in collisions involving deformable objects or non-conservative forces, the assumptions of the hard contact theory may not hold, and more complex models may be needed to accurately describe the collision. Nevertheless, because of its insufficient description and exclusion of significant physical processes that emerge as a result of the material and geometrical properties of the colliding components, it was concluded that hard contact theory is unsuitable to simulate the ATPID damper.

### **Soft contact theory**

The soft contact theory of collision is a method used to explain the behaviour of two objects colliding when at least one object is deformable. Unlike the hard contact theory, which assumes an instantaneous change in momentum during a collision, the soft contact theory takes into account the deformation of the objects and the duration of the impact. In a soft collision, the objects involved will deform, absorbing and possibly dissipating part of the kinetic energy of the system. Consequently, the objects may not return to their original shape after the collision. The resulting loss of kinetic energy can be observed. Additionally, the duration of the impact affects the collision. The longer the duration of the impact, the smaller force is exerted during the collision. Overall, the soft contact theory mainly provides a more accurate representation of collisions between objects with elastic and plastic properties. It accounts for the deformation and energy loss that occurs during the impact [11].

There are many different approaches to soft contact problems. They are based on linear or non-linear contact models and can take into account both elastic and viscoelastic phenomena [66, 67, 68]. A wide range of these models has been reviewed and described in the following section of the doctoral thesis. These models are presented using general equations, without a detailed explanation of the specific parameters used to describe them. After reviewing the literature, the most suitable model was chosen for modelling the impact phenomena occurring in the ATPID damper. This selected model is described in detail in the following chapter and applied for defining basic contacts between a grain and a flat surface and the derivation of the final formulation for contact forces used in numerical simulations.

*Linear viscoelastic model of the normal contact force*

Linear models of contact are the most commonly used in DEM [69, 70, 71, 72, 73]. To incorporate energy dissipation, the normal force  $F^n$  is divided into two parts: one models elastic repulsion, while the other models viscous dissipation. The elastic component behaves like an elastic spring and depends on the relative displacements of both objects while the viscous component depends on the displacement rate. By incorporating dissipation, these models fall into the category of viscoelastic force schemes. It is important to note that these viscoelastic models often take the linear form, which corresponds to the force of a damped harmonic oscillator:

$$F^n = F_{el}^n + F_{diss}^n = k_{lin}^n \xi + \gamma_{lin}^n \dot{\xi} \quad (3.8)$$

where  $k_{lin}^n$  is the equivalent stiffness spring, equivalent linear damping  $\gamma_{lin}^n$ , overlap  $\xi$ , and overlap rate  $\dot{\xi}$ . The advantage of the applied model is the possible analytical solution of the contact problem. Currently, it is possible to analyse contact problems in systems made of a variety of materials characterized by non-linear mechanical properties. Therefore, it is required to develop the discussed linear model.

*Non-linear elastic model of the normal contact force*

The Hertzian contact model [74] is a theoretical method that explains how two solid objects, such as spheres or cylinders, interact when they collide with each other. The model assumes that these objects are elastic, isotropic, and homogeneous and that their contact happens at a single point or a small area. The force of the contact is calculated by examining how the objects deform at their contact point. The general form of the

Hertz Theory contact force is as follows:

$$F^n = F_{el}^n = k^n \xi^{\frac{3}{2}} \quad (3.9)$$

The model also takes into account the objects' curvature and Young's modulus of the materials they are, which are included in the non-linear reduced stiffness  $k^n$ . Although the Hertzian contact model is extensively used in engineering, e.g. in designing mechanical systems like gears and bearings, it has some limitations. These include its inability to capture plastic deformation and surface roughness effects.

*Partly non-linear viscoelastic model of the normal contact force*

After the development of several force laws based on the Hertz Theory [74], which originally focused on elastic contacts, modifications were made to extend the approach to nonlinear viscoelastic models. The partly non-linear viscoelastic model for the normal contact force is a mathematical approach utilized to describe the conduct of materials that demonstrate elastic and viscous properties during loading and unloading conditions. This model considers the non-linear behaviour of the objects, which implies that the correlation between stress and strain is not linear, and the material's response is not directly proportional to the applied load. Lee and Herrmann (LH) [75] suggested a partially nonlinear model:

$$F^n = F_{el}^n + F_{diss}^n = k^n \xi^{\frac{3}{2}} + \gamma_{LH}^n \dot{\xi} \quad (3.10)$$

where  $\gamma_{LH}^n$  is a phenomenological dissipative factor. The dissipation force  $F_{diss}^n$  remains linearly related to the displacement rate  $\dot{\xi}$ . In the model, the spring's stiffness  $k^n$  (from Hertz Theory) is determined by both the elastic properties of the material and the geometry of the colliding objects. In the approach introduced by Lee and Herrmann coefficient of restitution increases as the initial velocity increases and a collision time decreases with an increase in the impact velocity.

### *Fully non-linear viscoelastic model of the normal contact force*

A fully nonlinear model was suggested by Kuwabara and Kono (KK) [76].

$$F^n = F_{el}^n + F_{diss}^n = k^n \xi^{\frac{3}{2}} + \gamma_{KK}^n \dot{\xi} \xi^{\frac{1}{2}} \quad (3.11)$$

The introduced model involves a dissipative factor,  $\gamma_{KK}^n$ , and spring stiffness. This model was also discovered independently by Brilliantov et al. [77], who identified  $\gamma_{KK}^n$  as a material property that can be determined from the bulk viscosities of the materials involved in the collision. However, since information about the bulk viscosities are often not available, Brilliantov et al. treated  $\gamma_{KK}^n$  as a parameter that can be adjusted. A modified Hertz-type force law with a slightly different exponent of the dissipative term was suggested by [78]. The force scheme is as follows:

$$F^n = F_{el}^n + F_{diss}^n = k^n \xi^{\frac{3}{2}} + \gamma_T^n \dot{\xi} \xi^{\frac{1}{4}} \quad (3.12)$$

with a spring stiffness  $k^n$  and a phenomenological dissipative factor  $\gamma_T^n$ , which results in a constant coefficient of restitution and a collision time that is velocity-dependent.

### *Elastoplastic (hysteretic) contact models*

There is a distinct group of materials that undergo permanent deformation as a result of the action of various forces. Thus, exceeding the yield strength results in a lack of return to the original shape. The study of plastic deformation caused by the collision of particles with a specific surface is an important topic in both basic research and practical applications. Various elastoplastic models, including linear and nonlinear models, have been proposed [79, 80, 81, 82, 83]. These models use different springs with various stiffness for loading and unloading periods, and some models even subdivide these periods further. A partially latching model, initially proposed by Walton and Braun [79], can achieve an ideal plastic force scheme. Multiple analyses conducted on the impacts of metal spheres have demonstrated an almost linear relationship between displacement and loading as well as unloading behaviours. The Walton-Braun model offers a straightforward analytic solution that yields a final particle deformation dependent on the velocity of the penetration. Conversely, Sadd proposed a model for investigating wave propagation in granular materials, which assumes material behaviour without incorporating any dissipation effects dependent on velocity [80]. In-

stead, the concept of deformation-dependent damping is introduced by integrating distinct non-linear springs to account for the three stages of loading, unloading, and reloading. Thornton proposed a theoretical model for the elastic-perfectly plastic material behaviour of spheres [81, 82]. The collision process is divided into three cycles: the first loading phase assumes elastic material behaviour according to Hertz Theory, and then the contact becomes ideal plastic after reaching the yield point. Finally, in the unloading phase, the force-displacement behaviour follows a non-linear elastic pattern. Despite their differences, all hysteretic models share the common characteristic of generating permanent deformations of the materials in contact. The thesis focuses on viscoelastic collisions, which do not result in any plastic deformation of the objects involved. Hence, a comprehensive discussion of the various hysteretic contact models was not provided. Interested readers are encouraged to refer to the cited literature for further information and understanding of the topic.

#### *Discrete and Finite Element Method*

The Discrete Element Method (DEM) and Finite Element Method (FEM) can be utilized to model sphere collisions in particle impact dampers. In DEM, particles interact dynamically and reach states of equilibrium when internal forces are balanced. This method traces the movements of individual particles to determine the contact forces and displacements of a stressed particle assembly. Numerically, DEM employs a time-stepping algorithm, assuming constant velocities and accelerations within each timestep, which is similar to the explicit finite-difference method for continuum analysis. DEM operates under the assumption that the timestep is small enough that disturbances cannot propagate further than immediate neighbours during a single timestep. Hence, in every case, the forces exerted on a particle are solely governed by its interactions with other particles in contact. The discrete Element Method (DEM) employs a cyclical process of applying Newton's second law to particles and a force-displacement relationship at contact points. The motion of individual particles is governed by Newton's second law, which takes into account both contact and body forces. Simultaneously, the force-displacement law is utilized to update the contact forces based on the relative motion occurring at each contact point [84, 85, 86, 87]. The DEM represents the material as a collection of particles that interact with each other via contact forces. This method is a perfect approach for problems involving the analysis of the dynamics of a

PID damper consisting of multiple elements (spheres). It turns out that many authors use the Discrete Element Method to describe the effectiveness of PID dampers, and their results are described in [88, 89, 90, 91, 92]. While particles of arbitrary shapes can be used, spherical particles are commonly used for their simplicity and computational efficiency. However, the collision of particles is a time-dependent process that involves the deformation of the particles due to contact. In some cases, this deformation cannot be treated as purely elastic, especially in ductile materials like metals [93]. As a result, interparticle penetration must be considered in the contact model of the DEM.

FEM is commonly used to model continuous materials that can be described by continuum mechanics, such as metals and plastics. It models the material as a continuous field of interconnected elements, enabling the analysis of stress and strain under different loading conditions. FEM is useful for simulating sphere behaviour during collisions as it accurately predicts stresses and strains that occur in the material, facilitating the design of structures that can withstand such stresses and strains [94, 95, 96]. To simulate more complex systems and materials, coupled DEM-FEM methods combine both approaches by exchanging information between the continuum and discrete domains at their interface. These methods are useful tools for modelling complex systems, such as rock fragmentation during blasting, granular flow in silos, and composite material behaviour, and designing more efficient materials and structures [97, 98, 99, 100].

The accomplishments of Rojek and his research team are worthy of special recognition for their comprehensive numerical and experimental analyses that include a detailed implementation of plastic phenomena in both the Discrete Element Method and the Finite Element Method [101, 102, 103, 104, 105]. In their papers, they addressed a variety of issues such as high-velocity impacts of copper particles, rigid-soft particle mixtures, multi-scale analysis, thermal conductance effects of sintered particles, 3D formulation of deformable structures, particle-reinforced composites, and intermetallic matrix composite manufacturing. Undoubtedly, these studies offer the potential for sophisticated DEM computations, allowing for the analysis of very complex issues that can not be resolved using simplified contact models.

### *Multiscale contact modelling*

Multiscale modelling is a very interesting approach which involves connecting different models in various scales or descriptions of matter and improving information about the phenomenon being studied. An example of a multiscale problem is the interaction between rough surfaces with various geometric characteristics at different scales, from the shape of touching objects to atomic fluctuations on nanoscale surfaces. Earthquakes exemplify a multiscale problem in time, where accumulated stresses over years are released within seconds, causing seismic waves. Spatial multiscale problems are more challenging to model than time multiscale problems because time is one-dimensional [106]. Many researchers have been inspired by the multiscale problem, leading to a variety of theoretical and computational studies with the aim of expanding diagnostic capabilities. Studies presented in [107] include the approach of the diagnosis of bearings using coupled electromechanical phenomena and the thermo-mechanical phenomena which allow exchanging of heat during collisions. Multiscale contact modelling theory provides a detailed understanding of various phenomena, such as the stress-strain response in shape memory alloys [108], identifying material parameters and traction field for soft bodies [109], examining the effects of friction and deformations in lubricated soft contacts [110, 111], and investigating spurious softening in the macroscopic response of elastic-viscoplastic composites [112].

### *Leidenfrost effect*

An interesting phenomenon to describe is the Leidenfrost effect, which is used to model the behaviour of grains in a specific range of operations. Researchers observed a phenomenon that a liquid droplet can hover over a solid surface with a thin layer of vapour forming between them when the solid is heated to a temperature much higher than the boiling point of the liquid. This phenomenon, known as the Leidenfrost effect, prevents the liquid from boiling and instead causes slow evaporation due to the insulating effect of the vapour film [113]. Lei was inspired by this effect and studied the granular Leidenfrost effect in vibrated beds with bumpy surfaces, discovering that under sufficiently high vibration conditions, the entire granular bed can levitate above the vibrating base. The occurrence of the Leidenfrost state gives rise to an unequal energy distribution among particles, creating a disparity between those in close proximity to the vibrating base and those within the bulk material. Zhang [114] further investigated

the rheological behaviour and optimal damping effect of granular particles in experiments. This approach provides an optimal way to explore the relationship between the Leidenfrost effect and characteristic parameters to improve damping performance [115, 116, 117, 118].

## Conclusions

The literature review provided an opportunity to explore several models which explain the contact forces arising during collisions. These models include diverse dependencies that allow them to describe a wide range of physical phenomena, from simple to complex. To develop a numerical model of the ATPID damper, it was essential to choose an appropriate model for this problem. However, it was discovered that the granulate and silencer housing materials have nonlinear physical properties. Hence, the linear model (Eq. 3.8) would not be suitable. Conversely, Hertz's model (Eq. 3.9) considers only elastic components. To address these limitations, a non-linear viscoelastic model, derived in [78] (Eq. 3.12), was selected. This model builds upon Hertz's contact theory and includes the ability to describe viscous phenomena, which are crucial in understanding the ATPID damper's behaviour.

## 3.2 Numerical model of the ATPID damper

The collisions between the particle and container walls and the resulting energy dissipation are the key phenomena in PID modelling. Characterization of the contact force in terms of grain overlap and overlap rate forms the basis of the soft contact theory. The effects of elastic repulsion and viscous dissipation are included in the description of the full spectrum of contact schemes based on these two factors. Hertz Theory is primarily used to define the contact force, both linearly and nonlinearly. A soft contact model has been chosen for the research because it more accurately captures the physical consequences of grain collisions while incurring a higher computational cost.

A comprehensive mathematical explanation of contact mechanics is necessary to understand the phenomena of the interaction of two bodies. Hertz proposed a few fundamental laws that describe an elastic contact [74]. Hertzian contact theory, in particular, enables analysis of the interaction between a specimen's flat surface and a sphere-shaped indenter, where the definition of the radius of the contact circle  $a$  is

calculated as:

$$a^3 = \frac{3RF_c}{4E_{eff}} \quad (3.13)$$

where  $R$  is the indenter radius,  $F_c$  is the indenter force and  $E_{eff}$  is the effective Young's modulus of the specimen and indenter defined as:

$$\frac{1}{E_{eff}} = \frac{1 - \nu_w^2}{E_w} + \frac{1 - \nu_p^2}{E_p} \quad (3.14)$$

where  $E_w$  is the specimen Young's modulus,  $E_p$  is the indenter Young's modulus,  $\nu_w$  is the specimen Poisson's ratio and  $\nu_p$  is the indenter Poisson's ratio. Subscripts  $w$  and  $p$  correspond to the container wall and particle (grain), respectively. Hertz also described the overlap  $\xi$  in terms of radius of contact circle  $a$  and indenter radius  $R$ :

$$\xi = \frac{a^2}{R} \quad (3.15)$$

By using Eq. 3.13 and Eq. 3.15, the overlap can be written as:

$$\xi^3 = \left( \frac{3}{4E_{eff}} \right)^2 \frac{F_c^2}{R} \quad (3.16)$$

The transformation of the Eq. 3.16 allows obtain final definition of the elastic contact force:

$$F_c = \frac{4}{3} E_{eff} \sqrt{R} \xi^{\frac{3}{2}} \quad (3.17)$$

In most cases when two bodies collide, viscoelastic characteristics are present and have to be taken into account simultaneously throughout the modelling process. Therefore, Hertz elastic contact force is extended by an extra viscous component to explain the general form in such a situation:

$$F_c = \frac{4}{3} E_{eff} \sqrt{R} \xi^{\frac{3}{2}} + \alpha \dot{\xi} \quad (3.18)$$

where  $\alpha$  is a damping factor and  $\dot{\xi}$  is an overlap rate. According to the classical theory of the mechanical systems oscillations, the damping factor  $\alpha$  can be expressed as a function of the system damping ratio  $\beta$ , mass  $m$  and stiffness  $k$ :

$$\alpha = 2\beta\sqrt{km} \quad (3.19)$$

Following the approach proposed by Tsuji [78], the stiffness  $k$  can be expressed as:

$$k = \frac{4}{3}E_{eff}\sqrt{R}\xi^{\frac{1}{2}} \quad (3.20)$$

By using Eqs. 3.18 - 3.20, a viscoelastic force can be found:

$$F_c = \frac{4}{3}E_{eff}\sqrt{R}\xi^{\frac{3}{2}} + 2\beta\sqrt{\frac{4}{3}E_{eff}\sqrt{R}\xi^{\frac{1}{2}}m\dot{\xi}} \quad (3.21)$$

By introducing reduced parameters of effective stiffness  $k_{eff}$  and damping  $c_{eff}$  :

$$k_{eff} = \frac{4}{3}E_{eff}\sqrt{R} \quad (3.22)$$

$$c_{eff} = 2\beta\sqrt{k_{eff}m} \quad (3.23)$$

the following formula may be used to define the viscoelastic contact force as:

$$F_c = k_{eff}\xi^{\frac{3}{2}} + c_{eff}\dot{\xi}\xi^{\frac{1}{4}} \quad (3.24)$$

The ATPID damper is represented in the proposed method as a system composed of a container and a single particle (grain), see Fig. 2.7. The primary assumption of the mathematical model is that both the grain movement and the absorber motion occur in the same direction. This implies that the model ignores a particle's motion (and associated contact forces) in a direction perpendicular to the motion of the absorber. The only form of contact that takes place in the ATPID damper, as was previously indicated, is the grain-container contact. Two contact forces grain - floor  $F_{c_1}$  and grain - ceiling  $F_{c_2}$  - appear as a result.

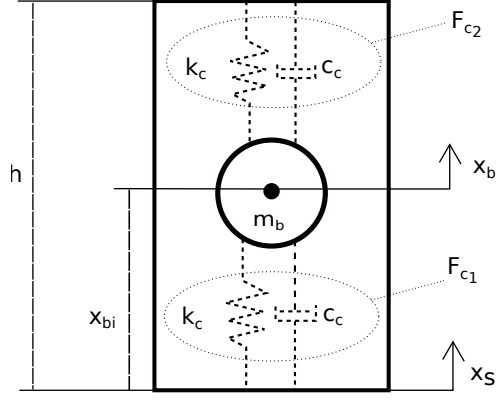


Figure 3.1: Mathematical basic model of the ATPID damper

A nonlinear contact model is used to characterize the contact forces (Eq. 3.24). The forces  $F_{c1}$  and  $F_{c2}$  in the proposed approach are defined as functions of grain overlaps ( $\xi_{c1}$  and  $\xi_{c2}$ ) and overlaps rates ( $\dot{\xi}_{c1}$  and  $\dot{\xi}_{c2}$ ) as follows:

$$F_{c1} = k_c \xi_{c1}^{3/2} + c_c \dot{\xi}_{c1} \xi_{c1}^{1/4} \quad (3.25)$$

$$F_{c2} = k_c \xi_{c2}^{3/2} + c_c \dot{\xi}_{c2} \xi_{c2}^{1/4} \quad (3.26)$$

where:  $\xi_{c1}$ ,  $\dot{\xi}_{c1}$  - overlap and overlap rate of the grain during the floor impact,  $\xi_{c2}$ ,  $\dot{\xi}_{c2}$  - overlap and overlap rate of the grain during the ceiling impact,  $k_c$  - reduced effective stiffness,  $c_c$  - reduced effective damping. The grain-container reduced effective stiffness is calculated using geometrical parameters and elastic material properties of grain and container walls, according to Eq. 3.22:

$$k_c = \frac{4}{3} E_{eff} \sqrt{r} \quad (3.27)$$

where  $r$  is the grain radius and effective Young's modulus is given by Eq. 3.14. The reduced damping parameter  $c_c$  is determined according to Eq. 3.23, assuming a critical damping condition ( $\beta = 1$ ) and mass of the grain  $m_g$ :

$$c_c = 2\sqrt{k_c m_g} \quad (3.28)$$

Analysis of Eqs. 3.25 and 3.26 demonstrate that prescribed contact forces can have negative values for particular stiffness and damping parameter values. By restricting the overlap value during the rebound of the grain from each container wall, only

positive values of contact forces are evaluated, hence eliminating the aforementioned non-physical effect in further computations.

Assuming the controllable container height  $h$ , its velocity  $\dot{h}$ , the initial position of grain  $x_{g_i}$ , its radius  $r$ , displacement of the container  $x_s$ , displacement of grain  $x_g$ , velocity of the container  $\dot{x}_s$ , and velocity of the grain  $\dot{x}_g$ , the overlaps and overlap rates can be described by the following equations:

$$\xi_{c_1} = \begin{cases} -x_{g_i} + r + x_s - x_g & \text{if } -x_{g_i} + r + x_s - x_g > 0 \\ 0 & \text{if } -x_{g_i} + r + x_s - x_g \leq 0 \end{cases} \quad (3.29)$$

$$\dot{\xi}_{c_1} = (\dot{x}_s - \dot{x}_g) \text{sgn}(\xi_{c_1}) \quad (3.30)$$

$$\xi_{c_2} = \begin{cases} x_{g_i} + r + x_g - x_s - h & \text{if } x_{g_i} + r + x_g - x_s - h > 0 \\ 0 & \text{if } x_{g_i} + r + x_g - x_s - h \leq 0 \end{cases} \quad (3.31)$$

$$\dot{\xi}_{c_2} = (\dot{x}_g - \dot{x}_s - \dot{h}) \text{sgn}(\xi_{c_2}) \quad (3.32)$$

Taking into account the definitions of the overlaps Eq. 3.29, Eq. 3.31 and overlaps rates Eq. 3.30, Eq. 3.32 the definitions of both contact forces for the case of positive overlaps take the form:

$$F_{c_1} = k_c(-x_{g_i} + r + x_s - x_g)^{3/2} + c_c(\dot{x}_s - \dot{x}_g)(-x_{g_i} + r + x_s - x_g)^{1/4} \quad \text{if } \xi_{c_1} > 0 \quad (3.33)$$

$$F_{c_2} = k_c(x_{g_i} + r - h + x_g - x_s)^{3/2} + c_c(\dot{x}_g - \dot{x}_s - \dot{h})(x_{g_i} + r - h + x_g - x_s)^{1/4} \quad \text{if } \xi_{c_2} > 0 \quad (3.34)$$

A changeable ATPID height  $h$  is one of the most innovative and interesting elements of the model. Eq. 3.34 reveals a nonlinear relationship between time-dependent damper height, its time-derivative, and upper contact force  $F_{c_2}$  as well as their effect on the damper response. Let us take notice that the particle velocity after collision with the damper ceiling is influenced by the ATPID height, and how this indirectly impacts the value of the lower contact force  $F_{c_1}$ .

The ceiling's minimal position,  $h_{min}$ , the ceiling's controllable range of movement,  $\Delta h$ , and the dimensionless control function,  $0 < \psi < 1$ , which describe the features of the admissible changes, are used to define the function of damper container height:

$$h = h_{min} + \Delta h \psi \quad (3.35)$$

A real movement of the damper height controlling element may be described by the control function  $\psi$  of the arbitrary form. In the considered case, a linear control function with two distinct tuning times will be used. The practical aspects of system implementation also contribute to the application of the linear modification of the damper height. The technique used to adjust the position of the container ceiling during experimental tests directly affects the suggested control function. The damper ceiling's position changes linearly as a result of the motor's constant current output as follows:

$$\psi = \begin{cases} 0 & \text{if } t < t_1 \\ \frac{t-t_1}{\Delta t_{12}} & \text{if } t_1 < t < t_2 \\ 1 & \text{if } t > t_2 \end{cases} \quad (3.36)$$

where:  $t$  - control time,  $t_1$  - activation start time,  $t_2$  - saturation start time,  $\Delta t_{12} = t_2 - t_1$  - activation period.

Finally, the whole model of the ATPID damper incorporates the definition of generated force obtained using the contact forces specified by Eqs. 3.33 and 3.34 as well as the equation of grain motion:

$$F_{ATPID} = -F_{c_1}(x_s, x_g, \dot{x}_s, \dot{x}_g) + F_{c_2}(x_s, x_g, \dot{x}_s, \dot{x}_g, h, \dot{h}) \quad (3.37)$$

$$m_g \ddot{x}_g - F_{c_1}(x_s, x_g, \dot{x}_s, \dot{x}_g) + F_{c_2}(x_s, x_g, \dot{x}_s, \dot{x}_g, h, \dot{h}) + Q_g = 0 \quad (3.38)$$

where the gravity force of the grain is  $Q_g$ . To determine the displacement of the grain  $x_g$  and contact forces resulting from applied kinematic excitation generated by displacement  $x_s$ , the equation of grain motion has to be solved. The ATPID absorber's force may be calculated using Eq. 3.37. Thus, both equations are required to determine the response of the damper under arbitrary kinematic excitation.

Fig. 3.2 shows the 2-DOF soft contact model of the mechanical system used in the

numerical tests. The proposed model's governing equations and initial conditions are provided by Eqs. 3.43.

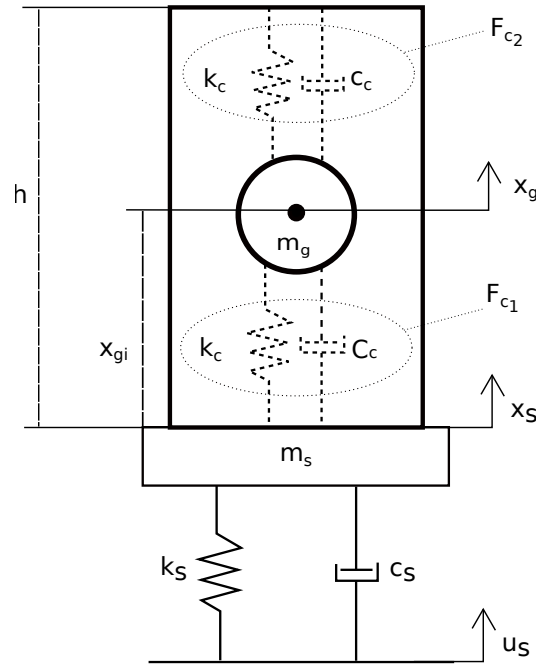


Figure 3.2: Scheme of the ATPID damper

$$m_s \ddot{x}_s + F_{ext} - F_{ATPID}(x_s, x_g, \dot{x}_s, \dot{x}_g, h, \dot{h}) + Q_s = 0 \quad (3.39)$$

$$m_g \ddot{x}_g + F_{ATPID}(x_s, x_g, \dot{x}_s, \dot{x}_g, h, \dot{h}) + Q_g = 0 \quad (3.40)$$

$$\dot{x}_s(t=0) = 0 \quad x_s(t=0) = -\frac{(m_s + m_g)g}{k_s} \quad (3.41)$$

$$\dot{x}_g(t=0) = 0 \quad x_g(t=0) = -\frac{(m_s + m_g)g}{k_s} + x_{gi} \quad (3.42)$$

$$F_{ext} = k_s[x_s - u_s] + c_s[\dot{x}_s - \dot{u}_s] \quad (3.43)$$

The model contains the beam (primary system) parameters:  $m_s$  - reduced mass,  $k_s$  - reduced stiffness,  $c_s$  - reduced damping,  $\ddot{x}_s$  - beam acceleration,  $\dot{x}_s$  - beam velocity,  $x_s$  - beam displacement,  $Q_s = m_s g$  - beam gravity force; the grain parameters:  $m_g$  - grain mass,  $\ddot{x}_g$  - grain acceleration,  $\dot{x}_g$  - grain velocity,  $x_g$  - grain displacement,  $x_{gi} = r$  - ini-

tial position of the grain in the container,  $Q_g = m_g g$  - grain gravity force;  $g$  - gravity; and excitation parameters:  $\dot{u}_s$  - support velocity,  $u_s$  - support displacement. Moreover,  $F_{\text{ATPID}}$  is a total force generated by the ATPID damper defined by Eq. 3.37.

At the beginning of the simulations, the system achieves a static equilibrium due to the provided initial conditions. To get the beam's oscillations around the initial equilibrium point, the displacements of the beam, container, and grain are shifted by  $x_s(t = 0)$ .

The function defining the motion of the structural support defines the applied kinematic excitation as:

$$u_s = A \sin(2\pi f t) \quad (3.44)$$

where the resonance frequency  $f$  depends on mass  $m_s$  and  $m_g$  as follows:

$$f = \frac{\sqrt{k_s}}{2\pi\sqrt{m_s + m_g}} \quad (3.45)$$

and amplitude of excitation  $A = 10$  [mm].

The modelling of the dynamic response of the system subjected to the aforementioned excitation includes phenomena like multiple grain-wall collisions, which are characterized by very short duration times and are represented by the nonlinear contact model. Therefore, a numerical solution to the equations of motion is required, together with a thorough evaluation of its correctness. The numerical techniques used in practice included the Implicit Rosenbrock third-fourth order Runge-Kutta method (Rosenbrock), Cash-Karp fourth-fifth order Runge-Kutta method (CK45), Fehlberg fourth-fifth order Runge-Kutta method (RKF45), and Livermore Solver for Ordinary Differential Equations (LSODE). A series of computations in the MAPLE program showed that when the absolute error tolerance and relative error tolerance are very small and near to  $10^{-10}$ , the results obtained using different approaches are comparable.

The next part of the dissertation will concentrate on the various aspects of grain and container variables, including generated contact forces, system kinematics, and the consequent effectiveness of vibration damping, which affects the system's response. Such parameters are supplied as tables at the beginning of each simulation.

### 3.3 Validation of the numerical model

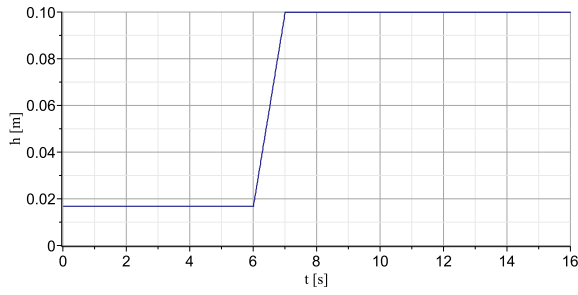
The results of basic experimental tests and numerical simulations using the system's reduced parameters were carefully compared to each other in order to confirm the mathematical model given by Eqs. 3.39 - 3.43. In the numerical simulations experimental component, a cantilever beam with mass  $m_b = 0.36$  [kg], was reduced to to the 1-DOF system. A conventional method was used to determine the reduced stiffness  $K_s$  associated with the first mode of vibrations. By performing a spectrum analysis on experimentally observed free vibrations of the tested object, the system's natural frequencies were identified. In order to provide the estimated reduced stiffness with an accurate value of the first natural frequency (3.02 [Hz]), the reduced mass was computed as  $m_s = 0.905m_b$ . In addition, to achieve comparable computational and experimental amplitudes of the free vibrations reduced damping  $C_s$  was found.

Finding the grain's reduced mass,  $m_g$ , was the next step in the modelling process. The initial natural frequency in the experimental investigation was assumed to be 2.862 [Hz] and 2.944 [Hz], respectively, and the mass of the grain was considered to be 10% and 5% of the total mass of the tested system. The decreased mass of the grain was considered to be 10% and 5% of the total mass of the reduced system in the numerical example, which produced identical results for the first system eigenfrequencies equal to 2.868 [Hz] and 2.947 [Hz], respectively. Physical characteristics of the reduced tested object ( $k_s, c_s, \nu_w, \nu_p, E_w, E_p$ ) are either known physically or computed based on preliminary experiments and are shown in Table 3.1.

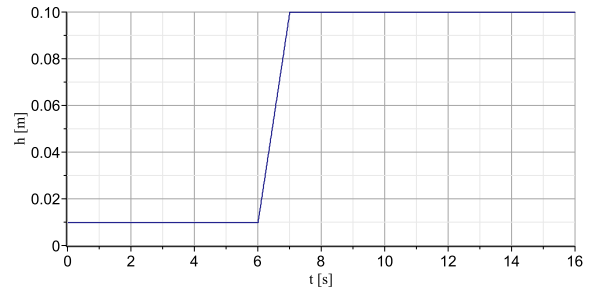
Table 3.1: Basic simulations parameters

$k_s$	$c_s$	$\nu_p = \nu_w$	$E_w = E_p$
117.6 [ $\frac{N}{m}$ ]	0.56 [ $\frac{Ns}{m}$ ]	0.2	$2.1 \cdot 10^8$ [Pa]

The damper activation start time  $t_1 = 6$  [s] and the activation period  $\Delta t_{12} = 1$  [s] were used to determine the assumed control function  $\psi$ . Eq. 3.35 assumes two different minimum heights for the controllable damper: 0.01 [m] for grain mass equal to 0.05M (Fig. 3.3a) and 0.017 [m] for grain mass equal to 0.1M (Fig. 3.3b). The minimum damper heights correspond to the different sizes of the grains. The maximum container height ( $h_{max}$ ) in both cases was equal to 0.1 [m].



(a)  $h_{min} = 0.01 \text{ m}$ ,  $m_g = 0.05M_s$



(b)  $h_{min} = 0.017 \text{ m}$ ,  $m_g = 0.1M_s$

Figure 3.3: Assumed changes of controllable damper heights

Table 3.2 contains all other container and particle parameters required for the numerical test. The results of the simulations of system vibrations are shown in Figs. 3.4 and 3.5.

Table 3.2: Parameters used in simulations

$m_g [kg]$	$h_{min} [m]$	$h_{max} [m]$	$r [m]$	$k_c [\frac{N}{m^{3/2}}]$	$c_c [\frac{Ns}{m^{5/4}}]$
0.05M	0.01	0.1	0.05	$1.031 \cdot 10^7$	841
0.1M	0.017	0.1	0.085	$1.344 \cdot 10^7$	1395.3

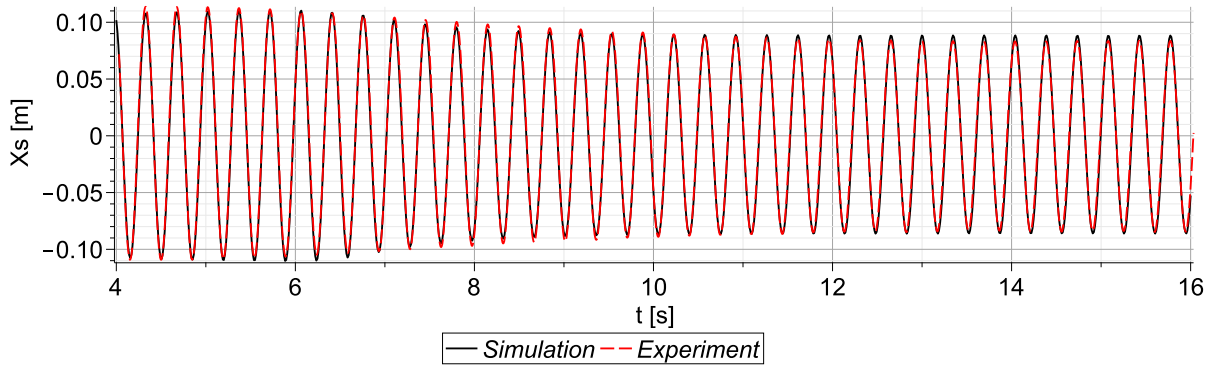


Figure 3.4: Comparison of the experimental and numerical results,  $m_g = 0.05M_s$

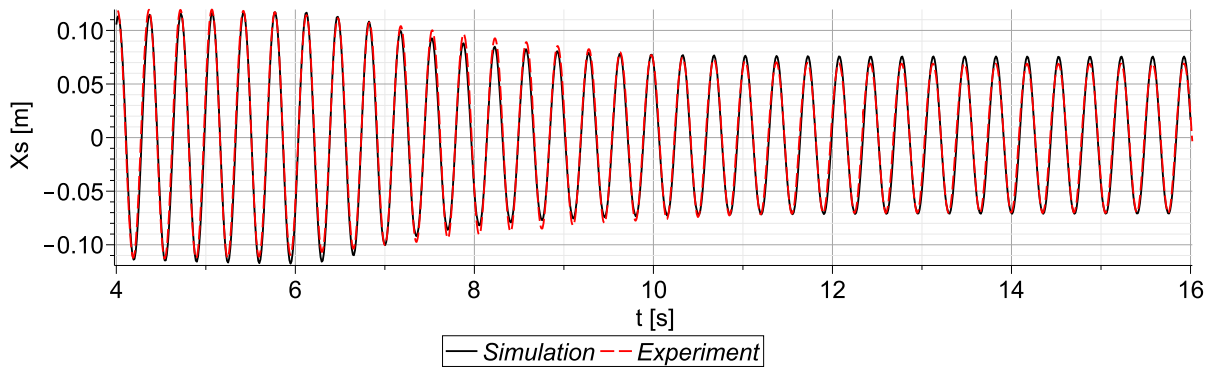


Figure 3.5: Comparison of the experimental and numerical results,  $m_g = 0.1M_s$

The three primary stages of the beam's response to the proposed harmonic excitation are as follows:

- The first stage when the grain is initially blocked ( $h = h_{min}$ ), the vibration becomes resonant and stabilizes in the range of  $4[s] < t < 6[s]$ .
- The second stage occurs when the controlling process is active and the damper ceiling rises to its highest point and the beam vibrations stabilize in the range of  $6.5[s] < t < 12[s]$ .
- The third stage, which occurs when beam vibrations are reduced and a steady-state is visible in the range  $12[s] < t < 14[s]$ .

For two alternative grain mass values, the presented results effectively validate the mathematical model. The displacement amplitudes derived from the experiments and numerical simulations closely match in both situations. The consistency between the two results also applies to different kinematic excitation amplitudes and frequencies. The above comparison shows that an operation of the ATPID damper can be effectively investigated using numerical simulations based on the proposed mathematical model.

The Root Mean Square Errors (RMSE) of the beam displacements corresponding to periods of the transient ( $6[s] < t < 10[s]$ ) and damped ( $t > 10[s]$ ) vibrations for each simulation  $X_{Sim}$  and experimental  $X_{Exp}$  result were determined using the following formula.

$$RMSE = RMS\left(\frac{X_{Exp} - X_{Sim}}{X_{Exp}}\right) \quad (3.46)$$

The aforementioned parameter was computed for five different grain masses (1%, 2.5%, 5%, 10%, and 20%), as well as for a range of stimulation frequencies (0.9, 0.95, 1, 1.05, and 1.1 of resonance frequency value). For various transient vibrations, the values of the RMSE of beam displacements are shown in Table 3.3 and for various steady-state damped vibrations, in Table 3.4. The proposed approach made it possible to show the consistency between the simulation and experiment when the grain impacts both container walls at resonance and in its near area.

Table 3.3: RMSE comparison of vibrations in transient range

	$0.9f_{res}$	$0.95f_{res}$	$f_{res}$	$1.05f_{res}$	$1.1f_{res}$
0.01M	0.016	0.079	0.059	0.062	0.019
0.025M	0.018	0.09	0.067	0.7	0.025
0.05M	0.019	0.1	0.075	0.079	0.032
0.1M	0.022	0.115	0.084	0.089	0.035
0.2M	0.027	0.129	0.094	0.101	0.039

Table 3.4: RMSE comparison of vibrations in steady-state range

	$0.9f_{res}$	$0.95f_{res}$	$f_{res}$	$1.05f_{res}$	$1.1f_{res}$
0.01M	0.019	0.087	0.075	0.08	0.023
0.025M	0.019	0.079	0.07	0.073	0.02
0.05M	0.018	0.073	0.064	0.067	0.017
0.1M	0.015	0.067	0.058	0.062	0.015
0.2M	0.012	0.061	0.053	0.057	0.014

According to the results shown in Tables 3.3 and 3.4, the RMSE of experimental and numerical system response for resonant excitations are similar in both of the assumed ranges, and they are 0.059 to 0.094 for transient vibrations and 0.053 to 0.075 for steady-state vibrations. The ranges near resonance reveal an increase in the RMSE coefficient, but their values are also small (maximum 0.129 for a transient range, and maximum 0.087 for a steady-state range). The obtained results demonstrate the possibility of using the proposed mathematical model for further numerical analyses. The proposed 2-DOF soft contact model of the ATPID damper and cantilever beam was named as Complex Model and will be used in Chapter 4 to describe the novel Predictive Control Algorithm.

### 3.4 Detailed analysis of the ATPID damper operating principle

The examination of the proposed system's governing equations (Eqs. 3.39 and 3.40) reveals that the ATPID damper's behaviour is complex and requires further investigation. By integrating the relationship between contact forces derived from the equation of grain motion (Eq. 3.40) into the equation of system motion (Eq. 3.39), it is possible to acquire a better understanding of the dynamic process under investigation. The

resulting equation has two equivalent forms that can be written as:

$$(m_s + m_g)(\ddot{x}_s + g) - m_g \left( 1 - \frac{\ddot{x}_g + g}{\ddot{x}_s + g} \right) (\ddot{x}_s + g) + F_{ext} = 0 \quad (3.47)$$

$$(m_s + m_g)(\ddot{x}_s + g) + m_g(\ddot{x}_g - \ddot{x}_s) + F_{ext} = 0 \quad (3.48)$$

The initial state of the analyzed system is described by the first component of the Eqs. 3.47 and 3.48 where the grain cannot move inside the container ( $h_{max} = 2r$ ) and the total system mass is the sum of the masses of the basic structure and the grain ( $M = m_s + m_g$ ). Although the second component in both equations is the same, it can be interpreted in two separate ways as two alternative ATPID operation principles. The first term of the second component of Eq. 3.47 defines the Mass Modification Effect (MME), which denotes a change in system mass  $\Delta m$  caused by the presence of the moving and colliding grain. In comparison, the second component of Eq. 3.48 defines the Pseudo-Inertial Force Effect (PIFE), which involves the generation of auxiliary force  $F_{iner}$  produced by grain movement. The PIFE effect is used to demonstrate the mathematical relation and similarities between the ATPID damper and inerters, which are currently common mechanical systems that use inertial forces based on the relative accelerations of system components [119, 120]. Both of the aforementioned operational principles explain a change between three different possible system states.

The first system state the situation when the damper is closed or the situation when grain may move ( $h_{max} > 2r$ ), and is pushed by one of the container walls, correspond to the first system state, which happens when the accelerations of the container and the grain are approximately equal  $\ddot{x}_g \approx \ddot{x}_s$ . Both the component denoting mass modification in Eq. 3.47 and the term indicating inertial force in Eq. 3.48 are equal to zero under such conditions. As a result, the two degrees of freedom (2 - DOF) system can be substituted by the system with one degree of freedom (1 - DOF) system with mass  $M = m_s + m_g$ , which is governed by the equation:

$$(m_s + m_g)(\ddot{x}_s + g) + F_{ext} = 0 \quad (3.49)$$

The second system state is when the grain is free-flying and does not collide against the walls of the container ( $\ddot{x}_g = -g$ ). The terms indicating mass modification in Eq. 3.47

and inertial force in Eq. 3.48 are then equal:

$$\Delta m = -m_g, \quad (3.50)$$

$$F_{iner} = -m_g(\ddot{x}_s + g) \quad (3.51)$$

In this situation, the pseudo-inertial force term has an untypical form that includes the grain mass and system acceleration, while the mass modification term indicates a decrease in the total system mass by the grain mass ( $M = m_s$ ). As a result, the equivalent 1-DOF system is represented by the simple equation:

$$m_s(\ddot{x}_s + g) + F_{ext} = 0 \quad (3.52)$$

The third state, which corresponds to the phenomena of a short collision with the grain rebounding from the container wall, denotes the situation where the accelerations of the grain and container are considerably different ( $\ddot{x}_g \neq \ddot{x}_s$ ). Then, the terms representing mass modification in Eq. 3.47 and inertial force in Eq. 3.48 then assume general forms:

$$\Delta m = -m_g \left( 1 - \frac{\ddot{x}_g + g}{\ddot{x}_s + g} \right) \quad (3.53)$$

$$F_{iner} = m_g(\ddot{x}_g - \ddot{x}_s) \quad (3.54)$$

In such a case, the pseudo-inertial force component represents the short and quick change of additional force, while the mass modification term describes a short and rapid change of system mass. Both of these quantities depend on the grain's mass as well as grain and mass accelerations. Additionally, they can take positive or negative values depending on the grain-wall collision case. Mass modification parameters and pseudo-inertial components are fully described by the model defined by Eq. 3.47 and Eq. 3.48, respectively.

By taking into account and analyzing the spectrum of the system's free vibrations with an ATPID damper (Figs. 3.6 and 3.7), the MME effect can be identified. The following values are applied to all simulation parameters:  $m_s = 0.905m_b$ ,  $m_g = 0.1M$ ,  $k_s = 427.6[\frac{N}{m}]$ ,  $c_s = 0.56[\frac{Ns}{m}]$ ,  $\nu_p = \nu_w = 0.2$ ,  $k_c = 1.334 \cdot 10^7[\frac{N}{m^{3/2}}]$ ,  $c_c = 1395.3[\frac{Ns}{m^{5/4}}]$ ,  $E_p = E_w = 2 \cdot 10^8$  [Pa].

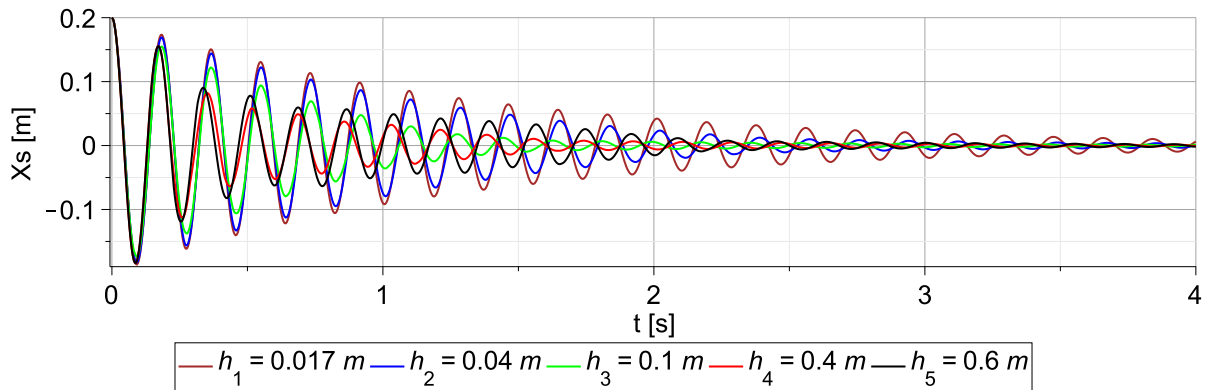


Figure 3.6: Free vibrations for various ATPID heights

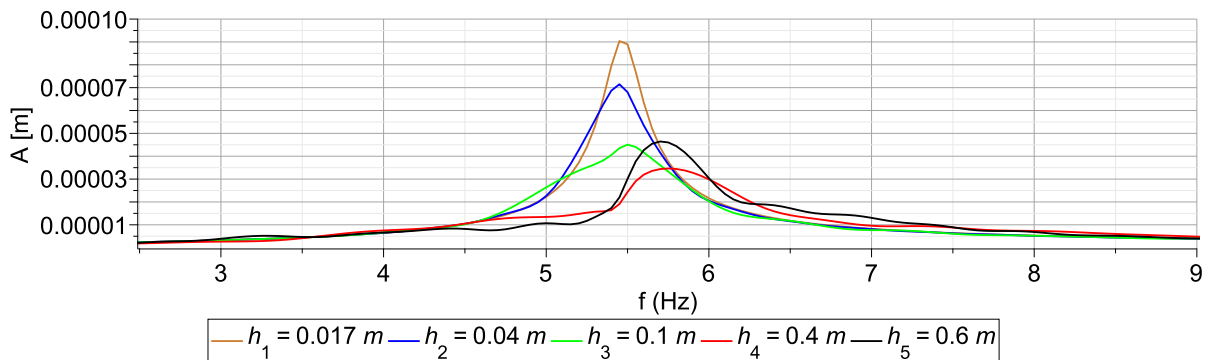


Figure 3.7: Spectrum of system free vibrations

One example of the MME is the spectrum change of the vibration spectrum. The natural frequency of the system's vibrations at a low container height ( $h = 0.017$  [m]) is  $f = 5.49$  [Hz], and results from the mass of the system's components, a beam, an ATPID compartment, and grain. The natural frequency of vibrations with a bigger container height ( $h = 0.4$  [m] or  $h = 0.6$  [m]) equals to  $f = 5.77$  [Hz] and refers to a system composed of a beam and a damper container with no grain. The dynamic features of the system are variable and depend on the damper ceiling position. For other situations of the container height, the natural frequencies are between above extreme values.

Moreover, the natural frequencies of the system for the two cases  $h_{max} = 0.4$  [m] and  $h_{max} = 0.6$  [m] ( $f = 5.77$  [Hz]) are comparable, however, the vibration amplitude for a larger container height is noticeably higher. It should be noted that while the effective mass of the system is identical to that demonstrated in the eigenfrequencies ( $f = 5.77$  [Hz]) for two situations of the container heights ( $h_{max} = 0.4$  [m] and  $h_{max} = 0.6$  [m]), the amplitude of the vibrations for a higher container height is noticeably bigger. The whole mechanics of the system (ATPID floor, ceiling, and grain displacements) for the two specified container heights were presented in Fig. 3.8 in an effort to identify the cause of the system's worse damping for higher container heights.

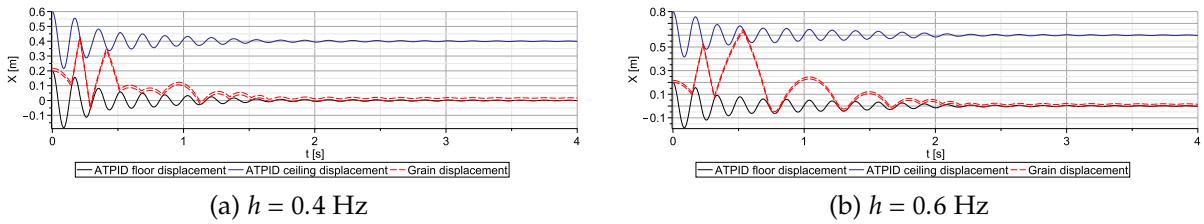


Figure 3.8: Damper (floor and ceiling) and grain movement for various container heights

In the situation  $h_{max} = 0.4$  [m], the grain regularly collides with the container's floor and ceiling during the first two vibration cycles. In contrast, when  $h_{max} = 0.6$  [m], the grain impacts happen irregularly throughout random process cycles. Because collisions take place over a longer period of time, the process presents better damping in the first case. Additionally, the Mass Modification Effect and the Pseudo-Inertial Force Effect (second components of Eqs 3.47 and 3.48), which become unpredictable and occur in random states of beam vibration, are responsible for worse damping abilities in the second case.

The ATPID's operating principle can be also understood by examining the change in system energy that occurs during the investigated process of free vibrations. The equation of beam motion (Eq. 3.39) can be integrated over its displacement in order to calculate the system's energy balance:

$$\int_{\Delta x_s} m_s \ddot{x}_s dx_s + \int_{\Delta x_s} F_{ext} dx_s + \int_{\Delta x_s} (F_{c1} - F_{c2}) dx_s + \int_{\Delta x_s} Q_s dx_s = 0 \quad (3.55)$$

By identifying the subsequent terms of Eq. 3.55 as the change of kinetic energy  $\Delta E_k^s$ , change of elastic energy  $\Delta E_{el}^s$ , viscous dissipation  $W_d^s$  and change of potential energy

$\Delta E_p^s$  the equation of the energy balance can be written in a form:

$$\Delta E_k^s + \Delta E_{el}^s + W_d^s + \int_{\Delta x_s} (F_{c_1} - F_{c_2}) dx_s + \Delta E_p^s = 0 \quad (3.56)$$

The total energy of the beam  $E_{tot}^s$  can be defined as a sum of kinetic  $E_k^s$ , elastic  $E_{el}^s$  and potential energy  $E_p^s$ , and according to Eq. 3.56, its change  $\Delta E_{tot}^s$  is caused by work done by contact forces generated in ATPID damper and viscous dissipation  $W_d^s$ :

$$\Delta E_{tot}^s = - \int_{\Delta x_s} (F_{c_1} - F_{c_2}) dx_s - W_d^s \quad (3.57)$$

The work done by contact forces produced in the ATPID damper has a significant impact on the change of the total beam energy and the efficiency of the vibration damping process since viscous dissipation is an uncontrollable process. Therefore, the study of the variations in the integral quantity will be the main focus of the following numerical examples. The work of the contact forces will be denoted by and given by the formulae:

$$W_{F_c}^s = - \int_{\Delta x_s} (F_{c_1} - F_{c_2}) dx_s = \int_{\Delta x_s} (F_{ATPID}) dx_s \quad (3.58)$$

has to be positive and possibly large in order to cause the decrease of total beam energy and efficient process of vibrations damping.

The plots presented in Fig. 3.9 reveal the change of work done by forces generated by ATPID damper  $W_{F_c}^s$  during the first impact of the grain against the lower container wall. The work is calculated between the initial time instant of contact and time instant of the permanent detachment of both objects.

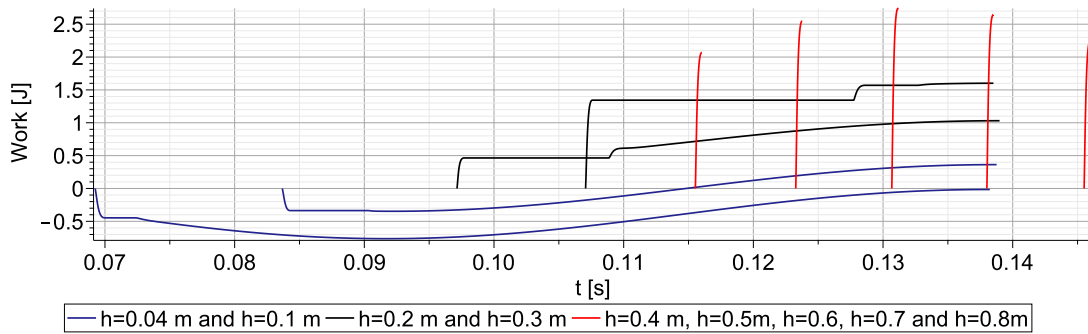


Figure 3.9: Change of work done by contact forces during the first impact of grain and container wall during the process of free vibrations for various container heights.

The first group of cases (navy lines) corresponds to extremely low damper heights ( $h_{max} = 0.04$  [m] and  $h_{max} = 0.1$  [m]), which results in the impact of the grain during the downward movement of the container when the directions of motion of both objects are the same. In such a case, after impact and a small grain rebound, both objects move together and then the grain is pushed by the bottom container wall. As a result, the contact force's initial effect on container displacement is negative, but it gradually improves during the second stage of impact when the grain is pushed upward. As a result, the total work performed by the contact force at the process' final time instant is close to zero or takes a small positive value.

The second group of examples (black lines) pertains to bigger damper heights ( $h_{max} = 0.2$  [m] and  $h_{max} = 0.3$  [m]) when grain impacts the container during upward movement of the container then the directions of the motion of the objects are opposite. In the first case, the second impact and the phase where the grain is pushed by the container wall come after a significant grain rebound. Contact forces perform larger work in both these processes. In contrast, in the second example, just a short pushing phase can be seen near the end of the process, and the second impact is similarly followed by grain rebound. Thus, the increase in energy happens mostly during the first impact and partially during the second impact. The work performed by contact forces is therefore significant in both cases.

The damper heights are the largest ( $h_{max} = 0.4$  [m],  $h_{max} = 0.5$  [m],  $h_{max} = 0.6$  [m],  $h_{max} = 0.7$  [m],  $h_{max} = 0.8$  [m]) in the third group of situations, which means that impact happens when the container is moving upward and at a relatively high velocity. In the studied cycle of vibrations, the grain impacts the bottom container wall, and then immediately strongly rebounds without subsequent contact with the cylinder bottom. In each situation taken into consideration, the contact forces' work increases for a short period of time when the bodies collide. As the container's pre-impact velocity increases, the change in work done by contact force raises, reaching its maximum value when the collision takes place close to the beam equilibrium state. In the following cases, when the height of the container is larger, the velocity of the container wall before the impact is lower and the work done by contact forces becomes smaller.

According to the previous study, the work done by contact forces is either close to zero or assumes a positive value after each impact, independently of the collision scheme, which is determined by the direction and velocity of the beam. The grain and walls of the damper can collide further for various grain and damper movement directions and velocities, but the three above described types of collisions are followed. As a result, the use of the ATPID damper always results in a reduction in system energy and an efficient process of vibration damping.

The total beam energy  $E_{tot}^s$  for each case was calculated in order to extend the investigation of the kinematic results provided in Fig. 3.6. The results are depicted in Figure 3.10. The plots enable a more in-depth analysis of the influence of various damper heights on vibration damping process during a longer period of time. When a collision between the grain and the container walls will occur when the grain is moving in the opposite direction than the beam. As a result of such impacts, the total beam energy is reduced thanks to the positive work done by the contact forces, effectively damping system vibrations. When the grain and the beam collide and both directions of the movement are the same, the work done by the contact forces temporarily decreases and the beam energy immediately increases. If collisions occur in the same direction of movement of the grain and beam, then the temporary increase in energy does not significantly affect the system's ability to attenuate, because as a result of the sticking effect in the next phase of the vibration, the energy of the system decreases.

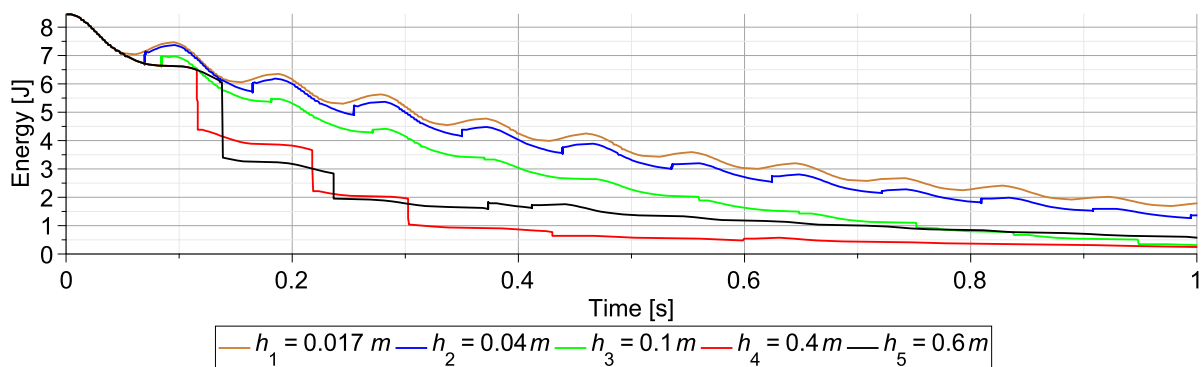


Figure 3.10: The total energy of the beam  $E_{tot}^s$  for various container heights

## 3.5 Sensitivity analysis

Eqs. 3.39 - 3.45 were used to determine the effects of various parameters (container height, grain mass, and excitation amplitude) on the dynamic response of the cantilever beam under harmonic excitation in order to analyze the sensitivity of the proposed damper. Fig. 3.11 shows the displacements of the free end of the beam during resonance excitation for various container heights. Additionally, grain, container floor, and ceiling displacements for different damper heights are shown in Fig. 3.12 and Fig. 3.13, for various grain mass in Fig. 3.14 and for various excitation amplitudes in Fig. 3.15.

### 3.5.1 Influence of the container height

The damper height is one of the most crucial system parameters from the vibrations attenuation point of view. Five different maximal container heights ( $h_1 \rightarrow h_5$ ) were considered in order to understand the differences in the system dynamic caused by the changing of the container ceiling position (Table 3.5). The system's dynamic response computed for such container heights is presented in Fig. 3.11. The remaining parameters of the functions  $h$  were constant and equal:  $h_{min} = 0.017$  [m],  $t_1 = 6.5$  [s],  $t_2 = 9$  [s] where mass of the grain is equal  $m_g = 0.1$ M and excitation amplitude  $A = 0.1$  [m].

Table 3.5: Parameters used in simulations

$$h_{max} \text{ [m]} \quad | \quad h_1 = 0.04 \quad | \quad h_2 = 0.08 \quad | \quad h_3 = 0.12 \quad | \quad h_4 = 0.16 \quad | \quad h_5 = 0.20$$

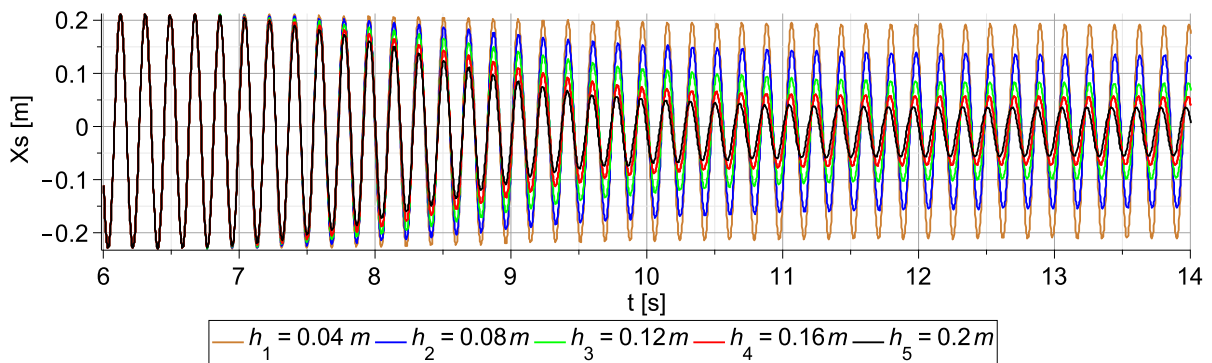


Figure 3.11: Displacements of the free end of the beam for various maximal container heights -  $h_1 \rightarrow h_5$

The container's maximum height determines the space available for grain movement, influences damping efficiency, and affects the vibration amplitudes of the damped system. As a result, in the ATPID control process, proper ceiling position tuning is required. The results shown in Fig. 3.11 reveal that there are considerable differences in the efficiency of vibration reduction obtained for various damper heights. The largest damping ( $h_5$ ) occurs when the maximum amplitude of the vibrations in the resonance range ( $x_s = 0.23$  [m]) is decreased by 78% and stabilizes at 0.048 [m]. Lower damping is evident for other examined maximal container heights  $h_4 \rightarrow h_1$ , and vibration amplitudes are reduced by 71%, 57%, 32%, and 5%, respectively.

The results of the simulations were used to determine the main reasons for the differences in vibration mitigation for various damper heights. Fig. 3.12 presents the grain, container floor, and ceiling displacements.

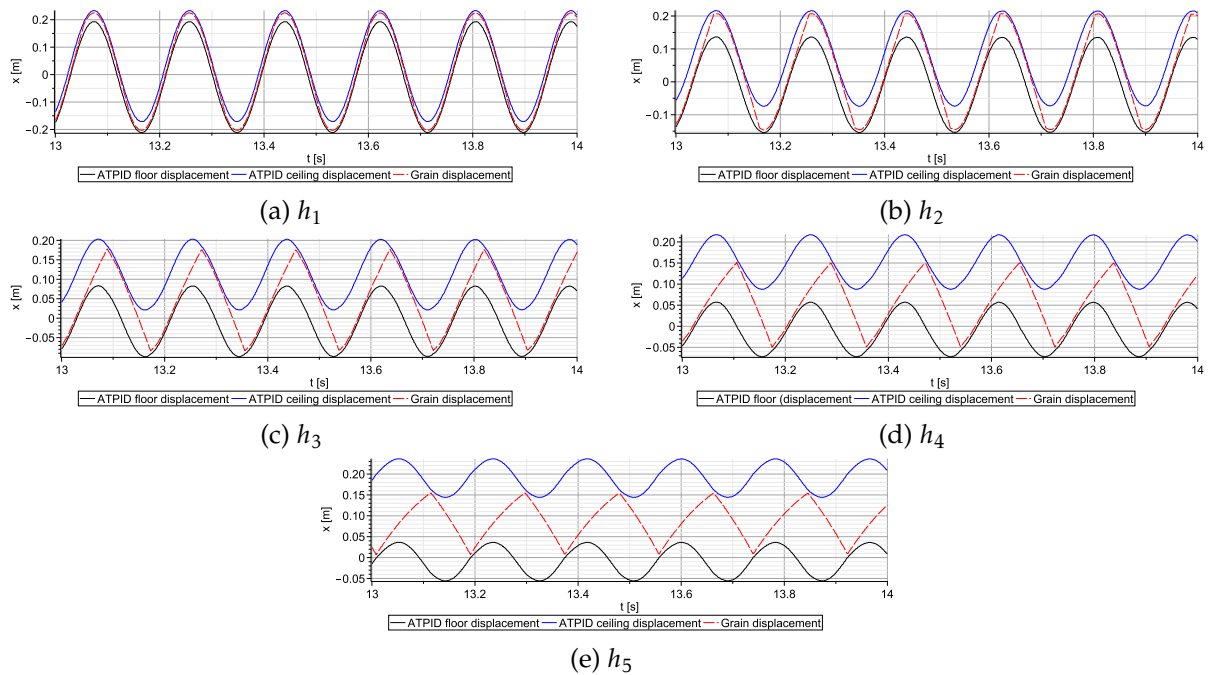


Figure 3.12: Damper (floor and ceiling) and grain displacement for various container heights ( $h_1 \rightarrow h_5$ )

For various ATPID container heights, the results are described in terms of the different forms of grain movement. The definitions of two impact types will be provided for the sake of clarification:

- When the grain is pushed by the container wall after impact and their velocities are identical, this is referred to as an impact with the sticking effect.

- The impact followed by an immediate grain rebound, in which the grain and wall move at significantly different rates, is what is known as a short impact without a sticking effect.

When the damper ceiling position ( $h_1=0.04$  [m],  $h_2=0.08$  [m],  $h_3=0.12$  [m]) is relatively low, the first type of ATPID operation takes place (Figs. 3.12a - 3.12c). In such a case the system response can be defined as a subsequent occurrence of the sticking effects between the grain and a lower or higher container wall, with intermediate non-contact periods of the grain movement being significantly shorter than the sticking stages. As a consequence, the system's effective mass and natural frequency are comparable to that of the closed damper. As a result, the ATPID's damping abilities are generally low, but they rise as the damper height increases.

The second type of operation occurs when the damper container is significantly higher ( $h_5=0.2$  [m]) and impacts without the sticking effect can be seen during every vibration cycle (Fig. 3.12e). As it was noted in the discussion of Eq. 3.47, the mass of the whole system is reduced significantly in this situation. As a result, the system's natural frequency is shifted into a new range, and the ATPID's damping abilities are much bigger than in the previously examined situations including the sticking effect (Figs. 3.12a - 3.12c). The sticking effect between the grain and the damper floor as well as the impact without a sticking effect between the grain and the container ceiling are both visible in Fig. 3.12d, which shows the third type of ATPID operation. The above analysis reveals that the ATPID damper is the most effective and the amplitudes of the steady-state vibrations are the smallest when only short grain-wall impacts (without sticking effect) occur in every period of vibrations (the second type of operation, Fig. 3.12e). The above conclusion is in agreement with a conclusion regarding ATPID effectiveness in damping of free vibrations, which was also the highest for the case of short grain impacts (cf. Figs. 3.6 and 3.7).

The following numerical simulations were conducted for the purpose of analyzing how the particle movement would change if the ceiling position were higher than previously assumed. Two damper heights were taken into consideration:  $h_6 = 0.3$  [m] and  $h_7 = 0.6$  [m]. Fig. 3.13 reveals grain as well as the ATPID floor and ceiling displacements.

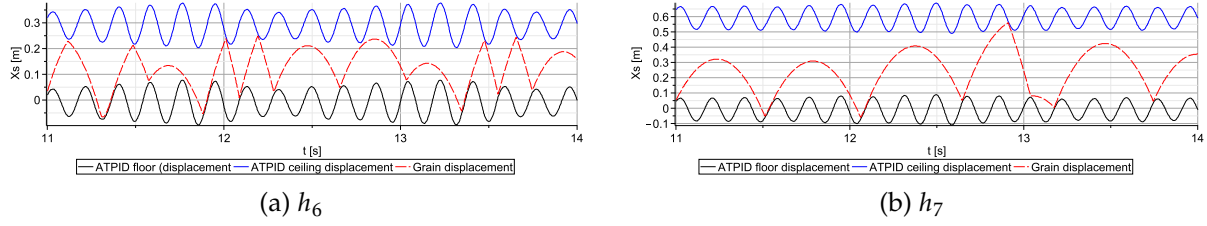


Figure 3.13: Damper (floor and ceiling) and grain movement for large container heights ( $h_6$  and  $h_7$ )

Focusing on the results, two novel ATPID operating principles random impacts and lack of ceiling impacts can be identified. The first type of operation (Fig. 3.13a) concerns a situation in which the grain collides with both the bottom and top wall of the container, but the collisions do not occur during every period of vibrations. When the particle can not reach the ceiling position and floor impacts do not occur during every vibration period, the second type of operation (Fig. 3.13b) occurs. Unpredictable grain movement within the container and low vibration damping efficiency are characteristic for both situations. Therefore, they are treated with as undesirable effects.

### 3.5.2 Influence of the grain mass

The calculation of the grain mass effect on the grain movement and the ATPID damping ability was another crucial component of the sensitivity analysis process. The particle mass  $m_g$  was assumed four different values:  $m_1 = 0.05M_s$ ,  $m_2 = 0.1M_s$ ,  $m_3 = 0.2M_s$ ,  $m_4 = 0.4M_s$ , where  $M = m_g + m_s$ . The excitation frequency for each case was computed under the assumption that it was a resonance frequency, according to the formula  $f = \sqrt{\frac{k_s}{m_g + m_s}}$ . The other parameters of the analysis were: the constant height of the damper  $h_{max} = 0.2$  [m] and the excitation amplitude  $A = 0.01$  [m]. The displacement of the damper floor, grain and damper ceiling are presented in Fig. 3.14.

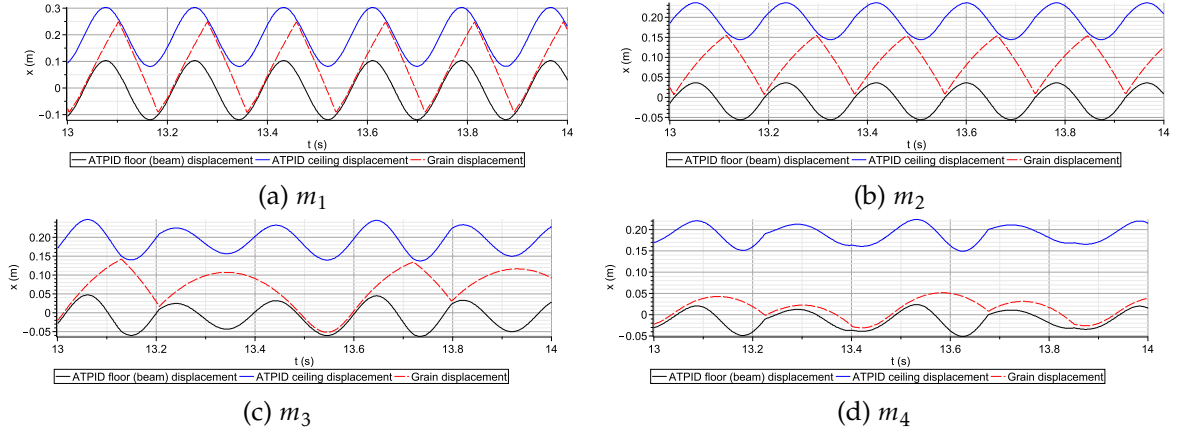


Figure 3.14: Damper (floor and ceiling) and grain movement for various grain mass ( $m_1 \rightarrow m_4$ )

The four previously described types of ATPID operation previously described can be observed for the proposed values of the grain mass ( $m_1 \rightarrow m_4$ ). The sticking effect between the grain and the damper floor or ceiling occurs for the proposed values of the system parameters for very low grain masses ( $m_1$ ) (Fig. 3.14a). A larger mass of the grain ( $m_2$ ) allows to observe the most effective system damping with the non-sticking contact of the grain with the damper walls (Fig. 3.14b). Further particle mass increase reveals the undesirable effect of random collisions (Fig. 3.14c), while even larger mass causes the situation when the grain-ceiling impacts do not occur (Fig. 3.14d). The analysis shows that grain mass significantly influences the type of grain movement, and that the ATPID height should be tuned for the selected grain mass.

### 3.5.3 Influence of the excitation amplitude

The amplitude and frequency of the excitation have an impact on the grain movement, ATPID's vibration damping ability, and the resulting displacement of the beam. In particular, the paper [64] in particular discusses different particle displacements as a function of a dimensionless acceleration factor dependent on the excitation amplitude. Here, I emphasize a simpler approach and take into account grain movement for four different excitation amplitudes:  $A_1 = 0.005$  [m],  $A_2 = 0.0075$  [m],  $A_3 = 0.01$  [m],  $A_4 = 0.02$  [m]. Each simulation assumes a constant damper height of  $h_{max} = 0.2$  [m] and a particle mass of  $m_g = 0.1M_s$ . Fig. 3.15 shows the displacements of the damper floor, ceiling, and grain.

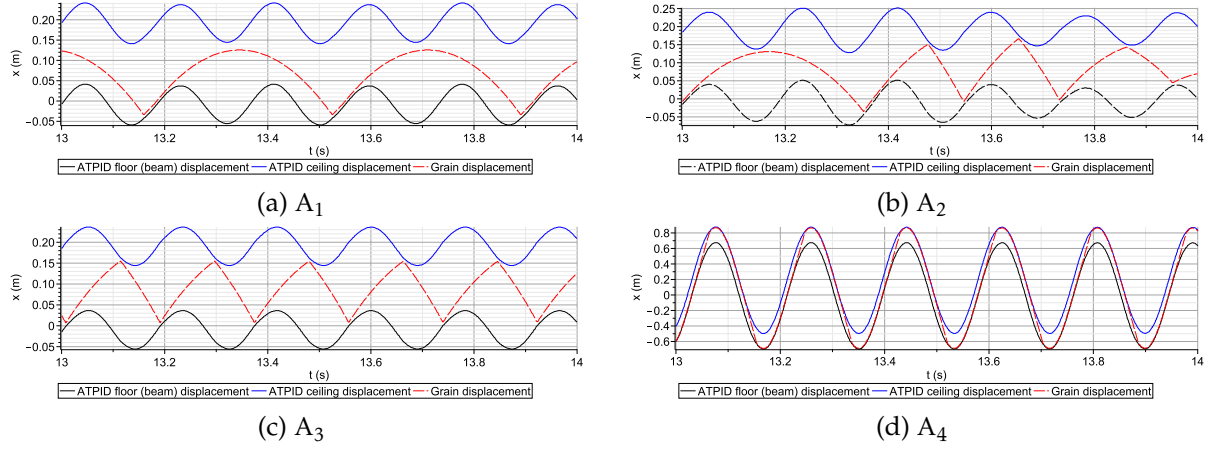


Figure 3.15: Damper (floor and ceiling) and grain movement for various excitation amplitudes ( $A_1 \rightarrow A_4$ )

The performed study reveals the same ATPID operation types as those in the previous cases of height and grain mass influence (Figs. 3.12, 3.13, 3.14)). For the low excitation amplitudes (Figs. 3.15a and 3.15b), the grain velocity and resulting beam acceleration at the end of each contact stage are too small to achieve the grain-ceiling impact (case  $A_1$ ), or the obtained impacts are irregular and unpredictable (case  $A_2$ ). However, Fig. 3.15c illustrates the favourable situation in which only impacts without a sticking effect are observed when grain mass and damper height are appropriately tuned to the analysed excitation amplitude. The velocity of the beam rises with increasing excitation amplitude, which also results in the undesirable sticking of the grain to the lower or upper ATPID wall.

Specific Damping Coefficient (SDC) is a parameter which allows to describe ATPID operation characteristics [121]. It can be defined as a ratio of the energy lost  $W(t_i)$  and initial energy  $E(t_i)$  per one cycle of vibrations:

$$\Psi(t_i) = \frac{W(t_i)}{E(t_i)} \quad (3.59)$$

Calculations for energy lost during a single vibration cycle include:

$$W(t_i) = E(t_i) - E(t_{i+1}) \quad (3.60)$$

The SDC calculations can be simplified by analyzing time instants when the system velocity equals zero, the associated kinetic energy disappears ( $E_k = 0$ ) and the total system energy equals the potential energy:

$$E(t_i) = \frac{kx(t_i)^2}{2} \quad (3.61)$$

By using Eq. 3.59, 3.60 and 3.61, one obtains the final formula for the SDC:

$$\Psi(t_i) = \frac{x(t_i)^2 - x(t_{i+1})^2}{x(t_i)^2} \quad (3.62)$$

For five different damper heights, the changes in the Specific Damping Coefficient for several cycles of beam vibrations during the unstable state of system operation ( $6[s] < t < 12[s]$ ) were calculated and presented in Fig. 3.16. The ATPID damping ability changes depending on the process time and container height, according to the SDC plots. The obtained results reveal that the damping ability for the lowest analysed container height  $h_1$  is negligible and that the highest damping efficiency is obtained for the container height  $h_5$ . In each case, the largest SDC value can be seen approximately in the middle of investigated damper activation period.

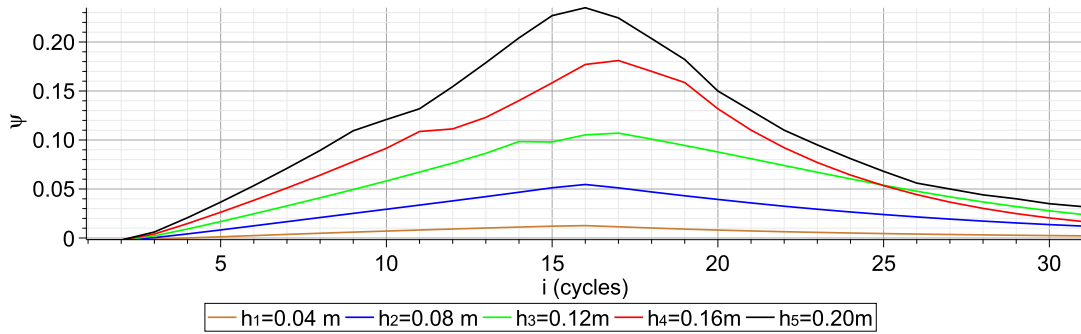


Figure 3.16: Specific Damping Coefficient of vibration during unsteady state of system operation

The SDC was also calculated for the ATPID damper heights equal to  $h_6 = 0.3$  [m] and  $h_7 = 0.6$  [m]. When the collisions between the grain and ceiling do not occur during every period of the vibrations, in such conditions, the unpredictability of collisions results in an unstable system response with oscillating vibration amplitudes. This is demonstrated by irregularly shifting Specific Damping Coefficients, which can take on positive or negative values.

The presented considerations prove that the appropriate choice of the damper height is crucial for the ATPID damping abilities and mitigation of the dynamic response of the considered system. This is a reason for proposing solutions in which it is possible to tune (in real time) the damper height and adapt it to the current system operation.

### 3.6 Energy analysis

The complex ATPID operation and the nonlinear influence of its parameters on damping ability were described in the previous sections. An energy analysis of the system must be carried in order to obtain a better understanding of the occurring physical processes. The section starts with an analysis of the grain-floor and grain-ceiling contact forces (Fig. 3.17), which play a crucial role in the changes in system energy. Further, I present the change of the total beam energy (Figs. 3.18 and 3.19), the entire system energy balance, which includes the work performed by the contact forces (Figs. 3.20 and 3.21) and the work produced by external excitation (Fig. 3.22).

#### 3.6.1 Overlaps, overlaps rates and contact forces

The nonlinear viscoelastic contact theory and the corresponding Eqs. 3.25 and 3.26 determine the grain-wall contact forces. Grain-wall overlaps and the rates of overlaps that occur during subsequent impacts are the parameters that are fundamentally important in the definition of the contact forces. The overlaps, overlaps rates, and contact forces in the study are presented in Fig. 3.17 for five different damper heights ( $h_1 \rightarrow h_5$ ).

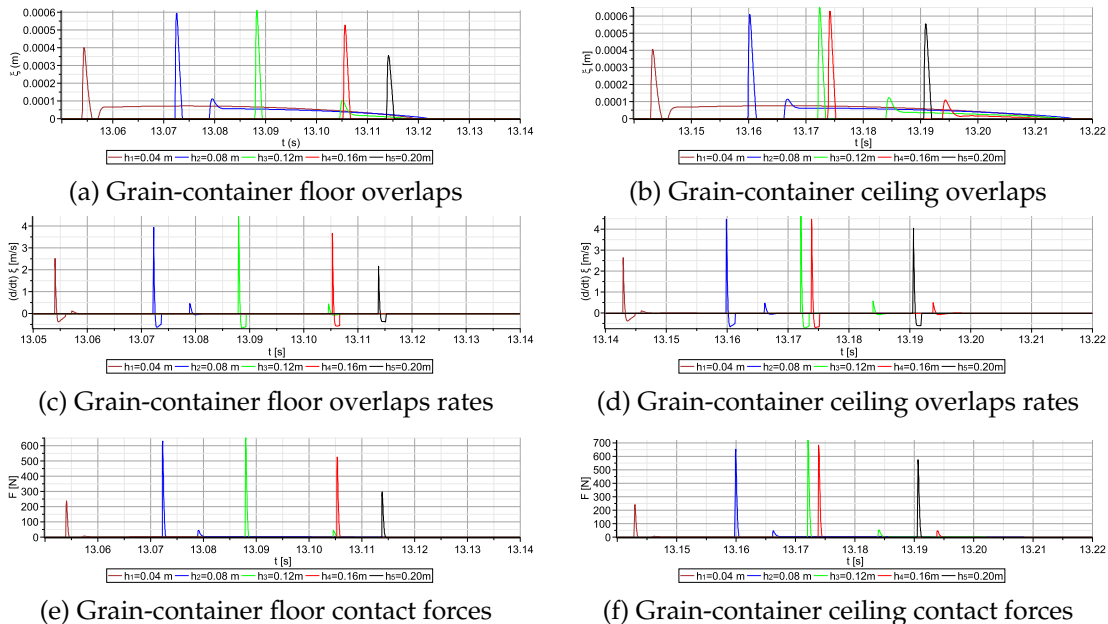


Figure 3.17: Overlaps, overlaps rates and contact forces for various container height -  $h_1 \rightarrow h_5$

The grain-floor and grain-ceiling overlap plots shown in Figs. 3.17a and 3.17b differ

noticeably for various cylinder heights. Two stages can be observed in both situations: the first one is a short peak with a large overlap amplitude, and the second one is a long period of time where the overlap is nearly constant before gradual decrease to zero. The first collision between the grain and the wall, that can be observed in each of the studied cases, constitutes the first stage. The second stage is the sticking effect that occurs when the grain is pushed by the container's bottom or top (cases  $h_1 \rightarrow h_4$  in Fig 3.17a and cases  $h_1 \rightarrow h_3$  in Fig 3.17b). During the first impact and the sticking stage, the grain-floor and grain-ceiling overlap rates (Figs. 3.17c and 3.17d) assume positive and negative values, respectively. The contact force plots (Figs. 3.17e and 3.17f) show high-amplitude peaks of force related to the initial impact and smaller peaks corresponding to the secondary impact at the beginning of the sticking stage.

### 3.6.2 Balance of system energy

The equations of motion (Eqs. 3.39 and 3.40) were integrated with respect to displacements  $x_s$  and  $x_g$  to obtain the equations of global energy balance of the beam and grain. It was carried out to demonstrate the influence of the contact forces on change of system energy and vibration damping:

$$\int_{\Delta x_s} m_s \ddot{x}_s dx_s + \int_{\Delta x_s} F_{ext} dx_s + \int_{\Delta x_s} (F_{c_1} - F_{c_2}) dx_s + \int_{\Delta x_s} Q_s dx_s = 0 \quad (3.63)$$

$$\int_{\Delta x_g} m_g \ddot{x}_g dx_g - \int_{\Delta x_g} (F_{c_1} - F_{c_2}) dx_g + \int_{\Delta x_g} Q_g dx_g = 0 \quad (3.64)$$

By identifying the terms denoting changes in kinetic energy and potential energy as well as work performed by external excitation and contact forces the equations for energy balance can be expressed in the following form:

$$\Delta E_k^s - W_{F_{ext}}^s - W_{F_c}^s + \Delta E_p^s = 0 \quad (3.65)$$

$$\Delta E_k^g - W_{F_c}^g + \Delta E_p^g = 0 \quad (3.66)$$

The equation of beam energy balance contains change of beam kinetic energy  $\Delta E_k^s$ , work done by excitation force on beam displacement  $W_{F_{ext}}^s$ , work done by both contact forces on beam displacement  $W_{F_c}^s$  and change of beam potential energy  $\Delta E_p^s$ . The equation of grain energy balance contains change of grain kinetic energy  $\Delta E_k^g$ , work done by both contact forces  $W_{F_c}^g$  on grain displacement and change of grain potential energy  $\Delta E_p^g$ .

Summing up the equations of the beam and grain energy balance (Eq. 3.65 and Eq. 3.66) allows to obtain the global energy balance for the entire system:

$$\Delta E_k^s + \Delta E_k^g - W_{F_{ext}}^s - W_{F_c}^s - W_{F_c}^g + \Delta E_p^s + \Delta E_p^g = 0 \quad (3.67)$$

Occurring in the above equation term indicating work done by contact forces on beam displacement  $W_{F_c}^s$  is an additive inverse of the work done by the system due to interaction with the grain  $\overline{W}_{F_c}^s$ :

$$W_{F_c}^s = -\overline{W}_{F_c}^s \quad (3.68)$$

Moreover, the difference of work done by the system due to interaction with the grain  $\overline{W}_{F_c}^s$  and work done by the contact force on the grain displacement  $W_{F_c}^g$  is the total work done on the contact element (contact spring and dashpot) and can be expressed as:

$$\overline{W}_{F_c}^s - W_{F_c}^g = D + \Delta E_p^c \quad (3.69)$$

where  $D$  is energy dissipation in the contact element and  $\Delta E_p^c$  is the change of potential energy of the contact spring, which vanishes in non-contact stage of the process. Thus, the energy balance for the whole system during the periods when the contact between ball and container wall does not appear takes a classical form:

$$\Delta E_k^s + \Delta E_k^g - W_{F_{ext}}^s + D + \Delta E_p^s + \Delta E_p^g = 0 \quad (3.70)$$

Eqs. 3.65 and 3.70 can be compared to demonstrate the differences between factors that influence beam energy and system energy. The work done by an external force and the work done by the system due to contact with the grain both contribute to the change of beam energy. The work done by external excitation and dissipation occurring during

grain-wall collisions, in turn, change the energy of the entire system. Let us observe that the grain's total kinetic and potential energy remains unchanged after each cycle of vibrations during the system's steady-state response:  $\Delta E_k^g = \Delta E_p^g = 0$ . Thus, according to Eq. 3.66, the work done by contact forces on the grain displacement equals zero:  $W_{F_c}^g = 0$  and according to Eq. 3.69, the work done by the system due to interaction with the grain is equal to total energy dissipation in the system:  $\overline{W}_{F_c}^s = D$ . This indicates that the work done by the beam as a result of its interaction with the grain  $\overline{W}_{F_c}^s$  is always positive and causes a reduction in the total energy of the beam as well as an attenuation of its vibrations. Additionally, the system's total energy dissipation decreases the energy of the beam while having no impact on the energy of the grain, which is advantageous from the vibration damping point of view.

The selected of the above defined energy and work terms were calculated for various container heights and presented in Figs. 3.18 - 3.21. Due to the fact that direct numerical computation of the work done by contact forces of extremely short duration is difficult and time-consuming, they were determined by computing all other energy and work terms and assuming that Eqs. 3.55 and 3.64 are a priori fulfilled.

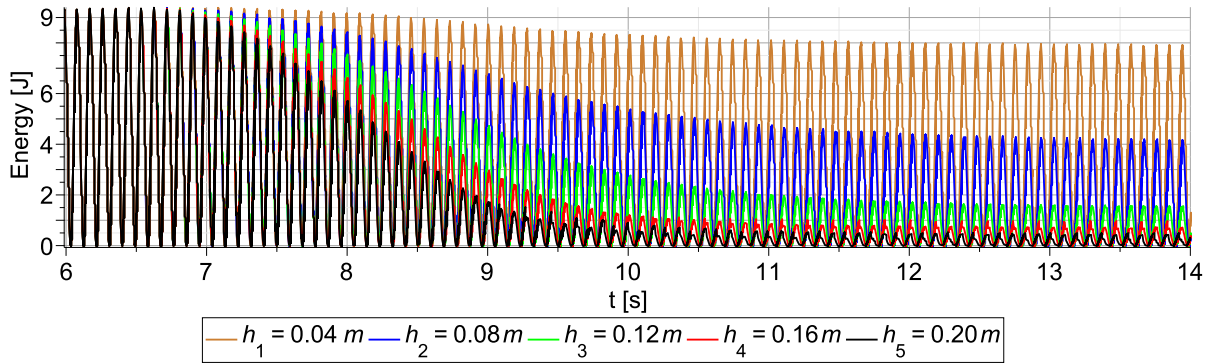


Figure 3.18: Change of the beam summary kinetic and potential energy for various container heights -  $h_1 \rightarrow h_5$

Fig. 3.18 shows the difference in the beam's summary kinetic and potential energy for various ATPID container heights. The maximum summary kinetic and potential energy value for the deactivated (closed) damper exceeds 9 [J]. The process of opening the ATPID reduces the maximum value of system energy in each considered situation. The vibration damping method is most successful for the largest container height under consideration,  $h_5$ . In such a case the beam's maximum total kinetic and potential energy is below 1 [J] during the steady-state response (for  $t > 12[s]$ ). As previously

stated, changes in the system’s natural frequency resulting from the particle’s movement can be considered as responsible for the observed process of vibration reduction. On the other hand, the occurrence of contact forces and the influence of these forces on the displacement of the beam could be used to describe such a process.

Eq. 3.65 reveals that the total energy of the beam changes due to both the permanent work done by external excitation and the work done by contact forces during impact periods. The height of the ATPID damper’s container affects both of the above work terms. The work done by the contact forces on beam displacement and changes in beam kinetic energy during impacts will also vary, in particular, because the changes of the contact forces are noticeably different for various damper heights, as depicted in Figs. 3.17e and 3.17f. The changes in the beam summary kinetic and potential energy damped steady-state vibrations for five various container heights were computed and shown in Fig. 3.19 in order to analyze such a situation.

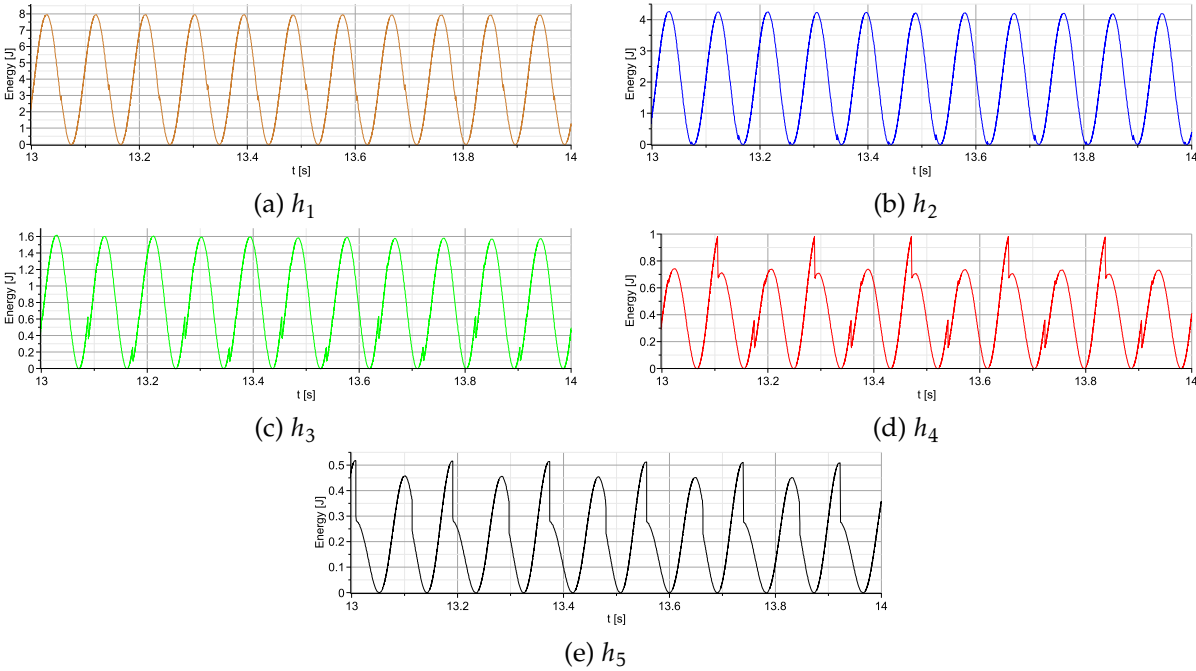


Figure 3.19: Change of the beam summary kinetic and potential energy for steady state response -  $13[s] < t < 14[s]$

In the case  $h_1$ , impacts begin to occur when the kinetic energy of the beam reaches about half of its maximum value in steady state. The energy of the beam during the primary stage of impact increases by 3.7 % of the maximal amplitude because the direction of the contact force and the direction of the beam movement are the same. In the situation  $h_2$  (Fig. 3.19b), when collisions take place while the beam’s kinetic energy is

almost zero and its energy increases by 3.5 %, an analogous situation is observed. The direction of the beam movement in the next three situations ( $h_3 - h_5$ ) is the opposite of the direction of the contact forces without a sticking effect, resulting in a decrease in the beam's energy in each collision. For example, in the case  $h_3$ , when the impact occurs when the kinetic energy is still relatively low, the energy is reduced by 15% and 12% for the grain collisions with the upper and lower walls of the damper, respectively. The effectiveness of impacts raises when the container height is increased because they occur closer to the beam maximum kinetic energy value. In the case  $h_4$ , the energy is reduced for the upper and lower impacts, respectively, by 35% and 16% of the maximal amplitude. The upper contact force changes the beam energy by 53% of the maximum amplitude and the lower contact force by 23% of the maximum amplitude for the most efficient case  $h_5$ , where the impact occurs when the kinetic energy of the beam is very near to maximal.

Analysis of the work done by the system due to the contact with the grain  $\overline{W}_{F_c}^s$  and work done by external excitation  $\Delta W_{F_{ext}}^s$  during the whole process provides additional information. For example, Fig. 3.20 shows the difference in the work performed by the system as a result of interaction with the grain  $\overline{W}_{F_c}^s$  for different container heights.

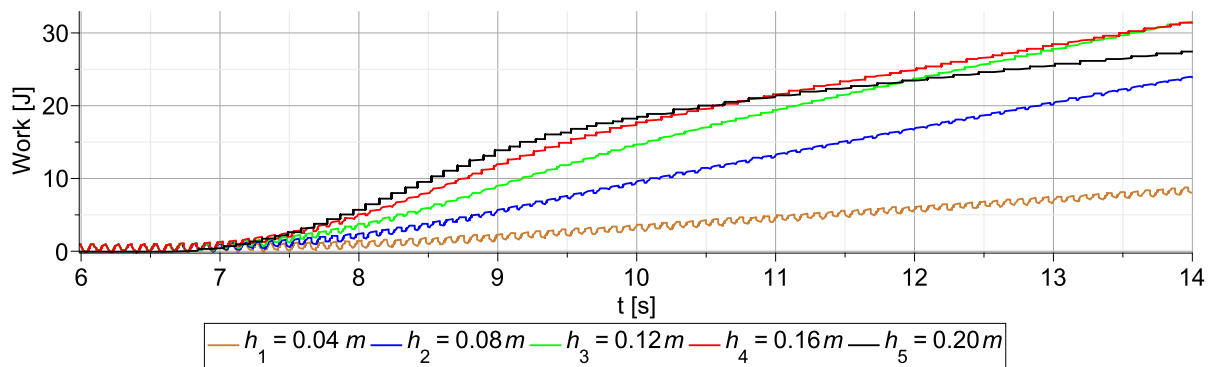


Figure 3.20: Work done by the system due to interaction with the grain  $\overline{W}_{F_c}^s$  and for various container heights -  $h_1 \rightarrow h_5$

Despite the fact that the contact forces that occur are completely different for each container height, the calculated work  $\overline{W}_{F_c}^s$  is always positive and increases gradually in all cases. The changes in work during the process have a nonlinear form. During the first part of the process, the work done by the system increases along with the container height. Consequently, it is the largest for the optimal container height  $h_5$ , which corresponds to the smallest vibration amplitudes. However, during the second part

of the process, such tendency is not maintained, and work computed for the optimal container height  $h_5$  becomes smaller than in the other cases ( $h_3$  and  $h_4$ ).

The short time plots ( $13[s] < t < 14[s]$ ) of the work performed by the system as a result of contact with grain are presented separately for each container height in Fig. 3.21 in order to provide a more detailed investigation. The plots in Figs. 3.21a and 3.21b correspond to situations in which the impact directions are the same as the beam movement directions in such situations. Each collision can be divided into two stages. The work done by the system on the grain during the main impact stage rapidly decreases (work is done by the grain on the system), which corresponds to an increase in beam kinetic energy. However, when the grain is pushed by the beam during the sticking stage, the system's work increases to a values higher than before the impact. In contrast, in cases  $h_3 - h_5$  the computed work increases during each collision and causes a permanent decrease of beam kinetic energy, which is favourable from the vibrations mitigation point of view.

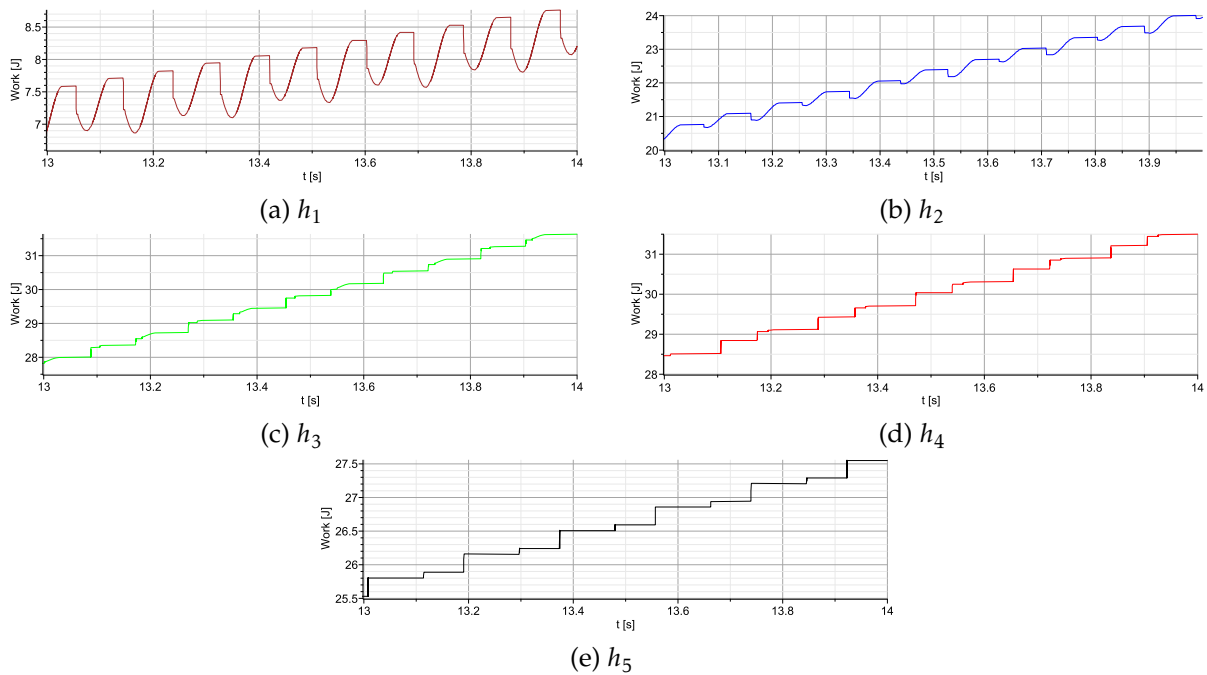


Figure 3.21: Work done by the system due to interaction with the grain  $\overline{W}_{F_c}^S$  for steady-state beam response -  $13[s] < t < 14[s]$

Due to the differences in the type of work performed by external forces in each situation, the ATPID damper's efficiency varies for different container heights. The system's natural frequency is modified due to a change of the container height, which also moves the excitation frequency out of its resonance range and decreases the ampli-

tudes and velocities of the system's vibrations. Fig. 3.22 presents the work performed by excitation forces  $W_{F_{ext}}^S$  and the work performed by the system as a result of interaction with the grain  $\overline{W}_{F_c}^S$  for two different container heights ( $h_1$  and  $h_5$ ), respectively, in order to explain the corresponding changes in the system energy.

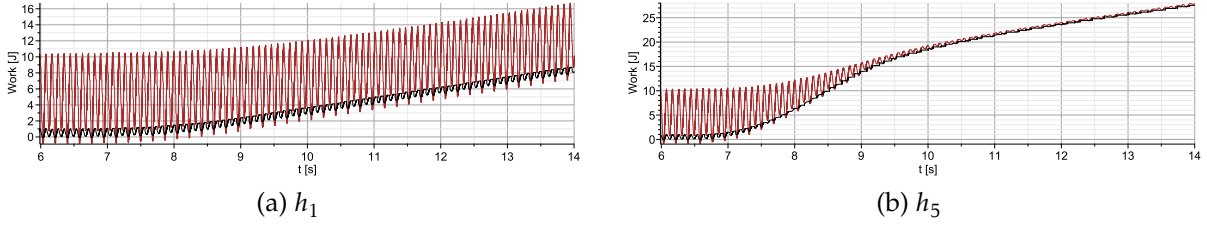


Figure 3.22: Work done by excitation forces  $W_{F_{ext}}^S$  (brown) and work done by the system due to interaction with the grain  $\overline{W}_{F_c}^S$  (black) for two container heights ( $h_1$  and  $h_5$ )

The average difference between the work done by excitation forces ( $W_{F_{ext}}^S$ ) and the work done by the system due to contact with the grain ( $\overline{W}_{F_c}^S$ ) is significant over the whole vibration process in the case when the height of the container is very low ( $h_1$ ) (Fig. 3.22a). This indicates that the rapidly oscillating component of the work produced by excitation forces has a significant role in shaping the system's total energy changes. As a result, the change in the system's energy is almost unnoticed. When the container's height ( $h_5$ ) is correctly tuned, oscillations in the work done by excitation forces gradually decrease until they are very small when a damped steady state is reached (Fig. 3.22b). Additionally, the system's work resulting from interaction with the grain is almost identical to the values of the work produced by excitation forces. As a result, the difference in the work produced by the two forces is relatively small, which corresponds to minimal oscillations in the system energy and an efficient beam vibration damping process.

### 3.7 Parameters optimization

The sensitivity of the dynamic response of the ATPID damper to three parameters (container height, grain mass, and excitation amplitude) was discussed in the previous section. The amplitudes of the steady-state beam vibrations  $x_s$  will be optimized in this section with to the maximum container height  $h_{max}$  for various grain mass  $m_g$  and excitation amplitude values A. According to Eqs. 3.71 - 3.73 the optimization values under consideration can be mathematically formulated as follows:

$$\text{Minimize:} \quad \max_{t \in (t_{min}, t_{max})} [x_s(A, m_g, h_{max}, t)]$$

$$\text{with respect to:} \quad h_{max}$$

$$\text{subject to:} \quad \text{governing equations: Eqs. 3.39 - 3.43}$$

$$A = A_i, (i = 1, \dots, 5) \quad (3.71)$$

$$m_g = m_i, (i = 1, \dots, 5) \quad (3.72)$$

$$h_{max}^* < h_{max} < h_{max}^{**} \quad (3.73)$$

The system parameters used in the numerical analysis of the optimization problem are equal:  $t_{min} = 12$  [s],  $t_{max} = 14$  [s] (range of damped steady-state vibrations),  $h_{max}^* = 0.017$  [m],  $h_{max}^{**} = 0.8$  [m] (full range of container height considered in the previous sections). Moreover, the subsequent values of decreasing grain masses  $m_g$  and excitation amplitudes A are presented in Tab. 3.6.

Table 3.6: Parameters used in the optimization problem

$m_g$ [kg]	$m_1 = 0.3M_s$	$m_2 = 0.2M_s$	$m_3 = 0.1M_s$	$m_4 = 0.05M_s$	$m_5 = 0.025M_s$
A [m]	$A_1 = 0.03$	$A_2 = 0.02$	$A_3 = 0.01$	$A_4 = 0.005$	$A_5 = 0.0025$

The formulated optimization problem was solved by performing a direct search of the parameters space. In Fig. 3.23, which is divided into five plots representing various excitation amplitude values, the analysis's results are displayed. For five different grain masses and a wide range of container heights, the vertical axis of each plot shows the maximum vibration amplitude during ATPID damped steady-state operation.

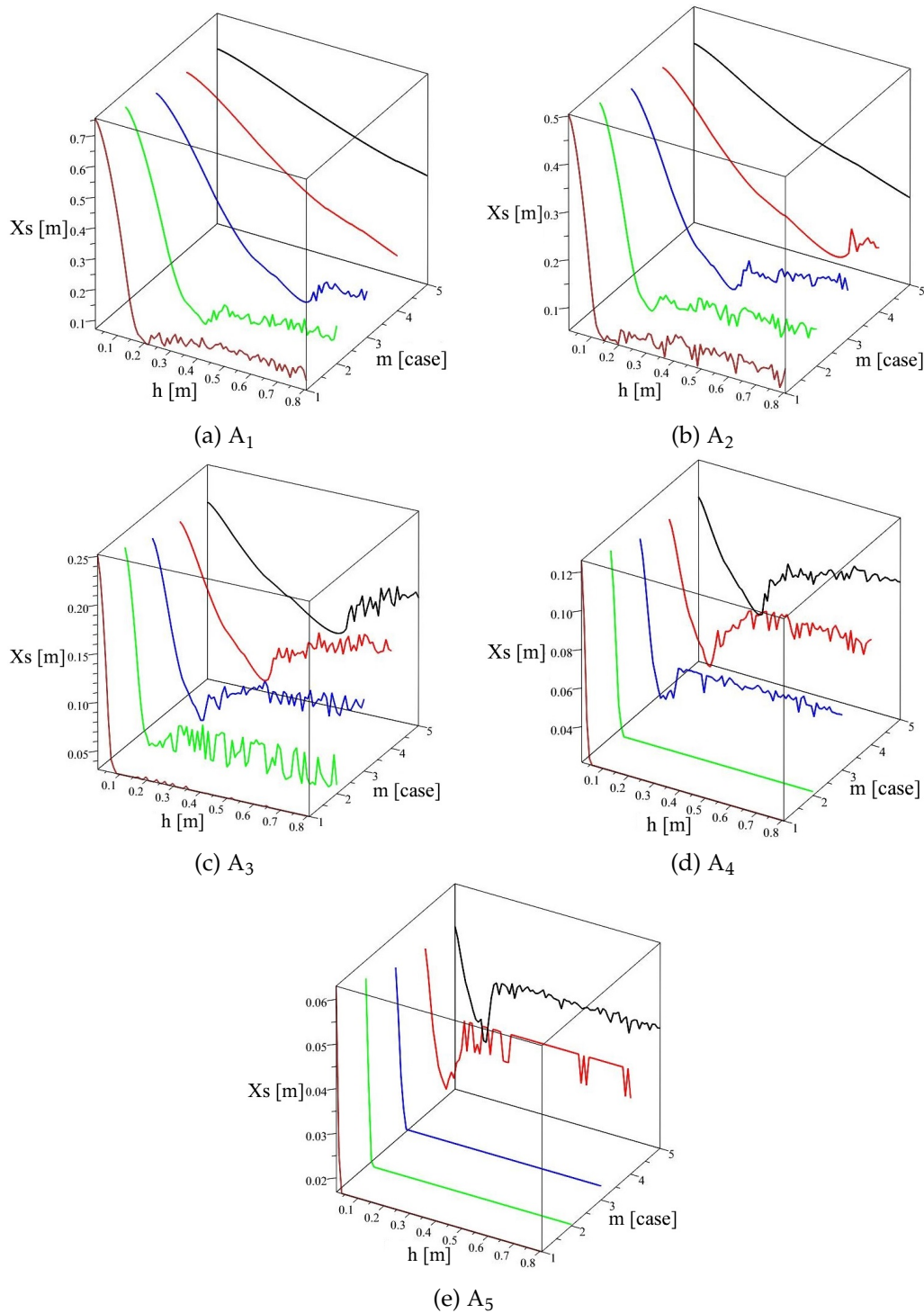


Figure 3.23: Optimization of the container height for various grain mass and excitation amplitudes

The type of ATPID operation (explained in the previous section) and the effectiveness of vibration mitigation are determined by the interaction of the ATPID container height, grain mass, and excitation amplitude. In the ideal scenario, it is expected that the selected container height will provide an impact without a sticking effect and shortest possible time of grain-wall contact in every cycle of vibration. According to

Fig. 3.23a, an optimal damper height differs for different grain masses and excitation amplitudes. For the  $m_1$  case, the optimal height  $h_{opt}$  for the  $m_1$  case is equal to about 0.2 [m], the  $m_2$  case  $h_{opt}$  is equal to 0.35 [m], and the  $m_3$  case  $h_{opt}$  is equivalent to 0.6 [m]. The global solution for cases  $m_4$  and  $m_5$  is higher than the upper bound of the damper height range that is assumed. The sticking effect between the grain and container walls, as was previously discussed, causes the worse damping ability for the container heights lower than optimal one. However, at container heights greater than the optimal one, the unpredictable movement of the grain without cyclic impacts on the lower and upper absorber wall results in the worse damping properties. Analogous conclusions can be applied to the Fig. 3.23b (cases  $m_1 - m_5$ ), Fig. 3.23c (cases  $m_2 - m_5$ ), Fig. 3.23d (cases  $m_3 - m_5$ ) and Fig. 3.23e for the cases  $m_4$  and  $m_5$ .

The rumble effect, which decreases the system response compared to the optimal one, is usually present after the optimal solution. However, the largest grain mass ( $m_1$ ) in Fig. 3.23c demonstrates the deviation from this principle. The optimal damper height is quickly reached with this solution, and the rumble effect is almost not visible. The process of damping is stabilized for larger damper heights, which corresponds to the constant value of the obtained vibration amplitude. The system's response, in this case, is equivalent (or only slightly worse) to that for the optimal damper height. The analogous situation is demonstrated in Figs. 3.23d and 3.23e for cases  $m_1$ ,  $m_2$  and  $m_3$ , respectively. For the case  $m_4$ , another phenomenon can be observed in Fig. 3.23e, where the rumble effect combines with the constant system response.

The important and interesting feature of the proposed particle impact damper is that each combination of grain mass and excitation amplitude requires a different optimal value of container height corresponding to the minimal vibration amplitude. On the other hand, it is expected that during real-life operation, the considered mechanical system will be subjected to different dynamic excitations, which will require different optimal values of damper parameters. Such a problem requires a technical solution providing control of the damper height in a real time, which is possible thanks to the proposed ATPID construction.

In order to compare damper efficiency for different excitation amplitudes, the parameter  $d$ , which is defined as the percentage ratio of the amplitudes of damped steady-state vibrations  $x_s^d$  and undamped steady-state vibrations  $x_s^{ud}$  (when the particle cannot move inside the container):

$$d = \left| 1 - \frac{x_s^d}{x_s^{ud}} \right| \cdot 100\% \quad (3.74)$$

Five graphs that that correspond to various particle mass are presented in Fig. 3.24 to demonstrate the obtained results. Each graph is composed of five plots showing the parameter  $d$  for given excitation amplitudes in terms of various ATPID damper heights.

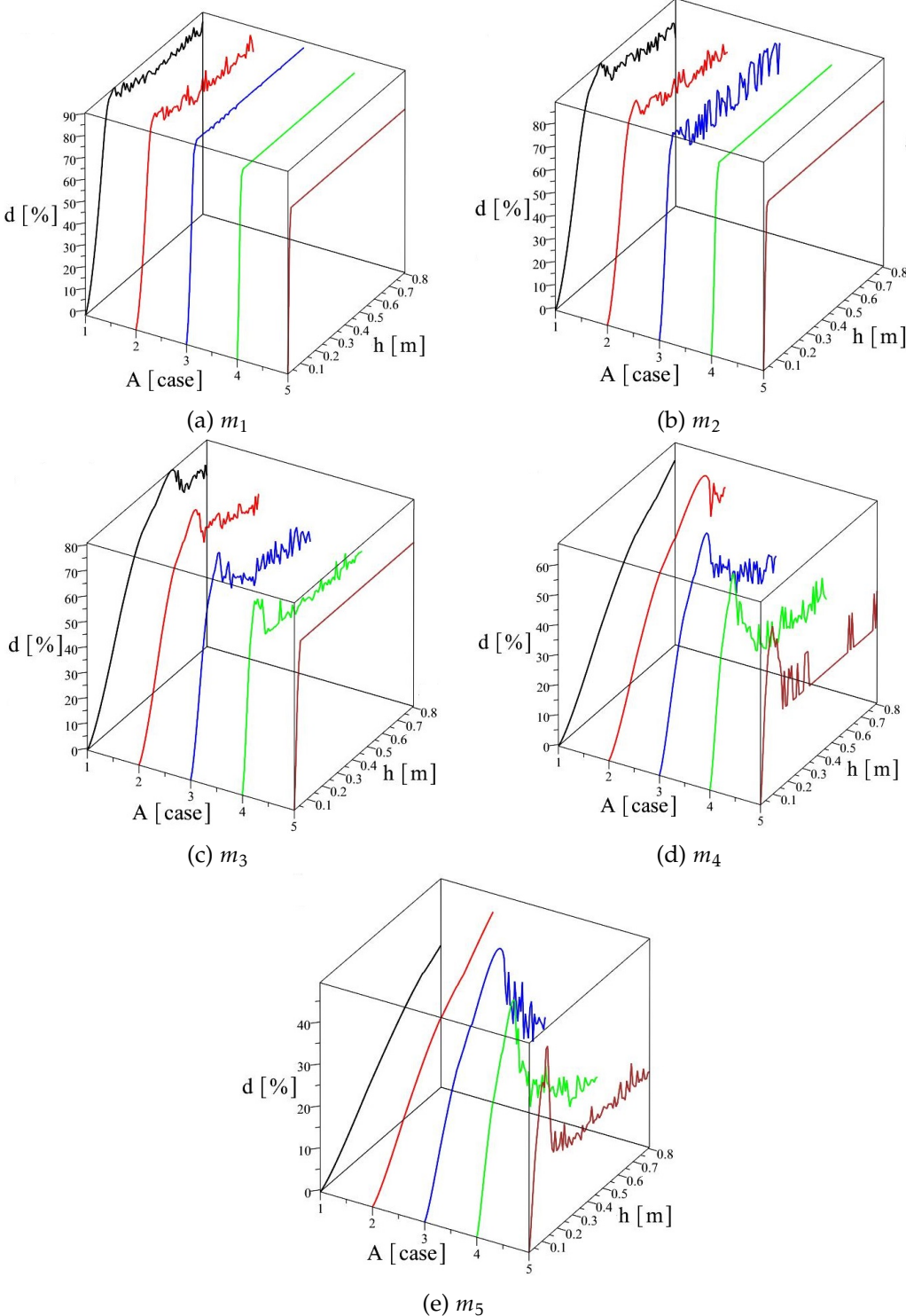
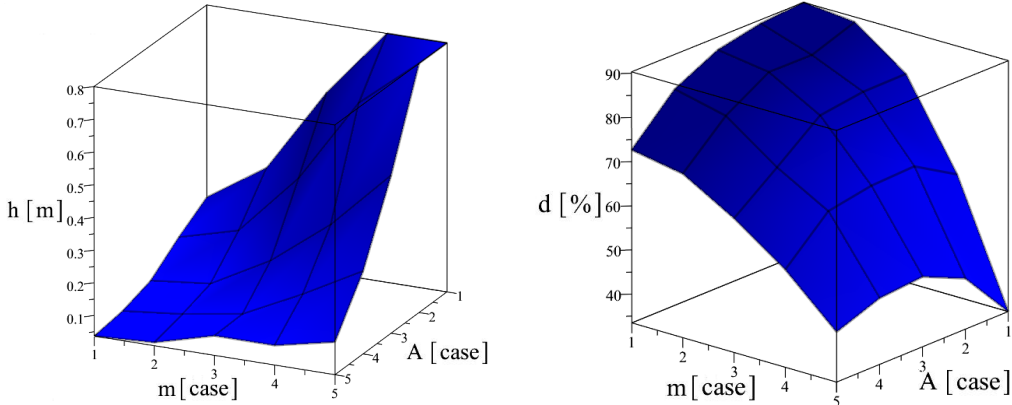


Figure 3.24: ATPID damping efficiency for various container heights, grain mass and excitation amplitudes

The presented plots allow for the estimation of the optimal container height and related damping effectiveness in relation to the excitation amplitude and grain mass. The analysis demonstrates that the efficiency of vibration mitigation is the lowest and does not approach 35 % for a small grain mass  $m_5$  and low vibration amplitude  $A_5$ , as demonstrated in Fig. 3.24e. When the excitation amplitude is increased, the particle movement is more efficient and the damper's efficiency can be increased ( $A_5 \rightarrow A_1$  for the case  $m_5$ ). Additionally, increasing the grain mass results in higher contact force values and a steady improvement in the damper efficiency (Fig. 3.24e  $\rightarrow$  Fig. 3.24a). The efficiency parameter  $d$  reaches 90 % for the maximum excitation amplitude  $A_1$  and the biggest grain mass  $m_1$ . It should be noticed that selecting a damper height that is too high for the excitation amplitude and grain mass can cause rumbling and significantly reduce the system's ability to attenuate vibrations.

The optimal damper heights for each combination of five different masses and five different excitation amplitudes were computed and presented in Fig. 3.25a based on the results from Figs. 3.23 and 3.24. The corresponding damping efficiencies were presented in Fig. 3.25b.



(a) Optimal container heights corresponding to various grain mass and excitation amplitudes (b) ATPID damper efficiencies for corresponding to optimal container heights, various grain and excitation amplitudes

Figure 3.25: Optimal results for various system parameters

The analysis of the results from Fig. 3.25a allows to conclude that the increase of the excitation amplitude and the reduction of the grain mass requires a larger damper height in order to obtain maximal vibration mitigation. In turn, Fig. 3.25b shows that the highest damping efficiency is obtained for the highest excitation amplitude and the largest grain mass. The obtained theoretical results reveal that the ATPID damper enables reduction of the resonance vibrations up to 90%. However, it should be noticed that the optimal solution is very close to the range in which the system may fall into an

undesirable rumble response.

### Experimental verification

Figs. 3.24 and 3.25b indicate that the ATPID damper is most effective in reducing beam vibrations, achieving around 90 % efficiency, when using a grain with a mass of 30 % ( $m_1$ ) and 20 % ( $m_2$ ) of the entire system's mass, and when the excitation amplitudes are  $A_1 = 0.03$  [m] and  $A_2 = 0.02$  [m]. Therefore, the test stand was adjusted accordingly to these values. The experimental tests were conducted for two cases: when the damper was deactivated (with a height of  $h_1 = 0.017$  [m]) and when the damper was optimally tuned (referred to as  $h_2$  in the figure legends). The results for the parameters  $m_1 = 0.3M_s$  and  $A_1 = 0.03$  [m] are presented in Fig. 3.26, while the results for the remaining parameters are listed in table 3.7.

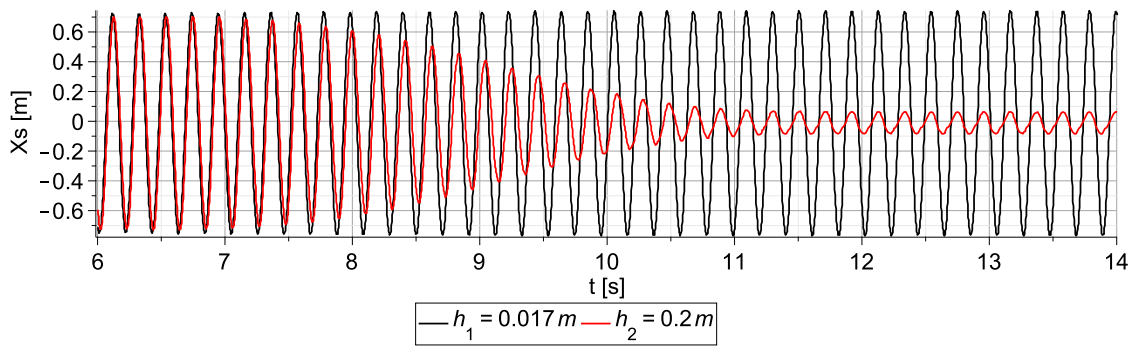


Figure 3.26: Comparison of the vibration amplitudes obtained in the experimental tests for the undamped system ( $h_1$ ) and the system with optimal ATPID height ( $h_2$ ) for the parameters:  $m_1 = 0.3M_s$  and  $A_1 = 0.03$  [m]

Table 3.7: Results of the undamped vibration amplitude  $x_s^{ud}$ , optimal damped vibration amplitude  $x_s^d$  and ATPID damper efficiency  $d$  for various grain mass  $m_g$  and excitation amplitudes A

$m_g$ [kg]	A [m]	$x_s^{ud}$ [m]	$x_s^d$ [m]	$d$ %
$m_1 = 0.3M_s$	$A_1 = 0.03$	0.745	0.065	91.4
$m_1 = 0.3M_s$	$A_2 = 0.02$	0.493	0.043	91.3
$m_2 = 0.2M_s$	$A_1 = 0.03$	0.698	0.064	90.8
$m_2 = 0.2M_s$	$A_2 = 0.02$	0.462	0.052	88.7

Upon examination of the experimental test results (Fig. 3.26 and Tab. 3.7), it is evident that the amplitude of beam vibrations in a damped steady state ( $x_s^{ud}$ ) is reduced by approximately 90 % compared to the beam response in resonance vibrations ( $x_s^d$ ) when the damper is deactivated. These experimental tests offer compelling evidence for the accuracy of the proposed numerical model and confirm the results obtained from the numerical analyses presented in Figs. 3.23, 3.24, and 3.25.

# Chapter 4

## ATPID damper control algorithm

### 4.1 State of the art

Prof. Masri from the Department of Civil Engineering of the University of Southern California and the scientists from other research institutions around the world, deserve a great credit for their work on the development of the classical Impact Damper. Since around 1969, they have been analyzing and describing the characteristics [15, 122] of such devices. They have conducted a series of experimental studies to determine the performance of impact absorbers subjected to random, harmonic, and stochastic excitations [123, 124, 125, 126], and mounted them on various complex primary structures. They have proposed several analytical models which describe the behaviour of ID in a simplified manner. In addition, their research has focused on the stability of systems with Impact Dampers [59, 127]. The knowledge obtained from their research papers has enabled the observation and formulation of criteria for their own control algorithm aimed at the most effective reduction of primary system vibrations. In the paper [128], the authors proposed an "active" Impact Damper in which real-time control is possible. In essence, the proposed device is a classical container containing a moving mass. By introducing appropriate limits, characteristic collisions between the auxiliary (moving) mass and the stops of the device can be obtained. From the vibration-damping point of view, the time of impacts plays a crucial role for the process effectiveness. The authors presented criteria describing the optimal motion of the auxiliary mass:

- the impacts have to occur when the velocity of the corresponding primary system mass reaches its maximum value,
- the velocities of two colliding masses have to be opposite to each other at the time

of impact.

The above conditions were implemented into a simple analytical model allowing for sensitivity and effectiveness analysis of the proposed control algorithm. The presented results are limited to a narrow range of parameters changes and demonstrate solutions that fulfill the above criteria defining effective vibration reduction.

The model used in this doctoral thesis is similar to that in [128]. Based on the research conducted in the thesis, there may be doubts about the correctness of the criteria presented by Prof. Masri. It appears that they do not consider all the relevant physical phenomena that can significantly affect the efficiency and optimal vibration damping. In the further part of the thesis, a novel Predictive Control Algorithm (PCA) will be proposed, which will include a set of assumptions constituting the criteria that must be fulfilled in order to find the optimal solutions. In the paper [128], the authors conducted an experimental verification of the aforementioned control algorithm using a special system that allowed for real-time adjustment of the device parameters. The scheme of this device is shown in Fig. 4.1.

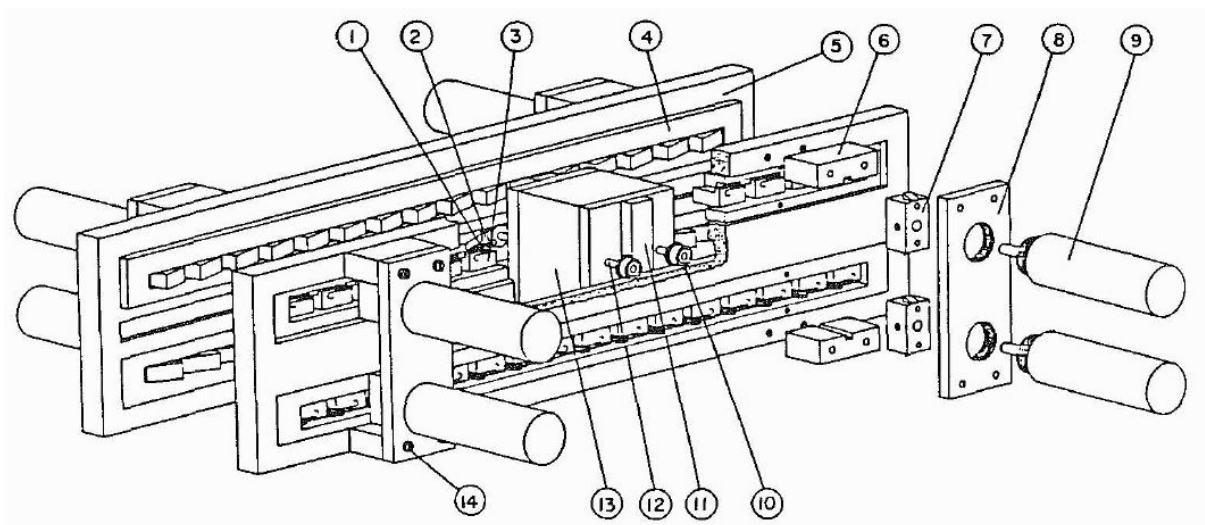


Figure 4.1: The scheme of the active impact damper device by Prof. Masri [128]

The proposed device consists of a container of a rectangular shape which is employed to restrict the movement of the auxiliary mass (13). An auxiliary mass mounted on a bearing (10) was permitted to move with minimal friction in tracks (12 and 14) located at the center of the container face plates (5), attached to the primary structure. The device included four panels (4) that could be moved to position of the stoppers (3) and initiate a collision between the auxiliary mass and the primary structure. These panels had the ability to move forwards and backwards in relation to the centerline of

the panel. The panels had 16 stoppers (3) which were attached to the moving panel (4) using pins (1 and 2) that enabled the auxiliary mass (11 and 13) to move freely in only one direction. The upper panels permitted unrestricted movement in one direction along the longitudinal axis (12) of the container, while the lower panels allowed movement in the opposite direction. As a result, the panels created an electromechanically-controlled ratchet-like mechanism. The electromechanical system consisted of a spacer (6), solenoid bracket (7), solenoid mounting plate (8) and magnetic solenoid (9). The primary objectives of this design were to eliminate the need for sensors to monitor the state of the auxiliary mass and to use simple control mechanism based on/off algorithm. This approach eliminated the requirement to calculate and provide the gap size, which allowed to reduce the computation time required for the decision-making process. As a result, the delay was shortened, providing more time for hardware activation.

Comparing the technical solution presented in this dissertation with the one shown in Fig. 4.1, many similarities can be observed. However, it should be noted that in this experimental and numerical studies, Prof. Masri has not included any phenomena related to gravity and friction. This fact significantly simplifies the solved problem. In reality, many systems are subjected to vertical motion, where gravity plays a significant role. This means that the behaviour of the system observed by Prof. Masri cannot be directly transformed into the behaviour of a similar system that would move vertically. Finally, it's also worth mentioning that the control strategy through the extension of specific stoppers can be described as a discrete control using a step function. The collision of the auxiliary mass depends directly on its dynamics, the dynamics of the primary structure, and the position of the stoppers. In the solution proposed in the doctoral thesis, it is also possible to influence the collision through the linear or non-linear motion of the moving ceiling. This expands the functionality and possibilities of the control strategy by applying a collision of a moving mass with a moving wall.

Additionally, Prof. Masri described his device as an active system. Based on its principle of operation, it is difficult to agree with such a classification. The control of the dynamics of the entire system is carried out by extending the appropriate stoppers, thus limiting the range of motion of the auxiliary mass and influencing the time of collisions. It is obvious that electrical energy is necessary to control the stoppers. However, the energy used does not directly affect the dynamics of the entire system. Only collisions, which are purely mechanical phenomena, have a direct impact on the system vibrations. For this reason, the presented device could be called a semi-active or

adaptive-passive device (because the control of the stoppers can be done in real-time). It should also be emphasized that in the following years, no author did any attempt to propose further technical solutions based on Tuned Impact Dampers or their technical counterparts which would expand functionality and eliminate the drawbacks of the "active" technical design proposed by Prof. Masri [14, 129, 22, 130].

## 4.2 General concept of the control strategy

The ATPID damper is a type of device that has the ability to tune the height and volume of the container in a real-time, which gives it the feature of being a controllable absorber. To enhance its functionality, the system can be equipped with components that enable to observe the vibrating structure and respond accordingly in order to reduce the resulting vibrations effectively, making it an adaptive system. Hence, it is crucial to develop an algorithm being able to determine the optimal height of the ATPID damper for the current operational conditions.

The obtained results indicate that the ATPID damper is a highly non-linear system. Consequently, development of the algorithm presents a challenging task, as it necessitates dealing with a complex problem that requires a verified numerical model. First, let us consider the situation where the ATPID damper is attached to a vibrating cantilever beam. The parameters of the system and the excitation have to be identified but at this stage, I omit the fact of the practical way of identification of the excitation amplitude. For the known excitation amplitude and using the numerical 2-DOF soft contact model of the damper developed in Chapter 3, a series of calculations can be made to determine the optimal height of the damper which provides the most effective reduction of the beam vibrations.

An algorithm, which can be used to obtain optimal ATPID height can be based on the numerical implementation of subsequent heights of the damper and observing damping of the steady-state system response. When the system's amplitude response in a given iteration is smaller than the response for the damper height set in the previous iteration, the damping coefficient is rising, and the process of increasing the absorber's height should be continued. The detailed steps of the described algorithm are presented below:

- The change in the height of the damper occurs periodically (e.g. every 4 [s]).
- The height of the damper changes by a constant value (e.g. 0.1 [m]).

- The opening time (i.e. the time after which the assumed value is achieved) is treated as a constant value (e.g. 1 [s]).
- After reaching the assumed height of the damper (in a given iteration), the algorithm observes the system response and checks the maximum amplitude of the beam vibration in a stabilized state, comparing it with the maximum amplitude of stabilized vibrations determined in the previous iteration (i.e. for the previous damper height).
- If the next value of the beam vibration amplitude is smaller than the previous one, the algorithm continues with the above steps.
- If the next value of the response amplitude is higher (i.e. the damping is worse), the algorithm returns to the previous height and considers it as optimal.

Fig. 4.14 is a graphical form of the above algorithm for exemplary parameters of the entire vibrating system.

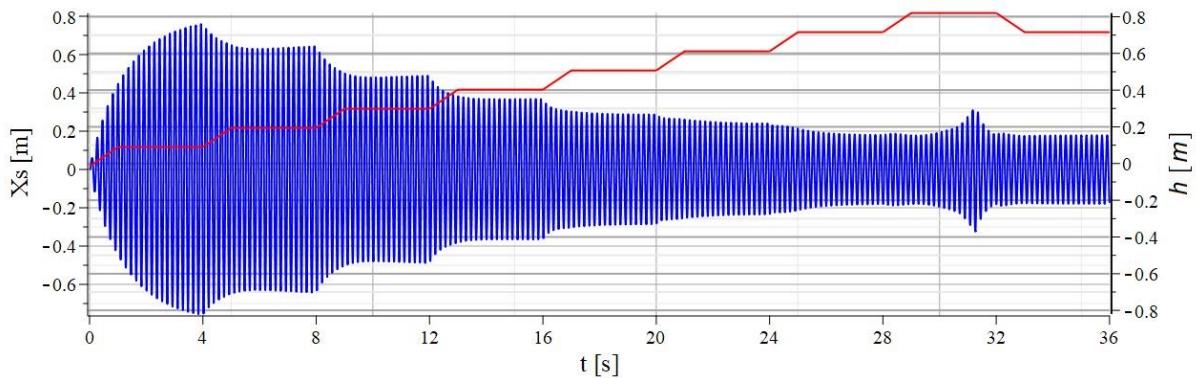


Figure 4.2: Amplitude of the system vibration ( $X_s$  - blue color) for various damper heights ( $h$  - red color) - the searching process of the optimal damper height

The results depicted in Fig. 4.14 demonstrate how the amplitude of the beam vibrations varies depending on the damper height. With each opening of the container, the vibration amplitude of the system decreases. Towards the end of the control process, it is observed that for one of the heights, the system exhibits a rumbling behaviour with larger vibration amplitudes, indicating that the height is tuned too high. Following the established assumptions, in such a scenario the algorithm returned to the settings from the previous iteration and the previously selected value can be considered as the optimal due to the previously determined nature of the amplitude change of the vibrations as a function of the damper height (Fig. 4.14).

The above algorithm has both advantages and disadvantages. The advantage is the ability to determine the optimal or close-to-optimal height (depending on the accuracy of the search). Real accuracy will depend on the time of calculations, the time between the changes, the time of each process of damper opening, and the constant value of the damper height between the iterations. The disadvantage is the long time required to find the optimal height. Often, this will be the time when the structure will already be destroyed due to the occurrence of resonance.

The algorithm presented above is a simple concept of the searching process for the optimal height of the damper for a given excitation amplitude. However, in reality, vibration amplitude changes in real-time and the process of controlling such a system have to be dynamic. Therefore, in the next step, the above concept will be expanded and described in detail as a general method of adaptive vibration damping. The development of real-time control strategies, which allow for effective adaptation of the ATPID damper to the actual working environment and improve a vibration mitigation process, is based on the obtained experimental results, numerical simulations, and optimization processes. The control strategy could be designed to adapt the damper height in real-time to the changing amplitude of the kinematic excitation. This section describes such a control method and provides numerical examples confirming its effectiveness in reducing steady-state vibrations.

The proposed real-time control strategy for the system subjected to a kinematic excitation of varying amplitude is based on a simple feedback control loop which is activated multiple times during the vibration mitigation process and repeatedly determines the optimal value of the damper height. A measured kinematic excitation and the amplitude of its frequency as determined by FFT (Fast Fourier Transformation) analysis provide the simplest form of the feedback signal for the control loop. The optimal damper height and corresponding voltage signal of the electric engine (Fig. 2.7) are provided by the output of the feedback control loop, which in turn determines the minimal amplitude of steady-state system vibrations. The appropriate container height for the detected excitation amplitude value can be efficiently determined using the results from the comprehensive analysis of the ATPID damper. Two different types of control system operations can be taken into consideration:

- It can be assumed that the optimal damper heights for the expected range of excitation amplitudes were computed before and saved in the hardware controller's memory. In this situation, the surface  $[A,m,h]$  from the carried out optimization process (Fig. 3.25a) can be used as a look-up table to choose the optimal container

height for the actual amplitude of kinematic excitation,

- it could possibly be considered that the optimal damper height is a variable that has to be calculated during the vibration mitigation process because it is not an a priori known factor. In this situation, the process of determining an optimal value can make use of previously identified fundamental properties of the system, which are reflected in dependencies between the damper height and a vibration amplitude (Fig. 3.23) or the damping percentage ratio (Fig. 3.24), especially the fact that the optimal height is the highest one at which the rumbling effect does not occur. Moreover, optimization for successive excitation amplitudes can create a data matrix  $[A, m, h]$ , which demonstrates that the optimal damper height depends monotonically but not linearly on the excitation amplitude,

Finally, the proposed control system (Fig. 4.3) uses a single feedback control loop and consists of the following parts::

- block for the on-line measurement or identification of the actual amplitude of the applied kinematic excitation,
- block for selecting the optimal container height corresponding to the identified excitation amplitude based on either: i) a pre-created look-up table with a list of the most appropriate container heights for a given grain mass and expected excitation amplitudes; or ii) an online optimization or direct search algorithm that applies the fundamental properties of the analyzed system,
- block for generation of the required voltage signal for the electric engine,
- block of the electric engine which provides that the appropriate height of the container is set.

The control loop takes a chosen component of the system's actual response, usually the amplitude of the beam vibration as its input parameter and utilizes it to identify the external excitation amplitude. The output of the control loop is the optimal height of the container, which is obtained by the applied engine using an optimal voltage signal. The input to the entire system equipped with ATPID includes the external excitation and the optimal container height obtained from the execution of the control loop. Both of these values contribute to the system's dynamic response.

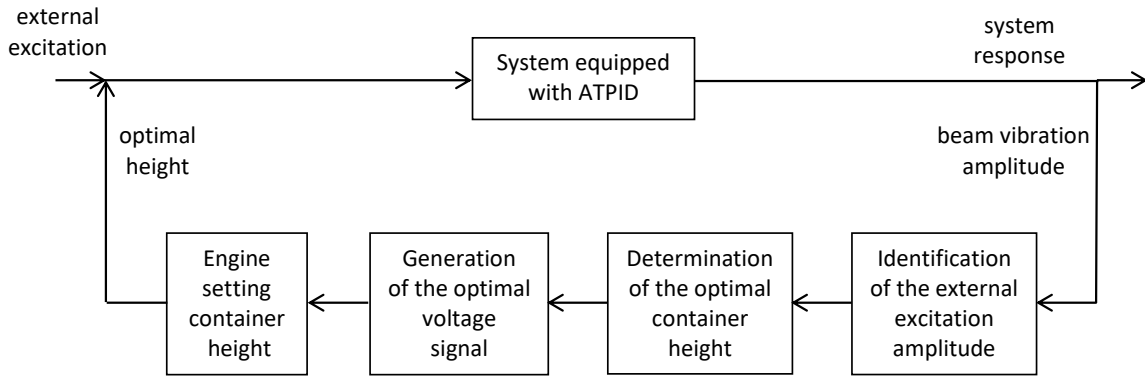


Figure 4.3: General scheme of the proposed control system

When the measurement system detects a change in the excitation amplitude during the vibration mitigation process (or its change exceeds a certain threshold), the application of the above feedback control loop is repeated several times. Such a procedure guarantees that the container height is adjusted in real-time for maximum performance, the ATPID damper operates adaptively, and the steady-state vibration is effectively mitigated.

### 4.3 Numerical simulations of real-time control algorithm

The following numerical examples show the operation of the previously proposed real-time control algorithm for adjusting the height of the ATPID to actual working conditions. The example reveals that the control algorithm effectively reduces steady-state vibrations caused by a harmonic kinematic excitation with variable, time-dependent amplitude. During the analyzed vibration mitigation process, the amplitude of applied kinematic excitation assumes three different values (Fig. 4.4). During the first 0.5 [s] the excitation amplitude linearly increases to 0.15 [m] and maintains a constant level at 0.5 - 6 [s]. During the following 2 [s] it linearly increases to 0.04 [m] and during the time period 8 - 13 [s] it is maintained at a constant level of 0.04 [m]. During the 1 [s] it linearly decreases to 0.03 [m], while during the final time period 14 - 20 [s] it is maintained constant at a constant level of 0.03 [m].

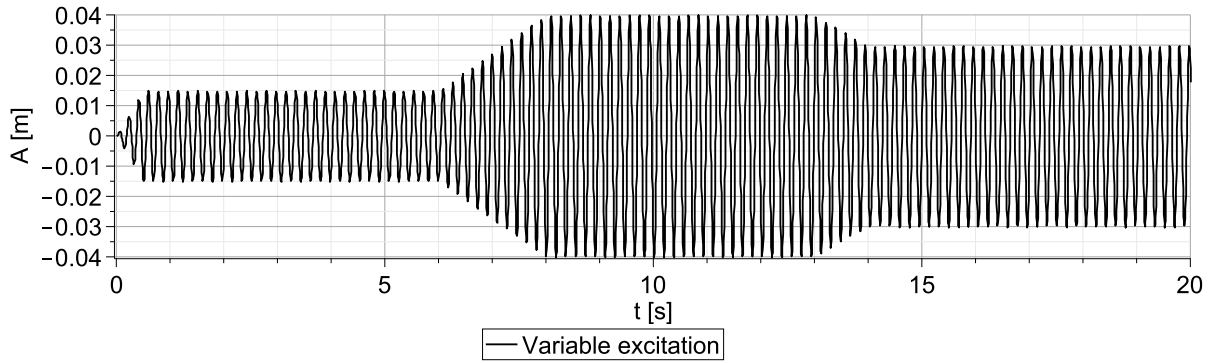


Figure 4.4: Change of the amplitude of applied kinematic excitation

The displacement of the system with a closed ATPID damper (container height equal to the grain size) is presented in Fig. 4.5. It can be observed that the initial steady-state of system response is reached after approximately 4 [s] and the corresponding displacement amplitude exceeds 0.3 [m]. The second steady-state (corresponding to the second vibration amplitude) is reached approximately at time instant 13 [s] and the corresponding displacement amplitude reaches 0.85 [m]. Eventually, the final steady-state is obtained also approximately at 17 [s] of the simulation and the corresponding displacement amplitude exceeds 0.65 [m].

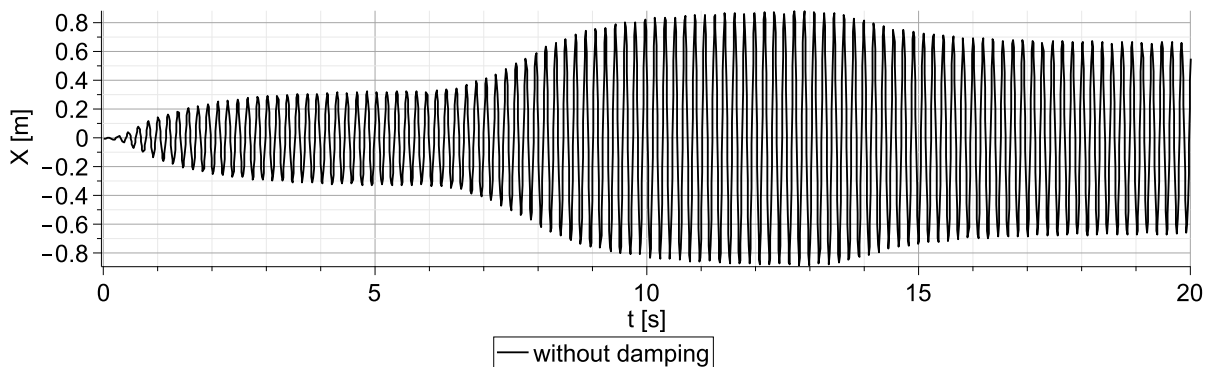


Figure 4.5: Displacement of the system with closed ATPID damper

The real-time control algorithm used in the following numerical simulations adjusts the damper actual height in accordance to the amplitude of the kinematic excitation that has been measured or determined. It is considered that at least two vibration cycles are required for precise measurement or identification of the excitation. On-line simulations of the system response for various container heights (and direct search of the successive heights) are used to identify the optimal value of the damper height during the vibration mitigation process. It is assumed that the process of determining the appropriate height is very short in comparison to the time required for the vibrations

mitigation. The process of changing the damper height has a constant rate of height change, and it requires less time to reach the final value than to find the next excitation amplitude. The values of the calculated optimal damper heights for the identified amplitudes (Fig. 4.6) are used as the reference points for the computation of the other optimal heights. Additionally, the process of finding the optimal container height is continued in the case of the lack of a change in excitation amplitude, by searching for values corresponding to predicted excitation amplitudes. This allows for the development and steady expansion of the database containing the set of optimal damper heights.

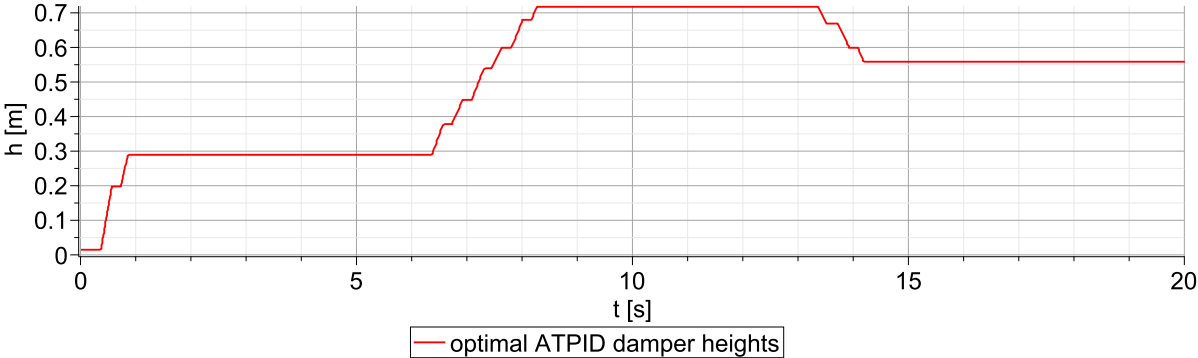


Figure 4.6: Change of the damper height obtained by application of real-time control algorithm

A comparison of the vibration amplitudes obtained in the system with a closed ATPID damper and the system with implemented real-time control strategy of container height is presented in Fig. 4.7. It can be observed that for the first excitation amplitude, the optimal damper height (Fig. 4.6) reaches 0.3 [m] and results in amplitude of steady-state vibrations of approximately 0.07 [m]. For the second excitation amplitude, the optimal damper height is equal above 0.7 [m] and the response amplitude reaches above 0.17 [m]. Finally, for the third excitation amplitude, the container height is equal 0.57 [m] for the amplitude of vibration of 0.13 [m]. Thus, it can be concluded that the obtained amplitudes of vibrations constitute less than 20% of the amplitudes of the undamped system. This confirms high efficiency of the proposed adaptive system and developed real-time control algorithm.

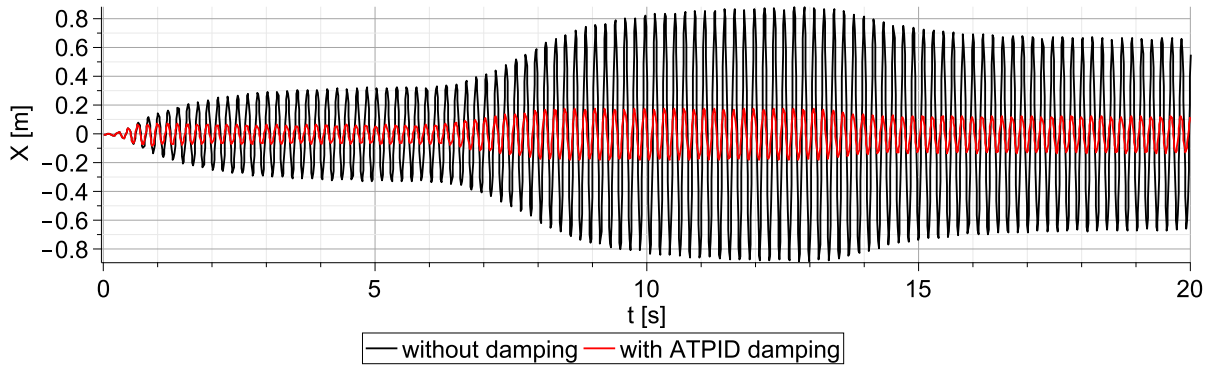


Figure 4.7: Comparison of vibration amplitudes obtained in the undamped system (black) and in the system with real-time control algorithm (red)

The operation of the entire system requires a hardware implementation of the proposed real-time control algorithm, which constitutes a separate research challenge and is planned in the next stage of the system development. The fully developed system will contain a hardware controller (such as the NI Compact Rio), a controlled electric engine that is currently in use, and a dedicated measurement system. Specific system for measuring system kinematics will include measurement cards, accelerometers, and laser sensors. It will also include software that enables data preprocessing techniques such as filtering and Fast Fourier's Transform. For the purpose of identifying the time history of external excitation and computing the actual value of excitation amplitude, the hardware controller will collect and save the measurement data. The optimal damper height corresponding to the identified excitation amplitude will then be determined using one of the methods described above, and the necessary control signal for the engine will be generated. Finally, the engine will change the damper height in real-time so that the system can respond to the shifting excitation and effectively reduce the system vibrations.

#### *Experimental verification*

The experimental tests were conducted to validate the proposed control algorithm, which had been developed using numerical analyses and taking into account the real-time variations in excitation amplitude. In the presented numerical example, each change in excitation value was implemented in a linear manner, resulting in successive amplitudes of 0.015 [m], 0.04 [m], and 0.03 [m] (Fig. 4.4). However, due to equipment limitations, it was not feasible to exactly replicate this numerical approach. Consequently, modifications were made to the research equipment to enable a stepped change in excitation amplitude, resulting in values of 0.03 [m], 0.02 [m], and 0.01 [m]. An example of the applied excitation amplitude is shown in Fig. 4.8.

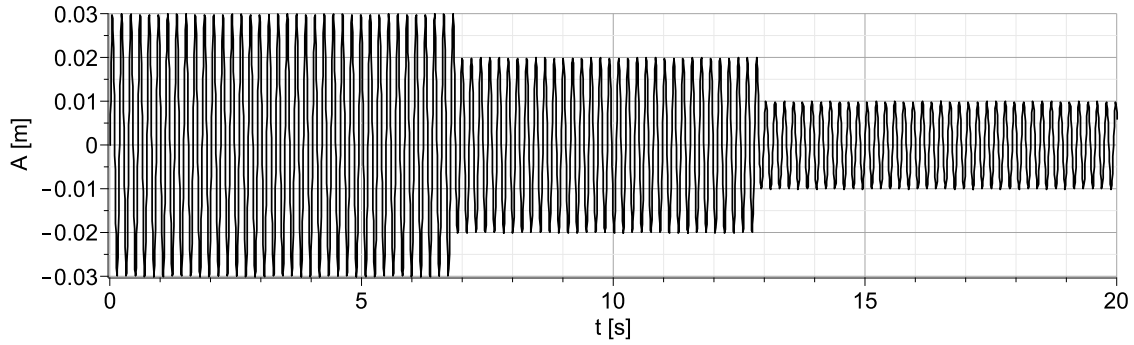


Figure 4.8: Change of excitation amplitude applied in the experiment

The described control algorithm was used to identify the optimal damper heights (in the range between 0.05 [m] and 0.5 [m]). During the computation, 101 discrete values of excitation amplitude were considered (with a step value equal 0.0045 [m]) and three different grain masses, namely 30 % (case 1), 20 % (case 2), and 10 % (case 3) of the total system mass were considered. Consequently, for each discrete value of excitation amplitude, three optimal damper heights were determined. This approach led to the creation of the look-up table containing the obtained data, which was then implemented into the Arduino Mega 2560 microcontroller.

The laser displacement sensor-based measuring system was used during the experimental tests to monitor the real-time kinematic excitation and the response of the beam's free end. The collected data was stored in the microcontroller's memory, which analyzed the input signal and determined the optimal container height as the one corresponding to the closest pre-recorded excitation amplitude value in the look-up table. The microcontroller then controlled the electric motor responsible for adjusting the position of the upper wall of the damper to achieve the optimal ceiling position. This control strategy was tested for all three cases of the grain mass. Figure 4.9 shows the real-time position of the ceiling obtained during the experimental tests.

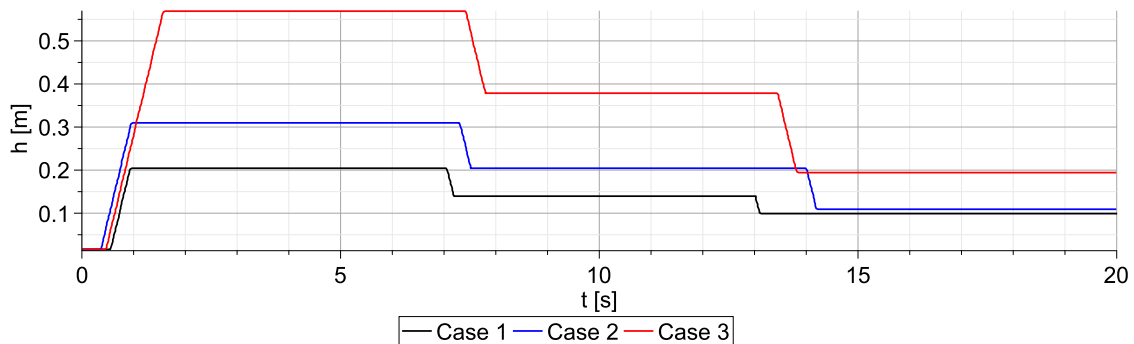


Figure 4.9: Experimental implementation of the ATPID damper control strategy for three different grain mass (cases)

The experimental results of the ATPID control strategy, as shown in Fig. 4.9, indicated that different optimal damper height values were achieved for each excitation amplitude and particle mass. The electric motor maintained a constant current, resulting in a uniform rate of change in damper height, but differences in the initiation time of each stage of damper opening or closing were observed. This was mainly due to the difference in amplitude changes in subsequent tests and the time required for the Arduino to identify the optimal damper height. The proposed control strategy was implemented for each grain mass case, and the displacement of the beam's free end was measured. Figs. 4.10 - 4.12 show a comparison of the cases of a closed damper and a damper with implemented control strategy.

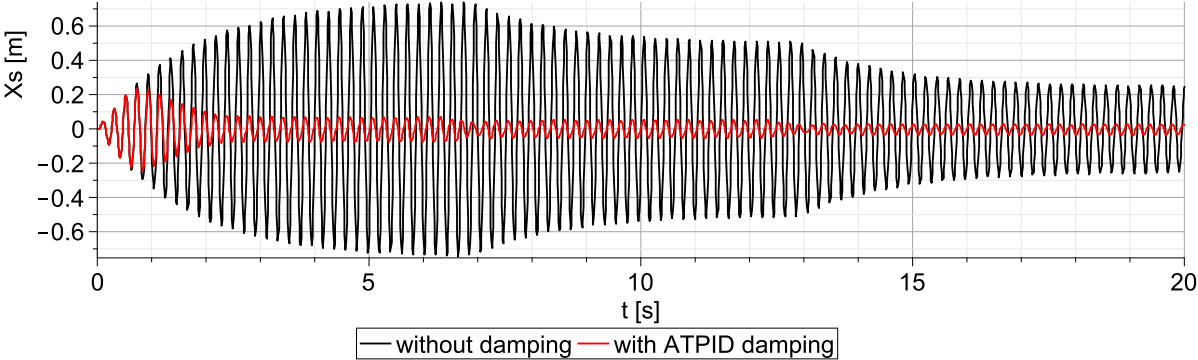


Figure 4.10: Comparison of measured responses of the beam vibrations for the case 1 ( $m_g = 0.3M_s$ )

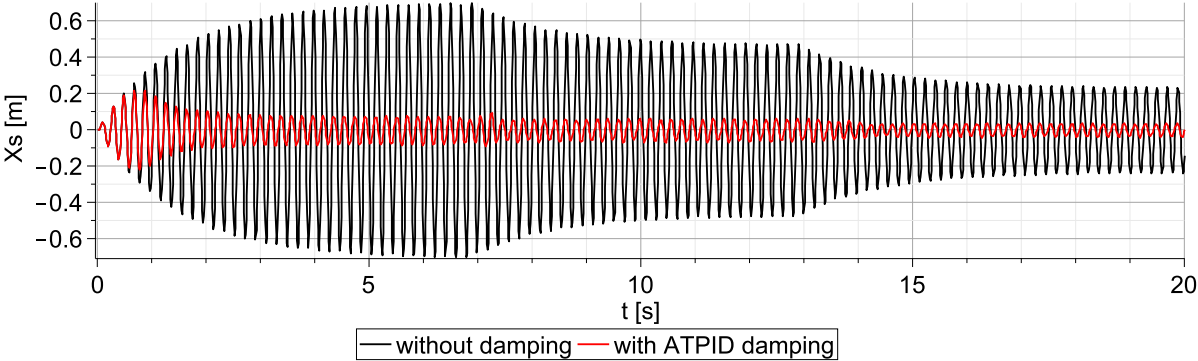


Figure 4.11: Experimental response of the beam vibration for case 2 ( $m_g = 0.2M_s$ )

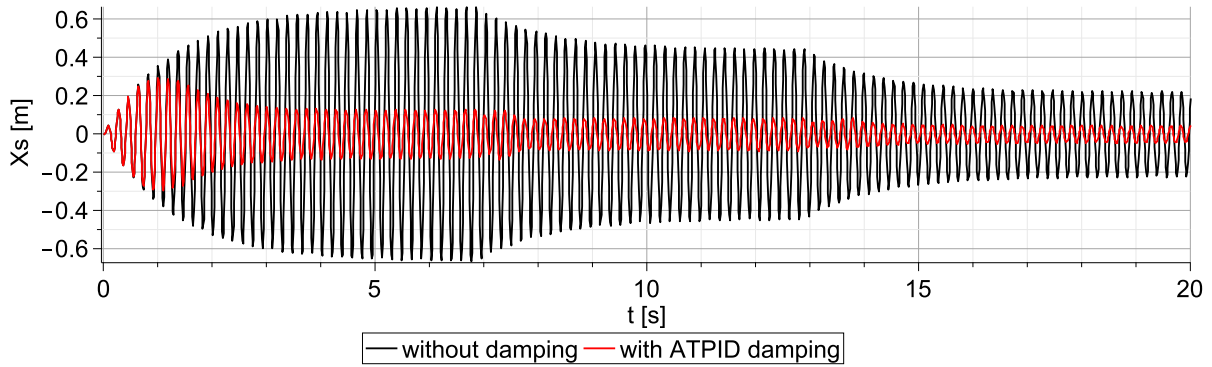


Figure 4.12: Comparison of measured responses of the beam vibrations for the case 3 ( $m_g = 0.1M_s$ )

Figs. 4.10 - 4.12 illustrate that the performed experimental verification enabled real-time control of the ATPID damper, and ensured maximum reduction of beam vibrations for dynamically changing excitation amplitudes (as shown in Fig. 4.8). This led to the reduction of resonant vibrations by approximately 90 % for case 1 ( $m_g = 0.3M_s$ ). For case 2 ( $m_g = 0.2M_s$ ), the vibration amplitude was reduced by 89 % for the largest excitation amplitude and 85 % for the smallest one. The lowest efficiency in reducing the beam is vibrations was observed in case 3 ( $m_g = 0.1M_s$ ), where resonant vibrations were mitigated by approximately 80 % throughout the beam's vibrations process. These results confirm the high effectiveness of the ATPID damper, which was previously described by numerical and experimental analyses. These studies of the control algorithm lay the groundwork for developing control algorithms that can identify optimal damper heights more quickly and efficiently.

#### 4.4 Predictive control algorithm (PCA)

From the previous studies of the ATPID damper principle of operation, it has been noticed that the movement of the grain changes depending on the height of the damper. The damper provides the most efficient vibration damping when the grain moves in a distinct pattern. Having those findings in mind, an algorithm for a given set of excitation parameters could quickly and easily find the height of the damper which results in the optimal movement of the grain was attempted to be developed. The features that define the optimal movement of the grain constitute the basis of the predictive control algorithm's criteria:

- Impacts occur when the direction of the primary system movement is opposite to the direction of the grain movement.

- Impacts occur when the velocity of the primary system is maximal or when its velocity decreases.
- Impacts occur in every period of vibrations. Otherwise, the system response will be unstable.
- The sticking effect between grain and walls should be avoided.

Before starting to implement Predictive Control the general assumptions have to be provided:

- The basic oscillating system is a cantilever beam.
- The excitation parameters (amplitude and frequency) can be identified during the process.
- The ATPID damper is deactivated at the start of the process (the grain is blocked).
- The beam is in resonance during vibrations for the closed ATPID damper.
- The physical and geometric parameters of the beam are known.

Based on the introduced assumptions and the control criteria, it is possible to propose a Predictive Control Algorithm (PCA), which allows to determine the optimal damper height. The diagram of a PCA is presented in Fig. 4.13.

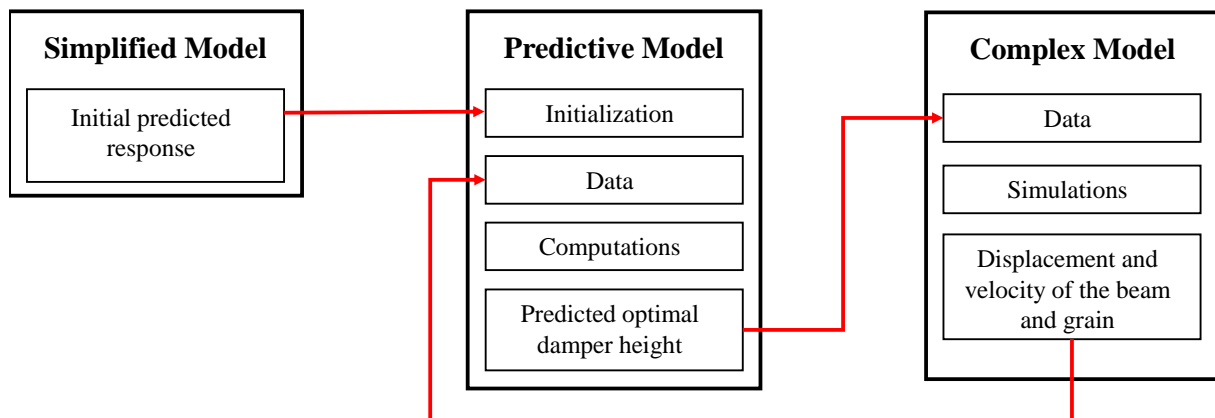


Figure 4.13: Scheme of the Predictive Control Algorithm

## Idea of the Predictive Control Algorithm

The following situation presents a basic vibrating structure subjected to resonant excitation, with an ATPID damper attached. The excitation and numerical model are known, so it is possible to predict the system response when the damper is deactivated and assumes the minimum possible height (it will not introduce additional damping). At this point, the question is, what is the optimal damper height for the most effective reduction of vibrations? It is possible to use the numerical model to check the system response for different damper heights and based on that determine the optimal one. Unfortunately, this method is time-consuming and, depending on the complexity of the system, can be long-lasting. Therefore, to find the optimal height of the damper providing effective vibrations reduction, an algorithm that shortens the time-consuming process of checking system responses for different heights is needed. According to the proposed concept, starting from a Simplified Model (SM), it is possible to predict the system response corresponding to damper height a height greater than the optimal height. Based on the obtained results and the previously defined PCA criteria, the initial damper height (the first guess) can be determined using the Predictive Model. In the first iteration of the calculations, this value will differ from the optimal one because of the application of the Simplified model containing significant simplifications and primarily predicting the system response in the range of vibrations when the ATPID damper height is too high. Although the obtained damper height is not optimal, it constitutes the initial stage of further calculations, which will introduce additional physical phenomena. This stage will utilize both the Complex model ( $CM_i$ ) and the Predictive model ( $PM_i$  where  $i$  constitutes a number of the iteration of the PCA algorithm). The Complex Model is the same 2-DOF soft contact model that was used in the main part of the ATPID damper modelling described in Chapter 3. These models will determine the dynamics of the system and the height of the damper respectively, and exchange data with each other. Iterative running of the Complex and Predictive Model set will allow to determine such a damper height that will be optimal or close to optimal. Finally, in order to find the height which is the most efficient, a searching process in the range close to the final height determined by the PCA algorithm will be performed.

Taking the above into account, a predictive control procedure can be constructed as follows:

$$\begin{aligned} \text{Minimize:} & \quad \max(x_s^d) \\ \text{with respect to:} & \quad h_{max} \\ \text{subject to:} & \quad \text{governing equations: 3.39 and 3.40} \\ & \quad \xi_{c_1} > 0 \Leftrightarrow \dot{x}_s > 0 \text{ and } \dot{x}_g < 0 \end{aligned} \quad (4.1)$$

$$\xi_{c_2} > 0 \Leftrightarrow \dot{x}_s < 0 \text{ and } \dot{x}_g > 0 \quad (4.2)$$

$$\xi_{c_1} > 0 \text{ and } \xi_{c_2} > 0 \text{ in every period of vibrations} \quad (4.3)$$

$$\xi_{c_1} > 0 \text{ and } \xi_{c_2} > 0 \Leftrightarrow |\dot{x}_s| \text{ is maximal} \quad (4.4)$$

$$t_c < \frac{\gamma}{2}T \quad (4.5)$$

where  $\gamma \ll 1$  and for this case it is assumed as  $\gamma \approx 0.1$ , where  $t_c$  - a single contact time,  $T$  - one period of beam oscillation,  $\max(x_s^d)$  - maximum amplitude of damped beam vibrations.

### Detailed description of the PCA algorithm

#### *Simplified Model*

The Simplified Model is a model that represents a reduced beam with an ATPID damper in two characteristic states. The first state is when the ATPID damper has a minimum height, as a result of which the grain is blocked. This means that throughout the entire process of resonant vibrations, the mass of the whole system consists of the mass of the beam and the particle. Due to the lack of grain movement, no additional forces are introduced into the system. In this situation, the beam and ATPID damper system can be presented as a 1-degree-of-freedom system, with the total mass of both elements. The equation of motion takes the form:

$$M_s(\ddot{x}_s + g) + k_s[x_s - u_s] + c_s[\dot{x}_s - \dot{u}_s] = 0 \quad (4.6)$$

where  $M_s = m_s + m_g$  and  $u_s$  is defined by Eq. 3.44.

The numerical solution of the Simplified Model (Eq. 4.6) and the 2-DOF soft contact model discussed in Chapter 3 showed that the system resonant response is the same (Fig. 4.14). The 2-DOF soft contact model, when the damper is closed, can be modelled as a 1-degree-of-freedom system without contact forces with the total mass of the beam and grain.

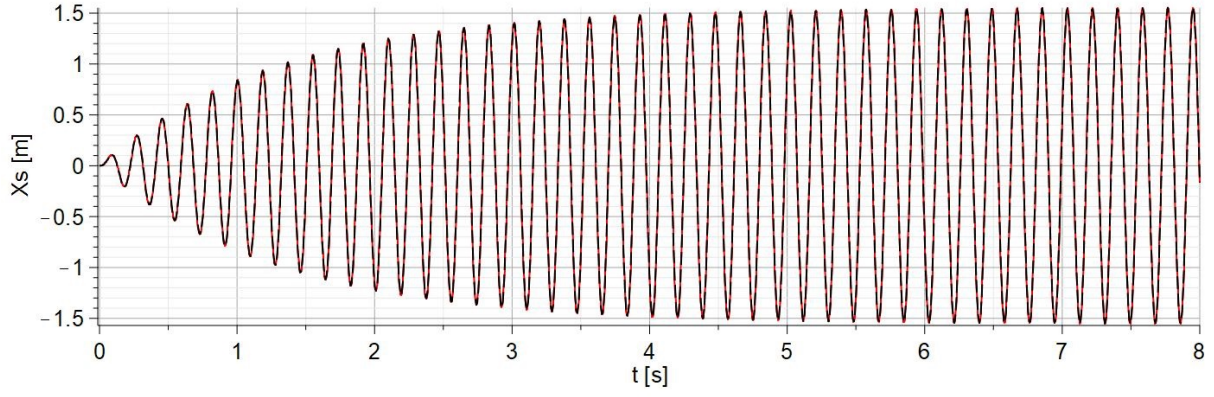


Figure 4.14: Comparison of the response of the beam vibration from the Simplified Model - red line (when  $M_s = m_s + m_g$ ) and 2-DOF soft contact model - black line (when the damper is deactivated)

The second type of vibration that can be studied using the Simplified Model is the situation when the mass of the system consists only of the mass of the beam. The situation in which the mass of the grain can be ignored requires that the contact between the particle and the cylinder walls is as rare and as short as possible. This case is possible only when the height of the damper is significantly greater than the optimal one and so large that the grain is unable to reach the upper wall position. A solution to such a case will allow to obtain important results necessary to determine the expected height of the damper. Therefore, an attempt was made to determine the analytical solution, which further will be used as a component of the Predictive Model. For the purposes of further consideration, it is assumed that the analytical solution of the Simplified Model is called the predictive solution of the vibrating system  $x_{pred}^s$  and describes oscillations around the equilibrium state considering the initial deflection  $x_{pred}^s(t=0) = -(m_s g)/k_s$  which correspond to the occurrence of the gravity forces. Therefore, the equation of motion can be represented as a system that does not take into account the component related to the force of gravity. The initial velocity is equal  $\dot{x}_{pred}^s(t=0) = 0$ . The equation of motion and its transformed version are described by Eq. 4.7 and Eq. 4.8, respectively:

$$m_s \ddot{x}_{pred}^s + k_s [x_{pred}^s - u_s] + c_s [\dot{x}_{pred}^s - \dot{u}_s] = 0 \quad (4.7)$$

$$m_s \ddot{x}_{pred}^s + k_s x_{pred}^s + c_s \dot{x}_{pred}^s = k_s u_s + c_s \dot{u}_s \quad (4.8)$$

The kinematic excitation takes the harmonic form:

$$u_s = A \sin(2\pi f t) \quad (4.9)$$

while the excitation rate is as follows:

$$\dot{u}_s = 2\pi f A \cos(2\pi f t) \quad (4.10)$$

where excitation frequency and natural frequency of the system are presented by Eqs. 4.11 and 4.12, respectively.

$$f = \frac{\sqrt{k_s}}{2\pi\sqrt{m_s + m_b}} \quad (4.11)$$

$$f_0 = \frac{\sqrt{k_s}}{2\pi\sqrt{m_s}} \quad (4.12)$$

The transformations of the above equations finally allow to determine the form of the equation of motion with harmonic force excitation. By substituting Eqs. 4.9 and 4.10 into the right-hand side of Eq. 4.8, the general harmonic form of the excitation is obtained as follows:

$$k_s u_s + c_s \dot{u}_s = k_s A \sin(2\pi f t) + c_s 2\pi f A \cos(2\pi f t) \quad (4.13)$$

The above equation can be reduced to a single trigonometric function that takes into account the reduced amplitude  $D_{red}$ :

$$D_{red} \sin(2\pi f t + \phi) = k_s A \sin(2\pi f t) + c_s 2\pi f A \cos(2\pi f t) \quad (4.14)$$

By using basic theory from the field of mechanical vibrations, a detailed formula can be derived to calculate the reduced amplitude of a harmonic force excitation:

$$D_{red} = \sqrt{A_0^2 + B_0^2} \quad (4.15)$$

where:  $A_0 = k_s A$ ,  $B_0 = c_s \omega A$  and  $\omega = 2\pi f$ . The final form of the reduced amplitude of the excitation is presented in Eq. 4.16.

$$D_{red} = A \sqrt{k_s^2 + c_s^2 \omega^2} \quad (4.16)$$

In the general case, the phase shift  $\phi$  can be calculated using the formula:

$$\phi = \text{atan} \frac{A_0}{B_0} \quad (4.17)$$

Generally,  $\phi$  is responsible for the shifting of the displacement of the beam vibration response in relation to the excitation waveform. In the considered case, this aspect is not significant. Additionally, for the sake of simplicity and transparency of further analyses of the grain motion inside the cylinder, it is assumed that the displacement response of the beam at the beginning of the simulation process ( $t = 0$ ) will be zero. This assumption unambiguously defines the values of the phase shift as  $\phi = 0$ . The final form of the equation of motion with harmonic force is:

$$m_s \ddot{x}_{pred}^s + k_s x_{pred}^s + c_s \dot{x}_{pred}^s = D_{red} \sin(2\pi f t) \quad (4.18)$$

It is expected that the system response will be in the form of a trigonometric function typical for steady-state vibrations:

$$x_{pred}^s = A_{pred} \sin(2\pi f t) \quad (4.19)$$

The amplitude of the expected solution can be calculated from the formula 4.20.

$$A_{pred} = \frac{D_{red}}{m_s \sqrt{4\beta^2 \omega^2 + (\omega^2 - \omega_0^2)^2}} \quad (4.20)$$

where:  $\omega_0 = 2\pi f_0$ .

In summary,  $x_{pred}^s$  is the displacement of the system, which has a mass equal to the mass of the beam. The frequency of excitation is calculated based on both the mass and the beam. In Fig. 4.15 the analytical solution in a stabilized state is shown for the following parameters:  $m_s = 0.905m_b = 0.3258$  [kg],  $m_g = 0.1M_s = 0.0362$  [kg],  $k_s = 427.6[\frac{N}{m}]$ ,  $c_s = 0.56[\frac{Ns}{m}]$ ,  $A = 0.07$  [m],  $f = 5.469$  [Hz],  $f_0 = 5.765$  [Hz].

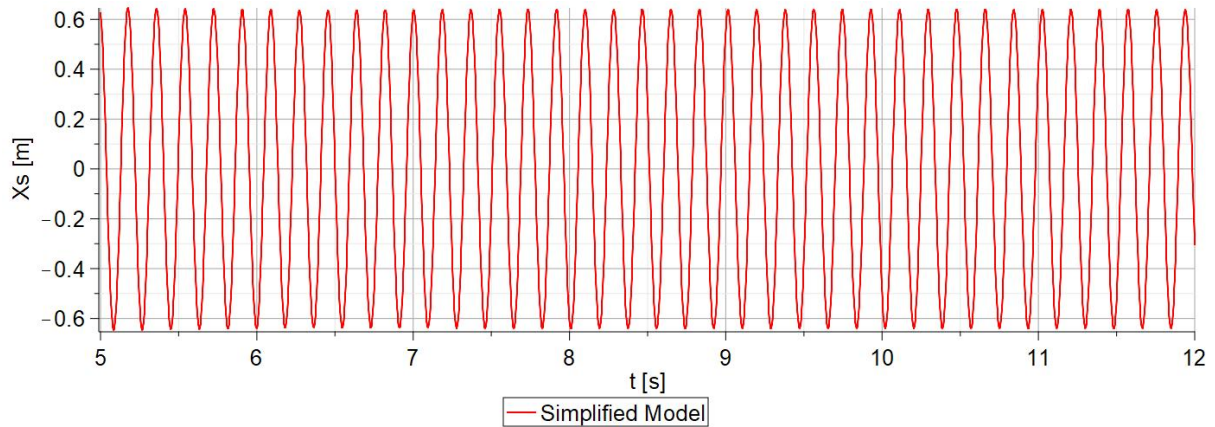


Figure 4.15: The predicted response of the system from the Simplified Model

The result from Fig. 4.15 was compared with a numerical simulation of a classical 2 DOF system model. At the beginning of the simulation, resonant vibrations were observed as the ATPID damper was closed. Then, the damper height was tuned to the optimal level for damping vibrations and this comparison was presented in Fig. 4.16.

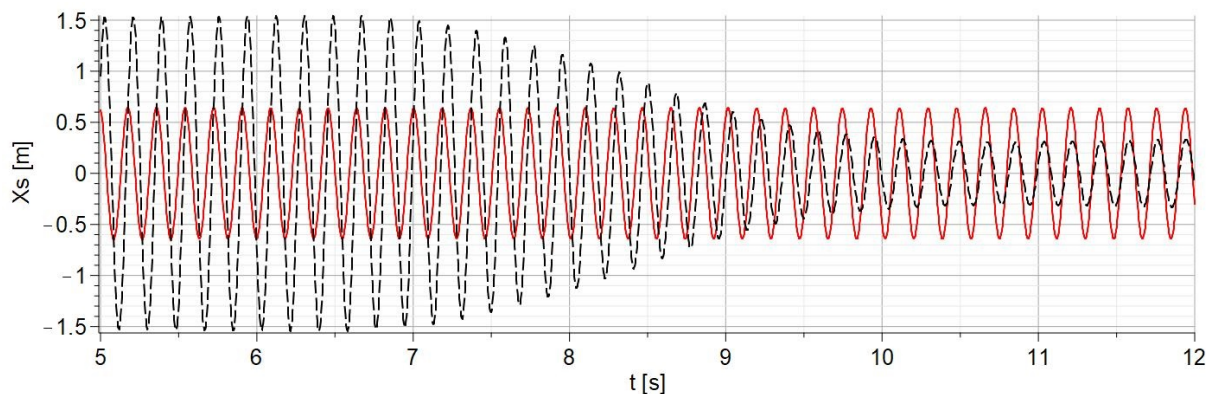


Figure 4.16: Comparison of the response of the beam vibration obtained from the Simplified Model - red line (when  $M_s = m_s$ ) and the 2-DOF soft contact model - black line (when damper height is optimal)

Analyzing the results shown in the above figure, it can be observed that the responses of both systems in a damped and stabilized state differ in terms of vibration amplitude. This difference is due to the fact that in the 2-DOF soft contact model, collisions between the grain and the walls are taken into account, thus introducing a disturbance responsible for additional phenomena that reduce the vibration amplitude. To prove this hypothesis, in the 2-DOF soft contact model, the damper height was also set significantly higher than the optimal one (Fig. 4.17) and the grain could not collide with the container ceiling.

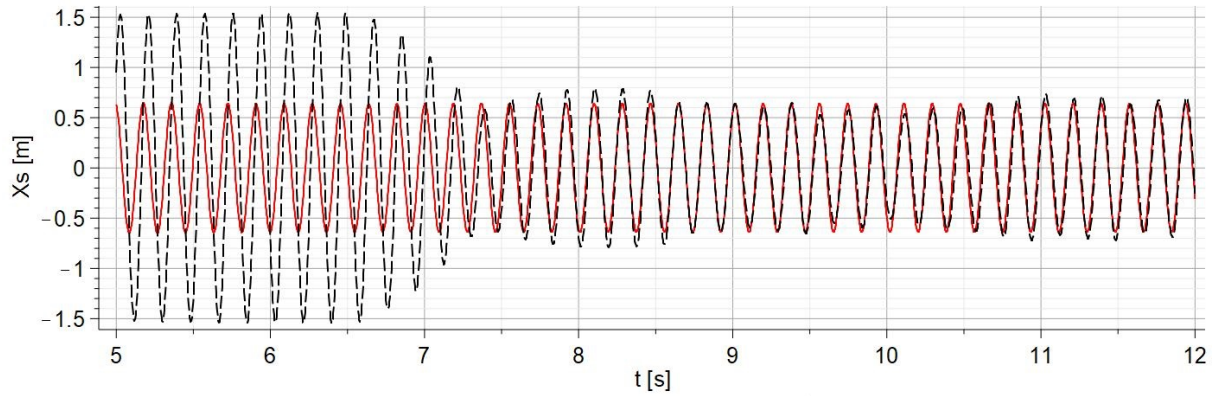


Figure 4.17: Comparison of the response of the beam vibration obtained from the Simplified Model - red line (when  $M_s = m_s$ ) and the 2-DOF soft contact model - black line (when the damper height exceeds the optimal height)

Fig. 4.17 shows that the response predicted using the Simplified Model system is similar to the response computed using the 2-DOF soft contact model when the damper height is assumed to be significantly higher than optimal. Such a comparison was made for other cases of the ratio between grain mass and mass of the entire system, which were analyzed in previous studies. It was revealed that for cases of particle mass in the range from 5 % to 30 % of the mass of the whole system, the differences in the amplitudes of vibration responses are negligible.

#### *Predictive model*

The purpose of the predictive model is to reflect the expected optimal movement of the grain and determine the height of the damper close to the optimal one. In the first iteration of calculations, from the Simplified Model, I obtain the beam displacement for a characteristic state, that is when the damper height is significantly larger than the optimal one. Additionally, from the sensitivity analysis of the system presented in Chapter 3, it is known that such vibrations often exhibit a rumble phenomenon, but the amplitude of these oscillations and the amplitude of system vibrations for the optimal damper height are relatively similar (Figs. 4.16 and 4.17). In the first iteration of calculations, the Predictive Model will attempt to find using the system response determined from the Simplified Model. The damper height at which the criteria for optimal particle movement could be fulfilled. To predict the movement of the particle in the container, a scheme of the model was proposed and is presented in Fig. 4.18.

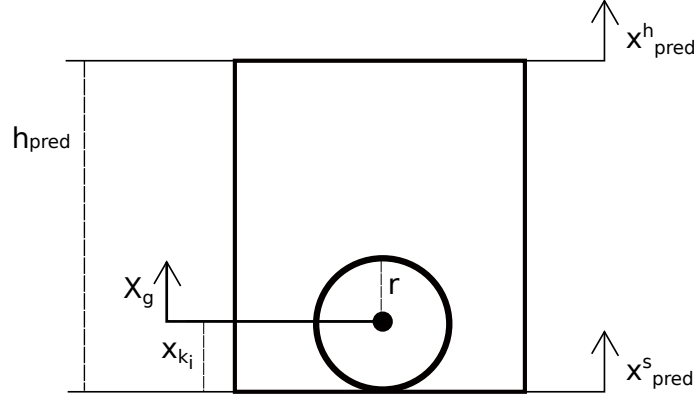


Figure 4.18: Scheme of the model for Predictive Model calculations

In order to simulate the movement of the grain in the container, it is necessary to determine the displacement of the bottom and the top wall of the damper. The displacement of the floor of the container is the predicted response of the system obtained from the Simplified Model  $x_{pred}^s$  (Eq. 4.7). The displacement of the upper part (ceiling) of the damper has the following form:

$$x_{pred}^h = A_{pred} \sin(2\pi f t) + h_{pred} \quad (4.21)$$

At this stage  $h_{pred}$  is unknown and the main goal of the algorithm is to determine this value. In the following step of the procedure, the initial condition of the simulation has to be established and the beam's location where the contact with the grain occurs has to be identified. This requires determining the time of the particle's impact with the lower part of the container  $t_{c1}$ . The displacement of the beam due to the  $t_{c1}$  can be expressed using the following equation:

$$x_{pred}^{t_{c1}} = A_{pred} \sin(2\pi f t_{c1}) \quad (4.22)$$

According to the previously introduced algorithm assumptions, the collision (without the sticking effect) with the bottom part of the container will occur when the beam velocity is at its maximum or the beam starts to decelerate:  $0 \leq 2\pi f t_{c1} \leq \pi/2$ . Therefore, the time of the first impact occurs in the time range:  $0 \leq t_{c1} \leq 1/(4f)$ . For the purpose of further analysis, it is initially assumed that the impact of the grain against the lower damper wall occurs when the velocity of the lower wall is maximal:  $t_{c1} = 0$  and then  $x_{pred}^{t_{c1}} = 0$ .

At this stage, it is necessary to assume the time  $t_{c2}$  at which the grain will collide with the upper part of the container. Based on previous research and introduced optimal criteria (impacts occur in every period of the vibrations), it is known that, in the

case of optimal particle movement, two collisions occur during one vibration period (one with the ceiling and one with the floor). Therefore, in general, the second collision has to occur when:  $\pi \leq 2\pi f t_{c_2} \leq \frac{3}{2}\pi$  and then  $\frac{1}{2f} \leq t_{c_2} \leq \frac{3}{4f}$ . Similarly to the situation with the first collision, for further consideration, it is assumed that the collision of the grain with the upper wall of the container will also occur when the beam reaches its maximal velocity. Therefore, the time of collision equals:  $t_{c_2} = \frac{1}{2f}$  and then the position of the beam during the collision of the grain with the ceiling of the damper has the form:

$$x_{pred}^{t_{c_2}} = x_{pred}^h(t = t_{c_2}) = A_{pred} \sin(2\pi f t_{c_2}) + h_{pred} \quad (4.23)$$

Before observation of the motion of the grain, it is necessary to know its equation of motion and the corresponding initial conditions. The initial position of the particle is determined by the position of the lower container wall at the time instant of impact:

$$x_{k_i} = x_{pred}^s(t = t_{c_1}) + r = r \quad (4.24)$$

Next, as a result of the impact, the grain acquires an initial velocity  $v_{k_0}$ . The main problem of the entire algorithm is the lack of information about the system conditions and dynamics in the initial phase of the calculations (before the simulation starts). With regard to the current situation, it is known:

- what is the initial position of the beam and the grain, and the initial velocity of the beam (i.e. at time  $t_{c_1}$ ),
- the velocity of the beam at the time  $t_{c_1}$  depends only on the excitation and the properties of the beam,
- the analytical solution for the dynamic response of the beam based on the Simplified Model does not take into account the contact forces, so it is not possible to observe disturbances in the beam response as a result of such phenomena by utilizing the Simplified Model.

The above facts cause that determination of the initial velocity of the grain immediately after the impact using commonly used mathematical methods is impossible. Therefore, a simplified method of determining the grain velocity has been adopted. To explain the proposed approach, the simulations of system response were performed using a 2-DOF soft contact model, where an optimal damper height was assumed and the velocity of

the particle and beam was determined in an optimally damped and stabilized state. The example results are presented in Figs. 4.19 and 4.20.

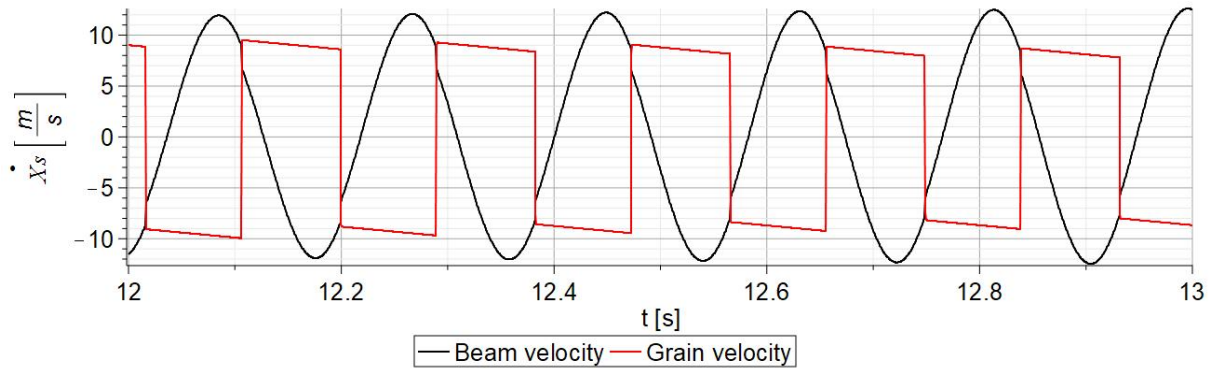


Figure 4.19: Example result of the beam and grain velocity obtained from a Classic Model with optimal height

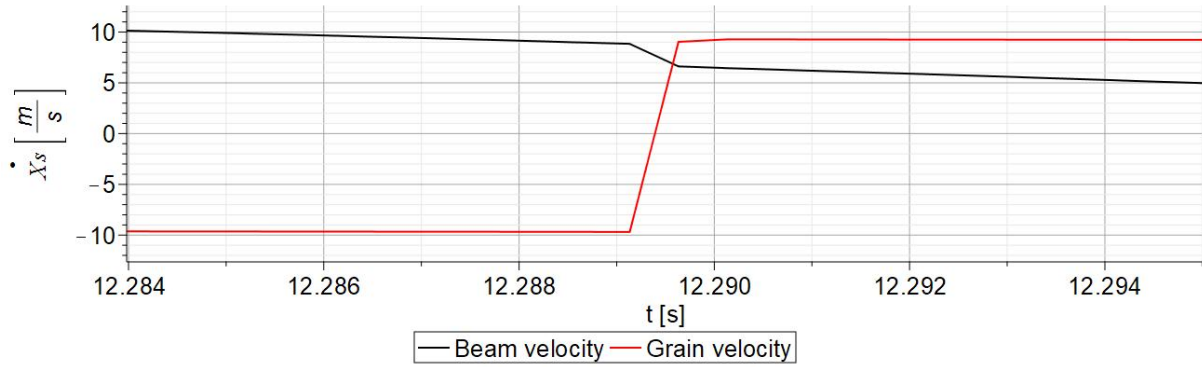


Figure 4.20: Beam and grain velocity for a classic model with optimal height - short range of the time

By analyzing Figs. 4.19 and 4.20 in detail, it can be observed that after the grain hits the floor or ceiling of the cylinder, it reaches a velocity close to the velocity of the beam before the impact. Based on these observations, it is assumed that in the first iteration of Predictive Model calculations, the initial velocity of the particle will be assumed to be equal to the velocity of the beam at the time of the collision, i.e. at time  $t_{c_1}$ . This assumption can be described by the formula:

$$V_{k_0} = \dot{x}_{pred}^s(t = t_{c_1}) = 2\pi f A_{pred} \cos(2\pi f t_{c_1}) \quad (4.25)$$

After the impact, the grain is expected to move without encountering any further collisions, and its motion can be described as an uniformly decelerated. Hence, the equation that describes value of the grain displacement at the time  $t_{c_2}$ , will take the following form:

$$X_g = x_{k_i} + V_{k_0}(t_{c2} - t_{c1}) - \frac{g(t_{c2} - t_{c1})^2}{2} \quad (4.26)$$

The collision of the grain with the upper wall of the damper will occur when:

$$X_g + r = x_{pred}^{t_{c2}} \quad (4.27)$$

Substituting the Eqs.4.21 and 4.26 into Eq. 4.27, the general form is as follows::

$$r + A_{pred}\sin(2\pi f t_{c1}) + V_{k_0}(t_{c2} - t_{c1}) - \frac{g(t_{c2} - t_{c1})^2}{2} + r = A_{pred}\sin(2\pi f t_{c2}) + h_{pred} \quad (4.28)$$

By transforming the Eq. 4.28, the general formula for the predicted height of the ATPID damper takes the form:

$$h_{pred} = 2r + A_{pred}\sin(2\pi f t_{c1}) + V_{k_0}(t_{c2} - t_{c1}) - \frac{g(t_{c2} - t_{c1})^2}{2} - A_{pred}\sin(2\pi f t_{c2}) \quad (4.29)$$

In the specific case of the previously assumed assumptions ( $t_{c1} = 0$  and  $t_{c2} = \frac{1}{2f}$ ), the equation simplifies to a special form which will be used in the first iteration of the calculations:

$$h_{pred} = 2r + V_{k_0}(t_{c2}) - \frac{g(t_{c2})^2}{2} - A_{pred}\sin(2\pi f t_{c2}) \quad (4.30)$$

#### *Application of the Simplified Model and Predictive Model*

The first iteration of calculations of the PCA algorithm (application of Simplified Model and Predictive model) was used to determine  $h_{pred}$  for 3 different excitation amplitudes  $A = 0.07$  [m],  $A = 0.05$  [m], and  $A = 0.02$  [m]. The results were compared against each other and presented in Figures 4.21 - 4.22. For an excitation amplitude equal to  $A = 0.07$  [m], the preliminary predicted height is  $h_{pred} = 1.98$  [m]. The optimal value was previously obtained using the 2-DOF soft contact model by searching the height of the damper over a wide range and identifying the value for which the vibration amplitude was minimal. The optimal height for these parameters is equal to 1.41 [m]. The determined height  $h_{pred}$  was included in the 2-DOF soft contact model and a numerical simulation was performed. The response of the system was presented in Fig. 4.21.

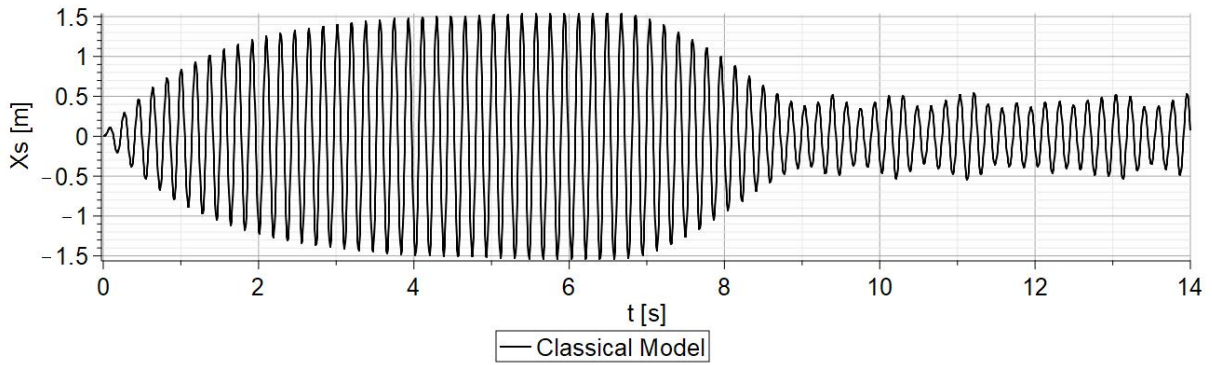


Figure 4.21: Response of the beam vibrations for 2-DOF soft contact model with initially predicted ATPID height for excitation amplitude  $A = 0.07$  [m]

Analyzing the results, it can be observed that the preliminarily determined height is larger than the optimal one, and a rumble effect is observed in beam vibrations. For the remaining vibration amplitudes,  $A = 0.05$  m and  $A = 0.02$  m, the preliminary predicted height  $h_{pred}$  is 1.4 m and 0.55 m, respectively. The vibrations of the beam for the above parameters determined by 2-DOF soft contact model are shown in Figs. 4.23 and 4.22.

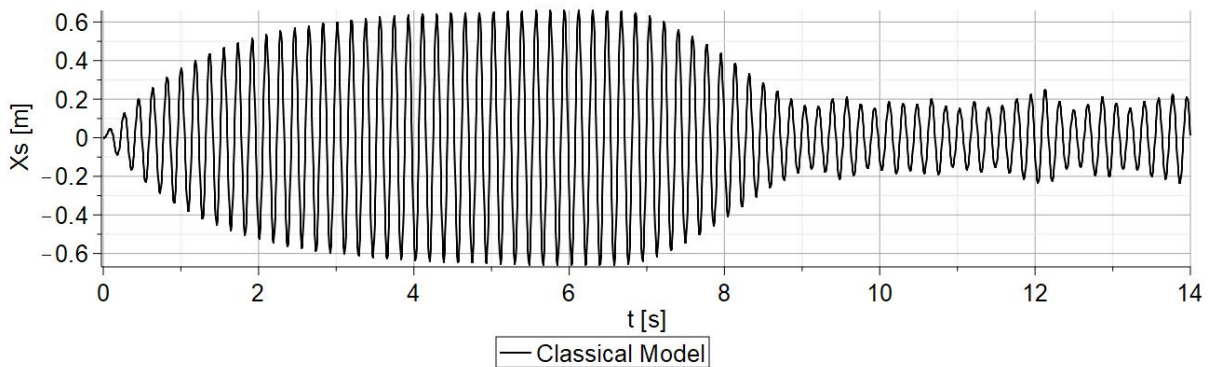


Figure 4.22: Response of the beam vibrations for 2-DOF soft contact model with initially predicted ATPID height for excitation amplitude  $A = 0.05$  [m]

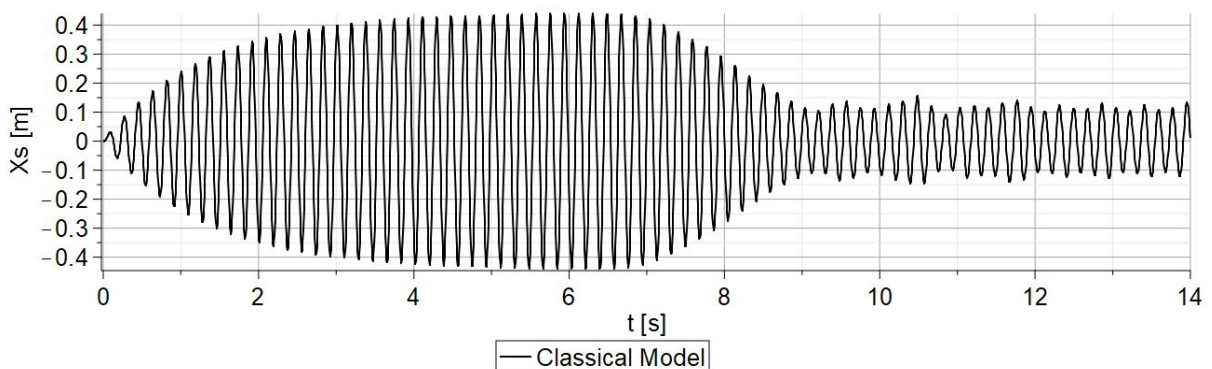


Figure 4.23: Response of the beam vibrations for 2-DOF soft contact model with initially predicted ATPID height for excitation amplitude  $A = 0.02$  [m]

The results from the plots in Figs. 4.21 - 4.23 demonstrate that in all three situations, the predicted height surpasses the height that would be most effective in decreasing mechanical vibrations in the tested system. Nevertheless, after the specified height  $h_{pred}$  is established, the system starts to vibrate in a chaotic manner because of the irregular movement of the grain in the container. Additional analysis will be performed to identify the optimal height of the damper so that the particle movement fulfill the predetermined criteria. Fig. 4.24 presents the initial stage of the grain movement inside the damper by utilizing the results obtained from both the first iteration of the Simplified Model and Predictive Model (SM + PM<sub>1</sub>),

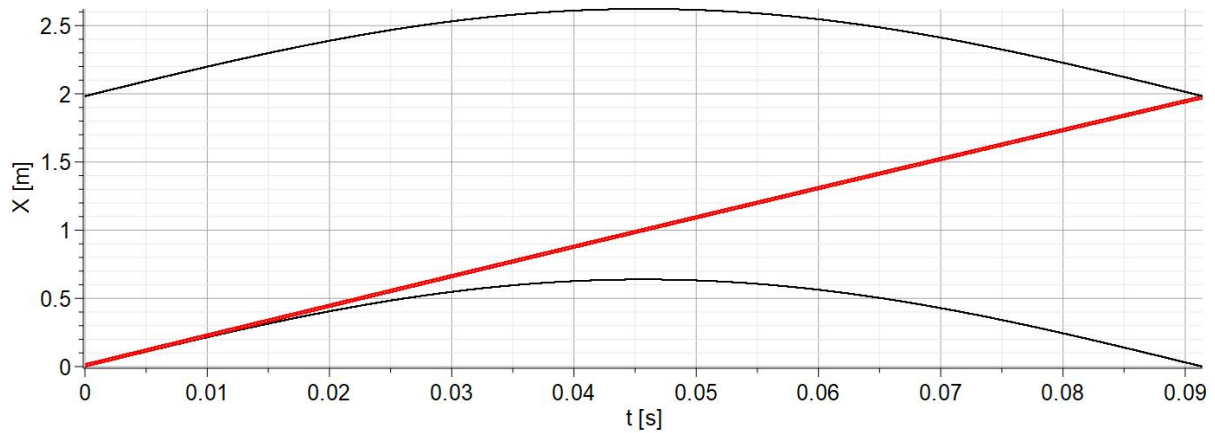


Figure 4.24: Upward motion of the grain in the container with initially predicted height  $h_{pred}$  from the Predictive Model

The displacement of the bottom wall of the container is given by the analytical solution  $x_{pred}^s$  obtained from the Simplified Model (Eq. 4.19). The displacement of the upper wall of the container can be determined as the sum of the displacement of the floor and the predetermined height of the damper (Eq. 4.21). Based on the initial velocity of the grain, its movement towards a collision with the damper ceiling can be observed. Both the initial collision with the bottom wall and the subsequent collision with the upper wall of the damper occur when the position of the beam assumes the zero value (when its velocity is maximum and in this case equal  $V_{grain} = V_{beam} = 21.96$  [m/s] after the collision between grain and damper floor). In order to proceed to the next analysis, the further trajectory of the grain was calculated. After contacting the upper wall, the velocity of the particle was assumed in a similar manner as at the beginning of the simulation (equal to the velocity of the beam before the collision). As a result, the displacement of the grain while moving downward was determined. Such results are presented in Fig. 4.25.

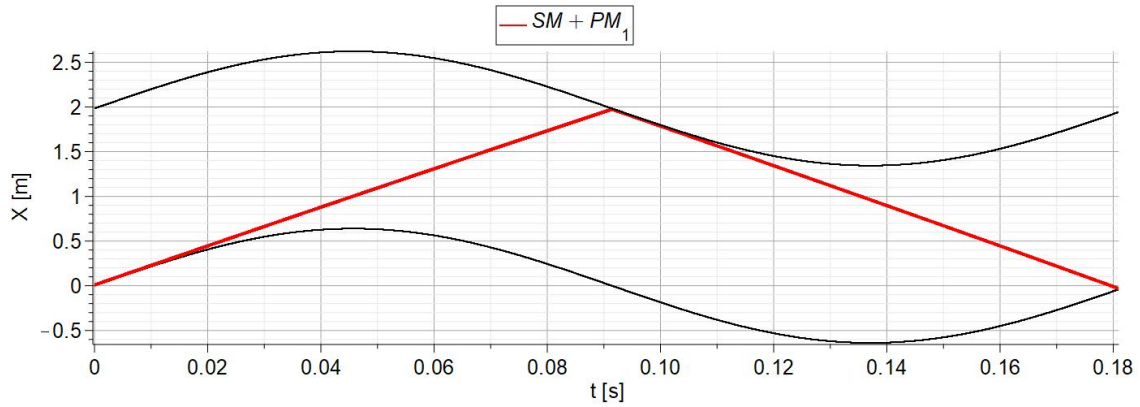


Figure 4.25: Upward and downward motion of the grain in the container with initially predicted height  $h_{pred}$  from the Predictive Model

Next, the time at which the grain collided again with the bottom wall of the damper was identified. The position and velocity of the beam and the particle at the moment of collision are respectively  $X_{beam} = -0.0402$  [m],  $X_{grain} = -0.0317$  [m],  $V_{beam} = 21.92$  [m/s] and  $V_{grain} = -22.79$  [m/s]. These values constitute the initial conditions for the simulation, which will be continued in the Complex Model.

*Application of the Complex Model and Predictive Model*

As was mentioned, the Complex Model is the same 2-DOF soft contact model that was used in the dedicated to the ATPID damper modelling (described in Chapter 3). It takes into account more physical phenomena (including collisions) compared to the Simplified Model. The main advantage is the ability to account for disturbances in the dynamics of the beam due to collisions with the grain. For the previously computed initial conditions and calculated primary height of the damper from the Predictive Model ( $PM_1$ ), the previous (first) simulation was continued with the use of the Complex Model ( $CM_1$ ) and the results are presented in Fig. 4.26.

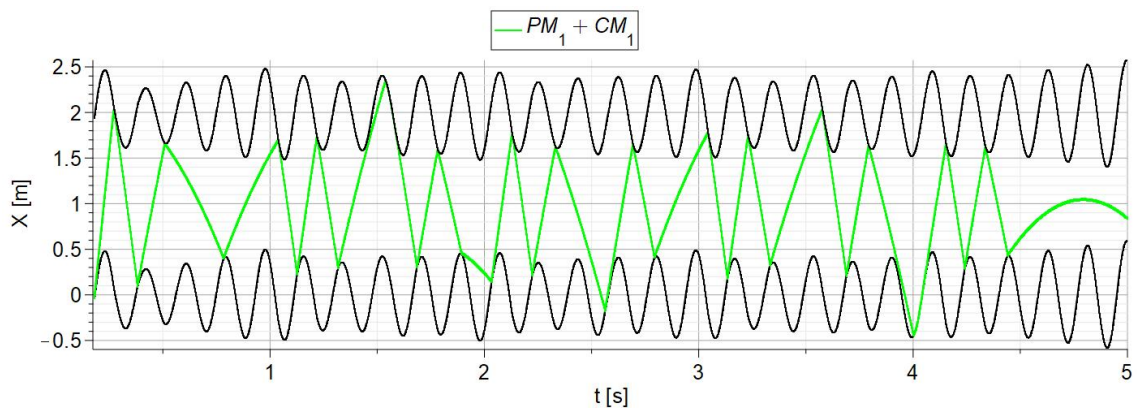


Figure 4.26: Motion of the grain and damper walls in the Complex Model with initially predicted height of the container from the Predictive Model

The graph indicates that for the calculated damper height, an unpredictable movement of the grain and a rumble effect occur which confirms that the determined height is too high. Therefore, it was decided to limit the analysis to the initial upward and downward motion of the particle until the next impact against the lower wall of the container. The detailed section of the graph under consideration has been presented in the following figure.

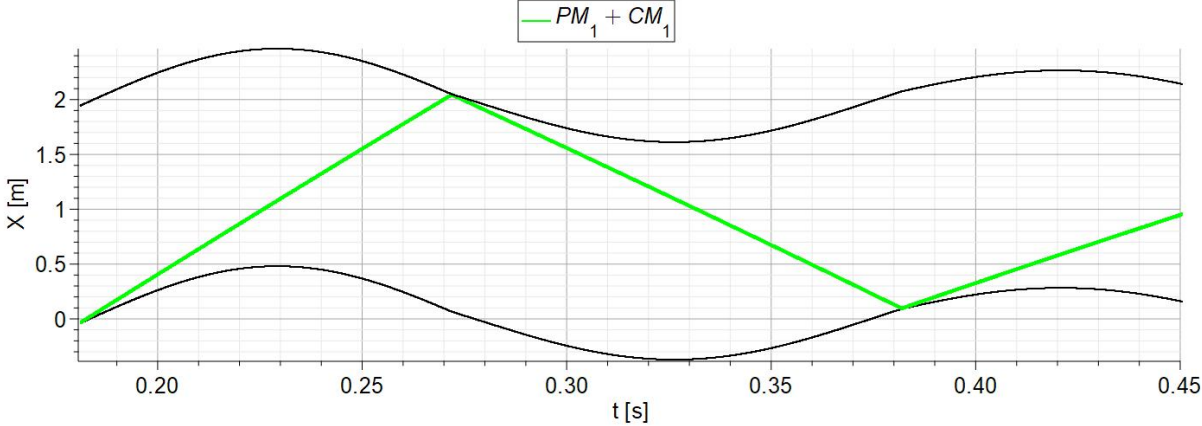


Figure 4.27: A short time motion of the grain and damper walls in the Complex Model with initially predicted height of the container from the Predictive Model

In the next step, it is essential to identify the end of the current simulation by determining the time at which the first impact of the particle with the bottom of the damper occurs. This is achieved by calculating the lower overlap and performing its detailed analysis. An illustrative plot is shown in Fig. 4.28 where the first lower overlap is identified in a wide range of time.

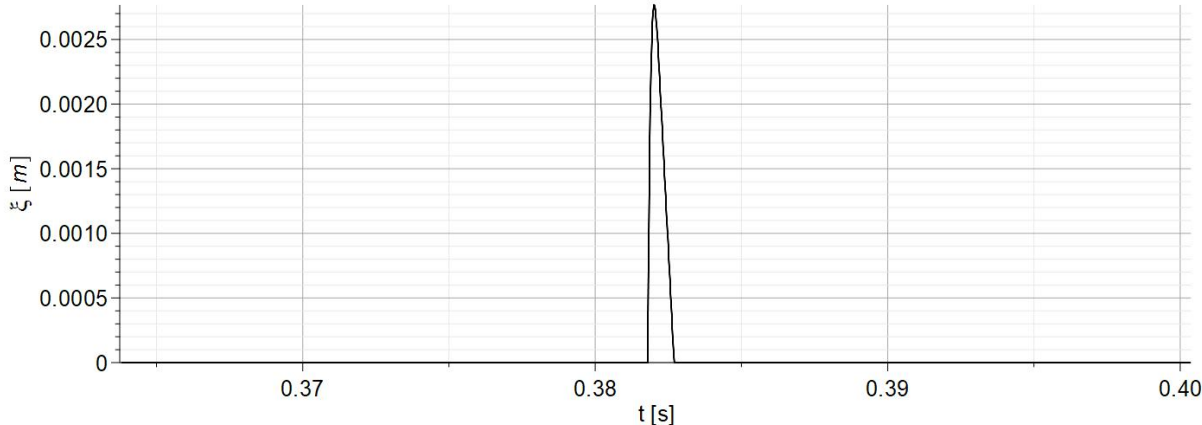


Figure 4.28: Identification of the grain collision (overlap) with the lower wall of the container

Next, the precise start time of the impact is identified, and based on that, the end time of the impact can be determined. This time denotes the end of the current simulation. A detailed plot describing the identified lower overlap is presented in Fig. 4.29.

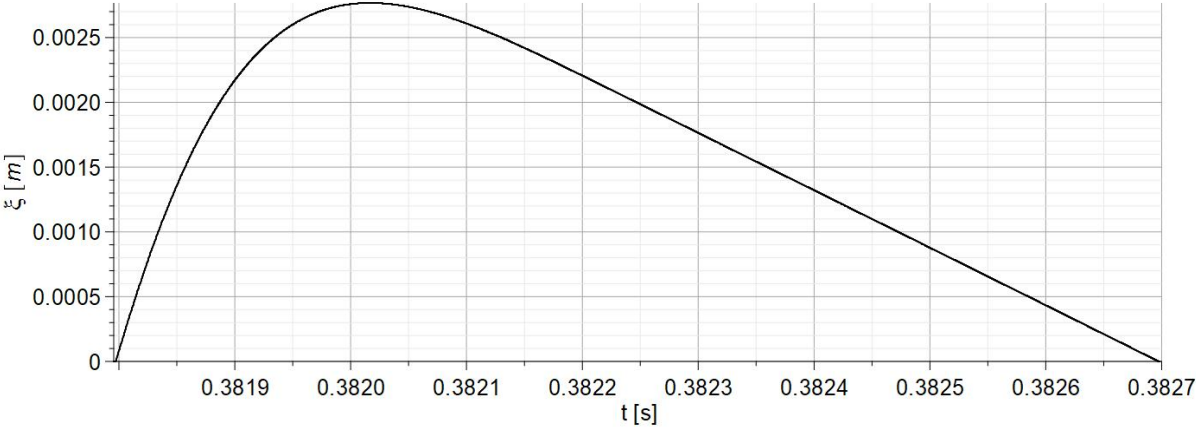


Figure 4.29: Detailed identification of the grain collision (overlap) with the lower wall of the container

In summary, the entire movement of the particle and the damper walls can be determined from the start of the Predictive Control Algorithm process, where the initial system response and damper height were determined. In particular, the first cycle of upward and downward movement of the grain and the damper can be computed using the Simplified Model and Predictive Model -  $SM + PM_1$ . The second cycle of upward and downward movement of the grain can be computed for previously determined damper height using Predictive Model and Complex Model ( $PM_1 + CM_1$ ) taking into account collisions described by soft contact theory. The plot of the grain’s movement inside the container from the beginning of the simulation is shown in Fig. 4.30.

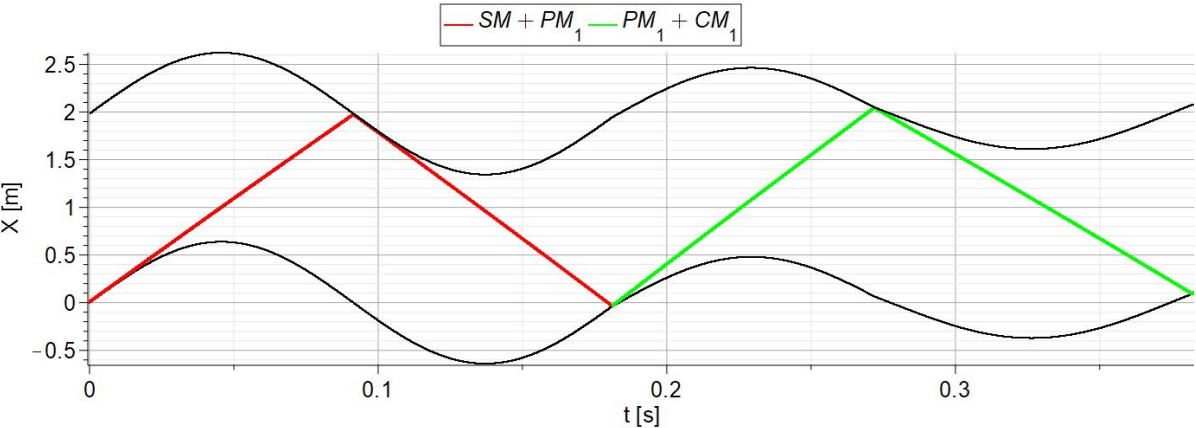


Figure 4.30: Motion of the grain and damper walls from the beginning of the calculations

The position and velocity of the beam and the grain at the end of the impact are  $X_{beam} = 0.097$  [m],  $X_{grain} = 0.1055$  [m],  $V_{beam} = 8.38$  [m/s],  $V_{grain} = 12.83$  [m/s]. These values will be treated as input data for further calculations in the Predictive Model.

The initial damper height was calculated using the formula 4.30 and by assuming a specific situation where all collisions occurred when the beam reaches maximum velocity. Therefore, the times of collision between the grain and the lower ( $t_{c1}$ ) and upper ( $t_{c2}$ ) walls of the container were assumed as 0 and  $1/(2f)$ , respectively. To determine the new height of the damper, one needs to use the general form of Eq. 4.29. To better describe the subsequent mathematical operations, the above formula is below:

$$h_{pred} = 2r + X_{beam} + V_{grain}(t_{c2} - t_{c1}) - \frac{g(t_{c2} - t_{c1})^2}{2} - A_{pred}\sin(2\pi f t_{c2}) \quad (4.31)$$

The times  $t_{c1}$  and  $t_{c2}$  denote the contact time of the grain with the lower and upper wall of the damper, based on the system response predicted  $A_{pred}$  using the Simplified Model. The response of the system from the SM differs slightly from the response of the system from the Complex Model, what is presented in Fig. 4.30. Therefore, the time  $t_{c1}$  should be determined by solving the equation 4.32.

$$A_{pred}\sin(2\pi f t_{c1}) = X_{beam} \quad (4.32)$$

The above equation has many solutions and the time  $t_{c1}$  can assume many values, but for further calculations, I take into account the value that is in the first period of vibrations. Therefore, to fulfill the assumption that the grain has to collide with the ceiling of the damper when it reaches maximum velocity, the time  $t_{c2}$  has to be equal to  $1/(2f)$ .

The Eq. 4.31 contains several constant components, such as the radius of the grain  $r$ , gravity  $g$ , the beam response amplitude determined from the Simplified Model  $A_{pred}$ . The assumption that the collision between the grain and the upper wall of the damper will occur when the beam velocity is maximal, which directly affects the value of the time  $t_{c2}$ . There are also terms that possess more physical characteristics due to viscoelastic collisions, primarily the position and velocity of the beam and grain at the end of the previous simulation and correspond to the times  $t_{c1}$  and  $t_{c2}$ . These values serve as initial data to calculate the new height  $h_{pred}$ . One of the main parameters is the initial velocity of the particle  $V_{k0}$ , which assumes the value from the end of the previous stage of the simulation:  $V_{grain} = 12.83$  [m/s]. These calculations also need to

be performed for a situation where the beam position  $A_{pred} \sin(2\pi f t_{c1})$  after the grain collision with the container floor is equal to the beam position at the end of the previous simulation  $X_{beam} = 0.097$  [m]. The solution of the equation yields a new time  $t_{c1}$ . Next, it is necessary to determine for which value of  $t_{c2}$  cyclic collisions between the particle and the upper part of the container will occur when the beam velocity is at its maximum.

The above assumptions allow determining the new height of the ATPID damper. For the newly determined height from the second iteration of the Predictive Model ( $PM_2$ ), simulations are continued using only the Complex Model ( $CM_2$ ). If the random movement of the grain without cyclic collisions with damper ceiling and floor is still observed without cyclic collisions with the damper ceiling and floor, the entire process of determining the damper height is repeated for new values of the particle and beam velocity and position. In most cases, however, longer observation of the grain's motion inside the container allows to conclude that the beam vibrations are stabilized and damped. An example of such analysis is presented in Fig. 4.31.

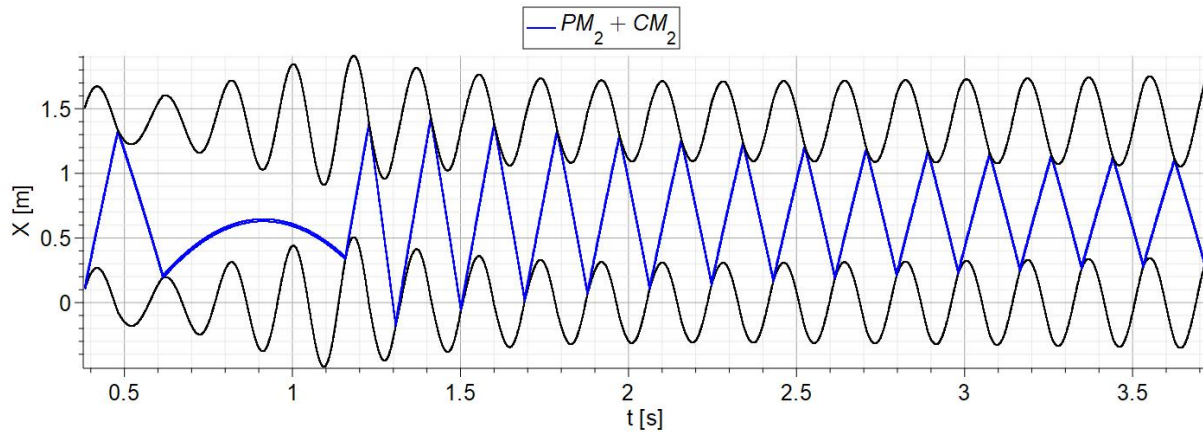


Figure 4.31: Motion of the grain and container for new predicted damper height

Analyzing the obtained results, it turns out that collisions between the particle and the container are cyclic and occur when the direction of the grain is opposite to the direction of the damper movement, the beam velocity is close to the maximum, and there is no sticking effect between the grain and cylinder walls. This means that all criteria for optimal grain movement are fulfilled. The movement of the particle inside the container controlled by the entire PCA algorithm is shown in Fig. 4.32.

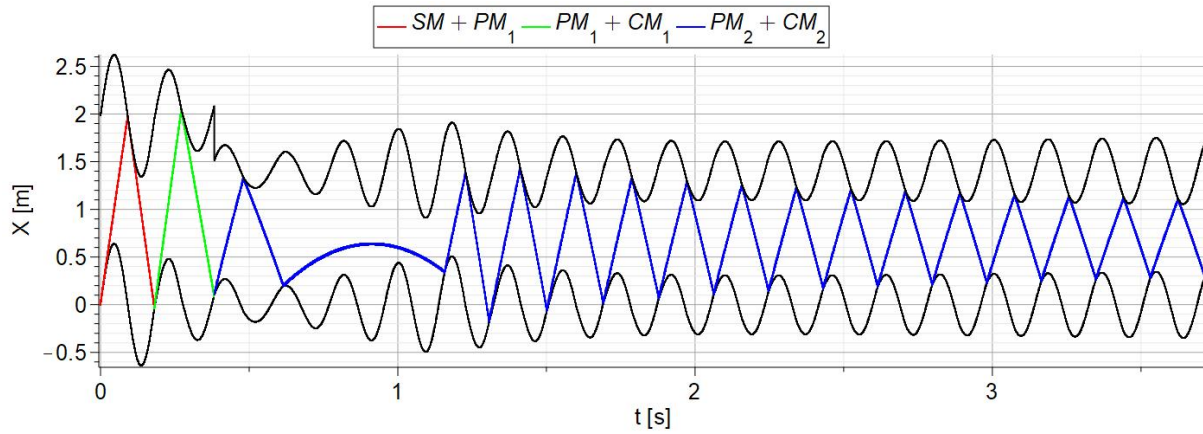


Figure 4.32: Motion of the grain and damper walls from the beginning of the calculations

The final value of the height determined using the PCA algorithm was named the initial optimal height. Despite this, once all the preliminarily assumed conditions are fulfilled, it is still important to ensure that the initially determined damper height is finally optimal, i.e., the amplitude of the beam's vibration response is minimized. Therefore, it is necessary to search through a range of values close to the last predicted height and determine for which height of the container the system's response is minimal.

#### Precise tuning of pre-determined ATPID height

The searching process involves decreasing the previously calculated damper height by 10% of its value and checking the changes in the system's response. The height decrease process is repeated until the system's response amplitude will start to increase. The last calculated height ( $h_{pred}$ ) value is then increased by  $\frac{h_{pred} \cdot 10\%}{1.5}$  and the beam's response is analyzed again. This stage is repeated until the system's response begins to deteriorate (the vibration amplitude starts to increase). The entire procedure is then repeated, and the damper height is changed by  $\frac{h_{pred} \cdot 10\%}{1.5n}$ , where  $n$  increases by 1 every time the transition from decreasing to increasing the height occurs and vice versa is performed. The results obtained from the PCA control algorithm itself are compared with the results from the searching stage, which involves exploring the range of values around the last calculated height, to ensure that the determined height is optimal and provides minimal beam vibration. The results and their comparison are presented below.

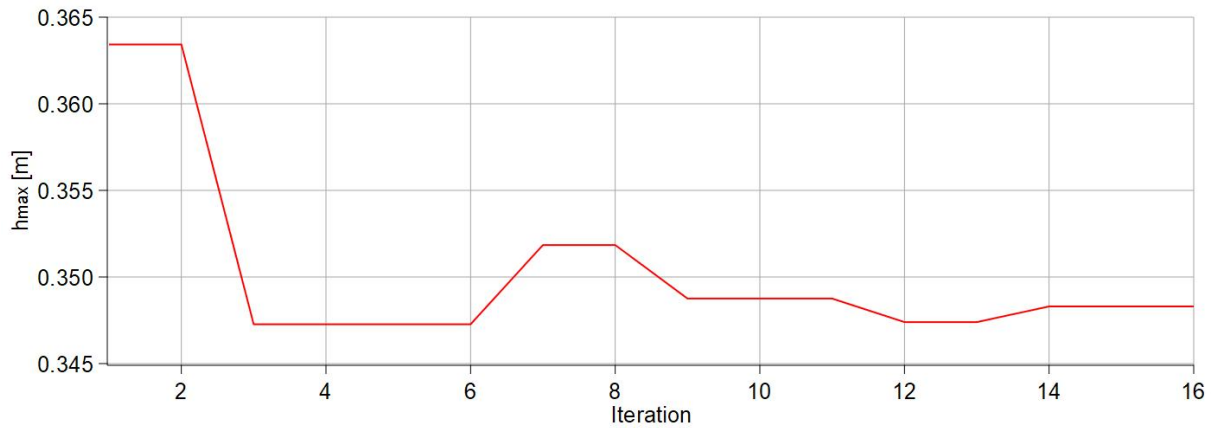


Figure 4.33: Example of the searching process for the optimal ATPID height

Successively determined damper heights obtained from the searching process are shown in Fig. 4.33. This is the final stage that allows determining the optimal height for which the amplitude of the vibration response of the system is minimal (Fig. 4.34). Fig. 4.33 shows a process in which alternately decreasing and increasing the damper height allows for describing the optimal height for the assumed system parameters.

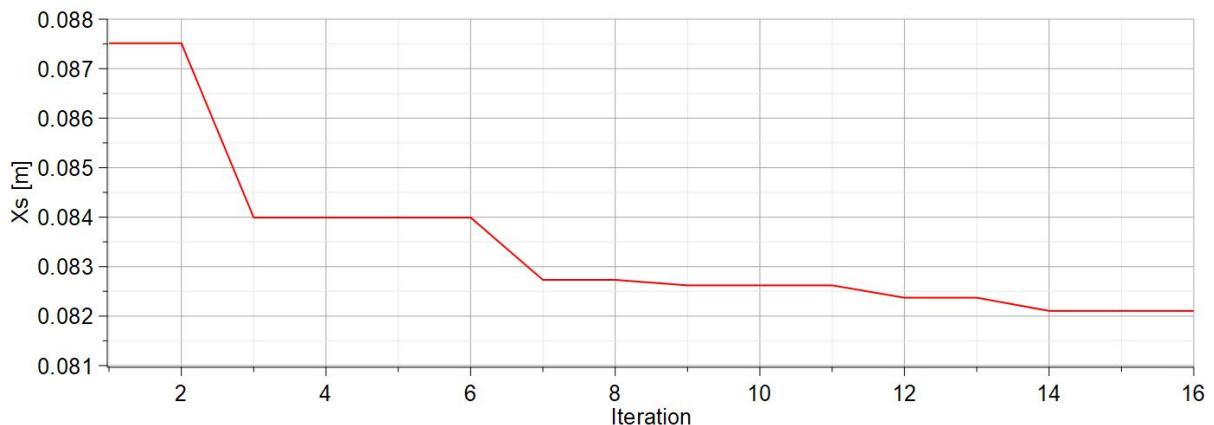


Figure 4.34: Example of the system response changes for the heights analyzed during the searching process

Fig. 4.34 shows the vibration amplitudes of the system for individual heights assumed in the search process. Analyzing this graph, it can be concluded that the beam vibrations are reduced throughout the process, which can clearly indicate the correctness of the algorithm for searching for the optimal height corresponding to minimal vibration amplitude. In the above case, it was enough to perform 16 iterations of calculations, which provided the optimal height of the ATPID damper was determined. In the general case, the scanning process will continue until successively determined heights will result in changes of vibration amplitude smaller than 1 %.

### Sensitivity analysis of the PCA algorithm

The presented control algorithm allows for determining the preliminary height of the damper, which calculated values were close to the optimal one. In order to determine the final optimal value of the container ceiling position, a searching process around the preliminarily determined height was applied. As a result, an algorithm was developed that enables prediction of the ATPID damper size for various system parameters, which provides that the vibrations will be most effectively reduced. Consequently, a sensitivity analysis of the proposed Predictive Control Algorithm was conducted. In the first assumed situation, optimal damper heights are determined (after PCA algorithm and searching process) for various excitation amplitudes and presented in Fig. 4.35. The remaining system parameters are constant and assume the values:  $m_s = 0.905m_b = 0.3258$  [kg],  $m_g = 0.1M_s = 0.0362$  [kg],  $k_s = 427.6[\frac{N}{m}]$ ,  $c_s = 0.56[\frac{Ns}{m}]$ ,  $A = 0.07$  [m] and  $f = 5.469$  [Hz].

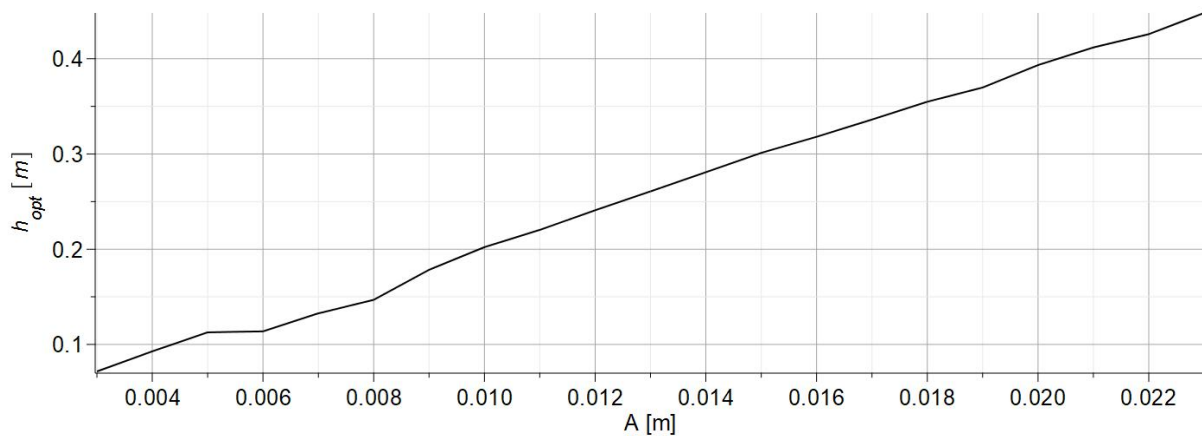


Figure 4.35: Change of the optimal ATPID height for a narrow range of excitation amplitudes

By analyzing Fig. 4.35, it can be observed that the change in optimal height for different excitation amplitudes gradually increases and is close to linear. These calculations were performed for a narrow range of amplitudes (up to 0.022 [m]). The results are interesting because the numerical model of the system is nonlinear. Similar analyses were conducted for a wide range of excitation amplitude changes (up to 1 [m]) and are presented in Fig. 4.36.

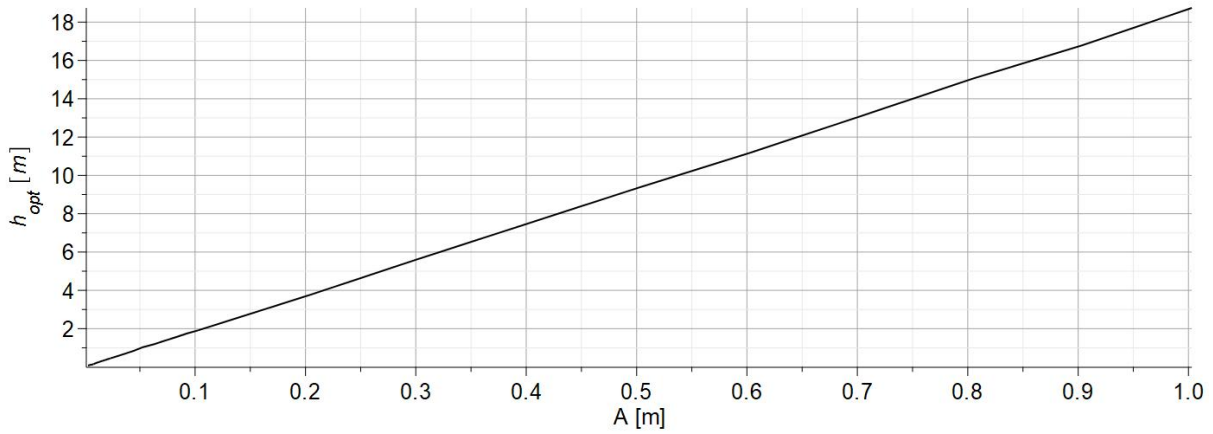


Figure 4.36: Change of the optimal ATPID height for a wide range of excitation amplitudes

Based on Fig. 4.35, it can be concluded that the change of the optimal heights for a wide range of excitation amplitudes is still linear. The next analyses that were conducted involved computing the percentage difference between the preliminary damper height value determined by the PCA algorithm and the final optimal height obtained through the search process. These results will serve as a parameter describing the effectiveness of the proposed PCA algorithm. The analyses were performed for a wide range (Fig. 4.37) and a narrow range (Fig. 4.38) of excitation amplitudes.

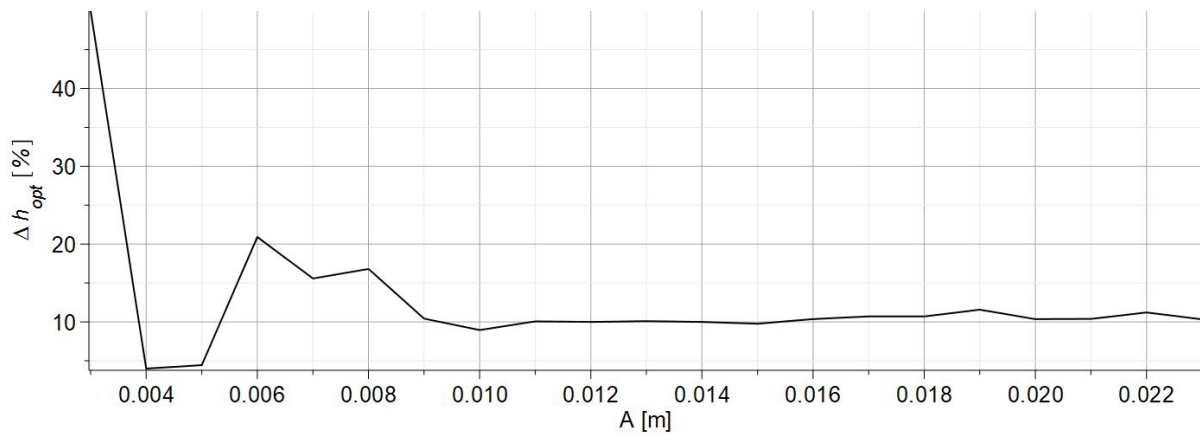


Figure 4.37: The percentage difference between the initial optimal height (determined from PCA) and the final optimal height (determined from the search stage) for a narrow range of excitation amplitudes

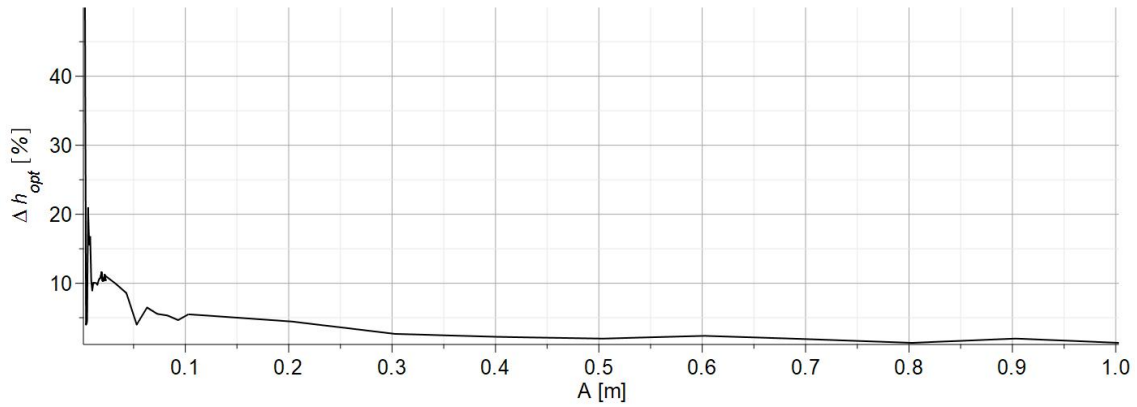


Figure 4.38: The percentage difference between the initially optimal height (determined from PCA) and the final optimal height (determined from the search stage) for a wide range of excitation amplitudes

Fig. 4.38 shows that the percentage error decreases to 4% as the excitation amplitude increases. An interesting phenomenon is the occurrence of large percentage discrepancies (from about 50% to 10%) for small amplitudes of excitation (up to about 0.1 m). Gravity is believed to be mainly responsible for discrepancies. Small excitation amplitudes correspond to small velocities and accelerations of the vibrating system and grain. This causes the grain in the open damper to remain in constant contact with the floor. Even when it does detach, the distance achieved between them is small. In such a case, it is difficult to correctly determine the height of the damper using the PCA algorithm while considering all the criteria that describe the optimal motion of the grain. As a result, the discrepancy between the initially determined height and the final optimal height is large. Next, optimal heights of the ATPID damper were determined for two other grain masses ( $m_g = 0.2M_s$  and  $m_g = 0.3M_s$ ) for a wide range of excitation amplitude changes. The results are shown in Fig. 4.39.

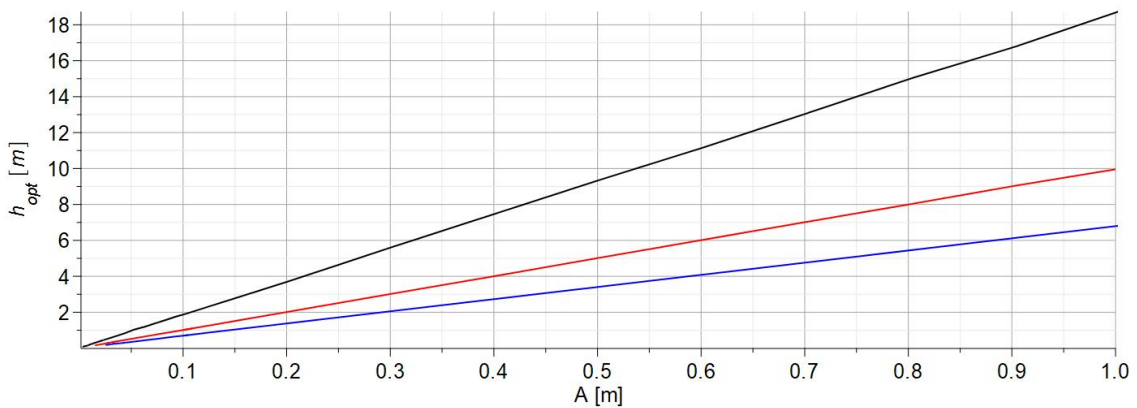


Figure 4.39: Change of the optimal ATPID height for a wide range of excitation amplitudes for three different grain masses:  $0.1M_s$  (black line),  $0.2M_s$  (red line),  $0.3M_s$  (blue line)

The linear relationship between the optimal absorber height and the excitation amplitude occurs in all three cases presented in Fig. 4.39. Calculations were also made for grain masses ranging from 10% to 30% of the total system mass. The optimal heights depend in a similar way on the change in amplitude and can be described by linear regression models with different slope parameters for each case. However, these results were not included in the figure for the sake of consistency and clarity. For the above three different cases, the effectiveness of the PCA algorithm was calculated for three different masses and the results are shown in Fig. 4.40.

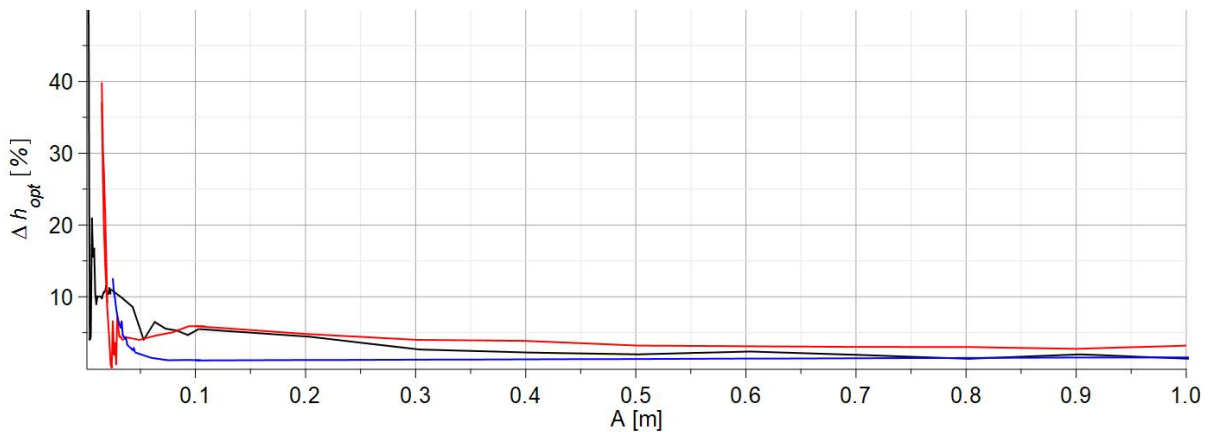


Figure 4.40: The percentage difference between the initial optimal height (determined from PCA) and the final optimal height (determined from the search stage) for a wide range of excitation amplitudes and three different grain masses:  $0.1M_s$  (black line),  $0.2M_s$  (red line),  $0.3M_s$  (blue line)

Based on the obtained results, it can be concluded that for the cases where the grain had different masses, the effectiveness of the algorithm depends on the value of excitation amplitude. For small excitation amplitudes (differences ranging from 40% to 10%). For increasing amplitude values, the error decreases and the difference between the initially determined height (from the PCA algorithm) and the height after the search stage is approximately 4%. These values can be considered as acceptable from a functional point of view. As previously mentioned, the small effectiveness of the algorithm for small excitation amplitudes is due to the significant influence of gravity on the dynamics of the system. To confirm the correctness of this assumption, the optimal damper heights (for cases with and without gravity) were determined for a wide range (Fig. 4.41) and a narrow range (Fig. 4.42) of excitation amplitudes, as well as for different grain masses (the results shown on the graphs concern a particle of a mass equal to 10% of the total system mass). Additionally, the percentage error determining the effectiveness of the PCA

algorithm was calculated and presented in Fig. 4.43.

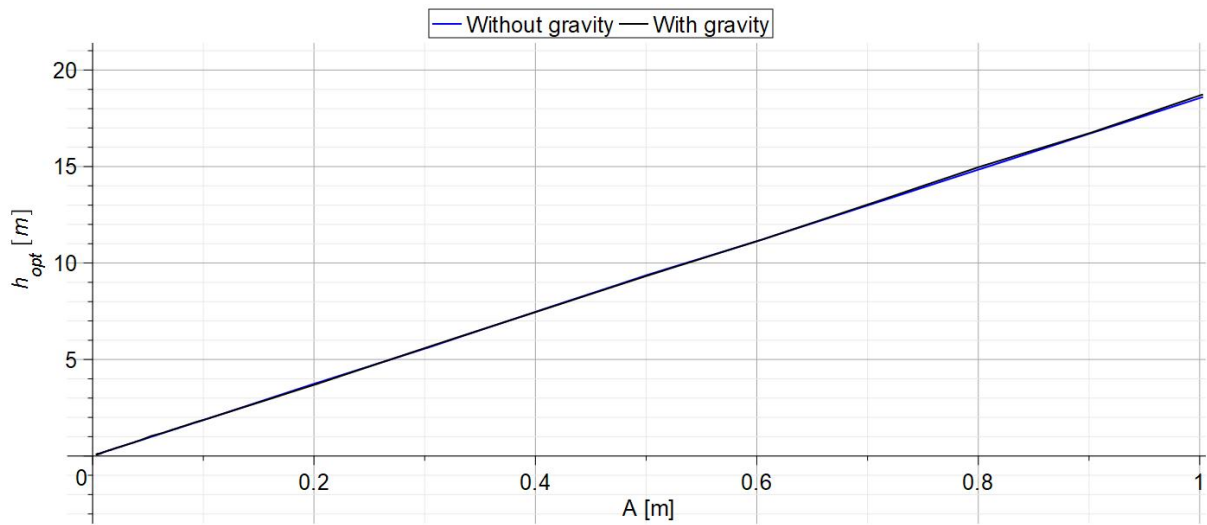


Figure 4.41: Change of the optimal ATPID height for a wide range of excitation amplitudes for the system taking into account and disregarding the force of gravity

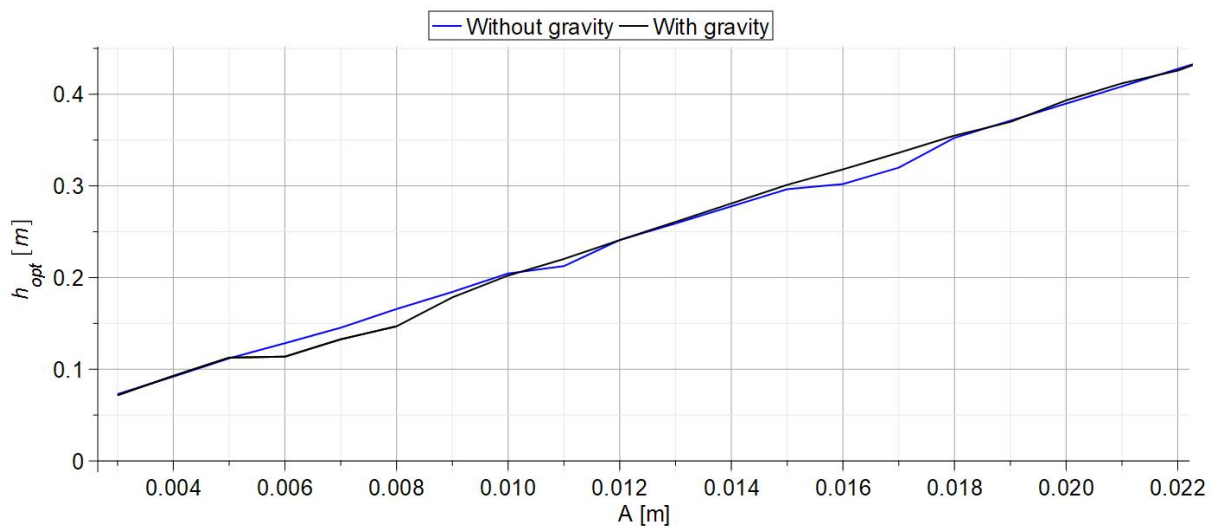


Figure 4.42: Change of the optimal ATPID height for a narrow range of excitation amplitudes for the system taking into account and disregarding the force of gravity

Figs. 4.41 and 4.42 present the linear correlation between the optimal height of the ATPID damper for various excitation amplitudes for two distinct system: one with gravity and one without gravity. The plots demonstrate that the optimal absorber height for the given amplitude remains almost the same regardless of whether gravity is considered or not, indicating no significant difference. A more precise analysis of the impact of gravity is provided by comparing the calculated errors for both considered cases. Fig. 4.40 presents a case where numerical analysis incorporates the influence of gravity and the error in the PCA algorithm calculations for small amplitudes is con-

siderably high. A corresponding scenario was computed by eliminating the impact of gravity from the system, and the efficiency results of the PCA algorithm were presented in Figure 4.43.

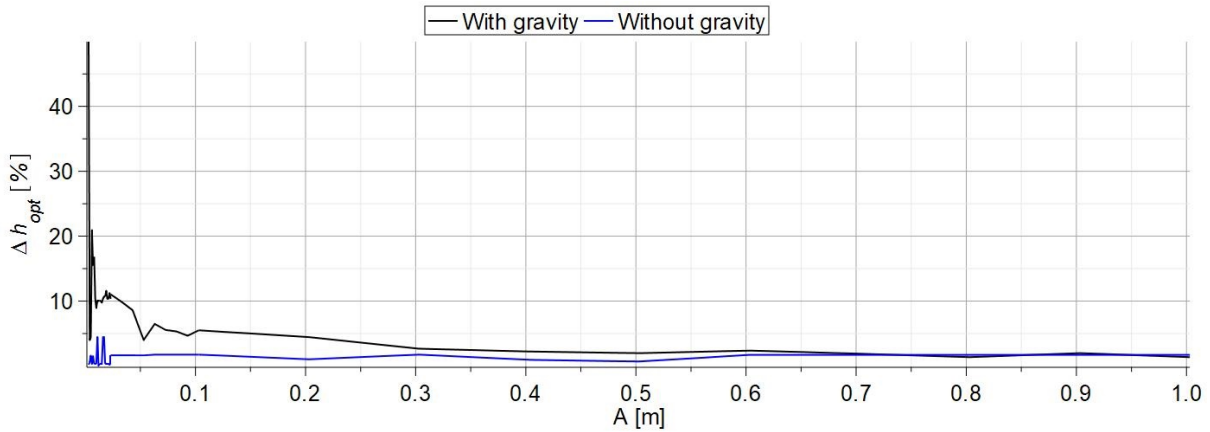


Figure 4.43: The percentage difference between the initially optimal height (determined from PCA) and the final optimal height (determined from the search stage) for a wide range of excitation amplitudes (system with and without gravity)

It turns out that the lack of consideration of the phenomenon of gravity causes the PCA algorithm to be very effective for the entire considered range of excitation amplitudes. The error between the results is small and equals approximately 4%. Considering the fact that for both systems (with gravity and without gravity) the determined optimal heights take almost the same values (Fig. 4.41), it can be concluded that in order to increase the efficiency of the control algorithm, a model without gravity can be used.

By examining Fig. 4.39, it is evident that the optimal height changes linearly in terms of the excitation amplitude. To further investigate, an interesting problem is the identification of the type of regression (linear or nonlinear) describing a correlation between the grain and various masses. Hence, an analysis was conducted to determine the optimal height of the ATPID damper for four different excitation amplitudes ( $A_1 = 0.9$  [m],  $A_2 = 0.2$  [m],  $A_3 = 0.1$  [m],  $A_4 = 0.03$  [m]), and for particle masses ranging from 10% to 30% of the total system mass. The obtained results are illustrated in Fig. 4.44.

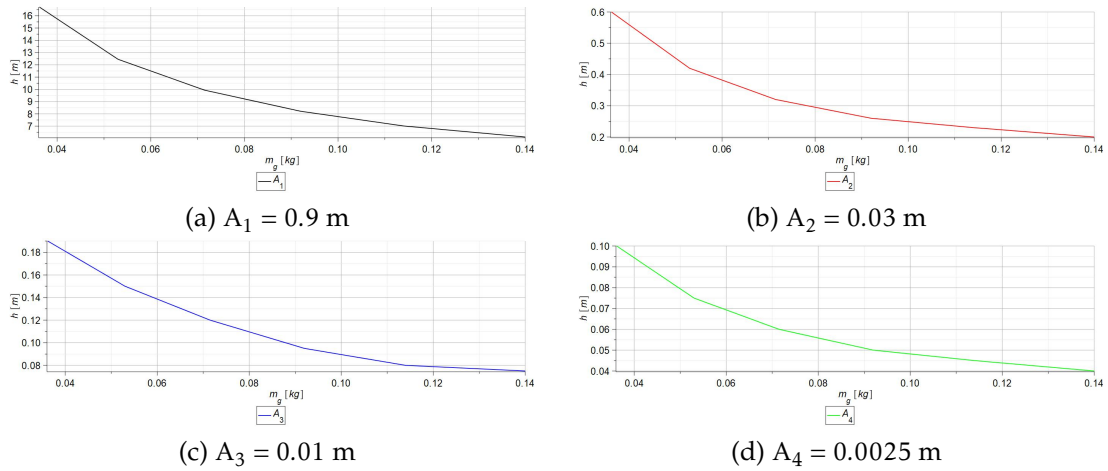


Figure 4.44: Change of the optimal ATPID height in terms of the mass of the grain (from 10 % to 30 % of the mass of the whole system) for various excitation amplitudes

The plots shown in Fig. 4.44 indicate that there is a non-linear relationship between the optimal height of the damper and the change of grain mass, regardless of the excitation amplitude. This non-linearity makes prediction of the system's behaviour difficult. Therefore, there is a need to develop algorithms that can quickly determine the optimal damper height for various combinations of excitation amplitudes and particle masses.

In the final stage of the analysis, the parameter  $d$  (defined as the percentage ratio of the amplitudes of optimally damped steady-state vibrations and undamped steady-state vibrations) was determined using the optimal height obtained from the proposed PCA algorithm and searching process in order to increase of damper effectiveness. The results are shown in Figs. 4.45 and 4.46.

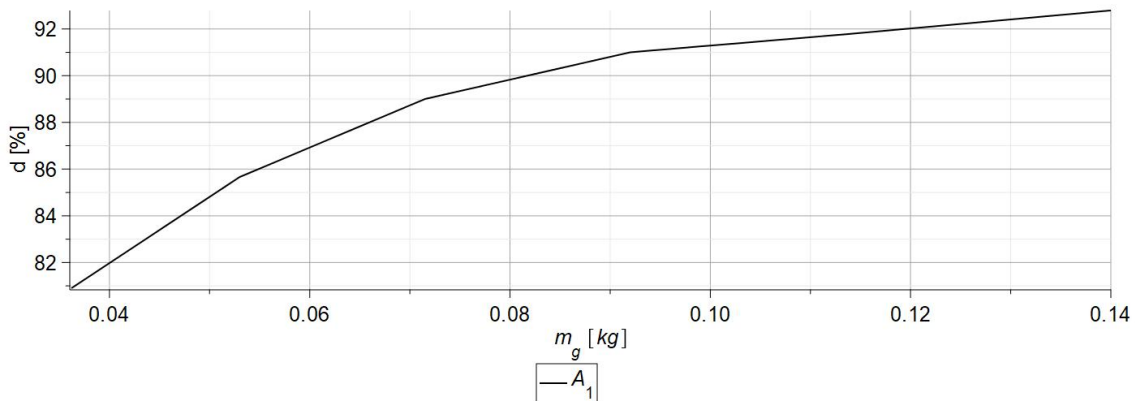


Figure 4.45: ATPID damper efficiencies corresponding to optimal container heights for various grain mass and excitation amplitude  $A_1$

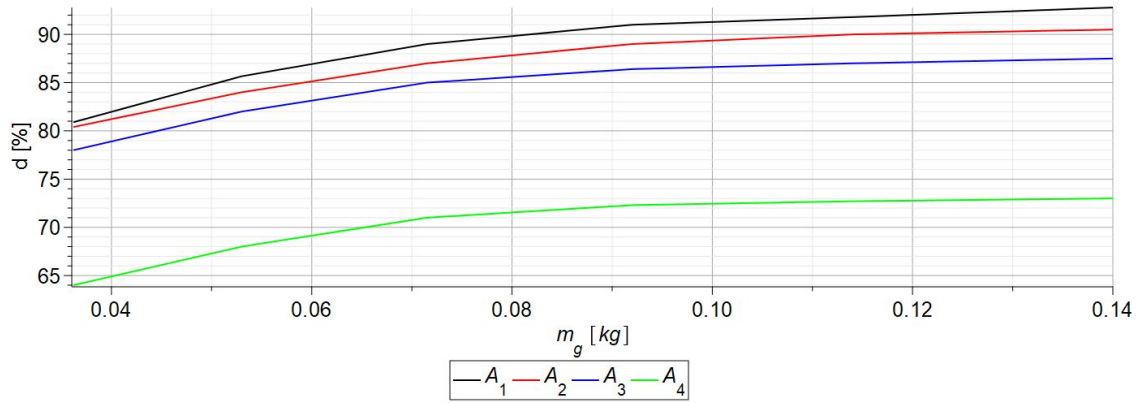


Figure 4.46: ATPID damper efficiencies corresponding to optimal container heights for various grain mass and excitation amplitudes

Fig. 4.46 shows that an increase of the mass of the grain improves the efficiency of the ATPID damper. For the applied excitation amplitudes, the vibrations of the system are reduced by approximately 92% for a mass equal to 30% of the mass of the whole system. It should be noted that the ATPID device was designed to damp vibrations as an additional component attached to the basic vibrating structure. Therefore, considering a larger mass is unnecessary because then the damper should be treated as a basic dynamic structure and then will play a dominant role in the whole system. For smaller masses of grain, the efficiency of the ATPID damper decreases non-linearly. For various amplitudes of the vibration, a different damping efficiency can be achieved. For the case  $A_1$  (black line) the maximal  $d$  can be obtained. For the lower excitation amplitude, a decreased damping efficiency can be observed.

These results confirm the previous calculations shown in Fig. 3.25. The difference between Figs. 3.25 and 4.46 is the method that allows to the determination of the optimal height of the damper. The sensitivity analysis of the PCA algorithm made it possible to assess the correctness of the algorithm and its effectiveness by comparing the obtained results with the results of previous analyses. Unfortunately, the disadvantages of the PCA algorithm include:

- The complete (identified) model of the vibrating structure (beam) and the excitation have to be known.
- The assumption of the grain's initial velocity (is simplified in the first iteration of the PCA algorithm calculation and adopted on the basis of observations).
- The PCA algorithm does not determine the optimal damper height for small excitation amplitudes with a high accuracy. Therefore, this algorithm is supported by the search process.

In order to eliminate the above disadvantages, the following solutions should be proposed in the future research:

- An algorithm that performs structural and parametric identification based on measurements of the vibrating system response.
- Replacing the intermediate data concerning the dynamics of the beam and the grain (used in the Predictive Model stage) by real-time experimental measurements.
- Omitting the influence of gravity.
- Replacing the PCA algorithm and searching process with a neural network model.

# Chapter 5

## Summary

Adaptive Tuned Particle Impact Damper (ATPID) is an innovative type of vibration attenuator, which consists of a container of a controllable size. It allows for dynamic tuning of the system damping and adaptation to the actual excitation.

The author proposed a prototype of the ATPID damper with the controllable height of the container and particle. A series of experimental studies of free and harmonic vibrations of the cantilever beam was conducted. As a part of the practical investigations, several parameters of the system and excitations were taken into account. The conducted research allowed to observe the fundamental behaviours for the initially selected range of damper parameters. It turns out that the effectiveness of vibration reduction in the system is significantly influenced by the height of the damper, which directly describes the change in the volume of the container in which the particle is located. It defines the space for grain movement without a sticking effect between the grain and walls of the damper. This is an important aspect in terms of the frequency of collisions and the duration of contact between the particle and the container. Additionally, the damping of vibrations is affected by the mass of the grain used in the damper. It can be clearly stated that the larger the mass of the particle causes increasing of the vibrations reduction. Studies conducted for different amplitudes of excitation (harmonic vibrations) and initial deflections of the beam (free vibrations) revealed a greater effectiveness in damping vibrations when larger amplitudes of beam vibration responses occur. Subsequently, an attempt was made to provide a theoretical description of the PID damper and the test stand.

Development of efficient methodology of ATPID modelling requires simplification of grain physical properties, soft contact theory based on the Hertzian model, optimization and control strategy as well as experimental validation. The presented re-

sults prove that the proposed method of ATPID modelling based on the soft-contact theory enables accurate simulation of the damper's influence on the mitigation of vibrating system response, which is confirmed by the satisfactory agreement with the conducted experimental tests. The developed mathematical model reveals the fundamental principles of ATPID operation, which include the Mass Modification Effect and Pseudo-Inertial Force Effect. The conducted sensitivity analysis discloses that the increase of container height and grain mass as well as the decrease of excitation amplitude cause gradual change in the type of grain movement from the permanent sticking to container walls through the short cyclic impacts to the chaotic motion with irregular impacts. Moreover, the sensitivity analysis allows to conclude that ATPID operation is the most efficient in the case of short cyclic impacts and to determine the corresponding ranges of container height, grain mass and excitation amplitude. In addition, the analyses based on Specific Damping Coefficient, contact forces and change of system energy indicate that container height is the most important ATPID parameter and reveal the desired range of its maximal values. Eventually, the solution of the optimization problem aimed at finding container height resulting in the most efficient mitigation of system vibrations discloses a decrease of optimal container height along with grain mass and its increase along with applied excitation amplitude. The largest efficiency of the proposed ATPID damper is found to be achieved for the largest grain mass and the largest excitation amplitude. In such a case, the proposed ATPID damper is extremely efficient and allows for reduction of the amplitudes of resonance vibrations up to 90 %. These results were verified by experimental tests.

Then, a general control strategy was proposed, allowing for the basic process of searching for optimal damper heights from the perspective of the most efficient vibration damping. This is a necessary element in the practical implementation of the damper's adaptive functionality. The test stand setup was expanded with a measurement system connected to Arduino microcontroller. The microcontroller identified currently occurring excitation in real-time based on measurements, and then, using a previously created map of optimal parameters, it read the required damper's height. The matrix of the optimal damper heights was created based on the mentioned general control algorithm. Due to the drawbacks and limitations of the initially proposed control algorithm, an attempt was made to create a Predictive Control Algorithm. The proposed feedback loop system based on numerical analysis and experimental measurements allowed for the quick determination of the optimal damper height value. The algorithm procedure involves alternately applying results from the Simplified Model

and Complex Model. These results are iteratively utilized by the Predictive Model, which determines intermediate values of the damper height. When the subsequently determined damper height values do not significantly differ from each other, the PCA algorithm ceases to operate. To ensure that the determined value is optimal, an additional searching process is conducted around the determined height parameter. It is found that even a small number of PCA algorithm iterations allow for satisfactory values of the container height to be determined, which differ slightly from the actual optimal damper height determined through the searching process. Sensitivity analysis was carried out to determine the effectiveness of the PCA algorithm for different parameter changes. It turned out that the algorithm has a high efficiency, and most of the determined values differ from the actual optimal values by less than 5 %. The algorithm's error exceeded 15 %, only in the extreme cases when it was difficult (and sometimes impossible) to fulfill all the criteria for optimal grain movement.

The objectives of the thesis were categorized into three distinct groups, each focused on experimental studies of the prototype, modelling of ATPID dampers, and developing control strategies. Consequently, the original contributions of the thesis can be attributed to advancements made in these three subsections.

*Achievements concerning the experimental studies of the ATPID damper:*

- Formulation of the disadvantages of the classic PID damper and determining the reasons for not using this type of device in the engineering environment.
- The proposition of the novel Adaptive Tuned Particle Impact Damper which construction eliminates the disadvantages of the classical PID dampers.
- Development of the ATPID damper by application of the electromechanical control system control which is innovative in such structures.
- Extension of PID-type damper functionalities and their prospective application as an alternative adaptive device in the engineering environment.
- Elaboration of experimental studies and initial characteristics of the ATPID damper for various conditions.

*Achievements concerning the numerical analysis of the ATPID damper:*

- Formulation of the theoretical model of Adaptive Tuned Particle Impact Damper based on nonlinear viscoelastic contact model of the grain-walls collision.

- Implementation of the control component which is innovative in such structures.
- Development of the model sensitivity analysis, energy balance and parameters optimization.
- Formulation of the detailed ATPID operation principles.
- Elaboration of the ATPID high damping efficiency for various parameters of the system.

*Achievements concerning the control strategies of the ATPID damper:*

- Formulation of the criteria for the optimal ATPID damper attenuation.
- Formulation of the basic concept of the ATPID control strategy.
- Experimental validation of the basic control concept effectiveness and feasibility.
- Formulation of the Predictive Control Algorithm which provides a quick determination of the optimal ATPID damper heights for any system parameters.
- Elaboration of the PCA algorithm effectiveness and sensitivity.

The doctoral dissertation lacks consideration and exploration of several important aspects. It seems important to study the effect of different grain densities and various materials and shapes of the damper container. Investigation of the influence of magnetism on the dynamics of the particle and improvement of the efficiency of the absorber is also an interesting phenomenon. Additionally, there is a potential to replace both the fundamental mechanical system model and the ATPID damper with an artificial neural network model. Artificial intelligence algorithms may also serve as viable alternatives to support or supplant ATPID damper control algorithms. Overall, the subject matter concerning machine learning is captivating and has shown significant advancement in recent years. The absence of theoretical and practical solutions for cyber-physical approaches in mechanical engineering is noticeable. The combination of existing adaptive technical system concepts with computer-based methods based on artificial intelligence algorithms is certainly an intriguing field of study.

The author hopes that the research will prove valuable for engineers involved in the design of adaptive mechanical vibration dampers and that the innovative concepts presented in the work will play a significant role in the development and promotion of the use of Particle Dampers in the engineering industry.

# Bibliography

- [1] Z. Lu et al. "Nonlinear dissipative devices in structural vibration control: A review". In: *Journal of Sound and Vibration* (2018). DOI: 10.1016/j.jsv.2018.02.052.
- [2] L. Gagnon, M. Morandini, and G. Ghiringhelli. "A review of particle damping modeling and testing". In: *Journal of Sound and Vibration* (2019). DOI: 10.1016/j.jsv.2019.114865.
- [3] S. Masri X. Lu Z. Lu Z. Wang. "Particle impact dampers: Past, present, and future". In: *Structural Control and Health Monitoring* (2017). DOI: 10.1002/stc.2058.
- [4] M. Trigui, E. Foltete, and N. Bouhaddi. "Prediction of the dynamic response of a plate treated by particle impact damper". In: *J Mechanical Engineering Science* (2014). DOI: 10.1177/0954406213491907.
- [5] K. S. Marhadi. "Particle impact damping: effect of mass ratio, material, and shape". In: *Journal of Sound and Vibration* (2005). DOI: 10.1016/j.jsv.2004.04.013.
- [6] H. Pourtavakoli, E. JR Parteli, and T. Pöschel. "Granular dampers: does particle shape matter?" In: *New J. Phys.* (2016). DOI: 10.1088/1367-2630/18/7/073049.
- [7] D. V. Iourtchenko M. F.Dimentberg. "Random Vibrations with Impacts: A Review". In: *Nonlinear Dynamics* (2004). DOI: 10.1023/B:NODY.0000045510.93602.ca.
- [8] S. Ema and E. Marui. "Damping characteristics of an impact damper and its application". In: *International Journal of Machine Tools and Manufacture* (1996). DOI: 10.1016/0890-6955(95)00073-9.

- [9] B. Blazejczyk-Okolewska. "Analysis of an impact damper of vibrations". In: *Chaos, Solitons Fractals* (2001). DOI: [https://doi.org/10.1016/S0960-0779\(00\)00146-6](https://doi.org/10.1016/S0960-0779(00)00146-6).
- [10] C.C. Cheng and J.Y. Wang. "Free vibration analysis of a resilient impact damper". In: *International Journal of Mechanical Sciences* 45.4 (2003). DOI: 10.1016/S0020-7403(03)00116-4.
- [11] J. Cheng and H. Xu. "Inner mass impact damper for attenuating structure vibration". In: *International Journal of Solids and Structures* 43.17 (2006). DOI: 10.1016/j.ijsolstr.2005.07.026.
- [12] F.S. Collette. "A combined Tuned Absorber and Pendulum Impact Damper Under Random Excitation". In: *Journal of Sound and Vibration* (1998). DOI: 10.1006/jsvi.1997.1666.
- [13] R. Vinayaravi et al. "Experimental investigation and theoretical modelling of an impact damper". In: *Journal of Sound and Vibration* 332.5 (Mar. 2013), pp. 1324–1334. DOI: 10.1016/j.jsv.2012.10.032.
- [14] J. P. Caffrey R. D. Nayeri S. F. Masri. "Studies of the Performance of Multi-Unit Impact Dampers Under Stochastic Excitation". In: *Journal of Vibration and Acoustics* (2007). DOI: 10.1115/1.2346694.
- [15] S. F. Masri. "Analytical and Experimental Studies of Multiple-Unit Impact Dampers". In: *The Journal of the Acoustical Society of America* (1969). DOI: 10.1121/1.1911581.
- [16] Cz. Cempel. "The multi-unit impact damper: Equivalent continuous force approach". In: *Journal of Sound and Vibration* (1974). DOI: [https://doi.org/10.1016/S0022-460X\(74\)80304-4](https://doi.org/10.1016/S0022-460X(74)80304-4).
- [17] C.N. Bapat and S. Sankar. "Multiunit impact damper—Re-examined". In: *Journal of Sound and Vibration* (1985). DOI: [https://doi.org/10.1016/S0022-460X\(85\)80015-8](https://doi.org/10.1016/S0022-460X(85)80015-8).
- [18] C. Snoun; M. Trigui. "Design parameters optimization of a particles impact damper". In: *International Journal of Interactive Design and Manufacturing* (2018). DOI: 10.1007/s12008-018-0463-y.

- [19] X. Huang et al. "Equivalent model and parameter analysis of non-packed particle damper". In: *Journal of Sound and Vibration* (2021). DOI: 10.1016/j.jsv.2020.115775.
- [20] X. Huang and X. Li. J. Wang. "Optimal design of inerter-based nonpacked particle damper considering particle rolling". In: *Earthquake Engng. Struct. Dyn.* (2021). DOI: 10.1002/eqe.3430.
- [21] X. Huang et al. "Equivalent model of a multi-particle damper considering particle rolling and its analytical solution". In: *Struct. Control. Health. Monit.* (2021). DOI: 10.1002/stc.2718.
- [22] Z. Lu, X. Lu, and S.F. Masri. "Studies of the performance of particle dampers under dynamic loads". In: *Journal of Sound and Vibration* (2010). DOI: 10.1016/j.jsv.2010.06.027.
- [23] Y. Wang et al. "Prediction methods for the damping effect of multi-unit particle dampers based on the cyclic iterations of a single-unit particle damper". In: *Journal of Sound and Vibration* (2019). DOI: 10.1016/j.jsv.2018.10.035.
- [24] A. P. Darby K. Li. "A buffered impact damper for multi-degree-of-freedom structural control". In: *Earthquake Engineering and Structural Dynamics* (2008). DOI: 0.1002/eqe.823.
- [25] Y. Wang, Z. Lu, and J. Du. "Experimental study on damping mechanism of buffered impact dampers". In: *Applied Acoustics* (2020). DOI: 10.1016/j.apacoust.2020.107492.
- [26] K. Li and A.P. Darby. "An experimental investigation into the use of a buffered impact damper". In: *Journal of Sound and Vibration* (2006). DOI: <https://doi.org/10.1016/j.jsv.2005.06.043>.
- [27] Y. Du and S. Wang. "Modeling the fine particle impact damper". In: *International Journal of Mechanical Sciences* (2010). DOI: 10.1016/j.ijmecsci.2010.04.004.
- [28] Y. Du, S. Wang, and J. Zhang. "Energy dissipation in collision of two balls covered by fine particles". In: *International Journal of Impact Engineering* (2010). DOI: <https://doi.org/10.1016/j.ijimpeng.2009.06.011>.

- [29] J.A. Rongong B. Darabi. "Polymeric particle dampers under steady-state vertical vibrations". In: *Journal of Sound and Vibration* 331 (2012), pp. 3304–3316. DOI: 10.1016/j.jsv.2012.03.005.
- [30] Z. Wang Y. Zhou Z. Lu B. Huang. "Experimental Comparison of Dynamic Behavior of Structures with a Particle Damper and a Tuned Mass Damper". In: *Journal of Structural Engineering* (2018). DOI: 10.1061/(ASCE)ST.1943-541X.0002213.
- [31] Z. Lu et al. "Experimental and analytical study on the performance of particle tuned mass dampers under seismic excitation". In: *Earthquake Engineering and Structural Dynamics* (2016). DOI: 10.1002/eqe.2826.
- [32] D. Wang P. Li A. Ghoshal Z. Lu. "Comparison Study of Vibration Control Effects between Suspended Tuned Mass Damper and Particle Damper". In: *Shock and Vibration* (2014). DOI: 10.1155/2014/903780.
- [33] H.F. Bauer. "Oscillations of Immiscible Liquids in Rectangular Container: A new damper for excited structures". In: *Journal of Sound and Vibration* (1984). DOI: 10.1016/0022-460X(84)90354-7.
- [34] V.J. Modi, F. Welt, and M.L. Seto. "Control of wind-induced instabilities through application of nutation dampers: a brief overview". In: *Engineering Structures* 17.9 (1995), pp. 626–638. DOI: 10.1016/0141-0296(95)00033-4.
- [35] T. Shimizu and S. Hayama. "Nonlinear response of sloshing based on the shallow water wave theory". In: *The Japan Society of Mechanical Engineers* (1987). DOI: 10.1299/jsme1987.30.806.
- [36] S. Takaeda Y. Saoka F. Sakai. "On the suppression of vibrations by tuned liquid column dampers". In: *Japan Society of Civil Engineers* (1988). DOI: 10.1117/12.432729.
- [37] E. Sonmez et al. "A study on semi-active Tuned Liquid Column Dampers (sTLCDs) for structural response reduction under random excitations". In: *Journal of Sound and Vibration* 362 (2016), pp. 1–15. DOI: 10.1016/j.jsv.2015.09.020.
- [38] P. Egger and L. Caracoglia. "Analytical and experimental investigation on a multiple-mass-element pendulum impact damper for vibration mitigation". In: *Journal of Sound and Vibration* (2015). DOI: 10.1016/j.jsv.2015.05.003.

- [39] M. Żurawski and R. Zalewski. "Damping of Beam Vibrations Using Tuned Particles Impact Damper". In: *Applied Sciences-Basel* (2020). DOI: 10.3390/app10186334.
- [40] M. Żurawski, B. Chiliński, and R. Zalewski. "Concept of an adaptive-tuned particles impact damper". In: *Journal of Theoretical and Applied Mechanics* (2020). DOI: 10.15632/jtam-pl/122431.
- [41] R. Zalewski, M. Żurawski, and P. Chodkiewicz. "Adaptacyjno-pasywny tłumik drgań wykorzystujący luźny materiał granulowany". In: *Patent P.43007* (2021-05-04).
- [42] W. Xiao et al. "Study on vibration suppression based on particle damping in centrifugal field of gear transmission". In: *Journal of Sound and Vibration* 366 (Mar. 2016), pp. 62–80. DOI: 10.1016/j.jsv.2015.12.014.
- [43] W. Xiao et al. "Research on Vibration Reduction Characteristics of Continuum and Noncontinuum System on Coupling for High-Power Gear Transmission Based on Particle Damping Materials". In: *Shock and Vibration* (2021). DOI: 10.1155/2021/8845526.
- [44] M. Heckel et al. "Granular dampers for the reduction of vibrations of an oscillatory saw". In: *Physica A* (2012). DOI: 10.1016/j.physa.2012.04.007.
- [45] W. Xiao et al. "Influence of particle damping on ride comfort of mining dump truck". In: *Mechanical Systems and Signal Processing* (2020). DOI: 10.1016/j.ymsp.2019.106509.
- [46] Z. Lu et al. "Experimental studies of the effects of buffered particle dampers attached to a multi-degree-of-freedom system under dynamic loads". In: *Journal of Sound and Vibration* (). DOI: 10.1016/j.jsv.2011.12.022.
- [47] J. Chen et al. "Experimental research on design parameters of basin tuned and particle damper for wind turbine tower on shaker". In: *Struct Control Health Monitoring* (2019). DOI: 10.1002/stc.2440.
- [48] P. Veeramuthuvel, K. Shankar, and K.K. Sairajan. "Application of particle damper on electronic packages for spacecraft". In: *Acta Astronautica* (2016). DOI: 10.1016/j.actaastro.2016.06.003.

- [49] Afsharfard Aref. "Application of nonlinear magnetic vibro-impact vibration suppressor and energy harvester". In: *Mechanical Systems and Signal Processing* 98 (2018). DOI: 10.1016/j.ymsp.2017.05.010.
- [50] A. Mitura and K. Kecik. "Modeling and energy recovery from a system with two pseudo-levitating magnets". In: *Bulletin of the Polish Academy of Sciences Technical Sciences* (2022). DOI: 10.24425/bpasts.2022.141721.
- [51] K. Kecik and A. Smagala. "Influence of Linear and Nonlinear Electromechanical Couplings on Vibration Absorber–Harvester System". In: *Nonlinear Mechanics of Complex Structures* (2021). DOI: 10.1007/978-3-030-75890-5\_10.
- [52] K. Kecik. "Nonlinear Dynamics and Energy Recovery of a Vibration Absorber/Harvester System with an Adaptive Suspension". In: *Journal of Vibration Engineering Technologies* (2022). DOI: 10.1007/s42417-022-00536-6.
- [53] R. M. Brach. "Mechanical Impact Dynamics: Rigid Body Collisions". In: *Wiley-Interscience* (1991).
- [54] M. Frémond. "Collisions Engineering: Theory and Applications". In: *Springer* (2016).
- [55] K. F. Malone and B. H. Xu. "Determination of contact parameters for discrete element method simulations of granular systems". In: *Particuology* (2008). DOI: 10.1016/j.partic.2008.07.012.
- [56] A. Popp and P. Wriggers. "Contact Modeling for Solids and Particles". In: *Springer* (2019). DOI: 10.1007/978-3-319-90155-8.
- [57] S. Hara Y. Kushida H. Umehara and K. Yamada. "Momentum exchange impact damper design methodology for object-wall-collision problems". In: *Journal of Vibration and Control* (2017). DOI: 10.1177/1077546317703202.
- [58] M. A. Silva and A. M. Wahrhaftig. "Remarks on optimization of impact damping for a non-ideal and nonlinear structural system". In: *Journal of Low Frequency Noise, Vibration and Active Control* (2000). DOI: 10.1177/1461348420940074.
- [59] T. K. Caughey S. F. Masri. "On the Stability of the Impact Damper". In: *Transactions of the ASME* (1966). DOI: 10.1115/1.3607659.

- [60] C. N. Bapat and S. Sankar. "Single Unit Impact Damper in Free and Forced Vibration". In: *Journal of Sound and Vibration* (1985). DOI: 10 . 1016 / 0022 - 460X (85) 90446-8.
- [61] N.Popplewell and M.Liao. "Simple Design Procedure for Optimum Impact Dampers". In: *Journal of Sound and Vibration* (1991). DOI: 10 . 1016 / 0022 - 460X (91 ) 90707-Q.
- [62] S. Ema and E. Marui. "A Fundamental Study on Impact Dampers". In: *Int. J. Mach. Tools Manufact* (1994). DOI: 10 . 1016/0890-6955 (94) 90009-4.
- [63] Y.S. Choo A.Q. Liu B. Wang and K.S. Ong. "The effective design of bean bag as a vibroimpact damper". In: *Shock and Vibration* (2000). DOI: 10 . 1155 / 2000 / 351576.
- [64] M.R. Duncan, C.R. Wassgren, and C.M. Krousgrill. "The damping performance of a single particle impact damper". In: *Journal of Sound nad Vibration* (2005). DOI: 10 . 1016 / j . jsv . 2004 . 09 . 028.
- [65] M. Gharib and M. Karkoub. "Design and experimental analysis of new industrial vibration dampers". In: *Journal of Mechanical Science and Technology* (2018). DOI: 10 . 1007 / s12206-018-0703-x.
- [66] J. Shafer, S. Dippel, and D. Wolf. "Force Schemes in Simulations of Granular Materials". In: *Journal de Physique I* (1996). DOI: 10 . 1051 / jp1 : 1996129.
- [67] A. Di Renzo and F. P. Di Maio. "Comparison of contact-force models for the simulation of collisions in DEM-based granular flow codes". In: *Chemical Engineering Science* (2004). DOI: 10 . 1016 / j . ces . 2003 . 09 . 037.
- [68] H. Kruggel-Emden et al. "Review and extension of normal force models for the Discrete Element Method". In: *Powder Technology* (2007). DOI: 10 . 1016 / j . powtec . 2006 . 10 . 004.
- [69] D.J. Parker et al. H.P. Kuo P.C. Knight. "The influence of DEM simulation parameters on the particle behaviour in a V-mixer". In: *Chemical Engineering Science* (2002). DOI: 10 . 1016 / S0009-2509 (02) 00086-6.

- [70] H.J. Herrmann M. Lätzel S. Luding. "Comparing simulation and experiment of a 2D granular couette shear device". In: *European Physical Journal. E, Soft Matter* (2003). DOI: 10.1140/epje/i2002-10160-7.
- [71] T. Matsushima. "3-D image-based discrete element modeling for irregularly-shaped grains". In: *Proc. 2nd Int. PFC—Symposium* (2004).
- [72] A. Boonsrirat S. Limtrakul and T. Vatanatham. "DEM modeling and simulation of a catalytic gas–solid fluidized bed reactor: a spouted bed as a case study". In: *Chemical Engineering Science* (2004). DOI: 10.1016/j.ces.2004.09.020.
- [73] S. Wirtz H. Kruggel-Emden E. Simsek and V. Scherer. "Modeling of Granular Flow and Combined Heat Transfer in Hoppers by the Discrete Element Method (DEM)". In: *Journal of Pressure Vessel Technology* (2006). DOI: 10.1115/1.2218349.
- [74] H. Hertz. "Über die Berührungsfester elastischer Körper. (On the contact of elastic solids)." In: *J. reine und angewandte Mathematik* (1882).
- [75] J Lee and H J Herrmann. "Angle of repose and angle of marginal stability: molecular dynamics of granular particles". In: *Journal of Physics A: Mathematical and General* (1993). DOI: 10.1088/0305-4470/26/2/021.
- [76] Goro Kuwabara and Kimitoshi Kono. "Restitution Coefficient in a Collision between Two Spheres". In: *Japanese Journal of Applied Physics* (1987). DOI: 10.1143/JJAP.26.1230.
- [77] N. V. Brilliantov et al. "Model for collisions in granular gases". In: *Phys. Rev. E* 53 (1996). DOI: 10.1103/PhysRevE.53.5382.
- [78] Y. Tsuji, T. Tanaka, and T. Ishida. "Lagrangian numerical simulation of plug flow of cohesionless particles in a horizontal pipe". In: *Powder Technology* (1992). DOI: 10.1016/0032-5910(92)88030-L.
- [79] O. R. Walton and R. L. Braun. "Viscosity, granular temperature, and stress calculations for shearing assemblies of inelastic, frictional disks". In: *Journal of rheology* (1986). DOI: 10.1122/1.549893.

- [80] Q.M. Tai M.H. Sadd. "A contact law effects on wave-propagation in particulate materials using distinct element modeling". In: *International journal of Non-Linear Mechanics* (1993). DOI: 10.1016/0020-7462(93)90061-0.
- [81] C. Thornton. "Coefficient of restitution for collinear collisions of elastic perfectly plastic spheres". In: *Journal of Applied Mechanics—Transactions of the ASME* (1997). DOI: 10.1115/1.2787319.
- [82] Z.M. Ning C. Thornton. "A theoretical model for the stick/bounce behaviour of adhesive, elastic-plastic spheres". In: *Powder Technology* (1998). DOI: 10.1016/S0032-5910(98)00099-0.
- [83] G. Ziętek and Z. Mróz. "A constitutive hardening model of coupled plastic deformation and martensitic transformation in steels". In: *Mechanics of Materials* (2016). DOI: <https://doi.org/10.1016/j.mechmat.2016.06.004>.
- [84] J. Chen H. G. Matuttis. "Understanding the Discrete Element Method: Simulation of Non-Spherical Particles for Granular and Multi-Body Systems". In: *Wiley Online Library* (2014). DOI: 10.1002/9781118567210.
- [85] M.A.J. Holmes et al. "Bending and twisting friction models in soft-sphere discrete element simulations for static and dynamic problems". In: *Applied Mathematical Modelling* (2016). DOI: <https://doi.org/10.1016/j.apm.2015.10.026>.
- [86] C.M. Wensrich and A. Katterfeld. "Rolling friction as a technique for modelling particle shape in DEM". In: *Powder Technology* (2012). DOI: <https://doi.org/10.1016/j.powtec.2011.10.057>.
- [87] Z. Syed, M. Tekeste, and D. White. "A coupled sliding and rolling friction model for DEM calibration". In: *Journal of Terramechanics* (2017). DOI: <https://doi.org/10.1016/j.jterra.2017.03.003>.
- [88] X. Lu Z. Lu and S. F. Masri H. Jiang. "Discrete element method simulation and experimental validation of particle damper system". In: *Engineering Computations: International Journal for Computer-Aided Engineering and Software* (2013). DOI: 10.1108/EC-08-2012-0191.

- [89] M. Sánchez and L. A. Pagnaloni. “Effective mass overshoot in single degree of freedom mechanical systems with a particle damper”. In: *Journal of Sound and Vibration* 330.24 (2011), pp. 5812–5819. DOI: 10.1016/j.jsv.2011.07.016. (Visited on 03/07/2019).
- [90] M. Sánchez and M. Carlevaro. “Nonlinear dynamic analysis of an optimal particle damper”. In: *Journal of Sound and Vibration* (2013). DOI: 10.1016/j.jsv.2012.09.042.
- [91] Z. Xu T. Chen K. Mao M. Y. Wang. “DEM simulation of particle damping”. In: *Powder Technology* 142 (2004), 154–165. DOI: 10.1016/j.powtec.2004.04.031.
- [92] D. N. J. Els. “Damping of rotating beams with particle dampers: Discrete element method analysis”. In: *IP Conference Proceedings* (2013). DOI: 10.1063/1.4812069.
- [93] K. Jurczak M. Chmielewski K. Bochenek J. Rojek S. Nosewicz and K. Pietrzak. “Discrete element simulation of powder compaction in cold uniaxial pressing with low pressure”. In: *Computational Particle Mechanics* (2016). DOI: 10.1007/s40571-015-0093-0.
- [94] J. Lengiewicz, M. Wichrowski, and S. Stupkiewicz. “Mixed formulation and finite element treatment of the mass-conserving cavitation model”. In: *Tribology International* (2014). DOI: <https://doi.org/10.1016/j.triboint.2013.12.012>.
- [95] Tijskens E. Ramon H. Dintwa E. “On the accuracy of the Hertz model to describe the normal contact of soft elastic spheres”. In: *Granular Matter* (2008). DOI: 10.1007/s10035-007-0078-7.
- [96] V. Roxling T. Ghandriz H. Elmqvist A. Goteman. “Generic Modelica Framework for MultiBody Contacts and Discrete Element Method”. In: *Proceedings of the 11th International Modelica Conference* (2015). DOI: 10.3384/ecp15118427.
- [97] S. Luding. “Cohesive, frictional powders: contact models for tension”. In: *Granular Matter* 10 (2008). DOI: 10.1007/s10035-008-0099-x.

- [98] D. Rathbone et al. "An accurate force–displacement law for the modelling of elastic–plastic contacts in discrete element simulations". In: *Powder Technology* 282 (2015). DOI: 10.1016/j.powtec.2014.12.055.
- [99] B. Storåkers, S. Biwa, and .L. Larsson. "Similarity analysis of inelastic contact". In: *International Journal of Solids and Structures* 34 (1997). DOI: 10.1016/S0020-7683(96)00176-X.
- [100] B. Storåkers, N.A . Fleck, and R.M. McMeeking. "The viscoplastic compaction of composite powders". In: *Journal of the Mechanics and Physics of Solids* 47 (1999). DOI: 10.1016/S0022-5096(98)00076-3.
- [101] S. Nosewicz J. Rojek D. Lumelskyj and B. Romelczyk-Baishya. "Numerical and experimental investigation of an elastoplastic contact model for spherical discrete elements". In: *Computational Particle Mechanics* (2019). DOI: 10.1007/s40571-018-00219-8.
- [102] J. Rojek, R. Kasztelan, and R. Tharmaraj. "Discrete element thermal conductance model for sintered particles". In: *Powder Technology* (2022). DOI: 10.1016/j.powtec.2022.117521.
- [103] K. Thoeni P. Hartmann and J. Rojek. "A generalised multi-scale Peridynamics–DEM framework and its application to rigid–soft particle mixtures". In: *Powder Technology* (2023). DOI: 10.1007/s00466-022-02227-1.
- [104] G. Jočbalis et al. "Comparative numerical study of rate-dependent continuum-based plasticity models for high-velocity impacts of copper particles against a substrate". In: *International Journal of Impact Engineering* (2023). DOI: 10.1016/j.ijimpeng.2022.104394.
- [105] K. Thoeni J. Rojek S. Nosewicz. "3D formulation of the deformable discrete element method". In: *International Journal for Numerical Methods in Engineering* (2021). DOI: 10.1002/nme.6666.
- [106] A.I. Vakis et al. "Modeling and simulation in tribology across scales: An overview". In: *Tribology International* (2018). DOI: <https://doi.org/10.1016/j.triboint.2018.02.005>.

- [107] M. Guessasma et al. "Multi-Scale and Multi-Physics Modeling of the Contact Interface Using DEM and Coupled DEM-FEM Approach". In: *Advances in Multi-Physics and Multi-Scale Couplings in Geo-Environmental Mechanics*. 2018. DOI: <https://doi.org/10.1016/B978-1-78548-278-6.50001-3>.
- [108] S. Stupkiewicz, M. Rezaee-Hajidehi, and H. Petryk. "Multiscale analysis of the effect of interfacial energy on non-monotonic stress–strain response in shape memory alloys". In: *International Journal of Solids and Structures* (2021). DOI: <https://doi.org/10.1016/j.ijsolstr.2020.04.006>.
- [109] T. Lavigne, S.P.A. Bordas, and J. Lengiewicz. "Identification of material parameters and traction field for soft bodies in contact". In: *Computer Methods in Applied Mechanics and Engineering* (2023). DOI: <https://doi.org/10.1016/j.cma.2023.115889>.
- [110] P. Sadowski and S. Stupkiewicz. "Friction in lubricated soft-on-hard, hard-on-soft and soft-on-soft sliding contacts". In: *Tribology International* (2019). DOI: <https://doi.org/10.1016/j.triboint.2018.08.025>.
- [111] S. Stupkiewicz et al. "Finite deformation effects in soft elastohydrodynamic lubrication problems". In: *Tribology International* (). DOI: <https://doi.org/10.1016/j.triboint.2015.03.016>.
- [112] P. Sadowski, K. Kowalczyk-Gajewska, and S. Stupkiewicz. "Spurious softening in the macroscopic response predicted by the additive tangent Mori–Tanaka scheme for elastic–viscoplastic composites". In: *European Journal of Mechanics - A/Solids* (2021). DOI: <https://doi.org/10.1016/j.euromechsol.2021.104339>.
- [113] X. Lei and C. Wu. "Optimizing parameter of particle damping based on (Leidenfrost) effect of particle flows". In: *Mechanical Systems and Signal Processing* 104 (2018). DOI: [10.1016/j.ymssp.2017.10.037](https://doi.org/10.1016/j.ymssp.2017.10.037).
- [114] X. Wang J. Fang K. Zhang T. Chen. "Motion mode of the optimal damping particle in particle dampers". In: *Journal of Mechanical Science and Technology* (2016). DOI: [10.1007/s12206-016-0305-4](https://doi.org/10.1007/s12206-016-0305-4).

- [115] P. Eshuis et al. "Granular Leidenfrost Effect: Experiment and Theory of Floating Particle Clusters". In: *Physical Review Letters* 95 (2005). DOI: 10.1103/PhysRevLett.95.258001.
- [116] W. Gafsi F. Chaari M. Haddar F. Djemal R Chaari. "Passive vibration suppression using ball impact damper absorber". In: *Applied Acoustics* (2019). DOI: 10.1016/j.apacoust.2017.09.011.
- [117] P. Chen X. Lei C Wu. "Optimizing parameter of particle damping based on Leidenfrost effect of particle flows". In: *Mechanical Systems and Signal Processing* (2018). DOI: 10.1016/j.ymsp.2017.10.037.
- [118] D. Wang and C. Wu. "A novel prediction method of vibration and acoustic radiation for rectangular plate with particle dampers". In: *Journal of Mechanical Science and Technology* (2016). DOI: 10.1007/s12206-016-0205-7.
- [119] I. F. Lazar, S. A. Neild, and D. J. Wagg. "Using an inerter-based device for structural vibration suppression". In: *Earthquake Engineering Structural Dynamics* (2013). DOI: 10.1002/eqe.2390.
- [120] K. Mnich et al. "Identification of friction in inerter with constant and variable inertance". In: *Meccanica* (2022). DOI: 10.1007/s11012-022-01547-z.
- [121] Binoy M. Shah et al. "Construction and characterization of a particle-based thrust damping system". In: *Journal of Sound and Vibration* (2009). DOI: 10.1016/j.jsv.2009.06.007.
- [122] S.F. Masri. "Theory of the Dynamic Vibration Neutralizer With Motion-Limiting Stops". In: *Earthquake Engineering and Structural Dynamics* (1972). DOI: 10.1115/1.3422718.
- [123] A. Papalou and S.F. Masri. "Performance of Particle Dampers Under Random Excitation". In: *Transactions of the ASME* (1996). DOI: 10.1115/1.2888343.
- [124] A. Papalou and S.F. Masri. "Response of Impact Dampers with Granular Materials Under Random Excitation". In: *Earthquake Engineering and Structural Dynamics* (1996). DOI: 10.1002/(SICI)1096-9845(199603)25:3<253::AID-EQE553>3.0.CO;2-4.

- [125] A. Papalou and S.F. Masri. "An Experimental Investigation of Particle Dampers Under Harmonic Excitation". In: *Journal of Vibration and Control* (1998). DOI: 10.1177/107754639800400402.
- [126] S.F. Masri and A. M. Ibrahim. "Stochastic Excitation of a Simple System with Impact Damper". In: *Earthquake Engineering and Structural Dynamics* (1973). DOI: 10.1002/eqe.4290010404.
- [127] S.F. Masri. "Steady-State Response of a Multidegree System With an Impact Damper". In: *Journal of Applied Mechanics* (1973). DOI: 10.1115/1.3422910f.
- [128] S. F. Masri et al. "Active Parameter Control of Nonlinear Vibrating Structures". In: *Journal of Applied Mechanics* (1989). DOI: 10.1115/1.3176143.
- [129] F. Arrate S. F. Masri R. Ghanem and J. P. Caffrey. "A data-based procedure for analyzing the response of uncertain nonlinear systems". In: *Structural Control and Health Monitoring* (2009). DOI: 10.1002/stc.322.
- [130] S. F. Masri Z. Lu and X Lu. "Parametric studies of the performance of particle dampers under harmonic excitation". In: *Structural Control and Health Monitoring* (2011). DOI: 10.1002/stc.359.